STREAMFLOW MODELING AND IMPACT OF CLIMATE CHANGE FOR BEAS BASIN IN HIMALAYA

Ph.D. THESIS

by

LAXMI NARAYAN THAKURAL

DEPARTMENT OF WATER RESOURCES DEVELOPMENT & MANAGEMENT
INDIAN INSTITUTE OF TECHNOLOGY ROORKEE
ROORKEE- 247667 (INDIA)
DECEMBER, 2014

STREAMFLOW MODELING AND IMPACT OF CLIMATE CHANGE FOR BEAS BASIN IN HIMALAYA

A THESIS

Submitted in partial fulfilment of the requirements for the award of the degree

of

DOCTOR OF PHILOSOPHY

in

WATER RESOURCES DEVELOPMENT AND MANAGEMENT

by

LAXMI NARAYAN THAKURAL

DEPARTMENT OF WATER RESOURCES DEVELOPMENT & MANAGEMENT
INDIAN INSTITUTE OF TECHNOLOGY ROORKEE
ROORKEE- 247667 (INDIA)
DECEMBER, 2014

INDIAN INSTITUTE OF TECHNOLOGY ROORKEE
ROORKEE

CANDIDATE'S DECLARATION

I hereby certify that the work which is being presented in the thesis entitled "**STREAMFLOW MODELING AND IMPACT OF CLIMATE CHANGE FOR BEAS BASIN IN HIMALAYA"** in partial fulfilment of the requirement for the award of the Degree of Doctor of Philosophy and submitted in the Department of Water Resources Development and Management of the Indian Institute of Technology Roorkee, Roorkee is an authentic record of my own work carried out during a period from January, 2008 to December, 2014 under the supervision of Dr. S. K. Mishra, Professor, Department of Water Resources Development and Management, Indian Institute of Technology Roorkee, Roorkee and Dr. Sanjay Kumar Jain, Scientist 'F' and Sh. Raj Dev Singh, Director, National Institute of Hydrology, Roorkee.

The matter presented in this thesis has not been submitted by me for the award of any other degree of this or any other Institute.

(LAXMI NARAYAN THAKURAL)

This is to certify that the above statement made by the candidate is correct to the best of our knowledge.

(R.D. Singh)	(S.K. Jain)	(S.K. Mishra)
Supervisor	Supervisor	Supervisor

Date:

ABSTRACT

Streamflow modeling is of foremost importance for appropriate planning, designing, development and decision-making activities of water resources. The snow-fed rivers originating from Himalayan basins receive ample amount of runoff generated from snow and glacier melt. Moreover, in a Himalayan basin, like the Beas river basin, snowmelt is a governing factor for runoff production. A systematic modeling of streamflow components in such complex terrain of Himalayas is an important and challenging issue in recent changing environment. A snowmelt model that precisely simulates the three components of streamflow namely snowmelt runoff, rainfall-runoff and baseflow are essential for modeling streamflow in Himalayas. The information on model inputs such as snow cover area, meteorological data, temperature lapse rate and other related parameters are mandatory for snowmelt models. The snowmelt modeling also enables to understand the catchment processes and the major impacts on the streamflow regime due to climate change. A probable change in climatic variables namely temperature and precipitation impact the hydrological processes and control the streamflow. Spatio-temporal variation in magnitude of streamflow due to climate change may affect potential water availability of surface water in future, operation of reservoirs and flood related analysis. Therefore modeling of streamflow and study of climate change impact on streamflow is of paramount importance.

Snow is an important key environmental parameter of earth's climatic system which not only affects the radiation budget of the earth but also influences the streamflow of mountainous rivers. A major source of runoff and groundwater recharge in middle and higher latitudes is the snowmelt runoff from seasonal snow covered areas and Himalayan mountain system forms one of the world's largest suppliers of freshwater. All the three predominant south Asian rivers namely the Indus, the Ganga and the Brahmaputra river systems originating from the Himalayan mountain system are snow and glacier fed. These rivers receive ample amount of snowmelt water and therefore are considered as the lifeline for the Indian sub-continent. The snow accumulated during winter season turns into a major source of runoff for these rivers during summer period. The spring and summer season runoff of a Himalayan river is mostly a contribution from snowmelt and is a dependable source of water for irrigation, generation of hydroelectric power and drinking water supply.

The lack of detailed systematic evaluation of the Himalayan water resources, first of all due to poor and inadequate network of hydro-meteorological observations and secondly, its

inaccessibility for being rugged, dangerous with harsh climatic conditions are the challenges demanding time for proper assessment of streamflow in these rivers. Even then, the available estimates show that water yield is almost double in the snow-fed higher Himalayan river basins than that of an equivalent peninsular basin mainly because of snowmelt and glacier melt contribution. The perennial nature of these rivers and the appropriate topographic setting of the Himalayan region provide exploitable hydropower potential in these regions. The effect of climatic change on the hydrologic systems, specifically on snow and glacier, have led to the alteration in timing and the amount of runoff in mountainous basins. Streamflow in the Himalayan rivers generated from the melting of snow and glaciers have a direct impact on the water resources of a region under these changing climatic conditions. Therefore, near real time snow cover estimation along with the accurate streamflow simulation and forecast under the changed climatic scenarios is of great importance in managing and planning the water resources of a region and also to minimize risk and loss from devastating floods caused due to rapid melting of snow and glacier under changing climate. Therefore, there exists a pressing need to properly assess the natural water resources in mountainous areas and their judicious utilization during different seasons and years for supporting agricultural production, water supplies, industries, energy generation and for functioning of ecosystem health. Moreover, to plan new upcoming hydropower and river valley projects on the river system of Himalayas accentuated the need of accurate and reliable estimation of runoff from snow and glacier. Therefore the present study envisages the assessment of streamflow estimation including snowmelt runoff and evaluation of the impact of climate change on streamflow.

Based on the literature review, the objectives of the present study have been set such as to interrelate snowmelt modeling and impact of climate change on streamflow, as follows:

- Snow cover assessment using multiple satellite images and assessment through a relationship developed between SCA and temperature.
- Determination of seasonally and topographically varying TLR using LST data estimated from thermal satellite images.
- Snowmelt runoff simulation for the Beas river using snowmelt runoff model.
- Trend analysis of temperature, precipitation and discharge data of Beas basin.
- Application of future scenarios on the basis of data analysis to investigate the impact of climate change on runoff.

The above objectives have been accomplished for the Beas river basin up to Pandoh dam. The Beas river originates from Beas Kund, a small spring near Rohtang Pass at an elevation of 4085 m and is an important river of the Indus river system. The length of the Beas

river up to Pandoh dam is 116 km. Among its major tributaries namely Parvati, Thirthan, Sainj Khad, Bakhli Khad, Parvati and Sainj Khad are glacier-fed. The catchment area of Beas river upstream of Pandoh dam is 5384.9 sq. km.

In the present study, snowmelt runoff has been modeled using SNOWMOD model. The important input of this model is snow cover area (SCA) and temperature lapse rate beside meteorological data and other parameters. Therefore, the main emphasis has been on estimation of SCA using different approaches and seasonally/topographically varying TLR. Further to evaluate the impact of climate change, trend analyses as well as generation of future scenarios have been the major areas of concern in this study. Finally, impact of climate change on streamflow has been studied on the basis of future scenarios.

Snow cover assessment

Vastness of the river basin area, time, and manpower constraints in data collection and seasonal changes in the information require fast inventory of the snow cover areas and its mapping. The scarce availability of field based information on the snow cover area (SCA) is a big constraint, rather a challenge, for carrying out snowmelt runoff studies in such a complex rugged terrain of Himalaya. Innovative space based sensor technology and digital image processing tools provide researchers and scientists to envisage snow cover monitoring and mapping for hydrology and water resources management and its impacts due to climate change. Remote sensing has emerged as a powerful active tool with its proficiency in mapping the snow cover area. Earlier NOAAA-AVHRR and IRS-WiFS data products were used in Himalayan basins. However, getting cloud-free data for most part of the year, particularly in the Himalayan region, is again a big deal. Consequently, Moderate Resolution Imaging Spectro radiometer (MODIS), a NASA space satellite, has been used for determination of SCA for the study area as it provides cloud-free scenes at a regular interval.The MODIS 8-day composite maps for a period of six years (2000-2005) were downloaded and processed to obtain snow cover depletion curves for the Beas basin. To check the efficacy of MODIS SCA, IRS-1C/1D WiFs and AWiFS satellite data have also been used for some of the dates. As per the analysis it was found that SCA estimated using MODIS is quite satisfactory compared to SCA obtained using WiFS and AWiFS satellite data. SCA was estimated mainly using MODIS satellite data available from 2000 onwards. A method using mean air temperature has been proposed to obtain SCA information when the satellite data was not available. An exponential relationship between SCA and CMAT has been generated for preparation of depletion of SCA. This

technique also supports in providing SCA for the previous years when the satellite data is not available or is cloud covered and hence reducing the quantity of satellite imageries.

Determination of Temperature Lapse Rate

Temperature Lapse Rate (TLR) is an important parameter necessary for temperature-based conceptual snowmelt runoff simulation. Earlier TLR was estimated from the ground based air temperature data recorded at meteorological stations. However, it is very difficult to establish meteorological stations in the complex Himalayan terrains with rugged and undulated topography and the available sparsely located network represents only local temperature. Thus, estimation of representative TLR values is extremely difficult and hence a fixed TLR value (=0.65 ^{o}C/100m) calculated from air temperature is most commonly and often used in snowmelt studies. Moreover, since TLR can vary both seasonally and regionally within different elevation zones, the use of fixed values of TLR in the snowmelt model may not be appropriate. Nowadays, remote sensing satellites provide a straightforward and consistent way to observe Land Surface Temperature (LST) over large scales with more spatially detailed information and these data well represent the terrain.

Spatio-temporal TLR was estimated for different dates (2001 to 2009) employing satellite based MODIS-LST maps and USGS-DEM for the Beas basin. In case of seasonal variation, TLR was the lowest during monsoon season whereas its variation with respect to topography showed that the lapse rate was low in lower altitudes than in higher altitudes.

Snowmelt runoff simulation

Streamflow was modeled for the Beas river basin using SNOWMOD, which is a temperature index based snowmelt runoff model. The model simulates the three components of streamflow i.e. snowmelt runoff, rainfall-runoff and baseflow independently and their sum provides the total streamflow. Employing the above variable TLR values the model was calibrated using daily data of 3 years (2002-2005) and these parameters obtained during calibration were used for validation of streamflow for a period of twelve years i.e. 1990-1993, 1993-1996, 1996-1999 and 1999-2002. The model efficiency (R^2) for snowmelt season of 1990-2002 varied from 0.68 to 0.80 and the difference in volume varied from -9.63% to 9.15%. During this period the snowmelt contribution varied from 24.07% to 34.62%, and rainfall from

30.48% to 41.85%. The average runoff generated from the snowmelt during the ablation period was 38.2% whereas remaining 61.8% was contributed from rainfall.

Trend analysis of temperature, precipitation and discharge data of Beas basin

For better understanding the trends in climatic variables namely temperature, rainfall and discharge of the Beas basin trend analysis was carried out using parametric (linear regression) and non-parametric (Mann-Kendall and Sen's slope Estimator) approaches both at annual and seasonal scales. The hydro-meteorological data of Beas river were collected from BBMB, Pandoh, Himachal Pradesh. Majority of stations showed increasing trends in mean annual temperature whereas one station (Manali) showed a decreasing trend over the last three decades. The annual rainfall indicated increasing trend at Banjar station, and decreasing trend at all other four stations with maximum decrease of -8.07mm/year at Sainj.

Seasonal analysis of rainfall trends showed that all stations during pre-monsoon, post-monsoon, and winter season experienced decreasing trend whereas all stations experienced increasing trend in monsoon seasons. A decreasing trend in discharge was observed at three stations Bakhli, Pandoh and Thalout while the other two stations Sainj and Tirthan indicated increasing trend at annual time scale.

Impact of climate change on runoff

For climate change impact assessment, in two ways scenarios were generated and applied. First of all, ten hypothetical scenarios for (T + 1°C, P + 0%), (T + 2°C, P + 0%), (T + 1°C, P + 5%), (T + 2°C, P + 5%), (T + 1°C, P + 10%), (T + 2°C, P + 10%), (T + 1°C, P - 5%), (T + 2°C, P - 5%), (T + 1°C, P - 10%), (T + 2°C, P - 10%) with respect to baseline scenario (T + 0, P + 0%) were generated to study the impact of climate change on streamflow. An increase of 1°C and 2°C in temperature increased the mean annual streamflow by about 9% and 8.69%, respectively.

Further, to assess the impact of temperature, projected temperature scenarios based on IPCC SRES A1B were generated and applied. To account for the change of SCA, modified snow cover depletion curves were prepared using exponential relationship between SCA and air temperature. The model was simulated with the change in temperature and modified depletion curves for the years 2040-43, 43-46, 46-49, 49-52 and 2093-96, 2096-99. The total

flow reduced for the years 2040-43, 2043-46, 2046-49, 2049-52 while for the years 2093-96 and 2096-99, it increased marginally. The snowmelt runoff decreased in all future scenarios.

The stream/snowmelt runoff modeling and impact of climate change studies for a Himalayan basin incorporating the unique technique of estimating SCA using mean air temperature and seasonally and topographically varying TLR have been used for the Beas basin for the first time, and promising results obtained. Overall, the significantly improved TLR and SCA estimates enhanced the model efficiency in simulating the streamflow. The assessment of hydrological impacts of climate change at basin scale for any Himalayan region is unique and crucial. The hypothetical and future projected scenarios furnished with the plausible future streamflow under the changing climatic conditions for the basin. Therefore, such studies are of great significance for accurate streamflow simulation and forecast of Himalayan rivers under contemporary and changing climate for proper planning and management of precious water resources.

ACKNOWLEDGEMENT

It is an opulent occasion for me to express my deep and sincere gratitude to my supervisors Dr. S. K. Mishra, Professor, Department of Water Resources Development and Management, Indian Institute of Technology, Roorkee, Dr. Sanjay Kumar Jain, Scientist-F and Sh. Raj Dev Singh, Director, National Institute of Hydrology, Roorkee, for their incessant and indefatigable invaluable guidance, inspiring constant support and encouragement at every step throughout the entire course of this research work I have no words to express my indebtedness to my supervisors for allowing to me to fulfill my dreams and ambitions through this research work.

I am extremely thankful to Director, National Institute of Hydrology, Roorkee giving me permission to undertake this research work and providing necessary support and facilities to complete it in a successful manner.

I express my sincere gratitude to Prof. Deepak Khare, Head of the Department of Water Resources Development and Management for providing the necessary facilities to accomplish the research work. I gratefully acknowledge Dr. Nayan Sharma, Chairman, Student Research Committee (SRC) and the committee members Dr. Deepak Khare, Dr. Manoj Arora and Dr. R. D. Garg for their constant encouragement and valuable suggestions during the course of study.

I am greatly thankful to Dr. Sharad Kumar Jain, Scientist-G and Head, Water Resources System division for his kind support and encouragement to achieve my goal. I am highly grateful to Sh. D. S. Rathore, Dr. A. K. Lohani, Dr. Sanjay Kumar and Sh. S. S. Kanwar for their constant support, technical suggestions, and being source of inspiration during the course of work. I am thankful to my colleagues Dr. Rakesh Kumar, Dr. R. P. Pandey, Dr. Senthil Kumar and Dr. Renoj Thayyen for insightful suggestions and encouragement. I am also thankful to my friends and colleagues Tanvear Ahmad, Furqan Ullah, Naresh Kumar, Neha Jain and Aakash Kumar for providing support and encouragement during my research work.

I am sincerely thankful to Dr. Vijay Kumar, Sc-F/ Director, Ministry of Earth Sciences, New Delhi for valuable suggestions and guidance. I am thankful to Dr. Ajanta Goswami, scientist, Indian Institute of Remote Sensing, Dehradun for incessant encouragement and technical discussions. I express my sincere gratitude to Sh. Rajesh Handa, SDO and Sh. Karam Veer Arora, official of BBMB, Pandoh for providing the necessary data and support during field visits.

I am also thankful to my scholar friends Ajay Kumar, Sandeep Shukla, Surendra Chandhania, Sunil Maskey, Vinit Jain and Sarita Gajbhiye for their valuable and timely help. I

am also thankful to technical and non-technical staff of Water Resources Development and Management department for their kind support during this period.

I am greatly thankful to my father Sh. Ayodhia Prasad and my mother Smt. Kanti Devi for their blessings. I am extremely grateful to my wife Sarvesh Thakural, and my son Yatharth and daughter Sudiksha, for understanding me and providing moral support, encouragement, inspiration, forbearance and sacrifice.

Above all, I am highly grateful to almighty God for giving me enough strength to complete the research work successfully.

Last but not the least my sincere thanks are due to all those who helped me directly or indirectly to complete this research work successfully.

Place: Roorkee (LAXMI NARAYAN THAKURAL)

Date:

CONTENTS

	Page No.
ABSTRACT	i
ACKNOWLEDGEMENT	vii
CONTENTS	ix
LIST OF FIGURES	xiii
LIST OF TABLES	xix
Chapter 1 INTRODUCTION	1
1.1 GENERAL	1
1.2 NEED OF THE STUDY	3
1.3 OBJECTIVES	4
1.4 ORGANISATION OF CHAPTERS	4
Chapter 2 LITERATURE REVIEW	7
2.1 BACKGROUND	7
2.2 SPACE BORNE SATELLITE REMOTE SENSING OF SNOW COVER	7
2.3 SNOW COVER MAPPING	9
2.4 TEMPERATURE LAPSE RATE (TLR)	13
2.5 SNOWMELT RUNOFF MODELING	15
2.6 SNOWMELT COMPUTATION	16
2.6.1 Energy Balance Approach	16
2.6.2 Degree-Day Approach	17
2.7 SNOWMELT RUNOFF MODELS	18
2.7.1 Statistical Models	18
2.7.2 Simulation Models	18
2.8 TREND ANALYSIS	22
2.9 CLIMATE CHANGE	26
2.10 SUMMARY	29
Chapter 3 STUDY AREA AND DATA AVAIALABILITY	31

3.1 INTRODUCTION 31
3.2 THE STUDY AREA 31
3.3 CLIMATIC CONDITIONS AND VARIATIONS IN STUDY AREA 32
3.4 GEOLOGY AND SOIL 34
3.5 HYDROPOWER POTENTIAL 35
3.6 STREAMFLOW CHARACTERISTICS OF RIVER BEAS AT PANDOH 36
3.7 AVAILABILITY OF DATA 37
3.8 REMOTE SENSING SATELLITE DATA 37
3.9 SATELLITE IMAGERIES AND DATA PRODUCTS 39
3.9.1 IRS-1C/1D and IRS-P6 39
3.9.2 Moderate Resolution Imaging Spectroradiometer (MODIS) 41
3.9.2.1 MODIS SNOW DATA PRODUCTS 42
3.9.2.2 MODIS land surface temperature data 44
3.9.3 DIGITAL ELEVATION MODEL 45
(a) Using SRTM 90 M Data 45
(b) Using USGS Data 46
3.10 HYDRO-METEOROLOGICAL DATA 47
3.11 SOFTWARE USED 47
Chapter 4 ASSESSMENT OF SNOW COVER AND ITS DEPLETION 49
4.1 BACKGROUND 49
4.2 INTRODUCTION 49
4.3 ASSESSMENT OF SNOW COVER AREA (SCA) 51
4.3.1 Using Remote Sensing Data 51
4.3.1.1 Preparation of SCA Maps and DEM 52
4.3.2 SCA Using Temperature Data 62
4.4 SUMMARY 69
Chapter 5 DETERMINATION OF TEMPERATURE LAPSE RATE 77
5.1 BACKGROUND 77
5.2 MEASUREMENT OF LAND SURFACE TEMPERATURE 77
5.3 LST RETRIEVAL FROM REMOTE SENSING DATA 81
5.4 TLR ESTIMATION 84

5.5 SUMMARY 92
Chapter 6 STREAMFLOW MODELING USING SNOWMOD 95
6.1 BACKGROUND 95
6.2 SNOWMELT RUNOFF MODELING 96
6.3 SNOWMOD-A SNOWMELT MODEL 97
6.4 DATA INPUT FOR SNOWMOD 99
6.5 MODEL VARIABLES AND PARAMETERS 99
6.5.1 Division of Basin into Elevation Bands 99
6.5.2 Precipitation Data and Distribution 101
6.5.3 Temperature Data: Spatial and Temporal Distribution 102
6.5.4 Degree-Days 104
6.5.5 Degree-Day Factor 105
6.5.6 Snow Cover Area (SCA) 107
6.5.7 Rain on Snow 107
6.6 COMPUTATION OF DIFFERENT RUNOFF COMPONENTS 108
6.6.1 Surface Runoff from Snow Covered Area 108
6.6.2 Surface Runoff from Snow-Free Area 110
6.6.3 Estimation of Subsurface Runoff 110
6.6.4 Total Runoff 111
6.7 CATCHMENT ROUTING 112
6.7.1 Surface Runoff Routing 112
6.7.2 Subsurface Routing 113
6.8 EFFICIENCY CRITERIA OF THE MODEL 113
6.9 CALIBRATION OF MODEL 114
6.10 SIMULATION OF STREAMFLOW 118
6.11 SUMMARY 129
Chapter 7 TREND ANALYSIS 131
7.1 BACKGROUND 131
7.2 INTRODUCTION 131
7.3 DATA USED 133
7.4 DATA PROCESSING 133
7.5 METHODOLGY 134
7.5.1 Regression Model 135
7.5.2 Sen’s Estimator of Slope 135

7.5.3 Mann–Kendall Test 136
7.6 TRENDS OF OBSERVED HYDRO-METEREOLOGICAL DATA 137
7.7 RESULTS AND DISCUSSION 138
7.7.1 Trends in Temperature 138
7.7.2 Trends in Rainfall 152
7.7.3 Trends in Streamflow 157
7.8 SUMMARY 162
Chapter 8 CLIMATE CHANGE AND ITS IMPACT ON STREAMFLOW 163
8.1 BACKGROUND 163
8.2 CLIMATE CHANGE MODELING 163
8.2.1 Climate Change and Issues 163
8.2.2 Climate Scenarios 166
8.3 HYDROLOGICAL MODELING FOR CLIMATE CHANGE 168
8.3.1 Coupling GCMS and Macroscale Hydrological Models 168
8.3.2 Downscaled GCM Climate Output for Use in Hydrological Models 168
8.3.3 Based on Hypothetical Scenarios as Input to Hydrological Models 169
8.4 STREAMFLOW MODELING UNDER CHANGED CLIMATE 170
8.4.1 Using Hypothetical Scenario 170
8.4.2 Streamflow under Future Projected Scenario 186
8.5 SUMMARY 196
CHAPTER 9 SUMMARY AND CONCLUSION 197
9.1 SUMMARY 197
9.2 CONCLUSIONS 198
9.3 SCOPE OF FUTURE RESEARCH WORK 199
9.4 MAJOR CONTRIBUTIONS 199
REFERENCES 201
ANNEXURE-I 232
ANNEXURE-II 233

LIST OF FIGURES

Figure No.	Title	Page No.
Figure 3.1	Location map of the Beas basin up to Pandoh Dam	33
Figure 3.2	Spatial distribution of hydrometric stations in the study area	48
Figure 4.1	Digital Elevation Model (DEM) of the Beas basin	54
Figure 4.2	Snow cover distribution in the Beas basin using MODIS images for year 2001	55
Figure 4.3	Snow cover distribution in the Beas basin using MODIS images for year 2002	56
Figure 4.4	Snow cover distribution in the Beas basin using MODIS images for year 2003	57
Figure 4.5	Snow cover distribution in the Beas basin using MODIS images for year 2004	58
Figure 4.6	SCA for the Beas basin using MODIS, WiFS and AWiFS images	59
Figure 4.7	Classified images of WiFS (a) 28 February, 2001 (b) 27 September, 2002	60
Figure 4.8	Classified images of WiFS (a) 14 May, 2004 (b) 11 December, 2005	60
Figure 4.9	Snow cover depletion curves for ablation period (March to October)	62
Figure 4.10	Snow cover depletion curves (SDCs) for the years 1990-1993	66
Figure 4.11	Snow cover depletion curves (SDCs) for the years 1994-1996	67
Figure 4.12	Snow cover depletion curves (SDCs) for the years 1997-1999	68
Figure 4.13	Observed and simulated SCA for band 4 and band 5 for year 2001	70
Figure 4.14	Snow cover depletion curves (SDCs) for the years 1990-1993 with 1^0C increase	71

Figure 4.15	Snow cover depletion curves (SDCs) for the years 1994-1996 with 1^0C increase	72
Figure 4.16	Snow cover depletion curves (SDCs) for the years 1997-1999 with 1^0C increase	73
Figure 4.17	Snow cover depletion curves (SDCs) for the years 1990-1993 with 2^0C increase	74
Figure 4.18	Snow cover depletion curves (SDCs) for the years 1994-1996 with 2^0C increase	75
Figure 4.19	Snow cover depletion curves (SDCs) for the years 1997-1999 with 2^0C increase	76
Figure 5.1	Flowchart for determining the TLR for the Beas basin	85
Figure 5.2	Scatter plots showing the relationship between elevation and MODIS-LST for pre-monsoon season	86
Figure 5.3	Scatter plots showing the relationship between elevation and MODIS-LST for monsoon season	87
Figure 5.4	Scatter plots showing the relationship between elevation and MODIS-LST for winter season	88
Figure 5.5	Scatter plots showing the relationship between elevation and MODIS-LST for post-monsoon season	89
Figure 5.6	Seasonal TLR for the Beas basin during 2000-2009	92
Figure 6.1	Structure of the SNOWMOD model	98
Figure 6.2	Area-elevation curve of the study area	100
Figure 6.3	Simulation of the Beas river at Pandoh for year calibration period i.e. 2002-2005	116
Figure 6.4	Simulation of the Beas river basin at Pandoh for the year 1999-2000	117
Figure 6.5	Simulation of the Beas river basin at Pandoh for the year 2000-2001	117
Figure 6.6	Simulation of the Beas river basin at Pandoh for the year 2001-2002	118
Figure 6.7	Simulation of the Beas river at Pandoh for the year 1990-1993	119
Figure 6.8	Simulation of the Beas river at Pandoh for the year 1993-1996	120

Figure 6.9	Simulation of the Beas river at Pandoh for year 1996-1999	121
Figure 6.10	Simulation of the Beas river at Pandoh for year 1999-2002	122
Figure 6.11	Simulation of the Beas river basin at Pandoh for the year 1990-1991	123
Figure 6.12	Simulation of the Beas river basin at Pandoh for the year 1991-1992	124
Figure 6.13	Simulation of the Beas river basin at Pandoh for the year 1992-1993	124
Figure 6.14	Simulation of the Beas river basin at Pandoh for the year 1993-1994	125
Figure 6.15	Simulation of the Beas river basin at Pandoh for the year 1994-1995	125
Figure 6.16	Simulation of the Beas river basin at Pandoh for the year 1995-1996	126
Figure 6.17	Simulation of the Beas river basin at Pandoh for the year 1996-1997	126
Figure 6.18	Simulation of the Beas river basin at Pandoh for the year 1997-1998	127
Figure 6.19	Simulation of the Beas river basin at Pandoh for the year 1998-1999	127
Figure 7.1	Maximum and minimum temperature Trends of Bhuntar station	139
Figure 7.2	Maximum and minimum temperature trends of Larji station	140
Figure 7.3	Maximum and minimum temperature trends of Manali station	141
Figure 7.4	Maximum and minimum temperature trends of Pandoh station	142
Figure 7.5	Average temperature trends of Bhuntar and Manali station	143
Figure 7.6	Average temperature trends of Larji and Pandoh station	144
Figure 7.7	Rainfall trends of Banjar and Bhuntar stations	153
Figure 7.8	Rainfall trends of Larji and Pandoh stations	154
Figure 7.9	Rainfall trends of Sainj station	155
Figure 7.10	Stream discharge trends of Bakhli and Pandoh stations	158
Figure 7.11	Stream discharge trends of Thalout and Sainj stations	159

Figure 7.12	Streamflow discharge trends of Tirthan station	160
Figure 8.1	Simulation for the years 1990-1993 under temperature rise of 1^0C	172
Figure 8.2	Simulation for the years 1993-1996 under temperature rise of 1^0C	173
Figure 8.3	Simulation for the years 1996-1999 under temperature rise of 1^0C	174
Figure 8.4	Simulation for the years 1999-2002 under temperature rise of 1^0C	175
Figure 8.5	Simulation for the years 1990-1993 under temperature rise of 2^0C	176
Figure 8.6	Simulation for the years 1993-1996 under temperature rise of 2^0C	177
Figure 8.7	Simulation for the years 1996-1999 under temperature rise of 2^0C	178
Figure 8.8	Simulation for the years 1999-2002 under temperature rise of 2^0C	179
Figure 8.9	Mean annual streamflow for various scenarios in Beas basin	180
Figure 8.10	Mean annual snowmelt runoff for various scenarios in Beas basin	180
Figure 8.11	Mean annual streamflow for different scenarios for each month in Beas basin	181
Figure 8.12	Mean annual snowmelt runoff for different scenarios for each month in Beas basin	181
Figure 8.13	Snowmelt runoff for temperature rise of 1^0C and 2^0C for year 1990-1993	182
Figure 8.14	Snowmelt runoff for temperature rise of 1^0C and 2^0C for year 1993-1996	182
Figure 8.15	Snowmelt runoff for temperature rise of 1^0C and 2^0C for year 1996-1999	183
Figure 8.16	Snowmelt runoff for temperature rise of 1^0C and 2^0C for year 1999-2002	183
Figure 8.17	Mean annual streamflow for temperature change only scenarios for each month in Beas basin	184

Figure 8.18	Mean annual snowmelt runoff for temperature change only scenarios for each month in Beas basin	184
Figure 8.19	Projected daily max. temperature for different time period for Manali station	192
Figure 8.20	Projected daily max. temperature for different time period for Larji station	192
Figure 8.21	Projected daily max. temperature for different time period for Bhuntar station	193
Figure 8.22	Projected daily max. temperature for different time period for Pandoh station	193
Figure 8.23	Simulation of streamflow for the Beas basin up to Pandoh	195

LIST OF TABLES

Table No.	Title	Page No.
Table 3.1	Average rainfall distribution in the Beas basin	34
Table 3.2	Distribution of major rock types in the Beas basin at sub-catchment scale	35
Table 3.3	Details of hydro-electric power in Himachal Pradesh	36
Table 3.4	Key parameters of IRS-1C/1D and IRS-P6 satellites	40
Table 3.5	Details of satellite data used in the study	41
Table 3.6	Sequential overview of MODIS-LST products	45
Table 3.7	General details of hydrometric stations in the Beas basin	48
Table 4.1	Estimated snow cover area from MODIS data for the Beas basin	61
Table 4.2	Coefficients and R^2 values for the ablation period	65
Table 5.1	Spectral and spatial resolutions of AVHRR and MODIS Thermal Infrared Bands	82
Table 5.2	Monthly Temperature Lapse Rate (TLR) values in the Beas basin during the period 2001-2009	90
Table 5.3	Seasonal and annual TLR for the Beas basin	91
Table 5.4	Values of TLR for the three zones in the study area	94
Table 6.1	Beas basin area covered in different elevation zones	101
Table 6.2	Raingauge and temperature stations used for different elevation bands	103
Table 6.3	Parameter values used in calibration of model	106
Table 6.4	Results of model simulation for the period 1990-2002 for the Beas basin	128
Table 6.5	Contribution of snowmelt and rainfall to the ablation and annual flows	129
Table 7.1	Details of the meteorological stations located in the study area	133
Table 7.2	Seasonal and annual trends of average temperature (T_{avg})	145
Table 7.3	Seasonal and annual trends of maximum temperature (T_{max})	146

Table 7.4	Seasonal and annual trends of minimum temperature (T_{min})	147
Table 7.5	Seasonal and annual trends of highest maximum temperature (H_{max})	148
Table 7.6	Seasonal and annual trends of lowest minimum temperature (L_{min})	149
Table 7.7	Seasonal and annual trends of temperature range (T_{range})	150
Table 7.8	Distribution of rainfall at different stations in Beas basin (1979-2009)	152
Table 7.9	Seasonal and annual trends in rainfall of different stations in Beas basin	156
Table 7.10	Seasonal and annual trends of stream discharge	161
Table 8.1	Mean annual runoff for different hypothetical scenarios for the Beas basin	185
Table 8.2	Projected maximum temperature for different time period for Manali station	188
Table 8.3	Projected maximum temperature for different time period for Larji station	189
Table 8.4	Projected maximum temperature for different time period for Bhuntar station	190
Table 8.5	Projected maximum temperature for different time period for Pandoh station	191
Table 8.6	Simulation of streamflow for the Beas Basin up to Pandoh	194
Table 8.7	Mean (annual) runoff for A1B scenario for Beas basin	195

Chapter 1

INTRODUCTION

1.1 GENERAL

Water is the second essential element among the five elements of nature namely earth, water, air, fire and space with cold and wet sensible qualities. Available as a vital natural resource is of utmost important for the subsistence of any kind of life on the planet earth. Its availability is highly variable with space and time. Water is of paramount importance and precious for the livelihood, from crucial drinking water to food production, production of energy to development of industries and from management of natural resources to environment conservation. The scarcity of water resources and its tremendous increasing demand, which is outcome of growing population, intensification of agriculture sector, industrial and urban expansion, has necessitated its proper planning and management. Streamflow modeling in this line is of great importance for designing and operating of hydraulic structures, forecasting and regulating floods, and evaluating the impact of climate change over a river basin under the harsh, complex and rugged terrain of Himalaya.

A large amount of fresh water is stored in the form of snow and ice in the mountains for which they are considered as 'water towers' of the world. A large portion of earth is covered with the mountains occupying with different climate regime, shape, altitude, extension and vegetation. Mountain regions constitute relatively small river basins but are the major source of perennial rivers providing significant river flows downstream. These regions accumulate about half of the world's fresh water from precipitation in the form of rain and snow and are expected to satisfy the bigger part of growing demand. Freshwater is locked up in Antarctica and Greenland in the form of permanent ice or snow, or in deep ground water aquifers. With the rapid and escalating changes in landscape of mountains along with the growing demands of mountain resources, fresh water availability is being affected. Vast terrestrial ecosystem on the earth is sustained by the snow and ice representing 80% of the total freshwater globally. The Himalayan region is widely known as Third Pole because it contains the largest reservoirs of fresh water reservoir in the form of snow and glacier outside the Polar regions.

Himalaya the great mountain system is an amalgamation of the Sanskrit words-"Him" for snow and "alaya" for abode meaning storehouse of snow and ice. It is the highest, youngest and sensitive mountain network system of Asia in the world with Tibetan Plateau to its North

and Indian subcontinent on its southern edge. Geologically, impact of Indian tectonic plate has led to the origin of Himalayas. This unique mountain network runs uninterruptedly in southerly arched for 2500 km between Nanga Parbat (8126 m) in west to Namcha Barwa peak (7756 m) in east with 240 km average width. The Himalayan mountain system has 530 peaks above 6000 m, hundreds above 7000 m and 14 peaks over 8000 m high (Goswami, 2007). After the two poles Antarctica and Arctic, Himalayas represent the highest deposition of snow and ice. It passes through the five countries namely India, Pakistan, China, Nepal and Bhutan. In India, it extends through the States of Jammu and Kashmir, Himachal Pradesh, Uttar Pradesh, Sikkim, Arunachal Pradesh, Nagaland, Manipur, Mizoram, Tripura and Meghalaya.

In Indian context, based on the distinct geology, geomorphology and physiographic features, Himalaya can be grouped into three transverse or parallel ranges running from Jammu and Kashmir in the west to Arunachal Pradesh zones in east often referred as the Greater Himalayas, the Lesser Himalayas and the outer Himalayas. Further, these zones are divisible into three main realms, western Himalayas, central Himalayas and eastern Himalayas on basis of differing spatial geographic elements. More than 12000 glaciers are nourished by the Himalaya (Kaul, 1999; ICIMOD, 2001). The area covered by these glaciers is about 33000 km^2 (Rai and Gurung, 2005). Himalayan region is the prime source of three major river systems, the Indus, the Ganga and the Brahmaputra. Himalayan rivers replenished by melt water from these glaciers drain Indian subcontinent and sustain the population living in the contiguous lowlands. Since Indian society is mainly agrarian with about 75% of the people depending on agriculture, the water resources generated from these perennial rivers is significant premeditated resource and is considered a boon for the development of country. Availability of abundant water due to snow/ice and glacier melt together with monsoon precipitation and with physical topographical setting, the Himalayas is bequeathed with significant, incredible and excellent hydropower potential for its river basins.

Snow and ice are the key features of the Himalayan river basins that contribute almost 58% of the total runoff primarily controlled by seasonal snow and glacial melt. Snow and glaciers act as reservoirs with vast storage of freshwater. Seasonal snow cover and glacial ice being the alluring elements of nature have always attracted the researchers and scientist for studying the zenith environment. These elements are important fresh water resources and equally imperative resources for the economical hydropower generation in a region. If available in an appropriate manner, is a boon for the development for the region, however also a potential root cause for natural hazards as strongly affected by climate change leading to enlargement and growing of glacial lakes, instability of permafrost regions, increasing avalanches in

mountain regions (Bernstein, 2007). Possible change in the climate and its adverse effects on the hydrological components pose a major threat to water resources sector all over the globe. Thus, adequate knowledge of hydrology and proper management of water resources can safeguard from serious deceleration of water quality and quantity.

The Himalayas act as a mountain barrier and plays a key role in sustaining and controlling the monsoon system over the Asian continent. The upper catchments of the major rivers originating from Himalayas are snow covered receiving substantial amount of runoff from snow and glacier melt. These rivers flow through steep varied topography, any variation in the climatic condition may have plausible impact on the precipitation influencing the surface water runoff at the downstream. Hence, besides well timed reasonable precise estimation of streamflow, there exists an imperative need to study the trend of important climatic variables and their impact on the streamflow regime of Beas river basin possessing enormous water resources potential. Hence time demands that there is great need to properly assess the natural water resource in Beas river basin for their judicious utilization during different seasons and years for supporting agricultural production, water supplies, industries, energy generation and for functioning of ecosystem health. The Beas river basin located in the western Himalayan region receives significant amount of runoff from snow and glacier melt. Snowmelt runoff in such basin forms an integral part of hydrological modeling for predicting streamflow.

1.2 NEED OF THE STUDY

In spite of the paramount significance of Beas river system, a means of survival for a large population of the northern region of India, only a few systematic studies on its snowmelt runoff assessment have been carried out so far. However, there still exist few research gaps which need to be addressed for this area. In a Himalayan basin, like Beas river basin, modeling streamflow becomes highly complex due to complex variability in different hydrological and meteorological parameters due to highly varying topography, along with changing landuse and landcover in a changing environment. Moreover, global warming and looming climate change in the region has further added more intricacy. For better addressing these major issues, the technological advancement like availability of new generation satellite data, can be advantageously employed to map snow cover area and determine seasonally and topographically varying lapse rate to improve the overall accuracy of snowmelt runoff simulation. Keeping in view these foremost active research aspects, there is need to carry out research work to model the streamflow, and studies related to changes in key climatic variables

and impact of climate change on the streamflow of Beas river basin. Streamflow modeling of a Beas river basin would lead to long-term hydrological yields of the basin, scenarios for future climate change, and impact of climate on runoff needed for development of effectual management strategies for the region. Thus, the present study conceived with the objectives mentioned in next section to model the streamflow and assess the impact of climate change in the Beas basin in Himalaya.

1.3 OBJECTIVES

With this background, the present study was initiated with the following interrelated objectives pertinent for streamflow modeling.

1. Snow cover assessment using multiple satellite images and assessment through a relationship developed between SCA and temperature.
2. Determination of seasonally and topographically varying TLR using LST data estimated from thermal satellite images.
3. Snowmelt runoff simulation for the Beas river using snowmelt runoff model.
4. Trend analysis of temperature, precipitation and discharge data of Beas basin.
5. Application of future scenarios on the basis of data analysis to investigate the impact of climate change on runoff.

The five interrelated objectives have been carried out for the Beas river basin up to Pandoh dam. The geographical area of the Beas river basin up to Pandoh dam site is 5384.9 $km^{2.}$ The Beas river is bounded by high peaks in North and East of the river valley. The river gushes through very steep rolling meadow in upper reaches. It cuts its way through the mountains and encounters many falls and confronts varied complex characteristic of the basin before reaching Pandoh.

1.4 ORGANISATION OF CHAPTERS

The coherent research work carried out in this thesis has been organized into nine chapters and below is the brief overview of these chapters.

Chapter 1 mainly focuses on the introduction of the research work, its importance and related issues. The need of study and objectives of the study have been also discussed in this chapter.

Chapter 2 deals with the theoretical background about the work carried out earlier in this area. A comprehensive literature review is presented on concerned topics associated with the research work like snow cover mapping, temperature lapse rate, runoff modeling, trends in climate variables and impact of climate change. The use of satellite remote sensing for mapping snow cover area and temperature lapse rate has also been reviewed. The studies carried out in general and particularly in the Himalayan region and in Beas basin have been reviewed and discussed.

Chapter 3 describes about the study area details, dataset and software's used for the present research work. The climatic conditions and seasonal variation, geology etc. in study basin along with hydropower potential of the river have been described. The availability of the space borne satellite and hydro-meteorological data are discussed. The satellites imagery namely Aqua/Terra-MODIS, IRS-1C/1D, Resourcesat-1 (IRS-P6) satellites and their scientific specifications, relative importance and capabilities for estimation of snow cover and lapse rate have been discussed in detail. The digital elevation models and their technical specifications used for the present work are also discussed in detail.

Chapter 4 describes the different modus operandi involved in mapping and estimating aerial snow cover area from multiple satellite images. A method for preparation of depletion of SCA using mean air temperature has been described under the conditions when no cloud-free satellite data is available or to generate snow covered area in a new climate to see the impact of climate change on snowmelt runoff studies.

Chapter 5 describes the importance, technical specifications and approaches for the retrieval of Land Surface Temperature (LST) from thermal satellite data. The methodology to determine lapse rate using LST maps and Digital Elevation Model (DEM) have been discussed. The lapse rate computed for different months, seasons and topography based (different elevation) for Beas basin is discussed.

Chapter 6 deals with the streamflow modeling using SNOWMOD, a temperature index based conceptual snowmelt runoff model. The snow cover area and temperature lapse rate estimated in chapter 4 and 5 respectively besides meteorological data and other parameters used in the model are discussed. The various processes involved in the melt modeling have been

systematically discussed. The results of the streamflow calibration and simulation along with efficiency criteria have been described in detail.

Chapter 7 addresses trend detection techniques for hydro-meteorological parameters. Trend analysis for climatic variables namely temperature, rainfall, and discharge data using parametric (linear regression) and non-parametric (Mann-Kendall and Sen's slope Estimator) approaches have been discussed. The results of trend analysis on seasonal and annual scale have been discussed in detail.

Chapter 8 deals with the climate change and its impact on runoff of the Beas river using SNOWMOD model. The impact of climate change on the streamflow and its different components under plausible hypothetical scenarios and IPCC SRES A1B temperature projected scenario have been carried and discussed in detail.

Chapter 9 summarises the conclusions and scope for future work.

Chapter 2

LITERATURE REVIEW

2.1 BACKGROUND

Himalayan mountain system is one of the world's biggest reservoirs of fresh water in the form of snow and glaciers. Runoff produced from the snow and glacier melt in the Himalayan basin significantly influence the river streamflow. Rapid snow and glacier melt due to climate change could affect the water availability and its management over a long-term. Therefore, it is important to precisely model the streamflow in such snow and glacier fed river basins. This chapter presents a review of relevant literature for streamflow modeling and impact of climate change on snow-fed Himalayan rivers. The valuable role and contribution of remote sensing in estimation of snowmelt runoff has been also carried out. Review of literature on snow cover mapping, temperature lapse rate, snowmelt runoff modeling, trend analysis and climate change have been presented in this chapter.

2.2 SPACE BORNE SATELLITE REMOTE SENSING OF SNOW COVER

Snow forms an integral part of hydrological modelling (Ohara et al., 2014a) for predicting the snowmelt runoff. Its spatial coverage or extent i.e. Snow Cover Area (SCA) together with physical properties are very significant input parameters for simulation and estimation of snowmelt contribution in the river flow. In mountain hydrology, remote sensing has potential in snow cover/glacier mapping, terrain analysis, hazard and vulnerability mapping and accessibility analysis. The researchers especially hydrologists are of more concern about the areal distribution of the snow, its condition and amount of water stored in the form of snow in a river basin. Remote sensing has emerged as a valuable and economical tool for acquiring information on snow cover for prediction of snowmelt runoff in a river basin. It provides researchers and scientists to envisage and monitor snow cover for analysis, hydrological modeling, prediction and forecasting for supporting decision making processes. Moreover, it has shown its ability in measuring the snow cover extent and glacier cover (Krishna, 1996, 1999, 2005) and physical properties of snow in complex, rugged mountainous terrain (Thakur et al., 2012, 2013) which are equally inaccessible, dangerous and harsh climatic conditions,

also measurement of which is not possible through conventional methods. Use of remote sensing data also provides low-cost synoptic view in multi-spectral at repetitive coverage over the larger areas.

Satellites are well suited to measure unique and spectrally varying reflectance of snow owing to high albedo of snow surfaces, presenting a good contrast with other natural earth surface materials except clouds. Usually, fresh snow has high albedo of 90% or more whereas old weathered snow with accumulated dust and litter may have low albedo of 40% (Foster et al., 1987) which is mainly dependent upon the properties of snow such as the grain size, shape, depth, water content, surface roughness and impurity. Advancement in satellite image processing techniques facilitates users in identifying the snow and the boundary of snow and snow-free areas precisely.

Snow for the first time was observed from the first image obtained from the Television Infrared Observation Satellite-1 (TRIOS) launched in April 1960 (Singer and Popham, 1963). Since then, satellite based space technology is being employed for snow studies with two types of techniques; one using optical remote sensing and another using the microwave remote sensing, each having its own advantages and limitations. Optical images from satellite remote sensing from 1980s have been usually used to monitor snow cover and glaciers (Matson et al., 1986; Dozier and Marks, 1987; Kulkarni, 1991; Hall et al., 2002a, 2002b; Kaab et al., 2002; Kargel et al., 2005; Kulkarni et al., 2006, 2010) and using passive imageries since1980s (Hallikainen, 1984; Chang et al., 1987). Also, since 1990s combined active and passive microwave imageries are used for this purpose (Dozier, 1998; Hallikainen, et al., 2003a, 2003b, 2004). But, the optical remote sensing lacks ability in producing snow cover maps in cloudy conditions (Frei and Robinson, 1999) or nighttime conditions (Carsey, 1992).

In optical multi spectral images the visible and mid infrared wavelength regions are used for SCA mapping because the snow cover and clouds spectral reflectance are very analogous at visible wavelengths below about 1 μm (Carsey et al., 1987; Massom, 1991; Konig et al., 2001) and achieve maximum diversion in near infrared wavelength (between 1.55 and 1.75 μm) region. It is this key property which plays an important role in discriminating snow from snow-free areas in the visible bands of spectrum. In comparison to most of the earthly or terrestrial objects, snow has high reflectance in visible wavelength and strong absorption in infrared spectral regions. Due to these characteristics, reflectance ratios in the visible and near infrared wavelengths are used for detecting snow (Riggs and Hall, 2002) and this rationing approach formed the basis for the extensively used snow cover mapping products for MODIS (Hall et al. 2002a; Hall and Riggs, 2007) using NDSI technique.

Nowadays large number of satellite data of various sensors with different spatial and temporal resolutions and different geographic extent are made available to user for different applications. The spatio-temporal inputs provided by satellites when integrated with GIS and hydrological models become a promising approach to quantify the surface runoff (Deshmukh et al., 2004; Gangodagamage and Aggarwal, 2012). Moreover, remote sensing technique is a practical means to obtain snow cover information in large, inaccessible, rugged terrains of Himalayan basins. Various studies have been carried out in Himalayan region using the satellite images namely for snow cover mapping in snowmelt runoff estimation (Rango et al., 1977; Gupta et al., 1982; Kulkarni et al., 2001; Singh and Jain, 2003).

The primary differences in remote sensing instruments lie in their spatial, temporal, spectral and radiometric resolutions. Optimization of one type of resolution generally involves some sacrifice in other types of resolution, e.g., the Indian Remote Sensing Satellite (IRS) 1C/1D (Linear Imaging Self Scanning) LISS II, Landsat Thematic Mapper (TM) has a much better spatial resolution than the IRS 1C/1D (Wide Field Sensor) WiFS and NOAA/AVHRR (23.5/30 m versus 188 m and 1 km pixel size respectively); however, the AVHRR can provide daily coverage for a given point and WiFS has a revisit period of 3 days, whereas the LISS and TM can only provide bi-weekly coverage. Modern age satellite, Terra/Aqua MODIS provides an inimitable advantage for mapping the daily and eight days snow cover and land surface temperature globally and continuously since its launch. The MODIS data products have overall higher accuracy produced utilizing the group decision systems giving users more confidence to use. MODIS uses the finer and higher radiometric resolutions (12 bits) for quantization of all its spectral bands in comparison to other sensors like (AVHRR's (10 bits) for detecting smaller differences in emitted of reflected energy. These data products provide more finely defined visible and infrared bands and deploy most precisely calibrating subsystems. The MODIS data products also incorporate adjustment for snow even in dense vegetation areas unlike earlier snow cover mapping approaches (Klien et al., 1998). The MODIS snow maps have augmented the valuable record by providing daily snow products with numerous spectral bands and superior resolution relative to other satellite products. The MODIS derived data products have the capability to discriminate snow from most clouds.

2.3 SNOW COVER MAPPING

The precise and periodic monitoring and mapping of snow cover is important for snowmelt runoff studies. The distributed models which incorporate the spatial variability of

basin physical geography and the meteorological inputs are competent to utilize detailed snow cover information including snow cover area. Traditional methods for measurement of snow cover like snow surveys are costly and hazardous and even then are not helpful in distributed models due to their site specific nature and lesser frequency. Tremendous advancement in technology during the 20th century facilitates the researchers and scientists to undertake research in this area. Recent use of automated measurement techniques of telemetering of snow pillow and storage gauges for precipitation have reduced upto some extent fieldwork but problem of point measurement of snow still persist. With massive advancement in space technology during the last decade provides us with large number of satellites to study the complex physical development of earth-atmosphere system (Konig et al., 2001). Space borne remote sensing satellite has emerged as a promising tool to monitor and map snow cover for hydrology and water resources management. Space based snow mapping when used with digital elevation models in mountainous regions provide realistic snow cover extent. Extraction of snow cover from a remote sensing data is a complex task and thus requires effective techniques to extract useful information on snow cover information from digital image acquired by variety of satellites and aircrafts at diverse spectral, spatial and temporal resolutions. With increasing demands for areal estimation of snow cover, a number of image information extraction techniques have been developed and utilized for the said purpose. The various digital image extraction techniques used for snow cover mapping are categorised as; manual delineation, change detection-based method, spectral ratios, spectral indices, per pixel image classification and sub-pixel image classification. There are numerous successful applications of snow cover mapping using satellite remote sensing. Some of them applied specifically for the Himalayan region are reviewed in detail.

Wang and Li (2003) employed three techniques of snow mapping; supervised classification, digital number and NDSI to map and extract snow cover area using the satellite data of Landsat TM, MODIS and NOAA/AVHRR. It was found that the best method for acquiring the snow index was different for each sensor depending upon the spatio-temporal resolutions and objective of application.

Gupta et al. (2005) used the remote sensing data to differentiate between dry/wet snows in glacerized basin of Himalayas using multispectral data of IRS-LISS-III for the period March to November 2000 and DEM. The satellite sensor data was converted to reflectance values and NDSI was computed and boundary between dry/wet snow was determined from spectral response data. Further, threshold slicing of images was done to obtain dry/wet snow areas for different satellite overpasses in the basin. It is suggested that the directly derived position and

extent of wet snow and exposed glacier ice data can enhance the hydrological simulations in such basins.

Krishna (2005) conducted a study for the assessment of snow and glacier cover in the high mountains of Sikkim Himalayas. The different visual and digital image processing in combination were carried out on multi date satellite data of IRS 1B and 1C (1992 to 1997) for analyzing the baseline inventory of snow/glacier, permanent snowline and the short-term temporal changes in it. The study highlighted the utilization of remote sensing and GIS tools in establishing snow/glacier cover extent for assessment of possible impacts of climate change in such mountainous areas.

Shimamura et al. (2006) conducted a study to evaluate different methods used for monitoring snow cover areas over the snowy Niigata prefecture plains, Japan. The snow cover areas were delineated using Landsat-7 satellite data in the springs of year 2002 and 2003. The three methods: visible reflectance, NDSI and snow index (S3) were intercompared and found that S3 index was able to map snow covered areas under forested areas without any reference data in comparison to other methods.

Kulkarni et al. (2006) utilized NDSI based algorithm to generate 5 and 10 day snow cover products from RESOURCESAT-1 (AWiFS) sensor data for the Himalayan region. The 5-daily product provided snow and cloud extent scene-wise whereas 10-daily product analyzed three scenes and provided estimates of maximum snow extent at basin wise. It was suggested that this technique is useful for the Himalayan region where mountain shadow conditions prevails.

Keshri et al. (2009) suggested two new indices Normalized Difference Glacier Index (NDGI) and Normalized Difference Snow and Ice Index (NDSII-2) for systematically discriminating and detailed mapping of Supraglacial terrain cover as such found in the Himalayas. The Chenab basin in the Himalayas was selected as test area and ASTER image acquired on 8 September 2004 during post-monsoon season was used for the study. The combination of these two indices along with NDSI allows discrimination of snow, ice and ice-mixed-debris (IMD) in three steps. In the initial step, NDSI index separates snow and ice from rest of terrain. In the second step, NDGI index is used to separate snow and ice from IMD and finally snow and ice separated using NDSII-2 index.

Negi et al. (2009a) carried out a study to map snow cover in Beas basin in Indian Himalayas using satellite data of IRS-P6 (AWiFS). For the mapping snow cover, a technique based on Normalized Difference Snow Index (NDSI) along with NIR band reflectance and vegetal information was used for snow cover distribution in Beas basin consisting rugged

terrain, snow under forest, patchy and contaminated snow. The cloud-free satellite images for year 2004-05 were used to estimate the snow cover distribution. A good correlation was found between increase/decrease areal extent of seasonal snow cover and ground observed snowfall (fresh) and standing snow data.

Negi et al. (2009b) carried out snow monitoring to regionally evaluate accumulation and ablation snow cover patterns in Pir Panjal and Shamshawari ranges of Kashmir valley. The multi temporal of IRS-1C/1D (WiFS) for the winter season of 2004-05, 2005-06 and 2006-07 was processed to generate region wise snow cover maps and estimate the areal snow cover extent using hybrid technique. The study illustrated the spatio-temporal variability in the seasonal snow cover within the Kashmir valley.

Kaur et al. (2009) carried out a study using NDSI technique to monitor variations in snow cover and snowline altitude in the Baspa basin situated in Kinnaur district of Himachal Pradesh. The snow cover for the basin was delineated for years 2004-05 and 2006-07 between the months of October and June using Resourcesat-1, AWiFS satellite sensor data. It was observed that 98% of basin area lies below the elevation of 5800 m and the lowest snowline altitude was found to be 2425 m in the month of February 2004-05 and 2846.25 m in March for the year 2006-07.

Kulkarni et al. (2010) at 5 or 10 days intervals monitored seasonal snow cover for 28 sub-basins of the Ganga and Indus river basins in the Himalayan region. The NDSI algorithm was used to extract the seasonal snow cover from the Advanced Wide Field Sensor (AWiFS) of Indian remote Sensing satellite (IRS) for a 3 years period (2004-2007) between the months of October and June. The area–altitude distribution and snow map were combined to estimate the snow cover distribution in different altitude zones for the individual basin and for the central and western Himalaya. It was observed that lowest snowline altitude was at 2480 m in winters during the three years period on 25th February 2005. During the year 2004-05, it was seen that the snow accumulation and ablation were continuous process throughout the winter period in the Ravi basin and snow area reduced from 90% to 55% in the middle of winter.

Gurung et al. (2011) conducted a study to examine the changes in the seasonal snow cover area in the Hindu Kush Himalayan (HKH) region using the satellite data of MODIS 8-day standard snow products. Based on the satellite data from 2000-2010, the average snow covered area of the HKH region was estimated to be 0.76 million km^2 which is found to be 18.23% of the total geographical area. During the spring season, snow covered area indicated a decreasing trend i.e. -1.04±0.97%. The decadal snow cover trends were found to vary with season and region.

Subramaniam et al. (2011) developed and implemented an automated algorithm to estimate snow cover by using AWiFs sensor of IRS-P6 (Resourcesat-1). The algorithm was developed using the spectral information of snow and other land cover noise in the Red, Near Infrared and SWIR bands. The algorithm was evaluated with several temporal images covering entire snow belt of Indian Himalayas (from Kashmir to Arunachal Pradesh) and found to be working satisfactorily. It was also found that alorithm identified snow pixels even in the presence of mountain shadow, clouds and water bodies and worked well with Landsat ETM and IRS III satellite data.

Pant et al. (2014) examined the dynamics of snow cover in Pinder watershed located in the central Himalayas, India. The NDSI technique was used to extract and quantify the snow cover from the satellite data of Landsat TM of three different time periods (1990, 1999, 2011). The study revealed that geographical extent of snow cover was 9.4%, 8.60% and 7.80 % in 1990, 1999 and 2011 respectively. It was concluded that about 2.7 km^2 of the snow cover area of catchment has been converted to snow-free area over the last two decades.

Panwar and Singh (2014) carried out a study to monitor seasonal snow cover in Yamuna basin from 2003 to 2010 (October to June). The NDSI algorithm was used to generate snow cover extent from AWiFS sensor of Resourcesat satellite in every five and ten daily interval. It was found that maximum snow cover in the Yamuna basin was 76% in the month of January and February. The study suggested that a NDSI value of 0.4 (as a threshold) can be taken to discriminate between snow and non-snow pixels.

2.4 TEMPERATURE LAPSE RATE (TLR)

Primordially, surface air temperature decreases with increase in elevation. This decrease in temperature with increasing elevation is termed as Temperature Lapse Rate (TLR). It is considered to be most important characteristics of local/regional climate. TLR varies with macro topography and its magnitude varies in different geographic locations as a function of energy balance regimes. Research studies conducted by Diaz and Bradleyy, 1997; Rolland, 2003; Tang and Fang, 2006; Mokhov and Akperov, 2006; Marshall et al., 2007; Blandford et al., 2008; Minder et al., 2010 have highlighted the importance of surface air temperature for determining the temperature range essential in many spheres, like hydrology, glaciology, agriculture, forestry and ecology.

TLR is one of the most important variables for modeling melt runoff from a snow/ice and glacier basins employing temperature index method. The TLR varies with region and

season. Due to sparse distribution of weather stations in mountainous terrain, it is difficult to obtain lapse rate seasonally as well as topographically. Very limited studies have been conducted to estimate the representative TLR values. As per practice, constant value of lapse rate of 6.5°C km^{-1} is used in most of the studies. Remote sensing technology has emerged as a supportive tool in this field. It provides a straightforward and reliable mode to observe Land Surface Temperature (LST) over large scales with more spatially detailed information. This information from satellite imagery would certainly help to estimate representative TLR values for Himalayan region and in turn would enhance the modeling of snowmelt runoff. Some of the important studies carried out for determining the TLR in the Himalayan region are reviewed and discussed here in brief.

Singh (1991) computed TLR for Sutlej catchment based on the temperature data for two sets of stations namely Rampur-Kalpa and Kalpa-Rakchham to better understand the distribution of temperature and incorporate its effect on snowmelt models. The results of the study showed that TLR values for the two sets of stations vary drastically, even though in the same region. The mean monthly TLR for the Rampur-Kalpa varies between 6.9-10.6, 5.4-7.9, 6.8-8.9 ^{0}C/km for maximum, minimum and mean temperatures respectively and for the Kalpa-Rakchham TLR values were observed between (-0.8)-5.1, 3.2-8.9, 3.0-5.3^{0}C/km. The study suggests using representative values of TLR in accordance with temperature data instead of a constant value for a basin.

De Scally (1997) determined the lapse rates from slope air temperature data for seven stations located in the Punjab Himalaya, Pakistan. The data collected over two snowmelt seasons was analyzed and a strong negative correlation between elevation and mean daily temperature was observed. The study suggests that the lapse rates values calculated for this region, ranging from 0.48 to 0.78 ^{0}C 100 $^{-1}$m^{-1} are normally higher than the values reported from other studies mainly due to relatively higher thermal regime of the area and cooling influence of snow cover at some high altitude stations. It is also suggested to use derived lapse rates carefully, as the lapse rate values varies between the individual pairs of stations, as well as between the two years.

Thayyen et al. (2005) carried out a Temperature Lapse rate study for Din Gad catchment located in Garhwal Himalaya during ablation period i.e. May to October for three years (1998 to 2000). The temperature data of three meteorological stations situated at different altitudes was analyzed for determination of suitable lapse rate of slope, for modeling snow/glacier runoff and mass balance of Dokriani glacier. It was found that monsoon months were having lower lapse rate values, as compared to other ablation months. The study

suggested that for hydrological modeling, temperature lapse rate values of alpine zone have to be monitored rather than adopting these values of other geographic locations or extrapolated from lower elevations of the Himalayas.

Jain et al. (2008b) determined the Temperature Lapse rate (TLR) for the Satluj river basin located in the western Himalayas from satellite datasets of National Oceanic and Atmospheric Administration/Advanced Very High Resolution Radiometer (NOAA/AVHRR) using the split-window algorithm. The TLR values obtained were in the range of 0.6-0.74°C/100 m in the study area. The study suggests a good agreement between the air temperature and LST retrieved from the satellite data of NOAA-AVHRR and MODIS-Terra.

Kattel et al. (2013) carried out temperature lapse rate study on the southern slope of the Central Himalayas. The surface air temperature data of 56 stations located at different elevation for a period of 20 years in Nepal was analyzed for monthly, seasonal, and annual characteristics of temperature lapse rates using linear regression model. It was found that highest temperature lapse rate occurred in the pre-monsoon season whereas lowest in the winter season. It was observed that a different pattern exists in this region than other mountain regions. The results also suggest different controlling factors on the magnitude of TLR values for individual seasons.

Pratap et al. (2013) reported near-surface temperature lapse rate (dT/dZ) variability in Dokriani Glacier catchment located in the Garhwal Himalaya for year 2011-2012 based on temperature data (maximum, minimum, average) from three automatic weather stations in the catchment. The mean monthly temperature lapse rate dT_{avg}/dZ, dT_{max}/dZ, dT_{min}/dZ were computed between three camp station namely Tela camp, Base camp and Advanced base camp. It was found that dT_{avg}/dZ was lower than 6.5 $^{0}C\ km^{-1}$ in monsoon months and higher in dry period between Tela camp-Base camp, Base camp-Advanced base camp and Tela camp Advanced base camp. A significant inter-basin regional variation in central and western Himalayas was also observed. The study emphasizes to use locally determined temperature lapse rate for hydrological and glacier modeling in Himalayan region, rather than regional or global lapse rates.

2.5 SNOWMELT RUNOFF MODELING

Concept of modeling involves replacing the complex parts of universe under contemplation with a model of similar nature but with simple structure (Eldho et al., 2006). Hydrological models at watershed or basin scale are fundamentals for the assessment, evolution

and management of water resources and understand the interplay between climate and surface hydrology (Eldho et al., 2009). In the Himalayan basins, snow is a key feature and a major source of fresh water. The hydrological models are exploited to quantify the runoff generated from the snow/ice and glacier melt under the changing climate.

Snowmelt in hydrology is the surface runoff generated or produced from the melting of snow. Globally, snowmelt runoff is considered as major component of the movement of water. The potential effects of snowmelt are triggered landslides, debris flow besides flooding which is a serious concern for community round the world. Snowmelt runoff modeling proffers an excellent opportunity, to study the physical processes of snow accumulation, snowmelt and runoff. The precise and reliable estimation of runoff and its components at daily time step is of prime importance to hydrologists, which is required for designing the river valley projects and forecast available water which helps them in proper water resource management, flood hazards assessment, and study the impacts of climate change. The basin models which simulate snowmelt runoff generally consist of two major components called snowmelt component and transformation component which generates the liquid water from the snowpack, available for runoff in the rivers. As per WMO (1996) classification, both components may be lumped or distributed or combination of two. Lumped and distributed models are further categorized on the basis of approach used for analysis i.e. energy balance approach or temperature index approach (WMO, 1986; Debele et al., 2009) to simulate the snowmelt process. The snowmelt processes are mainly dependent on net radiation, temperature and wind velocity (Singh and Singh, 2001).

2.6 SNOWMELT COMPUTATION

The snowmelt component of snowmelt runoff simulation models usually takes the energy balance or temperature index form to simulate the process of melting. The two approaches known as energy budget or energy balance and temperature index or degree-day are described below:

2.6.1 Energy Balance Approach

Snowmelt is driven mainly by energy exchanges at the snow-air interface. The generation of melt water is governed by the energy balance or heat budget of a snowpack. An energy balance methods explicitly handles relevant processes and involves in accounting of

incoming energy, outgoing energy, and the change in the storage for a snowpack for a given period of time. Finally, the net energy is expressed as equivalent of snowmelt. The energy balance equation of the snowpack (Singh and Singh, 2001) for any time interval is given by:

$$Q_m = Q_{nr} + Q_h + Q_e + Q_p + Q_g + Q_q$$

where, Q_m = Energy available for melting of snowpack, Q_{nr} = Net radiation, Q_h = Sensible or convective heat from the air, Q_e = Latent heat evaporation, condensation or sublimation, Q_p = Heat content of rain water, Q_g = Heat gained through conduction from underground and Q_q = Change of internal energy of the snowpack.

The above equation considers the different components of energy in the form of energy flux, defined as the amount of energy received on a horizontal snow surface of unit area over unit time. The positive value of Q_m will result in production of melt from snow. The energy balance of a snow surface is significantly affected by the presence of cloud cover and vegetal cover. Moreover, due to highly complex physical processes within snowpack and involved in snowmelt, and data scarcity, especially in the Himalayan region, application of this approach is rare and restricted to small, well instrumented or experimental watersheds and resulted in development of numerous snowmelt models ranging from purely statistical techniques, which neglects the physics involved behind the snowmelt process. Among all, the conceptual models are most popular and used extensively because they are compromise between realistic complex science and realistic simple practical.

2.6.2 Degree-Day Approach

In the Himalayan region, availability of the metrological data is very poor due to scanty network. Several studies have been made by using empirical relationships between air temperature and snowmelt runoff. For the mountainous regions, the daily temperature data, surface wind speed and humidity measurements are most commonly available. Thus, temperature indices are widely used in estimation of snowmelt as it has been recognized as the best index of heat transfer processes associated with snowmelt. Air temperature expressed in terms of degree-day is used for the snowmelt computations. The simplest and most common expression which relates daily snowmelt to temperature index is given as:

$$M = D(T_{air} - T_{melt})$$

where, M = daily snowmelt (mm/day), D = degree-day factor (mm ° C^{-1} day^{-1}), T_{air} = index air temperature (°C) and T_{melt} = threshold melt temperature (usually, 0°C).

Generally, in snowmelt studies daily mean temperature is the most commonly used index of temperature. The temperature index model is a conceptual snowmelt runoff (SMR) model which mainly requires daily data of air temperature, precipitation, discharge along with the degree day factor and snow cover information as input to simulate the daily snow melt runoff. In data limited Himalayan basins, these temperature index models have been extensively used in snowmelt estimation with fair degree of accuracy (Singh et al., 1997a; Prasad et al., 2005; Thakur et al., 2009; Jain et al., 2010 a,2010b).

2.7 SNOWMELT RUNOFF MODELS

Several snowmelt models have been developed to account snow accumulation and melting processes to meet specific needs and hydrologic conditions. In general, very few models are capable of handling the varied hydrologic condition (Tekeli et al., 2005a). The snowmelt models used for forecasting are basically classified into two categories namely (1) Statistical models (2) Simulation models and are described below:

2.7.1 Statistical Models

The statistical correlation models are normally exploited for forecasting the seasonal yields. The basic method use the correlation analysis to relate the contemporary snow cover or the past precipitation, or combination thereof to the observed seasonal runoff (U.S. Army Corps of Engineers, 1956). Other variables namely baseflow, soil moisture, high elevation and low elevation water equivalent or precipitation ratios, wind and areal snow cover extent have been added to the analysis to ameliorate the results (Anderson, 1973). Statistically developed snowmelt models relate the runoff volume to snowpack and antecedent conditions and are used for long-term forecast. Though, statistical methods are widely used but yet they are not capable to represent the intricate physical interaction of the snowmelt runoff processes.

2.7.2 Simulation Models

Snowmelt runoff modeling employs both the conceptual and physical approaches for simulation. The conceptual models exploit a mathematical relationship between snowmelt and

measured quantities to compute snowmelt without considering detailed physical processes and parameters that affects the melt. These models require less informational input but suffer from uncertainty about the degree of applicability of parameters estimated under one set of model conditions to other condition. On the other hand, physical based modeling involves observation/ collection, and compilation of obligatory meteorological and snow cover information for running, calibrating and validating such models. The simulation models are the potential tools both for forecasting and a means to improve the understanding of snowmelt processes. Several studies on stream/snowmelt runoff modeling have been reported in the literature. Some of them applied specifically for the Himalayan region are reviewed in detail.

Shashi Kumar et al. (1993) implemented Snowmelt Runoff Model (SRM) to simulate discharge for two study areas i.e. Beas basin upto Thalot and Parbati river upto Pulga dam located in western Himalayan region. The digital data of Landsat MSS was analyzed using sophisticated interpretation techniques for the runoff seasons of 1986 and 1987. The areal snow cover extent was evaluated for each elevation zone. This information along with meteorological data, degree-day factor, temperature lapse rate and runoff coefficients was used as input to run the snowmelt model. Simulation studies were carried out to obtain a good fit between the simulated and actual discharges measured at Thalout and Phulga dam site by user departments.

Singh and Quick (1993) carried out a study to simulate streamflow for the Satluj river at Rampur located in the western Himalayas by using the University of British Columbia (UBC) watershed model. Daily simulation was made for the whole watershed by treating it as a single entity and by splitting into two sub-basins namely upper sub-basin and lower sub-basin. The study showed that on combining two watersheds of different hydrological behavior into a single watershed reduces simulation or forecasting accuracy. It was also reported that areal distribution of precipitation is the most crucial factor in streamflow simulation because the model exploit precipitation-elevation relationships to build up snowpack.

Singh et al. (1997a) estimated average contribution of melt runoff from snow and glacier to the annual streamflow of Chenab river at Akhnoor in western Himalayan region using a water balance approach over a period of ten years. Variability of snow covered area was also made using satellite imagery for the same period. It was observed that about 70% of the total basin area was covered with snow during the months of March/April which reduced to about 24% by September/October. The estimated average contribution of the snow and glacier melt was found to be about 49%.

Singh and Jain (2003) developed and applied a snowmelt and rainfall runoff conceptual snowmelt model for simulation of daily streamflow for Satluj river basin, a mountainous basin located in western Himalayan region. The model satisfactorily simulated daily streamflow and its components namely rainfall, snowmelt and baseflow for an independent dataset of 6 years. It was observed that most of the peaks in streamflow were generated by rainfall, but the prolonged high flows were due to melting of snow. The model was also utilized to estimate the contribution from snowmelt and rainfall to seasonal and annual flows. The analysis suggested that more than two-third of annual flow was contributed from snowmelt runoff. Seasonal distribution of streamflow indicated that about 60% annual flow was generated during summer season and about 75% of this was obtained from snowmelt.

Prasad et al. (2005) used Snowmelt Runoff Model (SRM) to estimate snowmelt runoff in Beas basin upto Pandoh dam on a 10 day average basis. The various model inputs were derived from available maps, remote sensing data and hydro-meteorological data. The snow covered area in the basin was extracted from IRS-1C/1D (WiFS). A good agreement was seen between the observed and computed runoff with monthly average deviation of +4.6% and a coefficient of determination was 0.854.

Kumar et al. (2007) estimated the average contribution of melt runoff from snow and glacier in the annual streamflow of Beas river at Pandoh, Himachal Pradesh. The total water budget for the basin using the water balance approach was computed over a period of 15 years (199-2004). A study on variability of snow covered area was also made for the same period. It was found that about 45% (2375 km^2) of the total drainage area of the basin was covered with snow during the March/April and about 15% (780 km^2) is under the perpetual snow and glacier cover. The estimated average contribution of the snow and glacier melt was found to be about 35%.

Singh et al. (2008c) carried out a study for simulation of daily streamflow for the Gangotri glacier basin lying in central Himalayas. The SNOWMOD, a snowmelt model based on temperature index approach was used to simulate streamflow for the melt period of four years (2000 to 2003). The different simulated components of the streamflow clearly indicated that nearly all high peaks were attributed to melt. It was also concluded that on the seasonal scale, the basin receives 97% of runoff from glacier melt and only 3% is generated from rainfall runoff.

Jain et al. (2010a) applied snowmelt runoff model (SRM) for estimating the streamflow for the Satluj river basin lying in the western Himalayan region. The snow cover area for the basin was extracted from NOAA-AVHRR and MODIS remote sensing satellite and area

elevation curves were prepared from SRTM-DEM. The calibrated model was used to simulate streamflow for a period of 4 years i.e. 2000-2003 and 2004-05. The well recognized criteria like shape of outflow hydrograph, efficiency and volume difference were used for verification of streamflow accuracy.

Arora et al. (2010) simulated daily streamflow of two major tributaries of river Ganga, river Bhagirathi and river Dhauli Ganga using SNOWMOD snowmelt runoff model. The results indicated that both the tributaries have significant contribution from snow and glacier melt. In the Bhagirathi river, the maximum snow/ice contribution was found to be 63.81% to 77.95% whereas rainfall and baseflow contribution were in the range of 8.14% and 23.06% and 12.73% to 13.90% respectively, of the total discharge. It was also concluded that the average contribution of streamflow components; snowmelt, rainfall runoff and baseflow were found to be 70.54%, 16.30% and 13.14% respectively for the study period (1999-2002). In the Dhauli Ganga river, the maximum snow contribution was found to be 79.23% to 80.61% whereas rainfall and baseflow components contributed in the range of 6.91% to 17.67% and 11.40% to 13.95% respectively, of the total discharge. It was also concluded that the average contribution of streamflow components; snowmelt, rainfall runoff and baseflow were found to be 77.35%, 10.35% and 12.32% respectively for the study period (1983, 1984 and 1987).

Sharma et al. (2012) carried out a study to estimate the spatio-temporal variation of snow cover during the past decade and streamflow simulation for the Jhelum river basin using Snow Melt Runoff Model (SRM). The NDSI algorithm was used to estimate the snow cover extent from the satellite imageries of MODIS sensor. The study indicated large variation in the distribution pattern of snow cover and also falling trend was also observed in different sub-basins of the Jhelum river. It was seen that a strong correlation existed between snow cover extent-temperature, snow cover extent-discharge and discharge-precipitation, analyzed for different seasons. A modified version runoff model developed for smaller watersheds was used to estimate the monthly discharge contribution from different sub-basins to the total discharge of the Jhelum river.

Panday et al., (2013) utilized Markov Chain Monte Carlo (MCMC) method for examining and evaluating the performance of SRM, a degree day conceptual snowmelt model. The model was applied in the Tamor river basin lying in eastern part of Nepal Himalaya for simulating the daily streamflow during the hydrological years from 2002 to 2006. The SRM model coupled with the MCMC method presented better fit to observed flows, nevertheless failed to capture peak discharge during summer monsoon months. It was found that the estimated average snowmelt contribution to the total runoff was 29.7±2.9%, which comprised

4.2±0.9% from snowfall that promptly melts while rainfall contribution was found to be 70.3±2.6% in the basin.

Agarwal et al. (2014) estimated snowmelt runoff for the sub-basin of Ganga river; Alaknanda and Bhagirathi river basins upto Joshimath and Uttarkashi respectively using SRM snowmelt runoff model. The information on snow cover area was extracted from satellite imageries of MODIS, Landsat and AWiFS for Bhagirathi basin and IRS-P6 of Resourcesat-1 and Landsat (ETM+) for Alaknanda basin. It was observed that the maximum discharge occurred during the monsoon season (in July and August) and decreases in winter from October to February for the study period. In Bhagirathi basin it was found that the measurement runoff and computed runoff were about 3602.69 (10^6 m^3) and 3533.21(10^6 m^3) respectively and average runoff and average computed runoff were 114.20 m^3 and 112.0 m^3/s respectively for the study period (2002-2007). Also, overall snowmelt simulation for the Alaknanda basin for the study years 2000 and 2008 was found good.

Li et al. (2014) carried out a study to estimate the runoff and its components for two Himalayan basins namely the Wang Chhu basin and the Beas river basin located in Bhutan and India respectively. The Hydrologiska Byråns Vattenbalansavdelning (HBV) model was used to identify the runoff proportion from four components i.e. glacier melt, snow melt on glacier, snow melt outside glacier and rainfall. The results indicated that rainfall is the largest contributor to runoff in the Wang Chhu basin, whereas snow and glacier melt is manifestly dominant in Beas river basin.

2.8 TREND ANALYSIS

Water resources systems are designed and operated on the basis of assumption of stationary hydrology, if these assumptions are erroneous then existing procedures for design needs to be amended. The changes in temperature, precipitation, and other climatic variables are likely to influence the amount and distribution of runoff in all river systems globally. The detection of trends in hydro-climatic data, particularly temperature, precipitation, and streamflow is essential for assessment of impacts of climatic variability and its change on the water resources of a region. Trend analysis may thus focus on the overall pattern of change over time, help temporal and spatial comparisons for deriving future projections. Estimates of temperature anomaly were better estimated using long-term series data. Several statistical methods apply parametric and non-parametric approach for the detection of trends. Mainly four

stages are involved in the trend analysis; collection and preparation of suitable database, exploratory analysis of data, application of statistical tests, and interpretation of results.

Himalayan region aptly called the water tower of Asia is greatly to be affected due to change in climatic conditions and impact the streamflow of snow-fed rivers originating from the region. The Himalayan region, including the Tibetan Plateau, has shown consistent trends in overall warming during the past 100 years (Yao et al. 2007). Various studies suggest that warming in the Himalayas has been much greater than the global average of 0.74°C over the last 100 years (IPCC, 2007). Long-term trends in the maximum, minimum and mean temperatures over the north western Himalaya during the 20th century (Bhutiyani et al., 2007) suggest a significant rise in air temperature in the north western Himalaya, with winter warming occurring at a faster rate. Global warming has resulted in large-scale retreat of glaciers throughout the world. This has led to most glaciers in the mountainous regions such as the Himalayas to recede during the last century and influence runoff of Himalayan rivers. The climatic change/variability in recent decades has made considerable impacts on the glacier life cycle in the Himalayan region. Several studies have been carried out to investigate the changes in temperature and rainfall series and its association with climate change. Some of the important studies carried out for the Himalayas are reviewed and discussed here in brief.

Mirza et al. (1998) analyzed the trends and persistence in precipitation in the Ganges, the Brahmaputra and the Meghna river basins. Time series of annual precipitation of 16 meteorological sub-divisions covering these basins were examined for trends using Mann-Kendall rank statistic, student's t-Test and regression analysis, and first order autocorrelation analysis was used for persistence. The results indicated that precipitation was by-and-large stable in Ganga basin while sub-divisions of both Brahmaputra and Meghna basin had either increasing or decreasing trend. It was also concluded that persistence was not present in precipitation series of Ganga basin but existed in 2 common sub-divisions in Brahmaputra and Meghna basin.

Shrestha et al. (1999) analyzed the maximum temperature data of 49 stations in Nepal for the period (1971-1994). The results indicated warming trends after year 1977 ranging from 0.06 to 0.12^0C/year in most of the Middle mountain and the Himalayan regions whereas the Siwalik and Terai, southern plains regions showed warming trends less than 0.03^0C/year. It was observed from the distribution of seasonal and annual temperature trends that high rates of warming existed in regions at higher elevations (Middle Mountains and the Himalaya), whereas low warming or even cooling trends found in the southern region.

Fu et al., (2004) applied the Kendall's test to examine the hydro-climatic trends in the Yellow river watershed during the last half century. It was observed that watershed had become warmer with more significant rise in minimum temperature than maximum and mean temperatures. The change in precipitation trend was not found significant and the basin runoff depicted falling trend. These results were attributed mainly to the human activities, global warming, and changes in landuse/landcover along with other constraints such as accuracy in estimation of natural runoff, snowmelt, water transfer, ground water exploitation and precipitation characteristics. The homogeneity analysis showed that precipitation, maximum and minimum temperature were all heterogeneous and the trends varied both monthly and regionally.

Bhutiyani et al. (2007) carried out a study to examine the trends in long-term instrumental air temperature data across the northwestern Himalayas during the last century. The study reported significant increase in air temperature by about 1.6^0C with winters warming at a faster in the twentieth century in the study region. It was concluded that the increasing significant trends in the diurnal temperature attributed to rise in both maximum and minimum temperatures, with maximum temperature increasing much more rapidly.

Basistha et al. (2009) carried out a study to investigate changes in the rainfall pattern during twentieth century in the Indian Himalayas. The statistical tests were applied to detect trend and possible shift in rainfall using 80 years of data from 30 stations. The study suggested that 1964 was found to be the most probable year of change in monsoon and annual rainfall in the region. It was concluded that there was an increasing trend upto 1964 after which trend decreased during 1965-1980 for this region and changes were most explicit over the shivaliks and southern part of Lesser Himalayas.

Rai et al. (2010) statistical test were used to investigate the persistence, trend and periodicity in hydro-climatic variables in Yamuna river basin. The results indicated significant difference in the patterns of monsoon and non-monsoon rainfall in terms of persistence and periodicity and about 20% of rainfall time series indicated the presence of persistence. The study concluded that overall declining trend was examined in the annual and monsoon rainfall, annual and monsoon rainy days and aridity index along with a rising trend in onset of effective monsoon.

Kumar et al. (2010) analyzed rainfall and rainy days time series at five stations i.e Srinagar, Kulgam, Handwara, Quazigund and Kukarnag in Kashmir valley to decipher rainfall trends at seasonal and annual time scale. It was revealed that the during the year 1903-1982, annual rainfall showed decreasing trend at three stations (Srinagar, Kulgam, Handwara) and all

three stations showed a decreasing trend in monsoon and winter and increasing trend in pre-monsoon and post-monsoon rainfall. It was also seen that all the stations experienced a decreasing trend in monsoon and winter rainy days. Other two stations experienced decreasing trend in annual rainfall during the period 1962-2002.

Xu et al. (2010) applied Mann–Kendall (non-parametric) test to detect the trends in main hydro-climatic variables in the Tarim River basin, China for a period of 1960-2007. The results indicated that both mean annual air temperature and precipitation experienced rising trend. The annual streamflow showed a mixed trend of increasing and decreasing. Moreover, it was found that the mountain region upstream illustrated a rising trend while region downstream showed a falling trend.

Khattak et al. (2011) examined trends in various hydro-meteorological variables based on non parametric tests in the upper Indus river basin (UIRB) in Pakistan. The results indicated increased trend in winter maximum temperature for the upper, middle and lower region with the slopes of 1.79, 1.66 and 1.20 ^{0}C per 39 year, respectively. It was concluded that increased winter temperatures would possibly increase streamflow during winter and spring whereas flow will decrease during summer months.

Jain et al. (2012b) analyzed the trends in rainfall and temperature data series in northeast India for the period (1871-2008) at monthly, seasonal and annual time scale. It was examined that rainfall series at regional scale had no clear trend, although trends for some seasonal and hydro-meteorological sub-divisions existed. The temperature variables namely maximum, minimum and mean temperatures showed increasing trend and Sen's estimator of slope for the minimum, maximum and mean temperature was found to be 0.011(°C/year), 0.019(°C/year), and 0.015(°C/year) respectively.

Choudhury et al. (2012) analyzed the long term data (1983-2010) to detect trend in the weather variables using non-parametric tests in Umiam located at mid altitude in Meghalaya. The results of the study indicated that there was non-significant increasing trend (3.72 mm/yr) in the total annual rainfall and maximum temperature depicted a linear increasing trend (0.086 ^{0}C/year) whereas minimum temperature showed non-significant decreasing trend (-0.011^{0}C/year). A significant increasing trend (0.031^{0}C/year) was also observed in the mean temperature over the period.

Mishra et al. (2013) identified trends in climatic variables using non-parametric methods in the Kaligandaki river basin located in Nepal Himalaya. It was revealed from the spatial distribution of temperature trend that there were greater warming trends at higher altitudes. The increasing trends in temperature (approx. by 0.03 to 0.08^{0}C/year) were found in

different seasons whereas seasonal precipitation showed mixed trends in the study basin. It was seen that with the increasing trends in winter and spring temperature and decreasing trends in precipitation, a clear significant negative trend in SCA was identified during these seasons. The results indicated potential effect of global warming on the climatic variables, precipitation and snow cover area in higher mountainous region.

Kattel and Yao (2013) carried out a study to examine the recent trends at 13 mountain stations on the southern slope of the central Himalayas. The analysis was carried for temperature variables namely annual maximum, minimum and average temperature for a period of three decade (1980 to 2009) for the stations located between elevation range of 1304 and 2566 m amsl. From the spatial analysis of average temperature, it was found that most of the stations showed warming trends. It was observed that maximum temperatures had higher warming magnitude while the minimum temperatures showed larger variability. The temporal variations indicated a dramatic increase in temperature during the latest decade, especially in the average and maximum temperatures.

2.9 CLIMATE CHANGE

Climate has changed considerably throughout the history of the earth due to change in its forcing components, whether natural or anthropogenic. Potential climate change impacts on hydrology pose a threat to water resources systems throughout the world. One of the most important and immediate effects of global warming would be the changes in local and regional water availability, since the climate system is interactive with the hydrologic cycle. This global warming is likely to have significant impacts on the hydrologic cycle, affecting water resources systems (IPCC, 2001, 2007; Wurbs et al., 2005; Kavvas et al., 2006). Predicted changes in climate regime, and paradigm shift in temperature, rainfall and other atmospheric variables may have an impact on the availability of fresh water resources, frequency of extreme weather events (floods, droughts, cyclones), agriculture yield, functioning of ecosystems, melting of glaciers, sea level rise etc.

In order to provide an indication of the extent of impacts of climatic change on water resources, streamflow represents an integrated response to hydrologic inputs on the drainage basin. Generally, in order to evaluate the impact of climate change on streamflow two approaches are most widely used firstly, hypothetical plausible scenarios and secondly, scenarios based on the projected output from GCMs or RCMs. Several studies have been

reported in the literature on climate change and some specific to Himalayan region are discussed here.

Sharma et al. (2000) conducted a study for the Koshi river basin in central Himalayas to analyze the hydrologic sensitivity of the basin to potential climate change scenarios using distributed deterministic modeling approach. It was found that the runoff increase was higher than precipitation increase in all possible precipitation change scenarios applying contemporary temperature. Moreover, runoff decreased by 2 to 8% with the scenario of contemporary precipitation and 4 ^{0}C rise in temperature.

Singh and Bengtsson (2004) carried out a study using SNOWMOD, a conceptual hydrological model to assess the impact of climate change on the sensitivity of water availability in the Satluj river basin (western Himalayas) using hypothetical scenarios. It was observed that the impact of climate change was more on the seasonal water availability as compared to the annual.

Singh and Bengtsson (2005) investigated the impact of climatic warming on the melt and evaporation for the rain-fed, snow-fed and glacier-fed river basins in the Himalayan region. Based on the future projected hypothetical climatic scenarios in the study area, three temperature rise scenarios (by 1^{0}C, 2 ^{0}C and 3^{0}C) were used to quantify the effect of warmer climate. It was found that the melt reduced from snow-fed basins under the warmer climate, whereas it increased from glacier-fed basins.

Singh et al. (2006) carried out a study to investigate the impact of climate change on runoff of a glacierized small basin in the Himalayas. The SNOWMOD model was used to simulate the melt runoff and to assess the impact of climate change under the possible scenarios of rainfall and temperature, both individually as well as in combination on the monthly runoff distribution and total runoff for the summer season. The analysis incorporated six temperature scenarios (0.5 to 3^{0}C) and four rainfall scenarios (−10%, −5%, 5%, 10%). It was revealed that runoff increased linearly with increase in temperature and rainfall. It was also observed that the changes in runoff were more sensitive to temperature changes as compared to rainfall.

Arora et al. (2008) simulated the daily runoff for the Chenab river basin upto Salal gauging site using a simple conceptual snowmelt model to study the possible hypothetical scenarios of temperature and rainfall on the melt characteristics and daily runoff. The average value of increase in snowmelt runoff obtained were 10, 28, and 43% for the T+1 ^{0}C, T+2 ^{0}C and T+3 ^{0}C scenarios respectively. Whereas the average value of increase in total streamflow runoff were found to be 7, 19 and 28% for the T+1 ^{0}C, T+2 ^{0}C and T+3 ^{0}C scenarios respectively.

Jain et al. (2010b) carried out a study to investigate the of climate change on the streamflow for the Satluj river basin located in the western Himalayas based on three temperature projected hypothetical climatic scenarios (T+1, T+2, T+3°C). It was revealed that with the increase in temperature there was not much change in total flow, however change in the distribution of streamflow was noticed. It was concluded that more snowmelt runoff occurred earlier because of increased melting of snow, with reduced runoff during monsoon months.

Gain et al. (2011) carried out a study to investigate the impact of climate change on the low and high flows of lower Brahmaputra river basin (LBRB) for the A1B and A2 emission scenarios. Weighted discharge time series were used for the future trends in average flow and extreme flow for the period 1961-2100. It was observed that extreme low flow conditions are probable to occur less frequent and very strong increase in peak flows in the future. The study concludes that the A1B and A2 scenario projects the strongest increase in low flow and high flow respectively.

Neupane et al. (2013) used Soil and Water Assessment Tool (SWAT) to estimate the impacts of climate change on the hydrologic processes of the Kali Gandaki watershed located in central Himalaya, based on projected changes in climatic conditions. The model used modified weather inputs like average, minimum and maximum temperature, and precipitation changes for SRES B1, A1B and A2 for 2080s. The mean annual streamflow was found to be about 39% higher than the current values for maximum temperature and precipitation changes of A2 scenario and 22% less for the minimum changes of same scenario. Also, it was also observed that the projected snowfall and snowmelt were lesser than current average by about be 30% and 29% respectively.

Kulkarni et al. (2013) applied PRECIS model to examine the potential impact of global warming over the three sub-regions; the western, central, and eastern Himalaya of Hindu Kush–Himalayan (HKH) region. The 3 PRECIS simulations were carried out for IPCC A1B emission scenario for continues period 1961 to 2098 for monsoon season (June-September). The climate projections were examined over the short (2011–2040), medium (2041–2070), and long term (2071–2098). The study indicated that significant warming will occur towards the end of 21st century all over the HKH region. It was concluded that precipitation in summer monsoon is likely to be higher by 20-40% in 2071–2098 than baseline period (1961–1990).

Rajbhandari et al. (2014) carried out a study to assess the impact of climate change over the Indus river basin using high resolution regional climate model (PRECIS). The study analyzed IPCC SRES A1B scenario over 3 time slices i.e. near future (2011-2040), middle of

21st century (2041-2070) and distant future (2071-2098). The study suggests that overall there is non-uniform change in precipitation, with an increased precipitation in upper Indus basin and decreased in lower Indus basin with little change in the border areas. The projection results also indicated greater warming in the upper Indus basin than lower Indus basin and greater warming during winter than in other season.

Bharti et al. (2014) carried out a study to assess the impact of climate change on water resources development using SWAT model for the Koshi River basin located in Nepal. The projections were generated for the 2030s and 2050s under the IPCC's A2 and B1scenarios. It results indicated that impacts are likely to be scale dependent because little impacts were projected for annual and full-basin scales. But at sub-basin scale, it was found that projected precipitation increased under both scenarios in 2030s in the upper transmountain sub-watersheds and most of the basin in 2050s while decreased in 2030s in lower sub-basins. Flow volumes were projected to increase during monsoon and post-monsoon and decrease during winter and pre-monsoon seasons.

2.10 SUMMARY

In this chapter review of the studies carried out by different investigators in the past for estimation of snow cover area, temperature lapse rate, streamflow modeling, climatic variability and its impact on the streamflow has been presented. From the review it is seen that one of the major inputs required for snowmelt runoff modeling is lapse rate, which has not been given due weightage in earlier studies. Most of the studies have taken lapse rate as constant and only a few studies have considered the variation of lapse rate. Therefore, it is better to take into consideration the true representation of seasonal and topographic variations in lapse rate for obtaining precise estimate of streamflow.

Another important aspect in snowmelt runoff modeling is generation of snow cover depletion curves (SDCs). For this purpose, snow cover area at closer intervals is required for better assessment of SDC. Therefore use of number of satellite data is required for assessment of SDC. Keeping this in view, the research was taken up for Beas basin for estimation of streamflow which may used for various purposes including hydropower, irrigation and drinking etc. over different periods and seasons under continual changing environment.

Chapter 3

STUDY AREA AND DATA AVAILABILITY

3.1 INTRODUCTION

The country has been divided into 7 zones and 26 hydro-meteorologically homogeneous subzones out of which the hydro-meteorological subzone 7 is designated as western Himalayas subzone. The major Indus river systems and its five major rivers namely Jhelum, Chenab, Ravi, Beas and Sutluj emanates from the western Himalayan region covering the hilly terrain of Jammu & Kashmir and Himachal Pradesh. These rivers and their tributaries are snow-fed and rain-fed during summer and through groundwater in winter season and carries bountiful discharge throughout the year flowing through steep bed slopes, which can be harnessed for hydropower generation. To meet out the objectives of the research work, the Beas basin upto Pandoh dam has been selected as the study area. This study area was chosen for several reasons: Firstly, ease and safety of access which helped us for frequent ground truth verification, collection and availability of good data network in the basin, and secondly, to harness potential of Beas river for hydropower and irrigation purposes. Moreover, global warming and potential climate change, have further added another dimension of complexity on the hydrological regime of the snow-fed Beas river which needs to be timely addressed. Further, very limited studies have been carried out earlier to assess the impact of climate change on the streamflow and its components for Beas basin. The chapter presents the description of the Beas river basin and details of wide range of hydro-meteorological and satellite data incorporated in the study.

3.2 THE STUDY AREA

The Beas river is a primary river tributary of Satluj river in the Indus river system. The river originates from the foot of a small glacier Beas Kund at an elevation of 4085 m above mean sea level lying on southern slopes of massive Pir Panjhal range of Rohtang Pass in Kullu district of Himachal Pradesh. It flows almost in north-south direction upto Larji, from where it turns nearly at right angle and flows towards west upto Pandoh dam. The average bed slope above Larji is of order of about 30 m/km while the river slope decreases sharply and near the

Pong dam site, it is of the order of 1.89 m/ km. The length of the river upto the Pandoh dam is 116 km. The catchment of the Beas basin upto Pandoh dam is 5384.9 km^2, out of which 780 km^2 is under permanent snow. The average annual rainfall in the catchment is about 1800 mm. The altitude varies from 832 m near Pandoh to more than 5000 m near Beo-Toibba. Some of the major tributaries which join the Beas river upstream of Pandoh dam are: Parvati river near Bhuntar, Tirthan and Sainj rivers near Larji, Sabari nala near Kulu and Bakhli khad near Pandoh dam.

All these rivers are perennial and the flow varies considerably during different months of the year. A major portion of the catchment lies under degraded forests and cultivated land and therefore, the proportion of the silt and sand are of fine, medium and coarse configuration. Steep slopes are very common but are terraced at several places in the lower ranges upto an elevation of 1982 m for agricultural purposes. In certain reaches, thick forests exist mostly between elevations of 1830 m to 2744 m. A map showing the Beas basin upto Pandoh dam is given in Figure 3.1.

In year 1960, Indus water treaty was signed between India and Pakistan after which India came to possess exclusive share of water of three eastern rivers i.e. Satluj, Beas and Ravi. Bhakra Beas Management Board (BBMB) earlier Bhakra Management Board was formed under a master plan for harnessing and utilization of water of these rivers for irrigation, flood control and power generation. In order to meet these objectives, dams were constructed over the rivers. On river Beas two units comprising namely Beas-Satluj Link (Unit-I) and Beas Dam at Pong (Unit-II) were taken up for consistent and effective use of the flow of river Beas for irrigation supplies, flood control and for generating hydropower for the States of northern India. Beas-Satluj Link project basically meant for power generation. The main purpose of Pandoh dam on Beas river is to divert the Beas river water to Satluj river for generating power at Dehar power house. The reservoir of the dam extends about 9.25 km upstream of dam and has the gross storage capacity of 4100 hectare-meter.

3.3 CLIMATIC CONDITIONS AND VARIATIONS IN STUDY AREA

The altitude and aspect are the two crucial factors governing the weather and climate in the Himalayan region. Firstly, variation in altitude not only varies the climate, from hot and moist tropical in lower valleys to cool temperate at about 2000 m and towards Polar beyond 2000 m but also controls the climatic variables temperature and rainfall. Secondly, the aspect

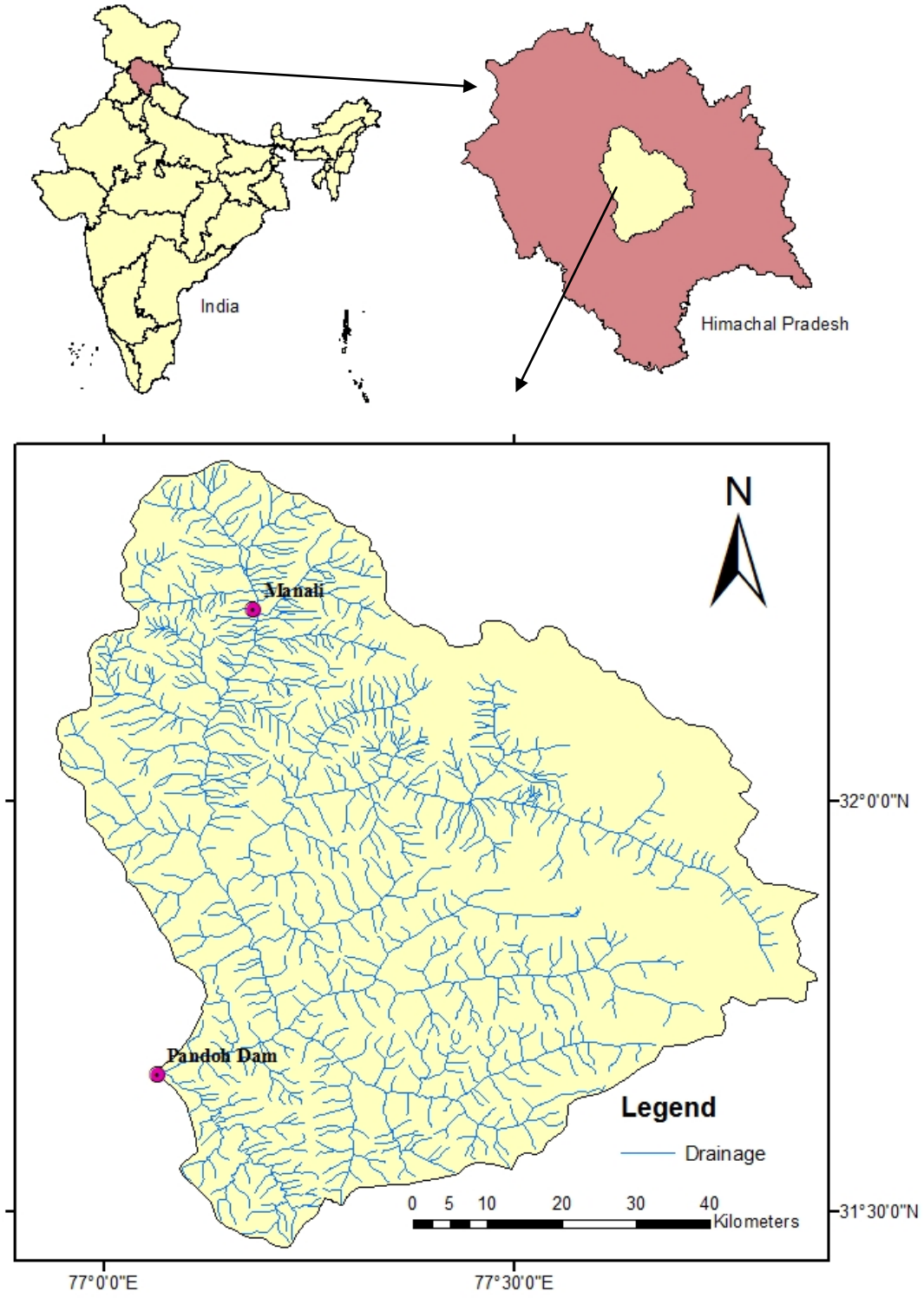

Figure 3.1: Location map of the Beas basin up to Pandoh Dam

has strong influence on temperature, as it affects the angle of sun rays. Usually in Northern Hemisphere south facing slopes are more exposed to sunlight and warm winds, and thus, these slopes in Himalayas are more sunny, warmer, wetter and forested, and also receive more rainfall whereas it is cold, dry and glaciated heavily in north facing slopes. The basin lies in the windward side of the middle Himalayas and hence receives heavy rainfall during the monsoon season due to moisture-bearing winds arriving from both Arabian Sea and Bay of Bengal. The study area enjoys the cold and dry climate and depending on the broad climatic conditions, four seasons viz., pre-monsoon (March-May), monsoon (June-September), post-monsoon (October-November) and winter (December-February) prevail over the basin. Though rainy months are spread from mid June to mid September, highest rain occurs in the month of July-August whereas lowest during October-January. A good amount of snowfall usually occurs in this region from December to February at an elevation above 2000 m and most of the parts of the Kullu remain under cover of snow.

Singh and Kumar (1997a) examined rainfall distribution in the Beas basin and found a distinct pattern of rainfall distribution for the outer and middle ranges of Himalayas, as given in Table 3.1. The table clearly indicates that higher rainfall occurs during the monsoon season than the other seasons in the basin.

Table 3.1: Average rainfall distribution in the Beas basin

Himalayan Range	Aspect	Rainfall (mm)				
		Winter	Pre Monsoon	Monsoon	Post Monsoon	Annual
Outer	Leeward (North)	179 (12.8%)	148 (10.6%)	985 (70.6%)	83 (5.9%)	1395
Middle	Windward (South)	317 (14.5%)	292 (13.3%)	1459 (66.6%)	122 (5.6%)	2190
	Leeward (North)	327 (31.1%)	210 (19.9%)	413 (39.2%)	102 (9.7%)	1052

3.4 GEOLOGY AND SOIL

The Beas river bed consists of large boulders and the geology of the catchment above Pandoh dam mainly comprises of alluvium, glacial deposits quartzite, sandstone and granites. In general, the soils vary from very shallow to moderately deep and very deep, yellowish brown to dark brown in colour. The texture of soil varies from sandy loam to silty clay loam

and clay. The texture of soil aid in providing useful information about the characteristics of soil which is directly or indirectly related to the growth of plants in the region. Moreover, relationship between soil texture and soil hydraulic parameters confers soil parameters for watershed hydrological models (McCuen, 1981) and information on antecedent soil moisture conditions are of great importance for event based rainfall-runoff modeling (Sahu et al., 2007). Both calcareous and non-calcareous soils are found in the basin. Various researchers have mapped the geology of Beas basin (Fuchs and Gupta, 1971; Chaku, 1972; Frank et al., 1973). The distribution of various major rock types in the Beas basin includes quartzites, gneisses, granites, schists, slates, marbles and metasediments and their distribution is given in Table 3.2 (Gupta et al., 1982).

Table 3.2: Distribution of major rock types in Beas basin at sub-catchment scale

Sub catchments	Area (km^2)	Generalised geographic elongation of the sub catchment	Major rock types
Manali	356.7	NNW-SSE	granite and metasediments
Sainj	746.9	E-W	granite, metasediments, and quartzites
Parvati	1742.4	S-E-NW TO NE-SW	granite, metasediments, and quartzites
Bhunter	3074.4	N-S TO E-W	granite, metasediments,, quartzites, limestones, slates and phyllites
Pandoh	5711.0	NNW-SSE	metasediments,granites, quartzites, limestones, slates and phyllites

3.5 HYDROPOWER POTENTIAL

The five major perennial rivers namely Chenab, Ravi, Satluj, Beas and Yamuna emanate from the western Himalayas and flow through the Himachal Pradesh and bless the State with significant hydropower potential. The bulk of potential available in Himachal

Pradesh of different river basins is at 20634 MW. The basin wise details of hydro-electric power generation in Himachal Pradesh are given in Table 3.3 (Slariya, 2013).

Table 3.3: Details of hydro-electric power in Himachal Pradesh

Basin	Currently operational	Under Execution	TEFR Ready	TEFR not Ready	Survey completed	Total
Yamuna	211.52	110	231	0	39	591.52
Satluj	3150.25	1280.5	1402	2227	1360.5	9420.25
Beas	1634.5	1330	736	856.5	25	4582
Ravi	1043.5	0	642.5	348	260	2294
Chenab	5.3	0	0	240	2503	2748.3
Total	6045.07	2720.5	3011.5	3671.5	4187.5	19636.07

It is discernible from Table 3.3 that out of the total estimated hydropower in the State, about 48% (nearly half) has been identified alone in the Satluj river basin. The Beas river basin ranks second in hydropower potential with more than 22% and more than 11% in Ravi and Chenab river basin. The largest 990 MW, Dehar hydro-electric power plant managed by Bhakra Beas Management Board (BBMB) receives water from Pandoh dam. The Larji hydropower project upstream of Pandoh dam has the installed capacity of 126 MW. Besides these, Allain Duhangan hydropower project (192 MW) and Malana hydropower project (86 MW) are among the private developers harnessing the hydropower of this area. The main upcoming hydropower projects in the basin are Sainj, Parbati-I, Parbati-II and Parbati-III.

3.6 STREAMFLOW CHARACTERISTICS OF RIVER BEAS AT PANDOH

Streamflow of river Beas consists of two components: one contributed from snow and glacier melt and another resulting from the rainfall over the basin. Generally, contribution from snowmelt starts from March and lasts till June/July depending on the accumulated snow pack water equivalent and prevailing temperature. The contribution from snowmelt increases continuously and exceeds the rainfall component as the summer season advances. Consequently, a major part of streamflow is generated during the pre-monsoon season from seasonal snow. During the monsoon season, rainfall component dominates and produces higher discharges and augment the river flow. Generally, higher discharges or floods are pronounced in the months of July and August, factually due to heavy rainfall in the lower reaches of the

basin. Normally, ablation of the seasonal snow which accumulates on the glaciers during the winter season begins at the end of May/June, and thereafter, glaciers start contributing to streamflow. They contribute to their utmost in the month of July and August. The melt runoff contribution from glaciers lasts till September/October. During the post-monsoon season, streamflow is presumed to be partly from the glaciers and occasional rainfall events. Minimum streamflow is observed during winter season because no melting occurs due to low temperature regime. The baseflow contribution during this period sustains the river flow and makes the mountainous rivers perennial.

3.7 AVAILABILITY OF DATA

Climatologically, the present study area falls in the lower Himalayan zone lying in the State of Himachal Pradesh in western Himalayas. As the streamflow of the river have contribution from rainfall as well as from snow and glacier melt, data on hydro-meteorology and areal extent of snow cover is essential for modeling. For the present research study, the hydro-meteorological and remote sensing dataset used is collected from two sources. The ground observed hydro-meteorological data is collected from the office of Bhakra Beas Management Board (BBMB), Pandoh during the field visit whereas the remote sensing data is either downloaded from internet or procured depending upon the access of satellite product.

3.8 REMOTE SENSING SATELLITE DATA

Mapping the earth's resources is a major challenge both technically and scientifically (Gupta et al., 2002, Srivastava et al., 2003). Among them water is an important and essential resource for the survival of humans and their well being. Timely and consistent information of water resources, especially in the Himalayan regions receiving substantial contribution from melting of snow/ice, glaciers and permafrost is crucial for optimal planning and utilization. This melt runoff generates numerous streams that nourishes the river and makes them perennial (Krishna, 2014). However, in the mountainous areas, due to the intricate rugged terrain, heterogeneous ground properties, and inaccessibility, snow cover estimation is a challenging mission. Use of satellite remote sensing is the only efficient way for monitoring the dynamically changing snow cover area at sufficiently large scale (Rango, 1996) and the land surface temperatures. Snow Cover Area (SCA) and Temperature Lapse Rate (TLR) are two

important input parameters for the hydrological modeling of snowmelt runoff estimation, flood forecasting, climate change studies etc. The information on these two parameters can be derived from the remotely sensed data of different satellites.

According to Hall and Martinec (1985), for a particular analysis, judicious selection of proper sensor taking into consideration factor like wavelengths, spatial and temporal resolution or frequency and timing of ground converge plays an important role. The remote sensing technique offers important advantages such as areal measurements, good spatial and temporal resolution, data availability in numerical formats and in less accessible regions. One of the great advantages of remote sensing data is its ability to provide areal information instead of point data which had rapidly increased its role in the field of snow hydrology. Even though a variety of remotely sensed devices are available, the greatest applications have been found in Visible (VIS) and Near Infrared (NIR) region of electromagnetic spectrum (Hall et al., 2002a). The main advantage of this is easy availability, interpretation and relatively easy distinguishing snow from snow-free area.

As snow forms an integral part of hydrological modeling in the Himalayan basins, its spatial coverage or extent i.e. Snow Cover Area (SCA) together with physical properties are very significant input parameters for simulation and estimation of snowmelt contribution in the river flow. Snow cover is important at all spatial scales (Rees, 2006). It represents an important geophysical variable for climate as it plays an important role in controlling the Earth's albedo (Wiscombe and Warren, 1980; Nolin and Stroeve, 1997) and in hydrology (Ross and Walsh, 1986; Barnett et al., 1989).

Previously, conventional methods of snow surveys based on manual ground measurements were used for snow cover information. These methods had limitations in monitoring of SCA in intricate climatic conditions of Himalayas due to inaccessibility, sparse location of ground stations and rugged terrains. Thus, snow monitoring, snow mapping, its estimation and analysis for snowmelt runoff is time consuming, for it is a convoluted process.

With the advancement in technology, manual measurement of snow cover is being replaced by the automatic weather stations. Now days, remote sensing is a popular tool for acquiring information about objects from measurements made at a distance without any physical contact with the objects. This tool is supplementing the ground based measurement techniques of snow cover area. However, ground information is very valuable and decisive in calibration and verification of other remotely sensed data available now a days. The main advantage of these satellite data is that they are continuous, cost effective and allow us to

monitor snow cover with high spatial coverage and repetition time even in the harsh, rugged and inaccessible areas.

The distribution of snow cover is a major function of topography and the climatic conditions prevailing in a craggy terrain. Digital Elevation Model (DEM) models being a function of geographic location are useful to model the elevation of terrain and provide the basic niceties essential to characterize the topographic features of a terrain. They are also used for automatic delineation of basins, channel network, land slope, average slope of stream segments etc. Thus, it becomes very important to derive the proper information of the terrain of the area as it is broadly used to understand the distribution pattern of snow with respect to change in topographic features. Presently, numbers of several techniques are available to generate DEMs which includes GPS, aerial photogrammetry and spaceborne technology etc. (Snehmani et al., 2013b). DEMs can be created at different spatial scales depending upon a specific application (Gupta et al., 2014).

In the present study, snow cover area, digital elevation model, land surface temperature information has been derived from the satellite data. For SCA estimation satellite data of Aqua/Terra MODIS, IRS-1C/1D-WiFS and AWiFS have been used. The data of two sets from Shuttle Radar Topographic Mission (SRTM) of 90 m spatial resolution and GTOPO30 with 1000 m spatial resolution were used for DEM, discussed earlier in section 3.9.3.

3.9 SATELLITE IMAGERIES AND DATA PRODUCTS

3.9.1 IRS-1C/1D and IRS-P6

Following successful launch of experimental satellites Bhaskara-1 and Bhaskara-2 in June 1979 and November 1981 respectively, the golden era of India's space exploration began with the launch of first indigenous and civilian Indian Remote Sensing Satellite, IRS-1A on 17 March, 1988 which laid a successful milestone in the Indian space programme and an IRS programme was commissioned. Currently, there are eleven satellites available in the IRS series to provide satellite data in varied spectral, spatial and temporal resolutions. The second generation IRS series IRS-1C and 1D with a mission to provide enhanced sensor and coverage features were launched on 28 December, 1995 and 29 September, 1997 respectively. Both of these satellites weighed 1250 kg and have onboard recorders to collect data. Both satellites carried three payloads namely Panchromatic Camera (PAN), Linear Imaging Self Scanner (LISS-3) and Wide Field Sensor (WiFS) with a spatial resolution of 5.8 m, 23.5 m and 70.5 m.

In continuation of IRS series, ISRO successfully launched its tenth satellite named as Resourcesat-1 or IRS-P6 on 17 October, 2013 from Bangalore onboard Indian PSLV-C5. This advanced version polar Sun synchronous orbit carries three payloads namely a Linear Imaging Self Scanner LISS-3, LISS-4 and AWiFS. The LISS-4, a high resolution sensor operates with spatial resolution of 5.8 m in three bands in the visible and near infrared bands of the spectrum and achieves five day revisit capability whereas the LISS-3, a medium resolution sensor with a spatial resolution of 23.5 m operates in three spectral bands in VNIR and one in SWIR band with 142 km swath. The data from high resolution sensor are valuable for urban planning and mapping application while medium resolution data is of great importance for vegetation discrimination, land mapping, and management of natural resources. The key parameters of IRS -1C/1D and IRS-P6 satellites are given in Table 3.4. Seventeen cloud free data of IRS-1C/1D and IRS-P6 were procured from National Remote Sensing Centre (NRSC), Hyderabad, India for the present study. The details of satellite data are provided in Table 3.5.

Table 3.4: Key parameters of IRS-1C/1D and IRS-P6 satellites

Parameter	IRS-1C/1D				IRS-P6/Resourcesat-1			
	Pan	Band	LISS-III	WiFs	Mono Mode	MX Mode	LISS-III	AWiFS
Spatial Resolution	5.8	Band 2 (Green)	23 m	-	-	5.8 m	23.5 m	56 m
		Band 3 (Red)	23 m	188 m	5.8 m	5.8 m	23.5 m	56 m
		Band 4 (NIR)	23 m	188 m	-	5.8 m	23.5 m	56 m
		Band 5 (SWIR)	70 m	-	-	-	23.5 m	56 m
Spectral Coverage	0.50-0.75 µm	Band 2 (Green)	0.52-0.59 µm	-	-	0.52-0.59 µm	0.52-0.59 µm	0.52-0.59 µm
		Band 3 (Red)	0.62-0.68 µm	0.62-0.68 µm	0.62-0.68 µm	0.62-0.68 µm	0.62-0.68 µm	0.62-0.68 µm
		Band 4 (NIR)	0.77-0.86 µm	0.77-0.86 µm	-	0.77-0.86 µm	0.77-0.86 µm	0.77-0.86 µm
		Band 5 (SWIR)	1.55-1.70 µm	-	-	-	1.55-1.70 µm	1.55-1.70 µm
Radiometric resolution	6 bit	all bands	7 bit	7 bit	7 bit	7 bit	7 bit	10 bit
Swath	70 km	all bands	142 km	810 km	70 km	23.9 km	140 km	740 km

(Source: Euromap, 2013)

Table 3.5: Details of satellite data used in the study

Year	Date	Satellite/Sensor	Path/Row
2000	29 March	IRS-WiFS	94/47
	02 October	IRS-WiFS	93/47
	18 December	IRS-WiFS	94/47
2001	04 February	IRS-WiFS	94/97
	28 February	IRS-WiFS	94/47
	11 May	IRS-WiFS	94/47
	31 October	IRS-WiFS	95/47
	14 November	IRS-WiFS	93/47
	23 December	IRS-WiFS	96/48
2002	30 January	IRS-WiFS	94/47
	18 February	IRS-WiFS	93/47
	11 May	IRS-WiFS	95/47
	27 September	IRS-WiFS	94/47
2004	14 May	IRS-P6 (AWiFS)	93/49
2005	24 October	IRS-P6 (AWiFS)	93/49
	17 November	IRS-P6 (AWiFS)	93/49
	11 December	IRS-P6 (AWiFS)	93/49

3.9.2 Moderate Resolution Imaging Spectroradiometer (MODIS)

The Earth Observing System (EOS) is a program of National Aeronautics and Space Administration (NASA) comprising series of artificial satellite missions and scientific instruments in Earth orbit designed for long-term global observations of the land surface, biosphere, atmosphere and ocean of the Earth. Moderate Resolution Imaging Spectroradiometer (MODIS) is a key instrument boarded on the platform of Terra (EOS AM)

and Aqua (EOS PM) satellites launched by EOS. Terra was successfully launched on December 18, 1999 aboard an Atlas IIAS vehicle from Vandenberg Air Force Base located northwest of Lompoc, California. This satellite at an altitude of 705 km orbits in a sun synchronous polar orbit timed such that it descends southward passing from north to south across the equator in morning. Another satellite Aqua (EOS PM-1) carrying the second MODIS instrument was launched on May 4, 2002 from Vandenberg Air Force Base, California. This satellite passes south to north over the equator in the afternoon. The land-imaging element of MODIS sensor appends the characteristics of both AVHRR and Landsat sensors to endow enhanced monitoring of the Earth surface globally. MODIS instrument on board on Terra and Aqua satellites view the whole Earth surface with swath of 2330 km (+ 55 o) every one to two days, obtaining data in 36 spectral bands, or wavelength groups (Hall et al., 2002a, MODIS, 2007). Among these 36 spectral bands ranging in wavelength from 0.4 μm to 14.4 μm, 11 are in the visible range, 9 in near Infrared range, 6 in thermal range, 4 in the short wave infrared (SWIR) range and 6 in the long wave infrared range (LWIR). The sensor maps the earth's surface in high radiometric sensitivity (12 bit) and in three different spatial resolutions viz. 250 m (band 1-2), 500 m (band 3-7) and 1 km (band 8-36).

MODIS design team has given substantial emphasis to instrument calibration and characterization, recognizing it as critical for generation of accurate long-term time series products required for global change studies (Justice et al., 2002). The data acquired from this satellite under goes five different levels of processing. The data from MODIS instrument are transferred to ground stations in White Sands, New Mexico through Tracking and Data Relay Satellite System (TDRSS). After, first Level-0 processing at EOS data and Operations System, the GES DAAC fabricates the Level 1A and 1B, geolocation and cloud mask products. The responsibility for generation of Level 2 and higher products are offered by MODAPS. The MODIS Level-3 (V003) generates earth gridded geophysical products mapped onto space and time grids. The MODIS Level-4 (V004) is the earth gridded model output or result analysis obtained from lower-level data.

3.9.2.1 MODIS snow data products

The MODIS snow maps have augmented the valuable record by providing daily snow products with several spectral bands and better resolution comparative to other satellite products. The MODIS derived data products have the capability to differentiate snow from

most clouds. The MODIS snow and sea ice products are globally accessible in various resolutions and projections to serve various user communities (Hall et al., 2002a, 2006; Riggs et al., 2006) and are disseminated via National Snow and Ice Data Centre (NSIDC) in Boulder, Colorado (Scharfen et al., 2000). The MODIS make use of fully automated and computationally prudent snow mapping algorithm technique for snow detection thus reducing subjective problems due to human biases. Seven bands (bands 1-7) of MODIS are especially designed to image the earth's land surface, corrected for atmospheric effects using aerosol and water vapour information. Among these seven bands MODIS snow mapping algorithm utilizes four bands (bands 1, 2, 4, 6). The MODIS identifies snow covered land, snow covered ice on inland water product globally. For identification and classification of snow on pixel by pixel basis, the snow mapping algorithm employs grouped criteria techniques by making use of Normalized Difference Snow Index (NDSI) and other spectral threshold tests (Hall et al., 2001). NDSI is analogous to the Normalized Difference Vegetation Index (NDVI) (Tucker, 1979, 1986; Townshend and Tucker, 1984). In snow map algorithm, the snow pixels need to satisfy the criteria applied in order of their appearance as below:

a. Pixel has nominal Level-1B radiance data

b. Pixel is in daylight

c. Pixel is on land or water

d. Pixel are unobstructed by cloud

e. Pixels have an estimated surface temperature < 283 Kelvin

The snow map algorithm of MODIS, based on rationing techniques is successful at local and regional scales. (Kyle et al., 1978) determined the use of ratio of a SWIR band to a visible band. This algorithm is based on long ancestry of NDSI technique for snow detection and was evolved using data of Landsat Mapper (TM) (Bunting and d'Entremont, 1982; Dozier, 1989; Hall et al., 1995; Klien et al., 1998; Hall et al., 2001; Hall et al., 2002a; Klien and Barnett, 2003). Due to higher reflectance of snow in the visible range (0.5-0.7 μm) of spectrum and lower in the short wave infrared range (1-4 μm) of spectrum (Nolin and Liang, 2000), MODIS automated algorithms make use of reflectance in bands 4 (0.545-0.565 μm) and 6 (1.628-1.652 μm) for calculation of Normalized Difference Snow Index (NDSI) (Hall et al., 1995).

On the other hand clouds have higher reflectance in both visible and near-IR wavelength of the electromagnetic spectrum (Rossow and Gardner, 1993). Based on these differences between snow/cloud reflectance and emittance characteristics, NDSI index also holds good in snow/cloud discrimination.

$$NDSI = \frac{Band4 - Band6}{Band\ 4 + Band\ 6}$$

The higher NDSI value indicates pure snow and NDSI decreases with mixing of other features in a pixel. MODIS bands 1 and 2 are also used by the algorithm to calculate Normalized Difference Vegetation Index (NDSI) values which are used with NDSI values to map snow in dense forests (Klien et al., 1998).

$$NDVI = \frac{Band\ 2 - Band\ 1}{Band\ 2 + Band\ 1}$$

Snow detection is achieved by using two groups of grouped criteria tests for snow reflectance characteristics in visible and near infrared wavelength regions. The first group criterion is for detecting snow in several conditions. In this criteria group of tests a pixel is mapped as snow if NDSI value is greater than 0.4, the reflectance in band 2 is greater than 0.11 and in band 4 reflectance is greater than 0.10. The other group of criteria tests is aimed to detect snow in dense vegetation in a better way by using bands 1 and 2 to calculate NDVI. In this criteria group, a pixel is also determined to be snow if NDSI and NDVI values in a defined polygon of a scatter plot of two indices and reflectance in band 2 (0.841-0.876 μm) is greater than 0.11 as well as reflectance in band 1 (0.62-0.67 μm) is greater than 0.1 (Hall et al., 2001).

3.9.2.2 MODIS land surface temperature data

MODIS is particularly useful for the LST product and its strength lies in its global coverage, high radiometric resolution and dynamic ranges for a variety of land cover form, and high calibration accuracy in manifold thermal infrared bands designed for retrieval of SST, LST and the atmospheric properties (Zhengming, 1999; Wan et. al., 2004, Mao et al., 2005). The MODIS-LST products are archived in Hierarchical Data Format-Earth Observing System (HDF-EOS). These MODIS-LST data products are produced in seven series (Zhengming, 2006). A summary of the sequence of MODIS-LST products is given in Table 3.6. The MODIS/Terra LST data are generated using the split window algorithm evolved by Wan and Dozier (1996). The LST algorithm employs data in band 31 and 32 of MODIS as inputs to the split-window at 11 and 12 microns respectively.

Table 3.6: Sequential overview of MODIS-LST products

Earth Science Data Type (ESDT)	Product Level	Nominal Data Array Dimensions	Spatial Resolution	Temporal Resolution	Map Projection
MOD11_L2	L2	2030 or 2040 lines by 1354 pixels per line	1km at nadir	swath (scene)	None. (lat,lon referenced)
MOD11A1	L3	1200 rows by 1200 columns	1km (actual 0.928km)	daily	Sinusoidal
MOD11B1	L3	200 rows by 200 columns	6km (actual 5.568km)	daily	Sinusoidal
MOD11A2	L3	1200 rows by 1200 columns	1km (actual 0.928km)	eight days	Sinusoidal
MOD11C1	L3	360° by 180° (global)	0.05° by 0.05°	daily	equal-angle geographic
MOD11C2	L3	360° by 180° (global)	0.05° by 0.05°	eight days	equal-angle geographic
MOD11C3	L3	360° by 180° (global)	0.05° by 0.05°	monthly	equal-angle geographic

The MOD11_L2 is the first LST product with a spatial resolution of 1 km for a swath (scene) obtained using the generalized split-window LST algorithm developed by Wan and Dozier (1996). The geolocation information (latitude and longitude) at a coarser resolution is stored with the products. The second product, MOD 11A1 is a tile of daily LST at a spatial resolution of 1 km produced by mapping the pixels of first LST product for a day to the Earth locations on sinusoidal projection.

In the present study, MOD11A2 has been employed which is 8-day LST product obtained by averaging from 2 to 8 days of MOD11A1 products which consist of 1200 km x1200 km tiles of 1km spatial resolution (0.928 km in actual) and sinusoidal map projection. The LST data is available as 16 bit unsigned integer while emissivity as 8 bit unsigned integer. MOD11A2 is encompass of daytime and nighttime LSTs, quality assessment, observation times, view angles, bits of clear sky days and nights, and emissivities estimated in Bands 31 and 32 from land cover types (LP DAAC, 2014).

3.9.3 DIGITAL ELEVATION MODEL

(a) Using SRTM 90 M Data

The Shuttle Radar Topography Mission (SRTM) is an international project led by the U.S. National Geospatial-Intelligence Agency (NGA), U.S. National Aeronautics and Space

Administration (NASA), the Italian Space Agency (ASI) and the German Aerospace Center (DLR). SRTM obtained elevation data on a near-global scale to generate the most complete high resolution digital topographic database of Earth, including three resolution products, of 1 km and 90 m resolutions for the world, and a 30 m resolution for the US (USGS, 2004). The elevation data used in this study is the 90 m resolution (3-arc SRTM), which consists of a specially modified radar system that flew onboard the Space Shuttle Endeavour during an 11-day mission in February of 2000. These two radar antennas operating in C and X-bands acquired elevation information over the landmass between 56 ^{0}S to 60 ^{0}N. All SRTM data are freely available at: http://seamless.usgs.gov/Website/Seamless/. The SRTM-DEM was downloaded from the USGS ftp site. These data are presently supplied free of cost for scientific study. The data were supplied in GeoTIFF format. The ERDAS Imagine software has been used to export the DEM to 32-bit data format. Many times variation in pixel intensity (digital numbers) occurs due to conflicting sensitivities resulting either from malfunctioning of detectors or due to topographic or/and atmospheric effects. These variations were corrected by radiometric calibration. The SRTM-DEM was available in Geographic latitude/longitude map projection with WGS84 datum.

(b) Using USGS Data

The USGS GTOPO30 is a global digital elevation model (DEM) resulting from a joint endeavors by the team of USGS EROS data center with a regular horizontal spacing at 30-arc seconds (nearly 1 km). This global model available in public domain was developed over a period of three years and completed in 1996. The DEM was evolved with an objective to serve the exigencies of geospatial data user groups for topographic data, both at regional and continental scale. Being a worldwide dataset, it covers the complete extent of Earth from 90 ^{0}S to 90 ^{0}S (latitude) and from 180 ^{0}W to 90 ^{0}E (longitude). The horizontal coordinate system of GTOPO30 is Latitude and longitude measured in decimal degrees, and referenced to WGS84 datum. The vertical units (in meters) exemplify elevation above mean seal level and range from -407 m to 8752 m.

The complete GTOPO30 has been alienated into 33 smaller tiles, also called as tiles to facilitate its electronic distribution. The area from 60 ^{0}S to 90 ^{0}S of latitude and from 180 ^{0}W to 90 ^{0}E of longitude is covered by 27 tiles, with each tile covering 50 degrees of latitude and 40 degrees of longitude. In this study, snow cover area and LST information elevation wise have

been extracted using SRTM and GTOPO30 DEM models respectively, which are important input parameters for a distributed snowmelt runoff model.

3.10 HYDRO METEOROLOGICAL DATA

The Bhakra Beas Management Board (BBMB) has setup a hydro-metrological network for the proper, safe, judicious regulation and operation of Pandoh dam. The hydro-meteorological data on temperature, rainfall and discharge covering the entire Beas basin have been collected from the office of BBMB at Pandoh, Himachal Pradesh. The observed daily maximum and minimum temperature data were available for four distinct stations namely Bhuntar, Larji, Manali and Pandoh located at different altitudes have been collected. The daily rainfall data has been collected for six stations namely Banjar, Bhuntar, Larji, Pandoh, Manali and Sainj.

The river flows are monitored and their discharge is measured in different tributaries by BBMB at five discharge sites on the river Beas namely Bakhli, Sainj, Thalout, Tirthan and Pandoh. The discharge observed at these stations was collected from the BBMB office at Pandoh. The spatial distribution of hydrometric stations in the study area is shown in Figure 3.2 and their general details are listed in Table 3.7.

3.11 SOFTWARE USED

ERDAS Imagine 9.3, an image processing and GIS software has been used for processing the satellite data before commencing the analysis. Arc GIS is the main GIS software used for GIS mapping while C++ program used for the statistical analysis. SNOWMOD snowmelt model has been used for streamflow modeling.

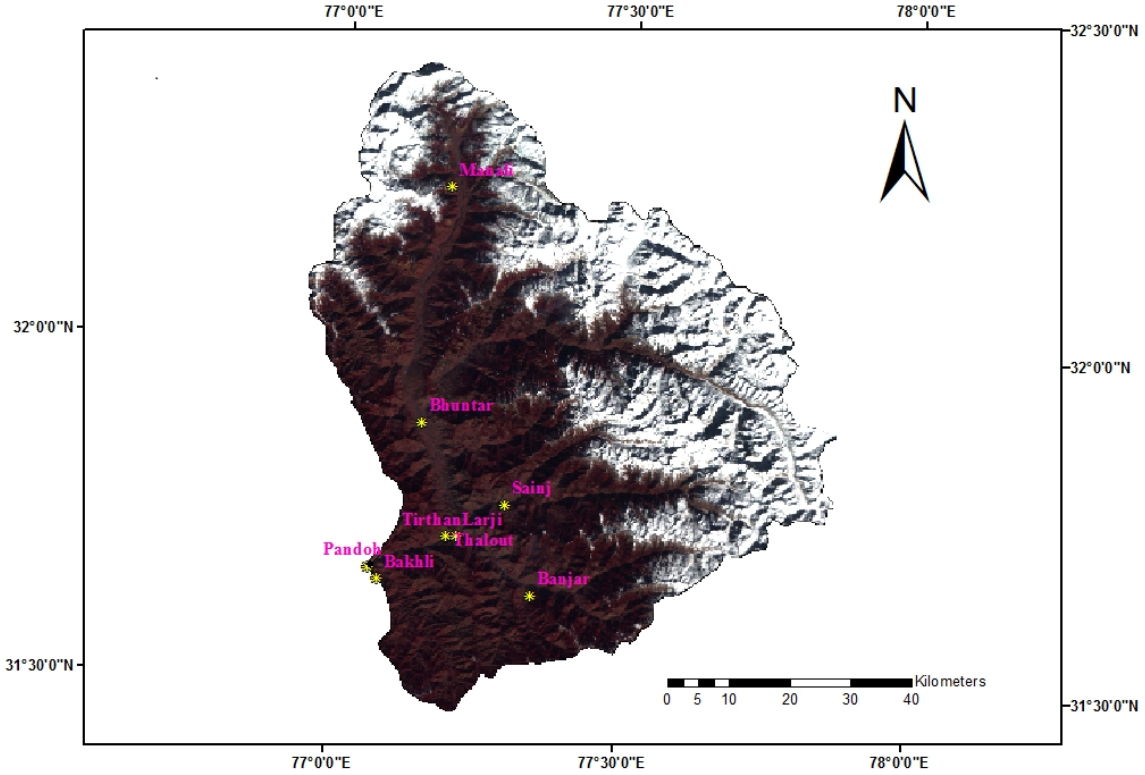

Figure 3.2: Spatial distribution of hydrometric stations in the study area

Table 3.7: General details of hydro-meteorological stations in the Beas basin

S. No	Station	Altitude (m)	Air temperature	Rainfall	Discharge
1.	Pandoh	899	1986-2009	1979-2009	1978-2005
2.	Thalout	933	-	-	1978-2005
3.	Bakhli	940	-	-	1978-2009
4.	Larji	995	1986-2009	1979-2009	-
5.	Tirthan	1043	-	-	1978-2009
6.	Bhuntar	1102	1986-2009	1979-2009	-
7.	Sainj	1348	-	1979-2009	1978-2009
8.	Banjar	1353	-	1979-2009	-
9.	Manali	1842	1986-2009	1989-2009	-

Chapter 4

ASSESSMENT OF SNOW COVER AND ITS DEPLETION

4.1 BACKGROUND

Snow Depletion Curve (SDC) is a significant input variable for streamflow modeling for the snow-fed river basins of Himalayas. Snow cover area information is required for preparation of SDCs. The complex and rugged terrain of Himalayan region obstructs in collecting areal SCA information manually. Thus, space technology based remote sensing has proved as a promising and vital source for deriving the valuable information of SCA at different temporal and spatial resolutions. The present study aims to estimate the spatio-temporal snow cover from multiple satellite imagery of different satellites such as MODIS, IRS-1C/1D and AWiFS. The continuous dataset of MODIS snow products have been classified into snow and non-snow categories for the period 2001-2005. The classified maps obtained from MODIS have been compared with the Snow Cover Area (SCA) maps estimated from IRS-1C/1D and AWiFS satellite imageries for some selected dates. More or less the area estimated using MODIS are comparable to the area obtained from IRS-1C/1D and AWiFS satellite images. Moreover, an exponential relation has been developed to derive SCA information using mean air temperature. This technique has been used to acquire SCA for the previous years (1990-2000) when the satellite data is unavailable or is cloud covered. The air temperature data of Manali station has been used to estimate the SCA of different elevation bands. This technique has proved to be simple, logical and conducive in providing propitious good results under the sophisticated environment of Himalayas. Further, SDCs were prepared for the years 1990-2000 and 2001-2005 based on snow cover area maps obtained from exponential relationship and satellite data respectively.

4.2 INTRODUCTION

Spatio-temporal coverage of snow is an important parameter for hydrological modeling for simulating and estimating the contribution of snowmelt to the river flows. Monitoring of snow cover is a big challenge in modeling the surface water distribution (Bergeron et al., 2013). Snow acting as reservoir of water controls the water supply and contribution of snowmelt. It is

a significant variable for the management of dams for being an excellent source for hydropower (Lavallee et al., 2006) which is cheap and renewable energy as well. On the other hand, abrupt melting poses an immense threat of flood in several areas.

Space based remote sensing technology is extensively used to map the snow, an important natural element with the higher albedo in comparison to other natural surfaces except cloud. Curiosity of researchers for knowing the distribution of snow for wide variety of reasons had made much evolution. It was in the middle of 1960s, Environmental Science Service Administration (ESSA-3) satellite which carried the Advanced Vidicon Camera System (AVCS) with the spectral range (0.5 - 0.75 µm) with a spatial resolution at Nadir of 3.7 km successfully mapped the weekly snow. Since 1966, National Oceanographic and Atmospheric Administration (NOAA) satellite is the first to map the snow cover on weekly basis; by utilizing variety of space borne sensors that provided daily and global observations of snow cover extent for monitoring the spatio-temporal variability (Robinson et al., 1993; Frei and Robinson, 1998; Salomonson and Appel, 2004). The MODIS is also mapping snow cover on daily basis since 2000 (Hall et al., 2002a; Riggs et al., 2006; Hall and Riggs, 2007). Nowadays, a large number of spaceborne sensors are available to provide satellite imageries with higher spectral, spatial and temporal resolutions, selection of which mainly depends on the need of commodity and study.

In the Himalayan region, the snow cover contributes substantially to the water resources in the summer months. However, a very little field information on snow/glacier is available or collected in this region (Shroder et al., 1993; Singh and Jain, 2002; Gupta et al., 2005). The satellite based data facilitate to ameliorate near real time simulation by providing continuous, complete spatial coverage and frequent data availability of the region. Thus, remote sensing has emerged as a valuable means to obtain viable information on snow cover in the large basins of Himalayas. Numerous researchers in recent decades have extensively used the satellite images for snow studies in the Himalayan region. A high temporal resolution is important particularly for monitoring changes in snow extent due to melt or accumulation. Several snowmelt runoff studies have been carried out in the Himalayan region by using satellite data driven snow cover (Rango et al., 1977; Gupta et al., 1982; Kulkarni and Bahuguna, 2001; Singh and Jain, 2003; Thakur et al., 2008; Jain et al., 2012a; Aggarwal et al., 2013, 2014). Dey and Goswami (1983) carried out a study to predict seasonal snowmelt runoff for Indus basin using NOAA-AVHRR data. The NOAA (AVHRR) and Aqua/Terra (MODIS) snow cover data are useful for snow studies for the basins having area above 200 km^2 (Rango, 1996). Also, the satellite data acquired from IRS LISS-II, LISS-III, Landsat TM and SPOT satellites are much more suited

for basins as small as 2.5 km^2, while IRS LISS-I and Landsat Multi Spectral Scanner (MSS) can be used for basins about 10 km^2 in size (Singh and Singh, 2001).

The multispectral images of Indian satellite, IRS (LISS-III) have been used for mapping dry/wet snow cover in Himalayas (Gupta et al., 2005). Passive microwave (SMMR) data has been used for the estimation depth and extent of snow cover for a part of Satluj basin in the Himalayan region (Saraf et al., 1999). (Gurung et al., 2011) have used MODIS snow products to monitor seasonal snow cover using remote sensing technique in Bhutan. Based on satellite derived information, a large number of studies have been carried out in the Himalayan region (Gupta at el., 1982; Agarwal et al., 1983; Dey et. al., 1988; Upadhyay et al., 1991; Thapa 1993; Jain, 2001; Singh et al., 2004; Thakur et al., 2006, 2011; Krishna and Sharma, 2013; Snehmani et al., 2013a). At present, many of the satellite data are freely available via World Wide Web (WWW) and can be accessed and downloaded free of cost through the internet service and data which is not available free of cost can be procured through specific agencies on nominal payment basis depending upon the nature of data.

The SCA significantly changes during spring and winter season and influences the streamflow of snow-fed Himalayan rivers which directly or indirectly exerts pressure on the various activities such as hydropower generation, reservoir operation, water management and lots of other developmental projects in the region. Thus, it is very essential to estimate the precise and consistent areal extent of snow cover of a river basin so that it can be used with confidence in simulating and predicting streamflow, and water balance studies for the existing or upcoming river valley projects in the region. The streamflow of Beas river up to Pandoh dam has significant contribution from snow/glacier melt. Keeping this in view, the present study has been taken for snow cover mapping using satellite data of MODIS, IRS-1C/1D WiFS and AWiFS. A simple and logistic exponential relationship between SCA and mean air temperature has been developed and used for estimating SCA for previous years when the satellite data is not available or is cloudy for the study area. Further for snowmelt runoff modeling for the basin, SDCs have been prepared using MODIS satellite data for years 2001 to 2005 and for years 1990 to 2000 using exponential relationship between SCA and temperature.

4.3 ASSESSMENT OF SNOW COVER AREA (SCA)

4.3.1 Using Remote Sensing Data

A snow cover mapping procedure involves in discriminating a pixel of snow from a non-snow pixel. Usually three techniques; reflectance statistics, training sites supervised

classification and Band ratio (Normalized Difference Snow Index) (NDSI) are applied for snow cover mapping for estimating the distribution and aerial extent of snow cover. Although, estimation of SCA from satellite images is a sensitive work under the complex Himalayan climatic conditions due to cloud cover and mountain shadow. The reflectance of snow is higher in the visible band and strong absorption is exhibited in the Short Wave Infrared (SWIR) band. A spectral band ratio can enhance features if there are differences in spectral slopes (Gupta et al., 2005). The NDSI utilize these spectral characteristics of snow and it is being developed using the concept of Normalized Difference Vegetation Index (NDVI) which is used for mapping vegetation through remote sensing data (Dozier, 1989; Hall et al., 1995; Gupta et al., 2005). The NDSI is defined as the difference of reflectance observed in a visible band (0.52-0.59 μm) and the short-wave infrared band (1.55-1.70 μm) divided by the sum of the two reflectance (Gupta et al., 2005). The MODIS snow cover algorithm is based on the high reflectance of snow in the visible band (band 4, 0.545– 0.565 μm) and low reflectance in the near infrared band (band 6, 1.628–1.652 μm), and it is also able to delineate snow in the mountain shadows. These two bands are used to calculate the NDSI (Hall et al., 1995), as follows:

$$\mathrm{NDSI} = \frac{\text{Visible Band} - \text{SWIR Band}}{\text{Visible Band} + \text{SWIR Band}} \tag{4.1}$$

The MODIS snow products have been exploited in the present study for the Beas basin for the estimation of snow cover area for a period of 2000-2005. The SCA has been also estimated from the satellite data of IRS-1C/1D WiFS and AWiFS for specific dates discussed earlier in chapter 3. Prior to snow cover mapping, all the imageries have been projected to a common projection system.

4.3.1.1 Preparation of SCA Maps and DEM

Notably MODIS snow data products are freely available to user's community via WORLD WIDE WEB (WWW). The satellite data were downloaded and processed thereafter. The maps were in sinusoidal projection and WGS84 datum. This sinusoidal projection was re-projected to Geographic Lat/Long and WGS84 datum. The entire MODIS snow data products were found to be geo-referenced very precisely (Jain et al., 2008a). The SRTM 90 m DEM has been downloaded. However, it was seen that MODIS snow data products and SRTM-DEM

were not geo-referenced precisely with respect to each other. Hence, image-to-image re-projection has been carried out for achieving better precision. For which all of the MODIS images and SRTM-DEM has been geo-referenced. As many as 32 GCPs were selected in the image. GCPs are the specific pixels in the image data for which both the file coordinates (in the image) known as the source coordinates and map coordinates (in the map) known as the reference coordinates. The GCPs were spread throughout the image so that the rectification is more reliable. The Root Mean Square Error (RMSE) value was kept within a pixel (mostly 0.2).

The next step was to convert the source coordinates to rectified coordinates. For this operation second-order, polynomial equation was used. The re-sampling was done using Nearest Neighbor method, which uses the value of the nearest pixel to assign to the output pixel value. The MODIS snow cover products are the classified images which are developed based on the NDSI technique used to extract information on snow cover area. These images were further used for classification, snow and lake ice was clubbed into snow category whereas remaining classes were categorized into non-snow. Also, the processed DEM of the study area has been classified. Using this classified DEM model, the relief of study basin has been divided into nine elevation zones with an altitude difference of 600 m and further used to derive basin characteristic (area-elevation curve) of the study area. The DEM for of the selected Beas basin is shown in Figure 4.1.

The entire dataset of MODIS images (2000-2005) was classified into two categories i.e. snow and non-snow. The SCA maps from January 2001 to December 2005 have been prepared. The SCA maps for period 2001 to 2004 are shown in Figures 4.2 to 4.5. Similarly, all the images of IRS-1C/1D WiFS and AWiFS have been also classified into snow and non-snow category using unsupervised classification scheme.These maps were compared with the SCA maps prepared from MODIS. It was seen that more or less the area estimated using MODIS are equal to the area obtained from IRS-1C/1D and AWiFS satellite images. The graphical representation of SCA estimation from these three sensors has been shown in Figure 4.6. Figure 4.7 and 4.8 show the classified images of WiFS and AWiFS respectively. Due to availability of continual and high temporal resolution of MODIS data, possibility of acquiring cloud-free data is better as compared to IRS-1C/1D and AWiFS data. This criteria make it unique for snowmelt studies. Therefore, MODIS SCA maps have been further used in this study for snowmelt modeling. Using these classified snow cover maps of MODIS, the total percentage of snow cover (weekly) in the present study area has been estimated for different dates, shown in Table 4.1.

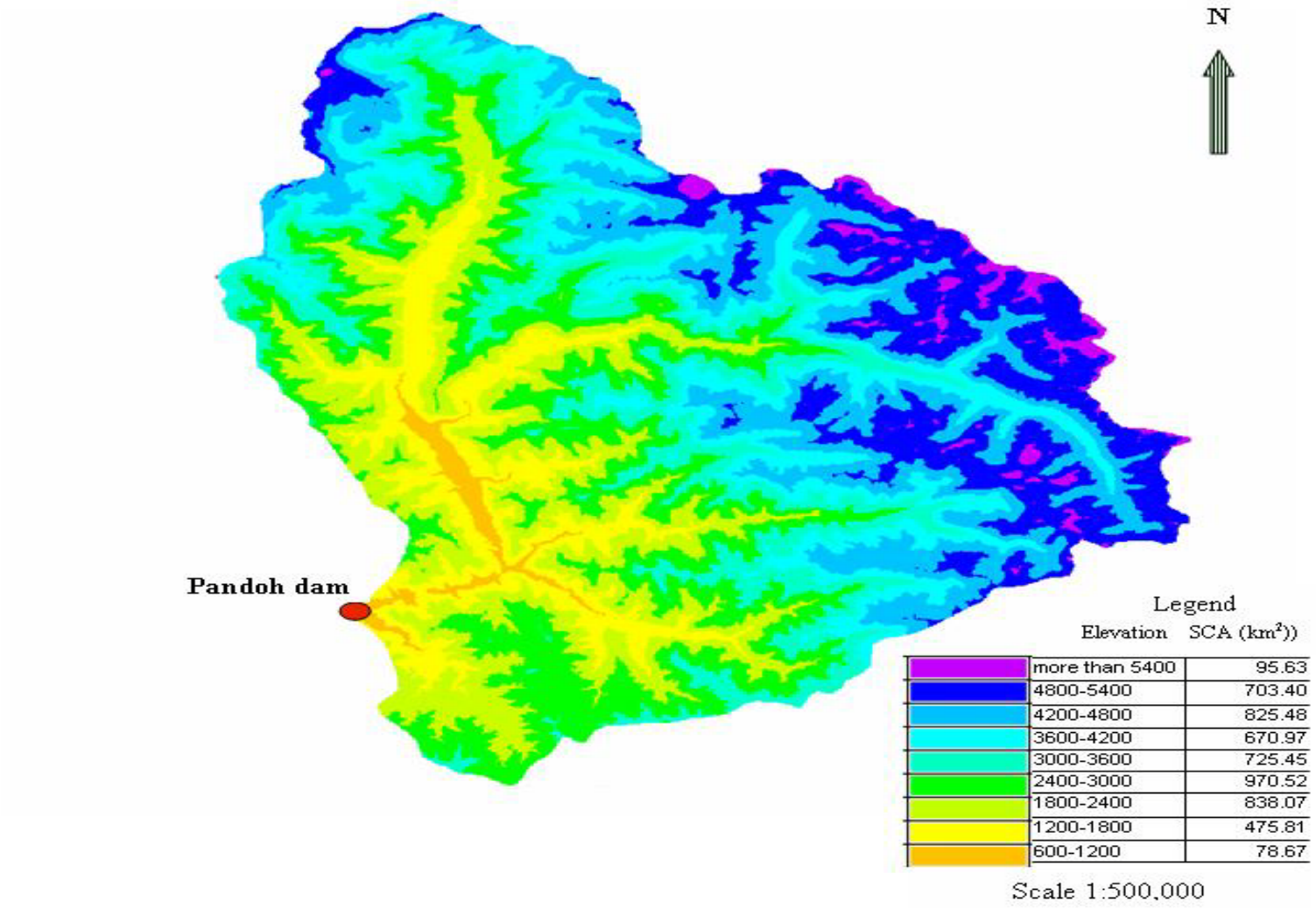

Figure 4.1: Digital Elevation Model (DEM) of the Beas basin

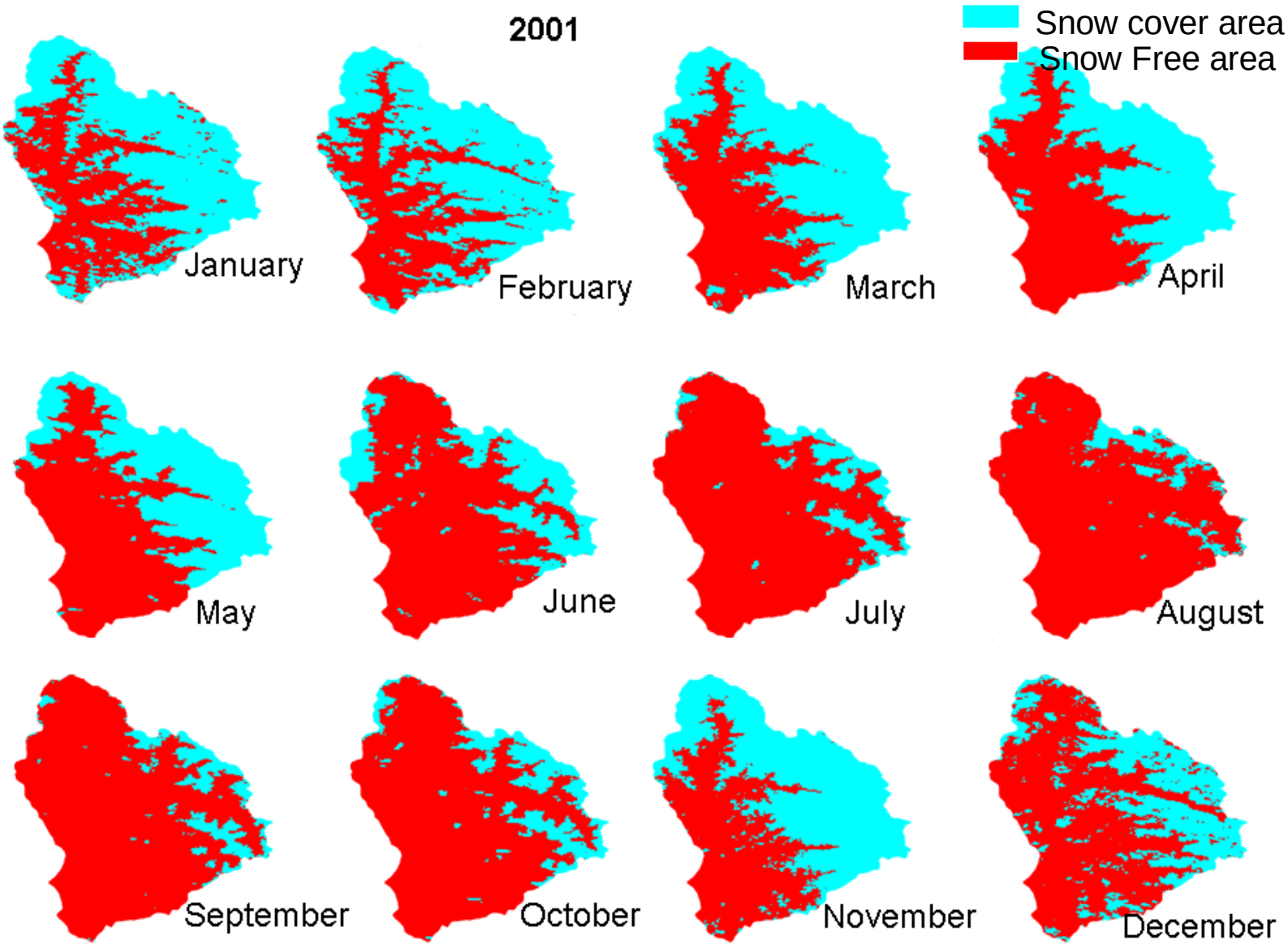

Figure 4.2: Snow cover distribution in the Beas basin using MODIS images for year 2001

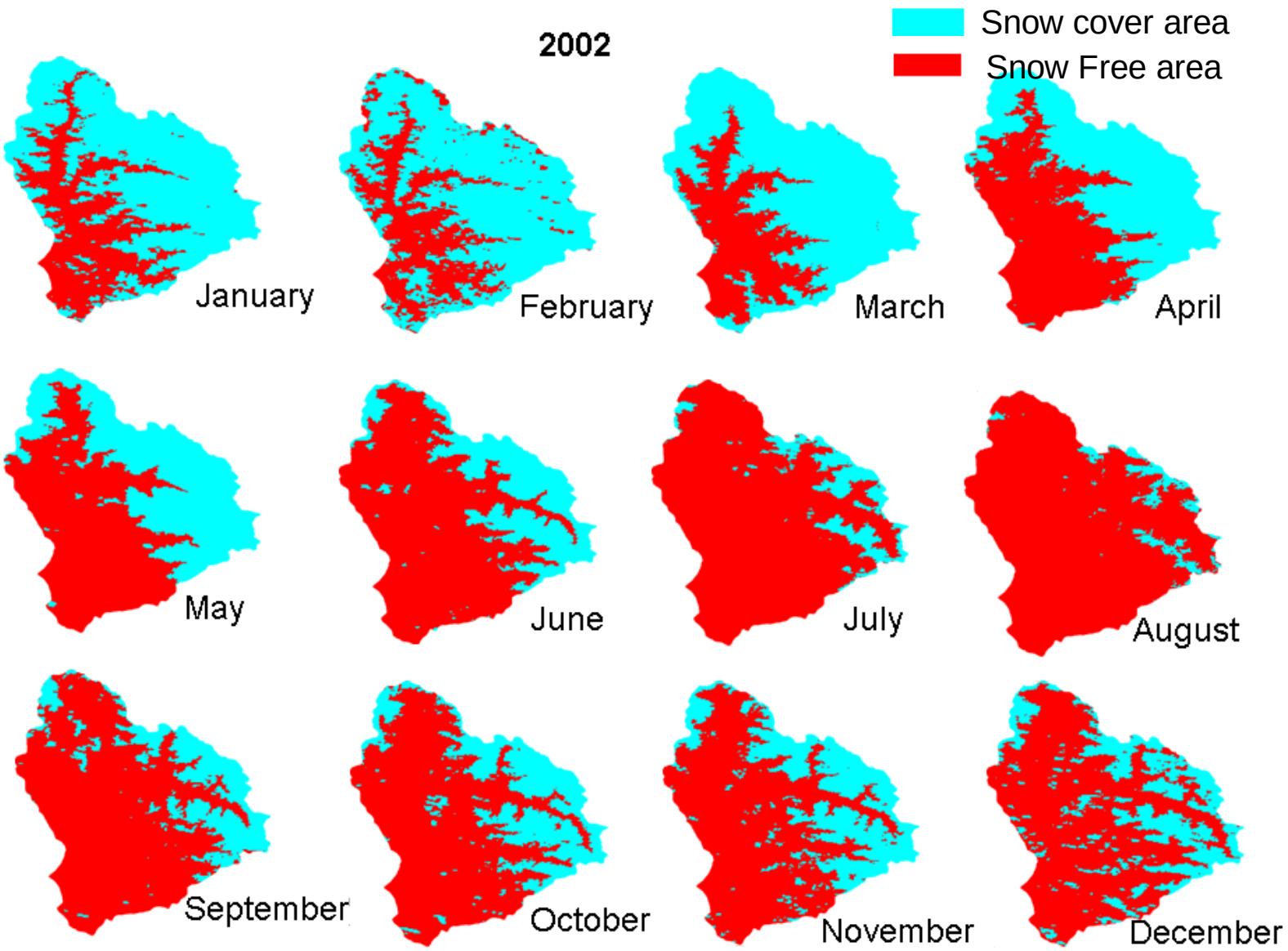

Figure 4.3: Snow cover distribution in the Beas basin using MODIS images for year 2002

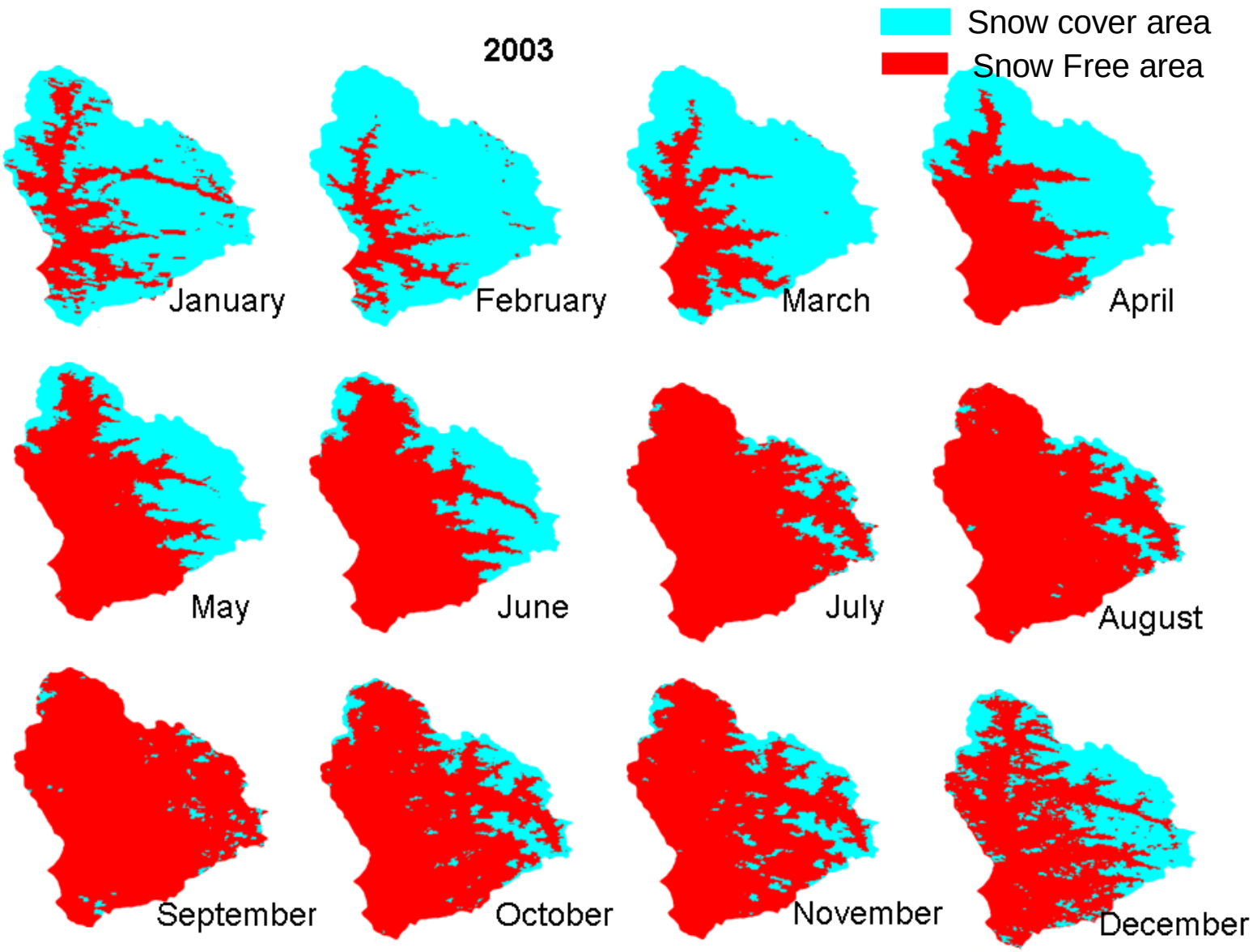

Figure 4.4: Snow cover distribution in the Beas basin using MODIS images for year 2003

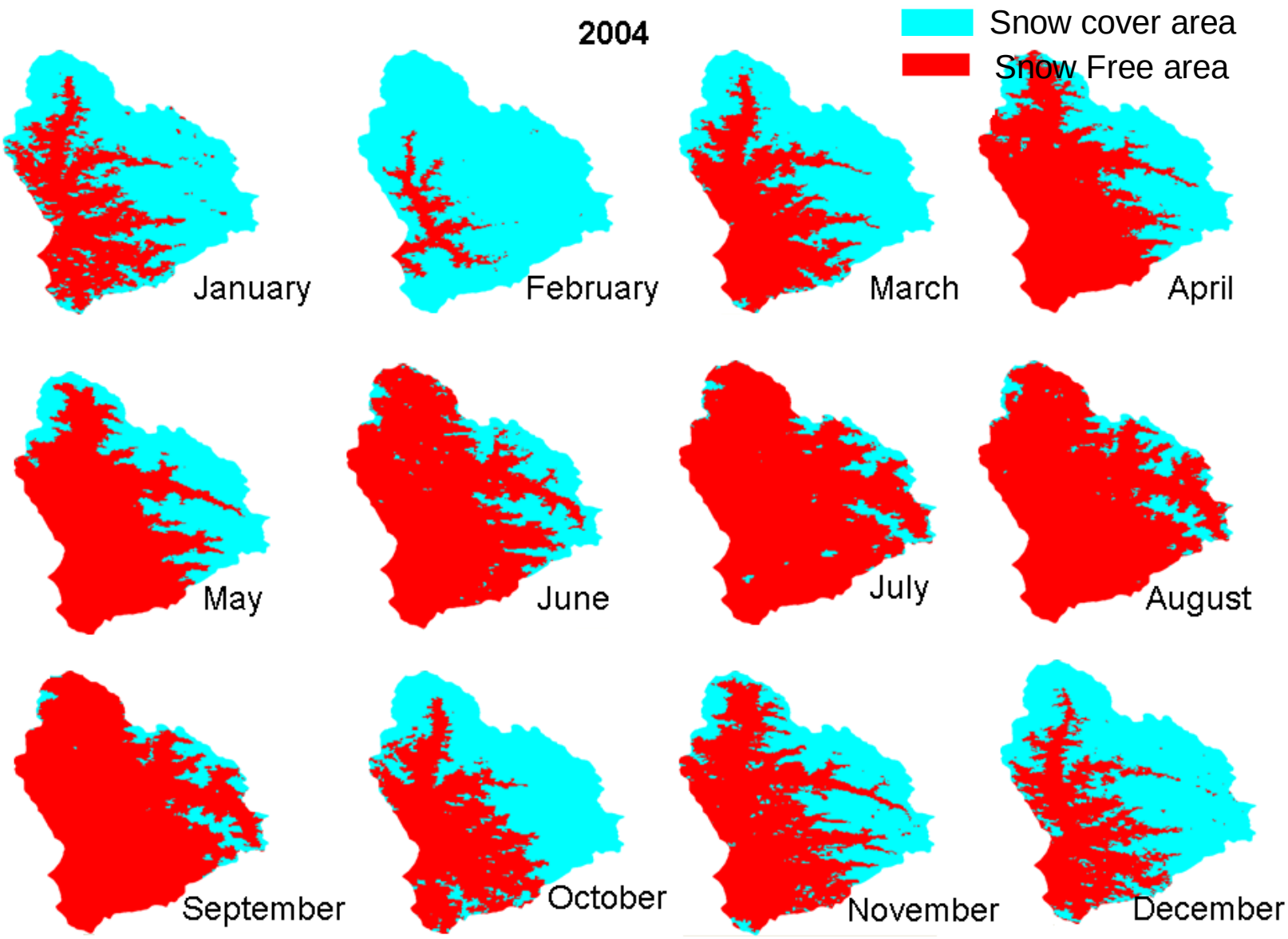

Figure 4.5: Snow cover distribution in the Beas basin using MODIS images for year 2004

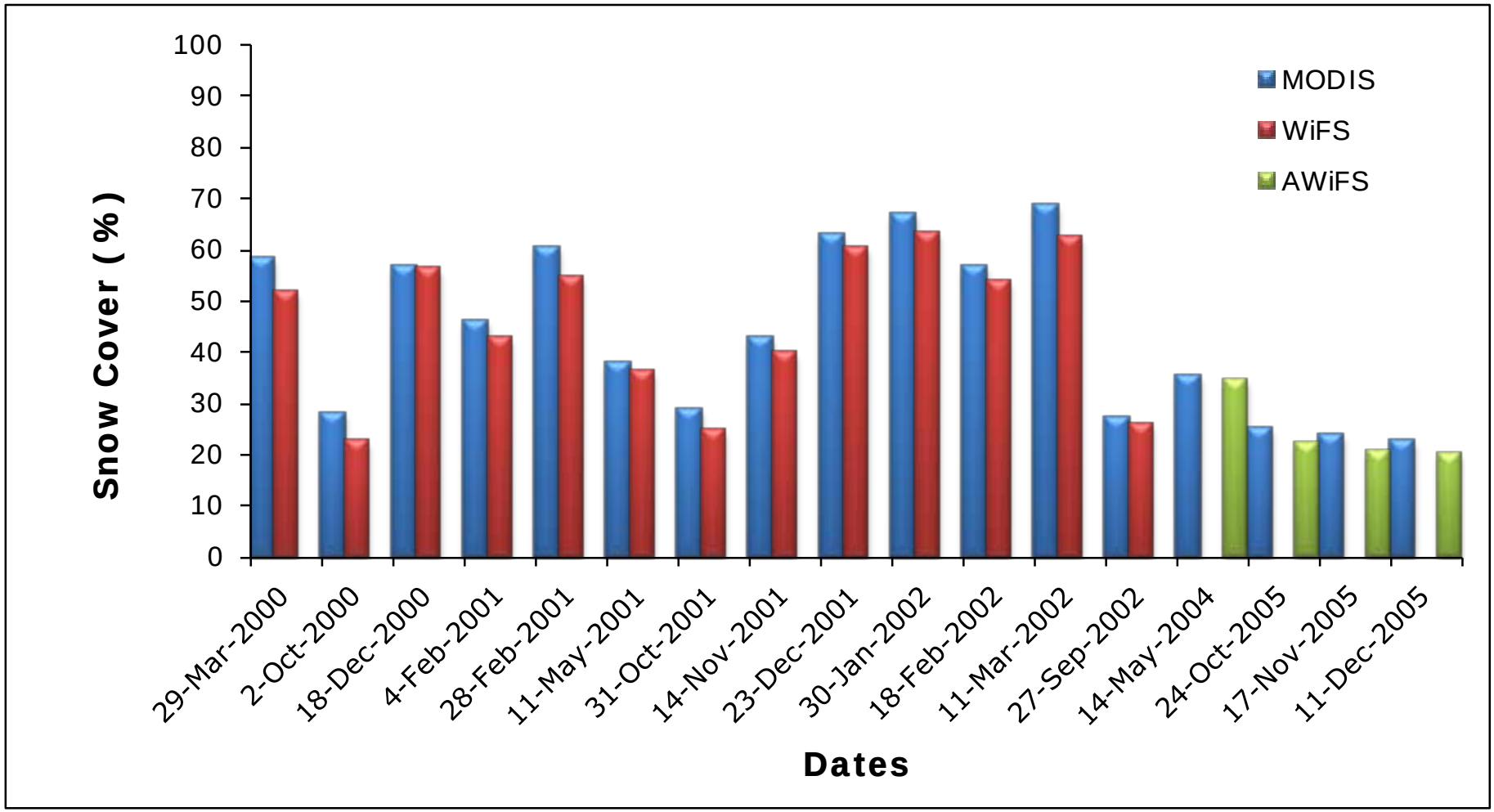

Figure 4.6: SCA for the Beas basin using MODIS, WiFS and AWiFS images

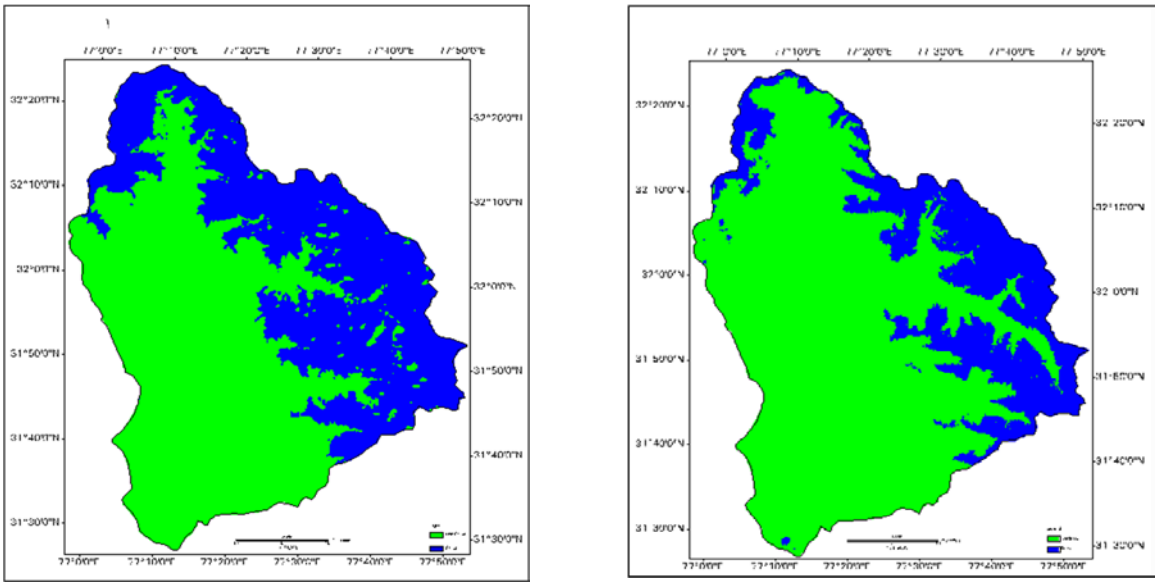

Figure 4.7: Classified images of WiFS (a) 28 February, 2001 (b) 27 September, 2002

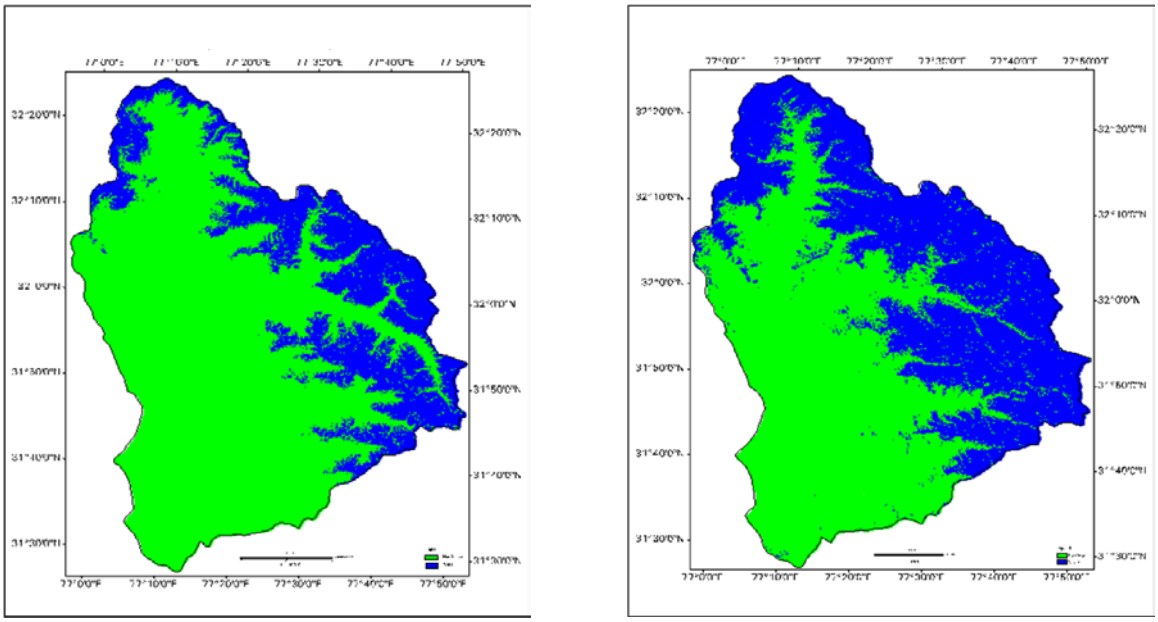

Figure 4.8: Classified images of AWiFS (a) 14 May, 2004 (b) 11 December, 2005

Table 4.1: Estimated snow cover area from MODIS data for the Beas basin

YEAR	2001	2002	2003	2004
March-1wk	65.11	73.65	67.75	71.13
March-2wk	70.09	87.62	71.61	63.63
March-3wk	54.58	68.44	61.35	55.43
March-4wk	64.62	66.33	47.93	48.28
April-1wk	63.63	48.23	66.69	42.47
April-2wk	62.68	59.45	55.78	39.98
April-3wk	48.31	51.11	50.92	36.76
April-4wk	51.76	45.47	49.4	39.33
May-2wk	46.56	56.81	39.03	45.16
May-3wk	43.06	45.29	39.2	54.7
May-4wk	37.98	38.9	35.45	35.51
June-1wk	34.99	35.59	37.11	37.16
June-2wk	31.19	29.12	30.23	31.8
June-3wk	25.1	28.7	19.21	37.11
June-4wk	22.21	21.42	22.16	21.47
July-1wk	12.66	27.53	11.43	21.84
July-2wk	9.05	11.91	10.77	17.81
July-3wk	11.04	10.68	10.35	9.01
August-1wk	8.45	14	8.96	11.56
August-2wk	9.49	8	9.34	13.93
August-3wk	10.35	9.16	9	10.92
August-4wk	9.48	14.84	10.71	9.39
September-1wk	11.79	10.34	11.12	11.37
September-2wk	16.01	19.55	12	10.33
September-3wk	20.74	19.04	13.05	12.84

Furthermore, for snowmelt runoff modeling, SCA is required for different elevation zones. For this purpose, classified DEM and MODIS SCA maps have been processed for all the dates. The SCA in each elevation zones were plotted against the elapsed time to construct the SDCs for the various elevation zones in the basin for all the years. SDC for the months of March to October for five years (2001, 2002, 2003, 2004 and 2005) are shown in Figure 4.9.

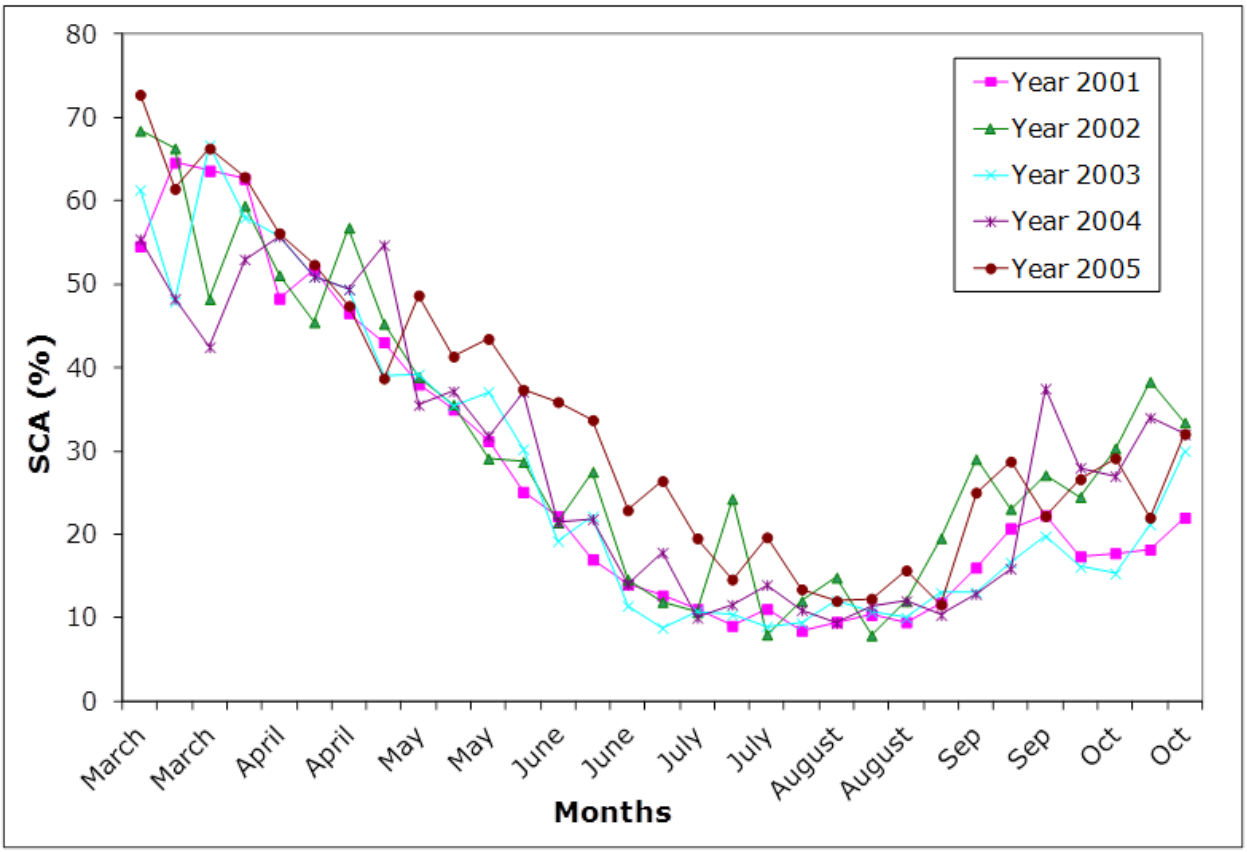

Figure 4.9: Snow cover depletion curves for ablation period (March to October)

4.3.2 SCA Using Temperature Data

Cloud cover is a major obstruction in operational monitoring of snow cover using optical remote sensing satellites. These satellites acquiring data in the optical region of electromagnetic spectrum lack the ability to produce SCA maps during cloud (Frei and Robinson, 1999). Consequently, snow cover information is obtained only for the cloud-free days and missed during cloudy days. For cloud cover problem, microwave remote sensing can be used to detect snow cover under cloud which includes data from both passive and active instruments. The passive remote sensing data are having its own limitation, coarse spatial resolution (~ 25 km) therefore they are not very much useful in snow mapping (Rango, 1996).

Active remote sensing with higher spatial resolution, such as Envisat ("Environmental Satellite"), Advanced Synthetic Aperture Radar (ASAR), Radarsat and European Remote Sensing (ERS) can detect snow cover under cloud easily (Guneriussen et al., 2001, Strovold and Melnes, 2004). To overcome the problem of temporary snow cover, the method involves extrapolating snow cover over a cloud obscured area (Li et al., 2008).

Temperature determines the fraction of precipitation that falls as snow and is the most important factor determining the timing of snowmelt. Moreover, air temperature and snow cover are inter-reliant phenomena having a definite relationship. When sufficient satellite data are not available due to cloud cover or due to some other reasons, then SDC can to be generated using temperature data. Under changed climate conditions also, modified SDC are required. Therefore to have SDC under such situations, a relationship between snow cover area and cumulative mean temperature is needed for each zone of the catchment. This procedure of having snow cover maps has two main purposes. First, it could potentially be used to generate snow cover maps when cloud-free satellite data are not available. Second, it can be used to generate snow covered area in a new climate to see the impact of climate change on snowmelt runoff studies.

As discussed before, SCA have been estimated using MODIS satellite data. This data is available from 2000 onwards, therefore, to have SCA for previous years, a method for preparation of depletion of SCA using mean air temperature has been applied. Because depletion of snow is a cumulative effect of climatic conditions in and around snow cover area, the Cumulative Mean Air Temperature (CMAT) at a nearby station should represent depletion of SCA.

In Himalayan basin, SCA starts melting in beginning of March. SCA in the basin is reduced by retreating of the snow line from the lower elevations of the basin towards the higher areas. The retreat rate is reduced as the thicker and denser snow packs are reached at the higher altitudes towards the end of the melting period. With the advancement of summer season, the snow cover starts melting in the upper part of the basin. As discussed by Singh and Kumar (1997b), increase of snow depth with elevation would result in thinner and low-density snow packs at the lower elevations and thicker and denser ones at the higher altitudes. The SCA reduces with time and at each point of time melt can be related to air temperature. Therefore, cumulative temperature over the melt period should represent the depletion of SCA (Singh et al., 2003; Tikeli, 2005b).

Rapid melting of snow, and thus the quick disappearance of SCA in lower elevations, was reported by Kattelman (1997). Gupta et al. (1982) derived a logarithmic relationship

between SCA and the volume of seasonal snowmelt runoff for Himalayan basins. Kaya (1999) and Tekeli (2005b) established a relationship between depletion of SCA in Karasu basin with CMAT on a daily basis for the years 1997 and 1998. This exponential relationship can be explained on the basis of distribution of snow in the basin (Singh et al., 2003; Tekeli, 2005b). An exponential relationship implies that initial increments in temperature lead to higher changes in the snow covered area than later increments in temperature of the same magnitude (Singh et al., 2003). These studies support the exponential relationship between SCA and CMAT used in the study.

Therefore, in this study also an exponential relationship between SCA and CMAT in the following form has been adopted.

$$Y=a*\exp(-bX) \qquad (4.2)$$

where, Y stands for SCA and X denotes the CMAT, while a and b are the coefficients to be determined. Since melting starts around beginning of March, reference date for computing CMAT was considered March 1. The above relationship has been developed for each year and found that it is not exactly same for each year, because snow cover varies each year. Therefore data of four ablation seasons for the years 2001-2004 have been used to establish the relationship between SCA and CMAT.

In the present study area, the SCA for zone 1, 2 and 3 are having almost no snow cover while zones 8 and 9 are having almost 100% snow cover area. Therefore these zones have not been considered in this study. The remaining zones 4, 5, 6 and 7 are having snow cover area which changes with time during ablation period, therefore relationship for these four zones have been developed. The station Manali having an altitude of 2100 m has been considered in zone 4. Mean daily air temperature was obtained using maximum and minimum temperature. There is no station available above the altitude of 2500 m. Therefore, for zones 5, 6 and 7 temperature of Manali station have been used and computed with the help of lapse rate (0.6°C) (Singh, 1991). The exponential fit to variation of SCA with respect to CMAT has been done for four zones. The computed coefficients in equation (4.2) are given in Table 4.2. The high R^2 values in Table 4.2 support the preliminary assumption of an exponential relationship between SCA and CMAT. The study is used for interpolation and simulating of SCA on the basis of temperature data and generation of SCA maps for climate change studies.

Table 4.2: Coefficients and R^2 values for the ablation period

Elevation zones	Coefficient a	Coefficient b	Coefficient of determination R^2
Zone 4	0.72	-0.0054	0.90
Zone 5	1.0	-0.0059	0.97
Zone 6	1.0	-0.0035	0.95
Zone 7	0.92	-0.0064	0.91

SDCs are very important in snowmelt runoff studies. For snowmelt runoff studies, SDCs in different elevation zones are required. Once the relationship between SCA and CMAT is derived, the SCA values for the missing dates can be found using the obtained relationship. In this way, SCA between the observation times can be interpolated and the depletion of the SCA from the basin can be simulated. Because SCA and CMAT are exponentially correlated, once the trend of depletion of SCA is established in the basin, it has been used for the other years using only CMAT data.

This approach has been applied for 11 years (1990-2000) for simulating daily SCA in the study basin. SDCs for zones 4, 5, 6 and 7 are shown for the years 1990 to 1999 in Figures 4.10 to 4.12. The simulated values can be used as input into a snowmelt runoff model (Martinec et al., 1998) to obtain the simulated discharges. As stated above, the relationship has been developed using data of four years, and therefore this relationship has been checked for one year data before applying for other years.

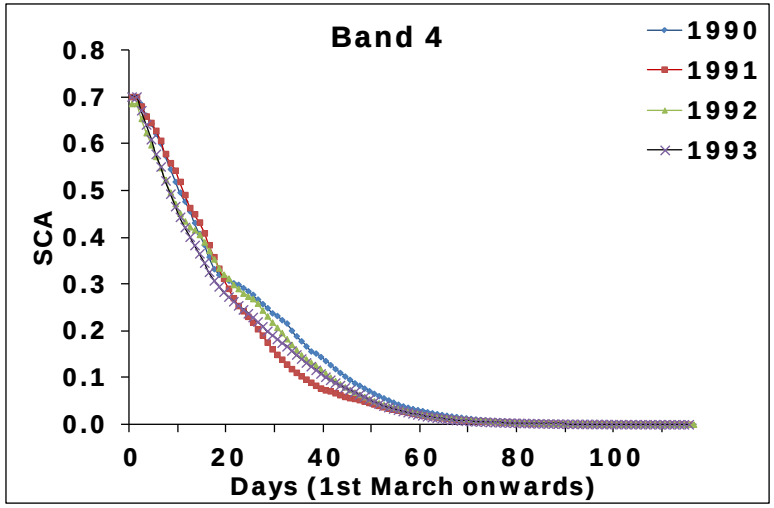

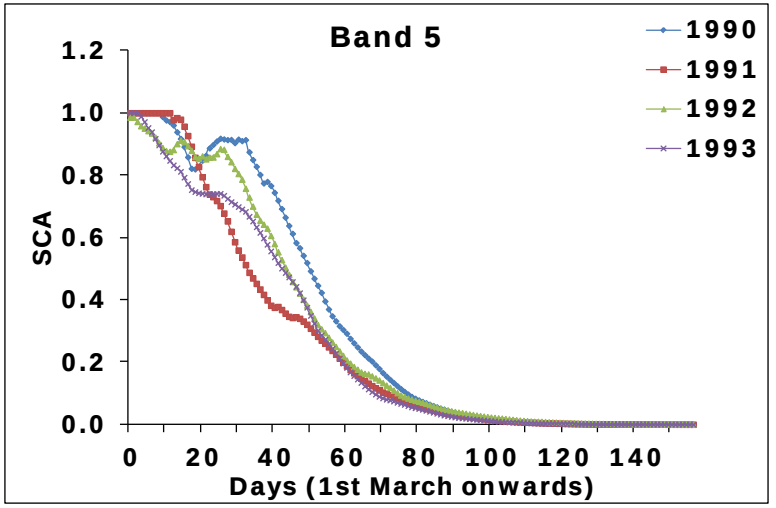

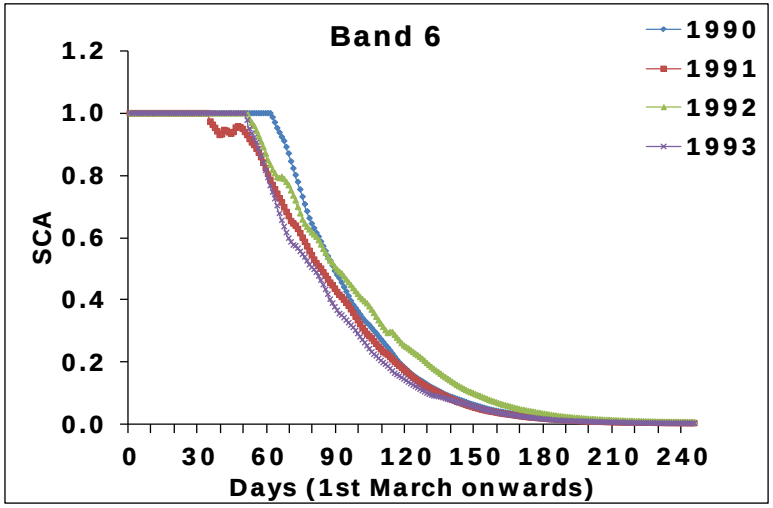

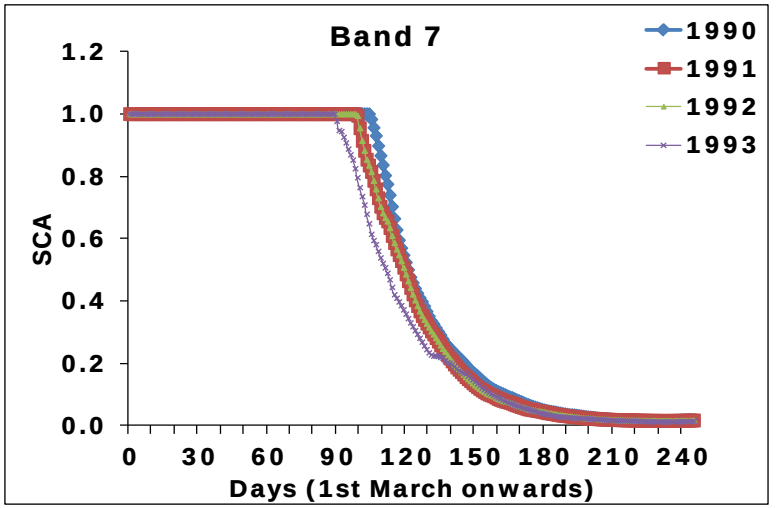

Figure 4.10: Snow cover depletion curves (SDCs) for the years 1990-1993

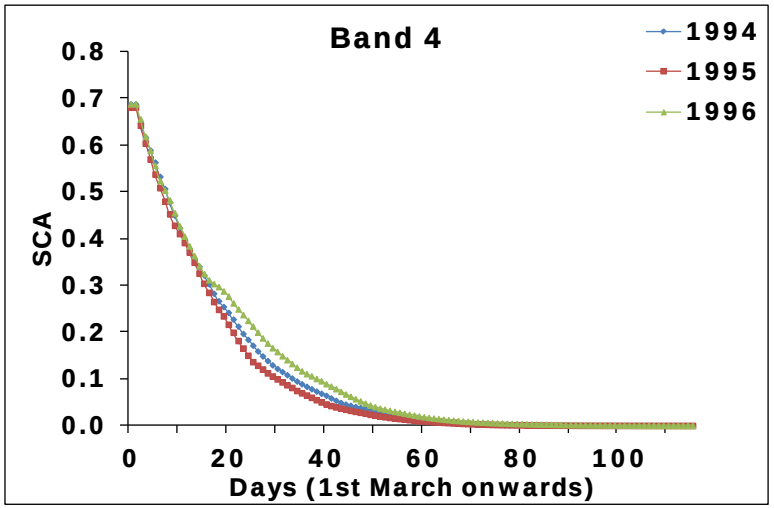

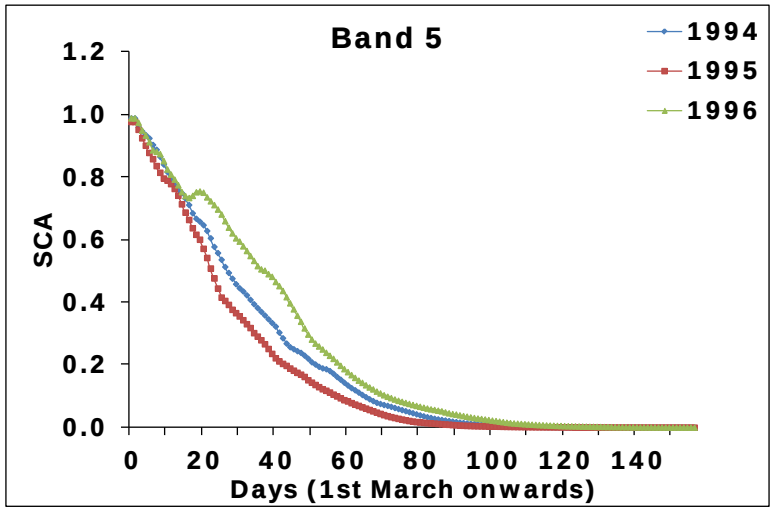

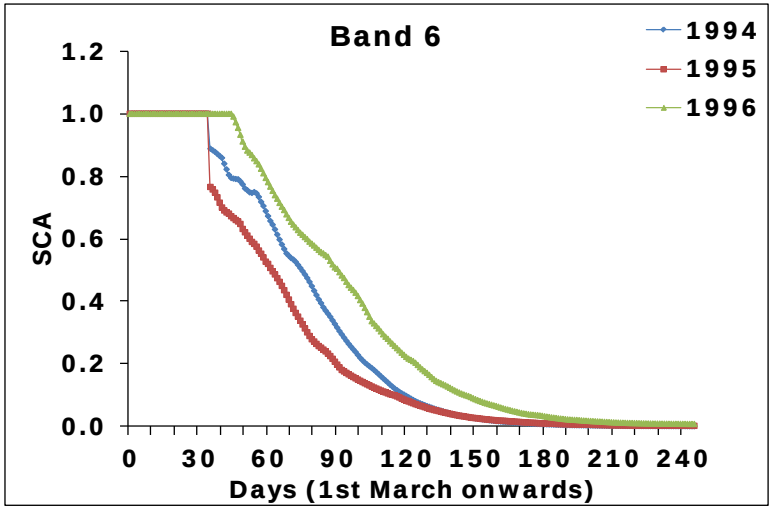

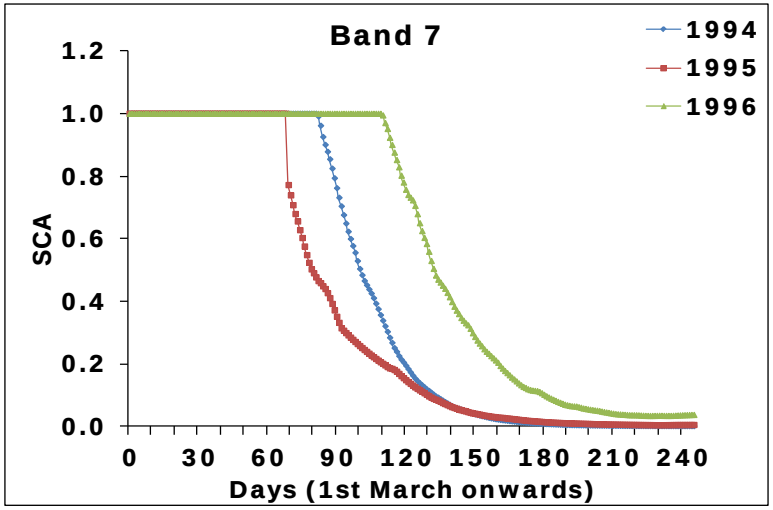

Figure 4.11: Snow cover depletion curves (SDCs) for the years 1994-1996

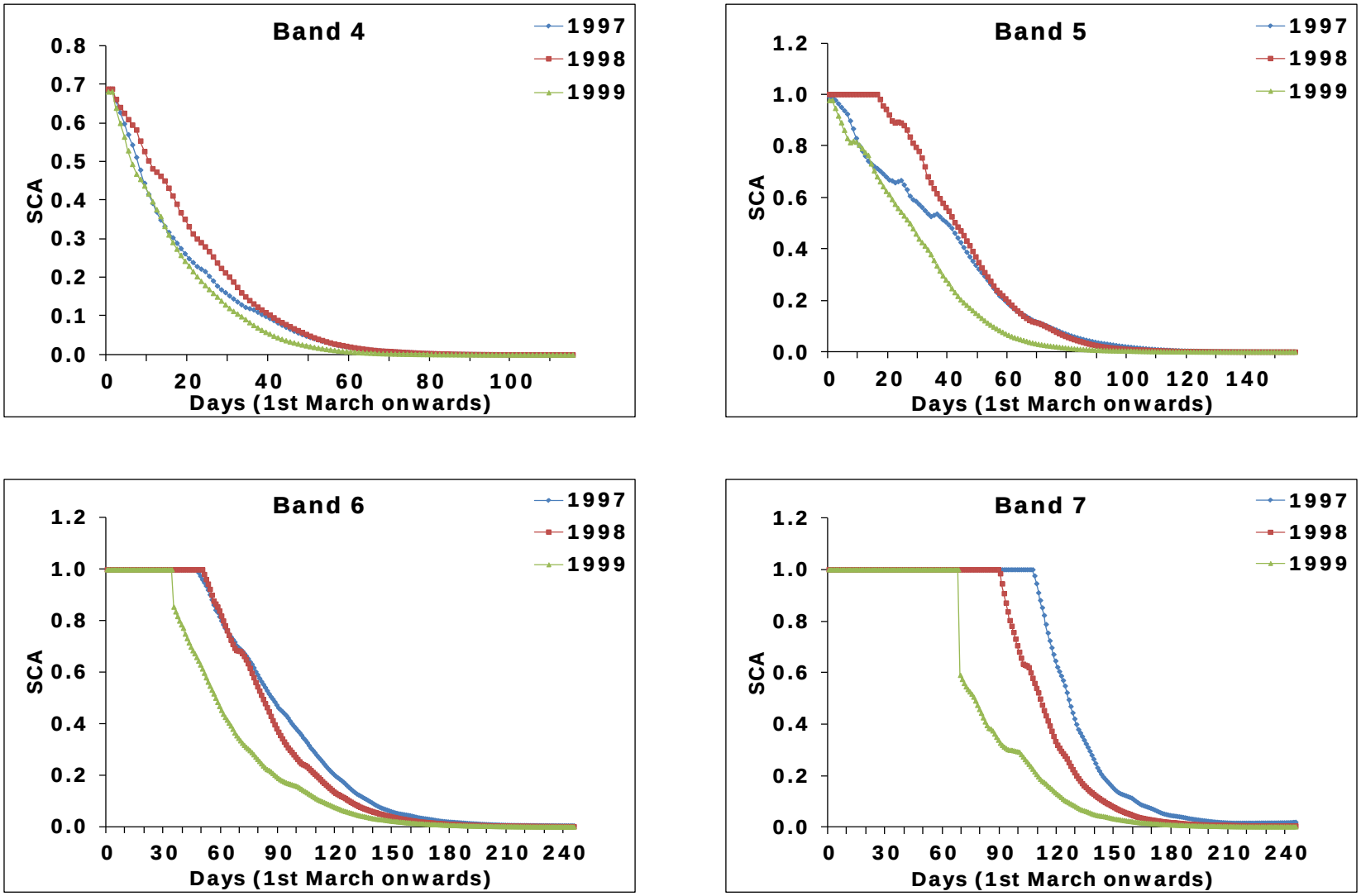

Figure 4.12: Snow cover depletion curves (SDCs) for the years 1997-1999

The SCA estimated using this relationship has been checked for one year i.e. 2001 and found that it matches well with the observed SCA as shown in Figure 4.13. In order to simulate the runoff in a new climate, it is necessary to determine a new set of SDC that would result from higher temperature. There will be a shift of the conventional SDC for a new warmed climate because in this situation, a greater part of the winter precipitation will be rain instead of snow. The relationship developed as above can be used to prepare modified SDC.

In the above relationship, change in temperature due to climate change will be considered to estimate the corresponding snow cover area. For example, if temperature is increased by 1°C, then corresponding SDC will advance by about 15-20 days. In this study, SDC for hypothetical climate change scenarios such as increase of temperature by 1 and 2°C have been generated. The new SDC generated for zone 4, 5, 6 and 7 are shown in figures 4.14 to 4.16 for increase of 1°C temperature while for 2°C rise SDC are shown in figures 4.17 to 4.19.

4.4 SUMMARY

The air temperature has been found as a dominating and most readily available meteorological parameter useful in snow hydrology. Since long, satellites have been in use for snow cover area estimation, but due to cloud cover and other related problems, it becomes difficult to acquire snow cover area information at regular interval. MODIS satellite data are found to be useful for studying snow cover area at a regular interval. In this study, snow cover area maps in different elevation zones for 2001-2005 have been prepared using MODIS data. The classified maps have been also compared with the snow cover maps estimated from IRS-1C/1D and AWiFS images for some selected dates.

For estimation of SCA in other years a relationship between mean daily air temperature and snow cover area have been developed. An exponential relationship has been found between SCA and cumulative mean air temperature (CMAT). The methodology adopted in this study is found to be suitable for computing the snow cover area based on observed air temperature values.

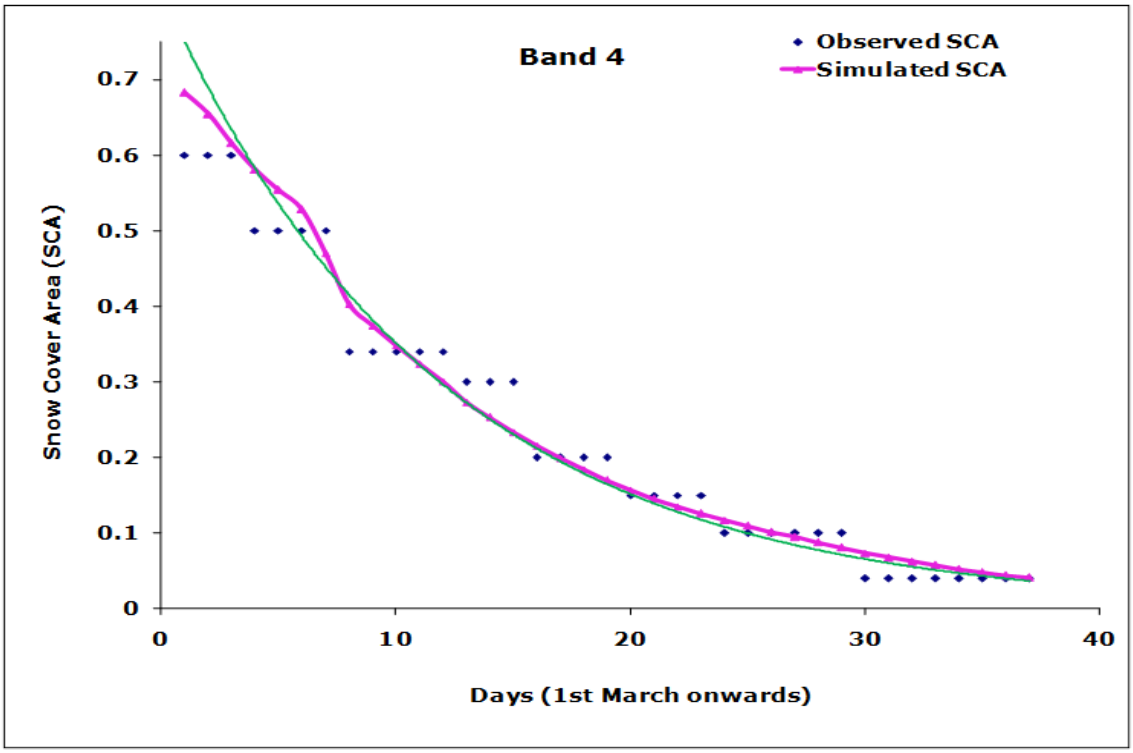

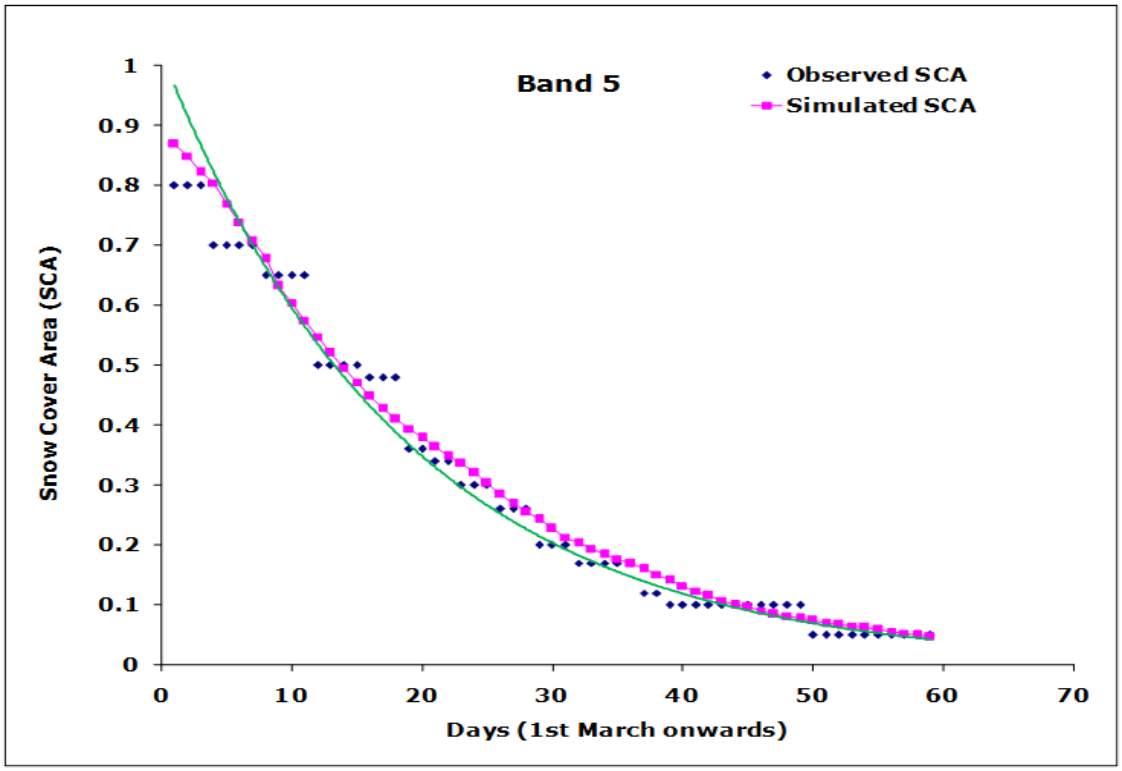

Figure 4.13: Observed and simulated SCA for band 4 and band 5 for year 2001

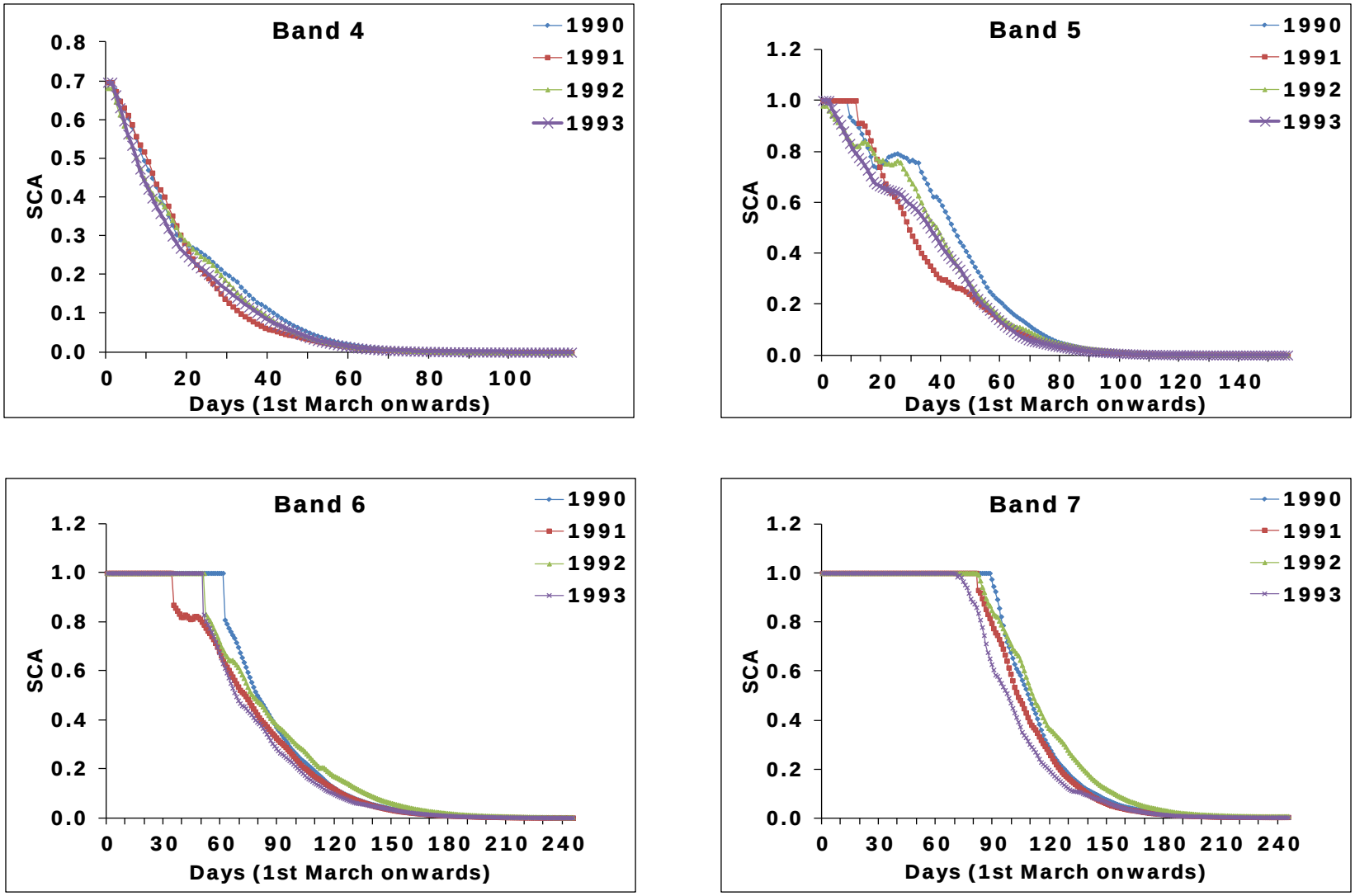

Figure 4.14: Snow cover depletion curves (SDCs) for the years 1990-1993 with 1^0C increase

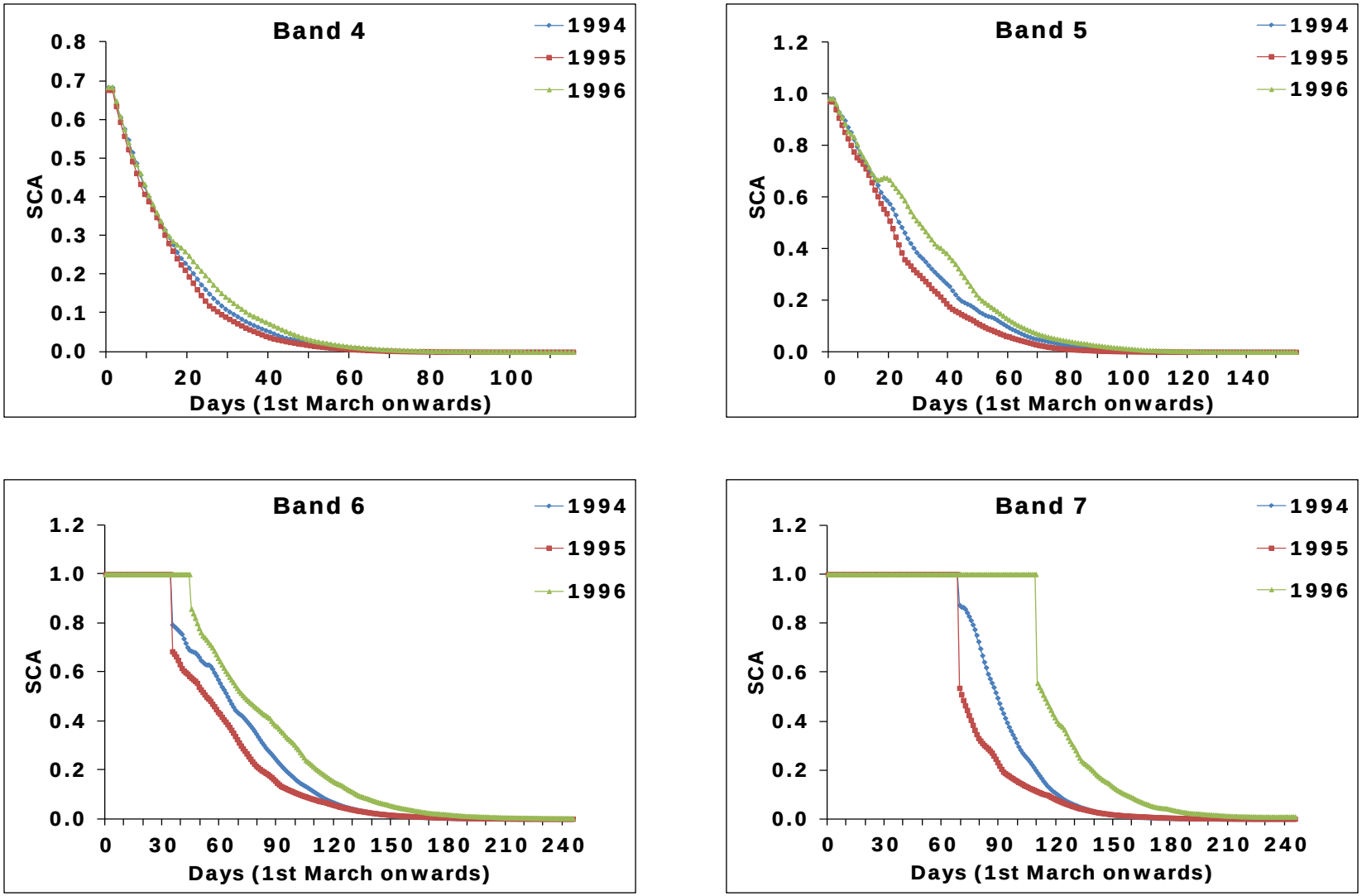

Figure 4.15: Snow cover depletion curves (SDCs) for the years 1994-1996 with 1^0C increase

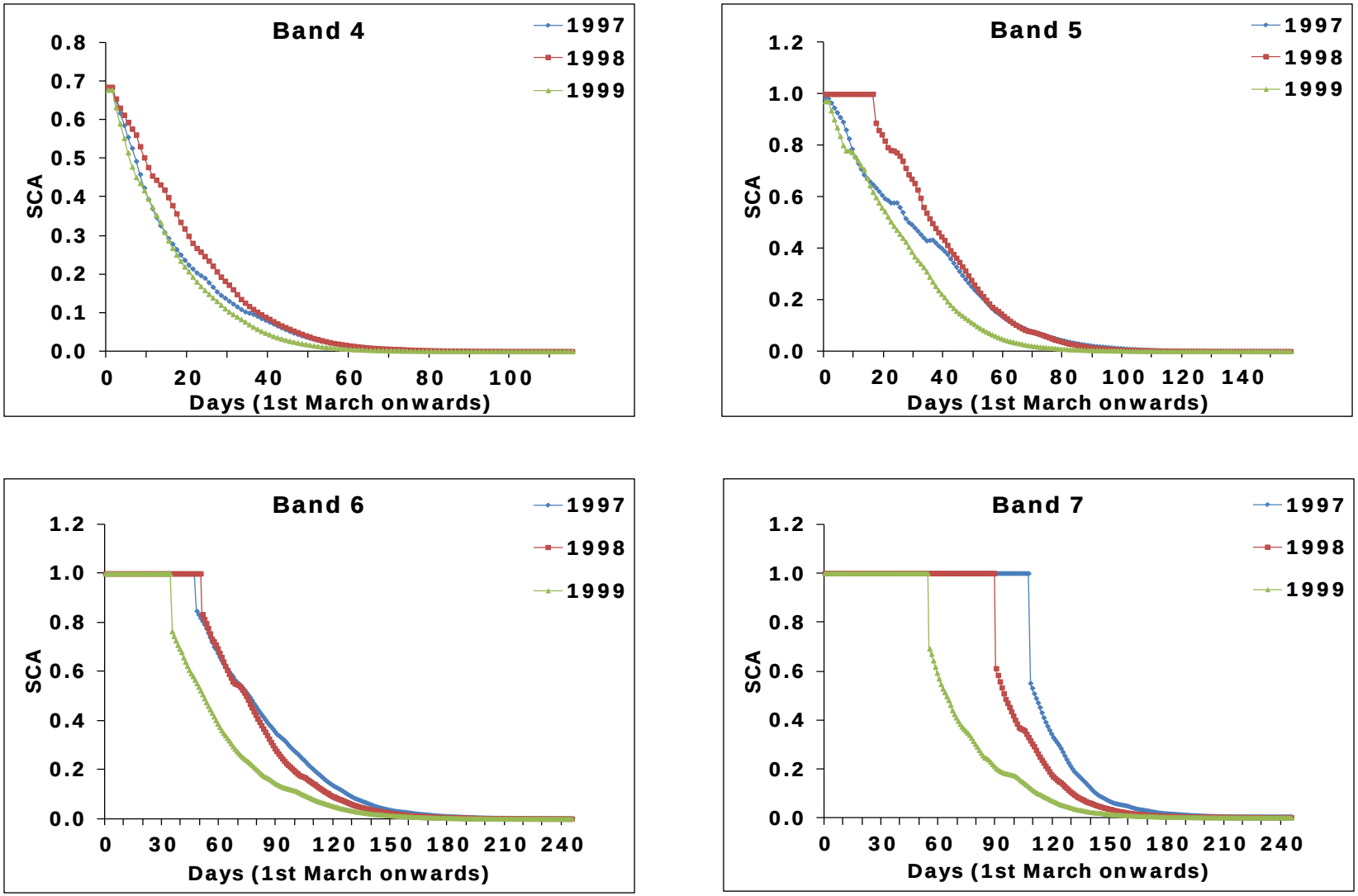

Figure 4.16: Snow cover depletion curves (SDCs) for the years 1997-1999 with 1^0C increase

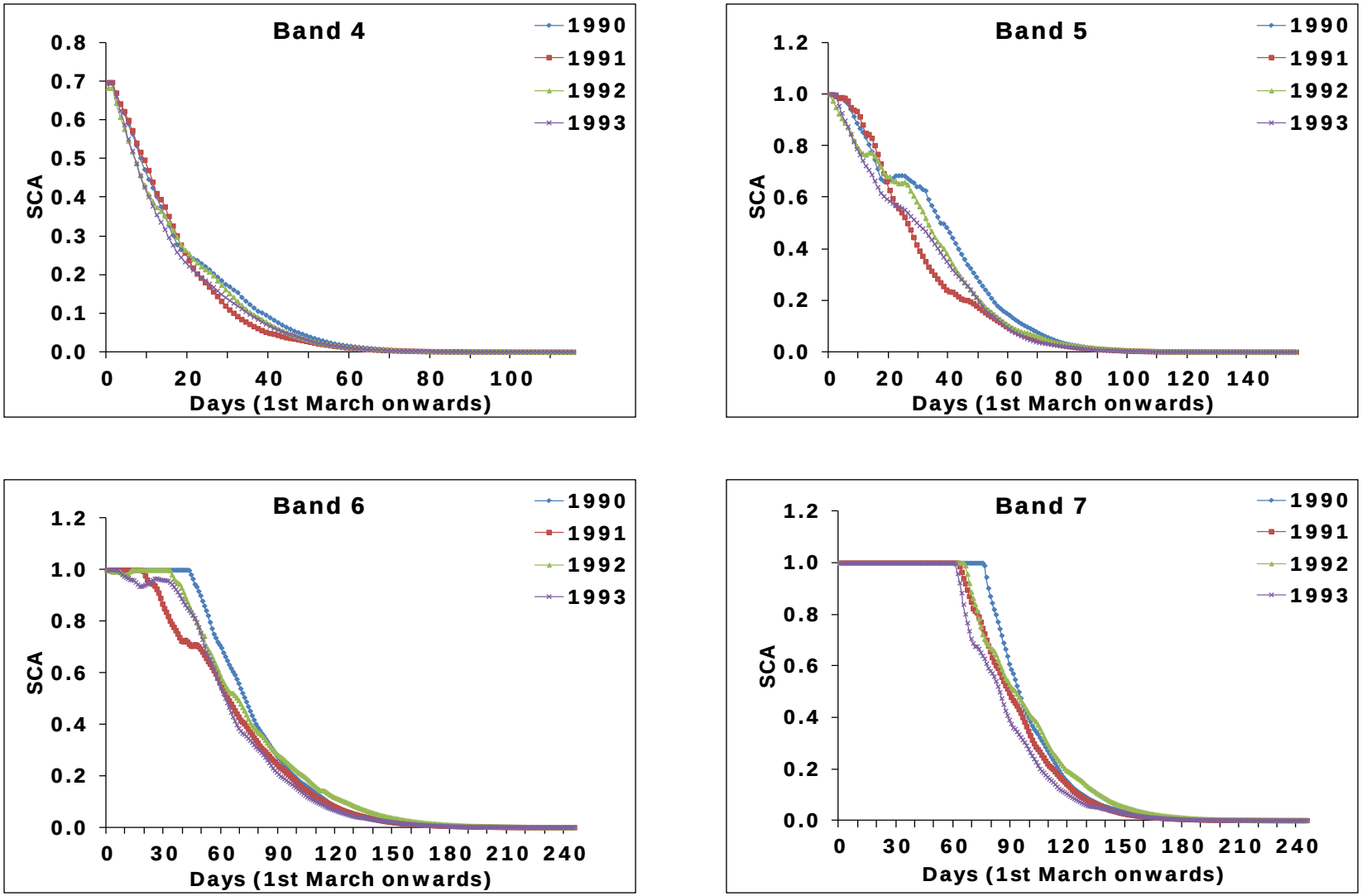

Figure 4.17: Snow cover depletion curves (SDCs) for the years 1990-1993 with 2^0C increase

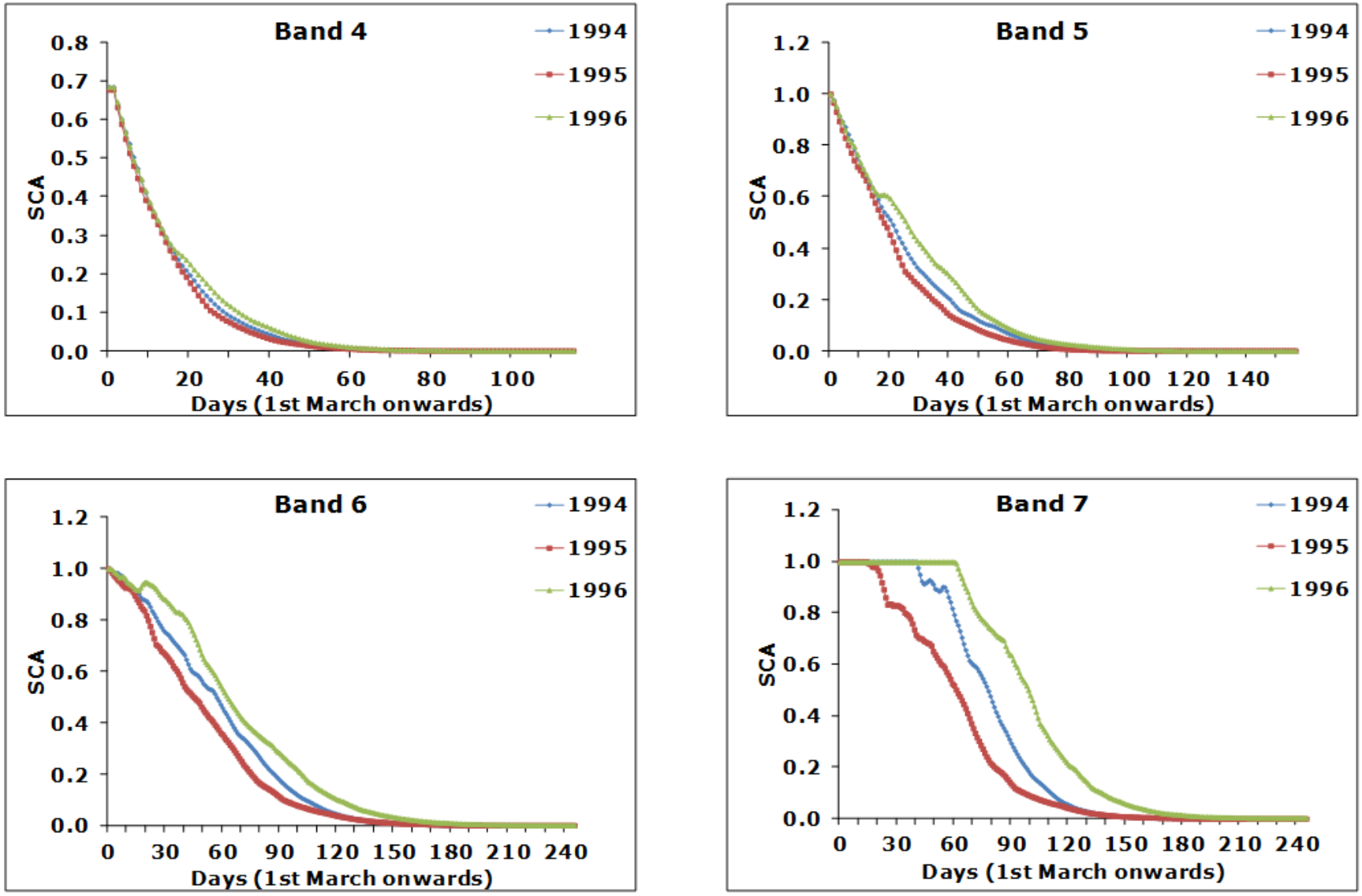

Figure 4.18: Snow cover depletion curves (SDCs) for the years 1994-1996 with 2^0C increase

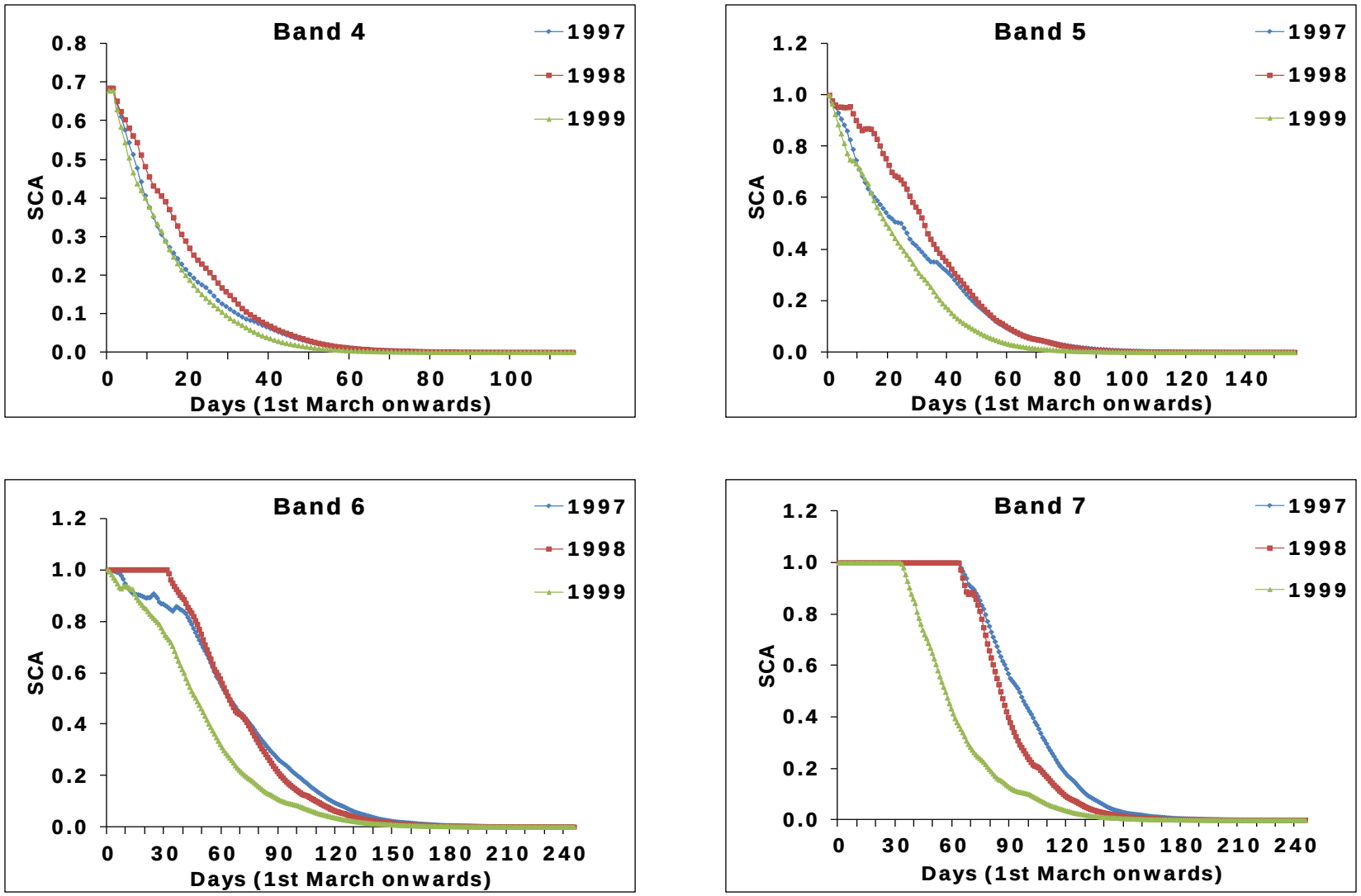

Figure 4.19: Snow cover depletion curves (SDCs) for the years 1997-1999 with 2^0C increase

Chapter 5

DETERMINATION OF TEMPERATURE LAPSE RATE

5.1 BACKGROUND

This chapter deals with the determination of Temperature Lapse Rate (TLR), an important parameter necessary for temperature-based conceptual snowmelt runoff simulation for the Beas basin. Earlier TLR was estimated from the ground based air temperature data recorded at meteorological stations. However, it is very difficult to establish meteorological stations in the complex Himalayan terrains with rugged and undulated topography and the available sparsely located network represents only local temperature. Thus, it is difficult to estimate representative TLR values and hence a fixed TLR value (=0.65 ^{o}C/100m) calculated from air temperature is commonly used in snowmelt studies. Moreover, TLR varies on seasonal and regional scales and also within different elevation zones. A very few studies have been carried for the assessment of TLR. TLR estimated from space borne satellite remote sensing provides a straightforward and consistent way to observe Land Surface Temperature (LST) over large scales with more spatially detailed information. In India one study has been carried out to assess TLR for Satluj basin using LST data. In this study variation of TLR was studied seasonally. Considering all these facets, in this study an attempt has been made to determine TLR employing satellite based MODIS-LST products for the Beas basin to see the variation of TLR seasonally as well as topographically. The USGS-DEM and MODIS-LST maps have been used to estimate TLR for different dates. Monthly, annually, seasonally and topographically varying lapse rates have been developed using these thermal satellite data for a period of nine years from 2001 to 2009.

5.2 MEASUREMENT OF LAND SURFACE TEMPERATURE

Temperature is regarded as the best index of heat transfer process allied with melting of snow. It is the prevailing temperature during precipitation which determines the type or form of precipitation reaching ground. Surface temperature is considered to be one of the most crucial parameter to estimate the effect of climate change on snow, ice and glaciers consequently affecting the streamflow of snow-fed rivers. Hence, the studies using LST information are of great importance with respect to the environmental and climate change scenarios.

In the lowest portion of earth atmosphere layer, temperature decline with an increase in altitude. This decline is called as temperature lapse rate, which is controlled by the equilibrium between heat convection from the surface and radiative cooling. The lapse rate varies with the latitude, altitude, season, and interaction between topography and weather. The lapse rate method takes into account the maximum air temperature measured at a reference station and extrapolates it over the entire basin via a functional relationship between air temperature and elevation data. This method assumes that a linear relationship exists between air temperature and elevation, and horizontal gradients are negligible due to topographic and orographic effects. This connection between temperature and altitude is essential for distinguishing the type or form of precipitation as rain or snow, reaching the ground, for precise streamflow modeling. Mostly in earlier studies in which lapse rate is one of the inputs, uniform and/or constant lapse rate have been used, which typically assume lapse rates of 6.0 or 6.5°C km^{-1} (e.g., Prentice et al., 1992; Arnold et al., 2006; Otto-Bliesner et al., 2006; Roe and O'Neal, 2010).

LST retrieved from space borne satellite remote sensing is the mean radiative skin temperature of an area of earth land surface which results from the mean balance of heating (solar) and cooling (land-atmosphere) fluxes. It is basically considered as determiner of the terrestrial thermal behavior of earth surface as it controls its effective radiating temperature. Various environmental studies and management activities of the Earth surface resources necessitate the knowledge of LST (Li and Becker, 1993). LST data is being potentially used nowadays in various studies in scientific and commercial domains for diverse applications including climate change, urban heat, crop monitoring, water management and geothermal and can provide valuable information about the physical properties of surface and climate, playing foremost role in many of the environmental processes (Dousset and Gourmelon, 2003; Weng, et al., 2004). Numerous researchers have used the knowledge of LST in many applications which rely on LST such as evapo-transiration modeling (Serafini, V.V, 1987; Bussieres et al., 1990), soil moisture estimation (Price J.C, 1990) and number of studies for climatic, hydrological, bio-geo-chemical and ecology (Schmugge, T.J and Andre, 1991; Running et al., 1994).

It is crucial to have reliable access of surface temperature estimates over the large spatio-temporal scales (Bohui Tang et al., 2008) as it is difficult to monitor and acquire such continuous information especially in rugged mountainous regions where meteorological stations are sparse and/or are irregularly distributed. For snowmelt runoff studies, air temperature data from meteorological station are spatially interpolated based on TLR equation

(Singh, 1991). Traditional LST data are collected by meteorological observation and then interpolated to gridded data. However, in some areas, especially in remote areas, spatial interpolation cannot provide satisfactory results from point observations due to the sparsely and salutatory distributed meteorological stations. Earlier spatial interpolation technique was commonly in use because even the developed countries used the ground measurements acquired from sparsely distributed stations, separated by hundreds of kilometers over the terrain (Jain et al., 2008a). Spatial coverage of the meteorological stations is even worse in developing countries (Lakshmi et al., 2001). Moreover, the application of conventional geo-spatial interpolation techniques remains a challenging task in complex terrain (Steinacker et al., 2006).

In such complex terrain, retrieval of LST data from remote sensing satellite has proved very supportive by providing high spatial and temporal resolution data, which is consistent with repetitive coverage with ability to measure the earth's surface conditions. LST, both at regional and global scales, is a key parameter in the physics of land-surface processes. It combines all the results of surface-atmosphere interactions and energy fluxes between the atmosphere and ground (Mannstein, 1987; Sellers et al., 1988). LST derived from the satellite data after appropriate aggregation and parameterization may be utilized to validate and improve meteorological model prediction globally (Price, 1982; Diak and Whipple, 1993). Satellite remote sensing provides a straightforward and consistent way to observe LST over large scales with more spatially detailed information (Xu et al., 2013).

Remote sensing sensors are used to monitor the temperature from space, which measure the infrared radiances leaving top of the atmosphere toward the satellite in the Thermal Infrared Region (TIR) region. These radiances are the integrating result of three fractions of energy; emitted radiance from the surface of earth, upwelling radiance from the atmosphere and the downwelling radiance from the sky (Weng et al., 2004) and can be utilized to derive brightness temperature (also called black body temperatures) using Planck's law (Dash et al., 2002).

Over the time, new technologies have emerged which have ameliorated and simplified the measurement of surface temperature from space radiometry in terms of instrumentation, technique, and as well as computation. The temperature index based snowmelt runoff models are simple to understand and run (Singh, 1991). Thus, several models based on this method have been developed and are more commonly in use for snowmelt runoff simulation. Due to the varied topography in mountainous regions, mostly conceptual snowmelt runoff models are used for simulation which divides the basin into elevation bands according to the basin relief. Precise information of temperature for each elevation band is needed to run the snowmelt model. For which either, the manually measured air temperature are extrapolated based on the

TLR method (more susceptible to error) or LST maps generated from satellite data are two alternative. The TLR regionally and seasonally varies (Running et al., 1987; Aber and Federer, 1992) and also fluctuates throughout the day. Hence, region and season specific information of TLR and its variation are quiet important for temperature index snowmelt models. Consequently, keeping in view all the aspects including easy availability, cost effectiveness, high spatio-temporal, and compatibility with models, the satellite driven LST information is a better alternative for the snowmelt runoff models.

However, in Indian context, few studies using a constant value of TLR (=0.65^{0}C per 100 m) computed from the air temperature data were carried out in different catchments with varying relief (Thapa, 1980; Bagchi, 1981; Jeyram et al., 1983; Agarwal et al., 1983; Seth, 1983; Jain, 2001). But some recent studies (Jain, 2001; Haritashya, 2005) expressed the need of using the actual TLR values for improving the snowmelt runoff estimates. Singh (1991) carried out sensitivity analysis of TLR in Beas basin and observed that a difference of 1 ^{0}C in lapse rate influenced the snowmelt runoff computation by 27-37%. Due to sparse studies on TLR from the Himalayan region and necessity of appropriate knowledge of LST distribution over the time and space for better results in climate change studies. There exists a pressing need to precisely determine variation of TLR on monthly and seasonal scale for the Himalayan region.

Conversely, air temperature which is a common weather parameter is the measure of heat content of air, described as the measure of average speed or kinetic energy level of molecules being influenced by the intricate set of interactions among the biosphere, lithosphere and atmosphere. The radiation transfer, sensible heat transfer, movement of air mass, and location with respect to water bodies are the components that controls the temperature of a place (Gusso and Fontana, 2005; Ritter, 2007).

The difference between air temperature and LST varies notably with the surface water status, roughness length and wind speed. However, seasonal trends of the two variables can be correlated. A strong correlation established between LST and air temperature (Gusso and Fontana, 2005; Jain et al., 2008b). Kawashima et al., (2000) reported a good correlation between the two variables with a standard error of 1.4 ^{0}C to 1.8 ^{0}C. Raj and Fleming (2008) observed a difference of 1- 2 ^{0}C between the observed field data and the retrieved data. Hence , the MODIS-LST retrieved from satellite data are the considered best alternative as they provides a continuous dataset with precise radiometric calibration (Jain et al., 2008b) for the snowmelt runoff modeling.

5.3 LST RETRIEVAL FROM REMOTE SENSING DATA

Land Surface Temperature (LST) is a key parameter for snowmelt runoff studies in the Himalayan region. LST estimated from the satellite technology can be determined from the energy thermal sensors receiving the thermal emissions in wavelength region (10.5-12.5 μm) emitted from land surface. Normally, LST is defined as the skin temperature of ground surface. An urgent need is pointed out for long-term remote sensing based LST (skin temperature) data in studies related to global warming, to improve the conventional limits of 2 meter World Meteorological Organization (WMO) surface air temperature observations (IPCC, Houghton et al., 2001). LST for the bare soil, is the soil surface temperature while for snow, it is the snow surface temperature. Space based satellite remote sensing technology provides a better choice to map this parameter at large scale. Various efforts have been made from time to time for retrieval of LST information from remote sensing data. To acquire this parameter from satellite in the thermal infrared wavelength region, it is essential take into account emissivity and to correct the signals recorded for the perturbations created by the atmosphere along the path between the surface of Earth and the sensor (Becker and Li, 1990). Ever since the thermal data had become accessible, lots of efforts were made to retrieve the LST data from the space borne satellite data and algorithms were proposed to deal with varied sensors onboard diverse satellites. Based on the channels used by the sensors, these algorithms were broadly classified into three categories; single-channel methods, multi-channel methods, and multi-angle methods. Mainly, two developed approaches are used to retrieve LST from the multispectral TIR images (Schmugge et al., 1998). The first approach makes use of a radiative transfer equation for correcting the at-sensor radiance to surface radiance, followed by emissivity model for separating the surface radiance into temperature and emissivity (Schmugge et al., 1998, Friedl, 2002) while the second approach enforces the split–window technique for sea surfaces to land surfaces with assumption that the emissivity is similar in the channels used for split-window (Dash et al., 2002). The remote sensing based thermal infrared (TIR) data is associated directly to the LST through the radiative transfer equation (Li et al., 2013).

The split-window was firstly proposed by McMillin in 1975 to estimate the temperature of sea surface from the remote sensing data. Subsequently, a variety of split-window algorithms were evolved and customized to retrieve LST from the satellite sensors with spatial resolution varying from several hundred meter to several kilometers having quasi temporal resolution. Presently, most of the algorithms are widely and effectively applied to retrieve LST from the satellite sensors of Advanced Very High Resolution Radiometer (AVHRR) and MODIS. The

split-window algorithms are generally applied to correct the atmospheric influences of satellite imagery acquired by two contiguous thermal channels positioned in atmospheric window (between 10 μm and 12 μm). The initial issue in determining LST is to translate the satellite radiance into surface brightness temperature. In order to retrieve brightness temperature, the channels need to be calibrated. The two adjacent thermal infrared channels 4, 5 and 31and 32 of NOAA-AVHRR and MODIS are used respectively for retrieving the brightness temperature. These retrieved brightness temperatures are thereafter converted into LST using split-window method. Yu et al. (2008) provided the spectral and spatial resolutions of AVHRR and MODIS presented in Table 5.1.

Table 5.1: Spectral and spatial resolutions of AVHRR and MODIS Thermal Infrared Bands

AVHRR-3			**MODIS**		
Band	Spectral Bandpass* (μm)	HSR#	Band	Spectral Bandpass (μm)	HSR
4	10.300-11.300	1100	31	10.780-11.280	1000
5	11.500-12.500	1100	32	11.770-12.270	1000

* Full width Half Maximum positions # HSR= Horizontal Spatial Resolution at nadir, commonly referred to as pixel size (per side)

Several equations have been derived by many researchers to be used for retrieving LST (Price, 1984; Becker and Li, 1990; Sobrino et al., 1994; Vidal, 1991; Ulivieri et al., 1992; Wan and Dozier, 1996; Caselles et al., 1997; Yu et. al., 2009). Due to different atmospheric absorption characteristics of two channels in infrared band, the split-window algorithm facilitates to correct or remove the atmospheric effect. However, accuracy of split-window algorithm depends upon the magnitude of difference between the two surface emissivities in the channels (Becker, 1987). (Wan and Dozier, 1996) proposed a generalized split-window algorithm for the retrieval of LST from MODIS products, is expressed as:

$$T_s = C + \left(A_1 + A_2 \frac{1-\varepsilon}{\varepsilon} + A_3 \frac{\Delta\varepsilon}{\varepsilon^2} \right) \frac{T_{31} + T_{32}}{2} + \left(B_1 + B_2 \frac{1-\varepsilon}{\varepsilon^2} + B_3 \frac{\Delta\varepsilon}{\varepsilon^2} \right) \frac{T_{31} - T_{32}}{2}$$

$$\varepsilon = (\varepsilon_{31+}\varepsilon_{32})/2$$

$$\Delta\varepsilon = \varepsilon_{31} - \varepsilon_{32}$$

where, Ts =LST, T_{31} and T_{32} = MODIS band 31 and 32 brightness temperature.
ε_{31} and ε_{32} = MODIS band 31 and 32 surface emissivity. A1, A2, A3 B1, B2, B3 and C are regression coefficients.

Various investigations have been conducted to retrieve LST information using TIR radiations emitted from surfaces by applying split-window algorithm (Price, 1984; Becker and Li, 1990; Prata and Platt, 1991; Coll et al., 1994; Coll and Caselles, 1997; Sobrino and Raissouni, 2000; Jain et al., 2008b; Tseng et al., 2011; Zhong et al., 2011; Salama et al. 2012). Barsi et al. (2003) used single channel algorithm to estimate LST utilizing Landsat images. Sobrino et al., (2003) estimated LST from Moderate Resolution Imaging Spectroradiometer (MODIS) data using split-window algorithm. Jacob et al. (2004) compared the values of LST and emissivity obtained from data of ASTER and MODIS sensors. Jain et al. (2008b) computed lapse rate using LST maps in different seasons for Satluj river basin, western Himalayan region. Presently, two most popular remote sensing satellites; National Oceanic and Atmospheric Administration (NOAA) and Moderate Resolution Imaging Spectroradiometer (MODIS) are widely used to retrieve LST. Only few snowmelt runoff studies have been carried out in the Himalayan region by various researchers during the course of time (Thapa, 1980; Bagichi, 1981, Jeyram et al., 1983; Agarwal et al., 1983; Seth, 1983; Jain, 2001; Haritashaya, 2005; Gowswami, 2007).

MODIS has its unique ability to derive LST at both regional and global scales. Its multiple thermal infrared (TIR) channels, designed with high radiometric resolution, high calibration accuracy and dynamic ranges for a variety of land cover types; to retrieve SST, LST and atmospheric properties (Zhengming, 1999) and make it a useful product in various fields. The MODIS-LST data product is retrieved using the split-window algorithm method developed by Wan and Dozier (1996). The temperature recorded by the sensors is in Kelvin with view angle depend algorithm applied to direct observations. The split window algorithm makes use of MODIS bands 31 and 32 at 11 and 12 microns respectively.

The information of precise TLR value for snowmelt runoff modeling is of paramount importance for Himalayan region especially in Beas basin with highly varied topography with

limited meteorological observatories. In the present study, variation of temperature lapse rate has been determined seasonally as well as topographically using MODIS-LST maps.

5.4 TLR ESTIMATION

TLR estimation mainly requires two types of satellite dataset which comprises the DEM and LST map. The GTOPO30 DEM with a horizontal grid spacing of 30 arc sec (approx. 1 Km) and MODIS11A2 for LST maps have been downloaded. The satellite data has to be processed before commencing the analysis. The projection parameters of DEM were in Geographic Lat/Long with WGS84 as spheroid and Datum. The MODIS-LST maps were available in HDF file format with the sinusoidal projection and contain 12 SDSs in a single downloaded HDF file. Out of the 12 SDS of MOD11A2 products, the layer MODIS _LST_Day_1km and MODIS_LST_Night_1km were used in this study.

Before using the two dataset, they were brought to a common projection system. For this the LST maps were converted from HDF file format into img raster format and were then re-projected to Geographic Lat/Long with datum-WGS84 using model maker in ERDAS Imagine. All the MODIS data products were found to be very accurately geo-referenced. After re-projection of images, the Beas basin boundary was used to extract Area of Interest (AOI) from DEM and LST maps for years 2001-2009. The average LST maps were prepared from the two SDS. Further, using average LST map and GTOPO30 DEM, TLR was determined for different periods during the years 2001 to 2009. The methodology has been shown in Figure 5.1.

To better understand the mathematical relation between the LST (dependent variable) and elevation (independent variable), regression analysis was performed. The initial step involved was to plot the two variables in two dimensions as a scatter plot. The scatter plot provides an opportunity to have visual inspection of the data prior to running a regression analysis. The LST values obtained from MODIS were plotted against elevation, as shown in Figure 5.2 to 5.5. It is obvious from the scatter plots that as elevation increases, temperature decreases linearly.

The least square method has been applied to obtain the equations of regression or best fit line. The generalized equation of the regression or the best-fit line is represented as follows:

$$Y = -aX + b \tag{5.1}$$

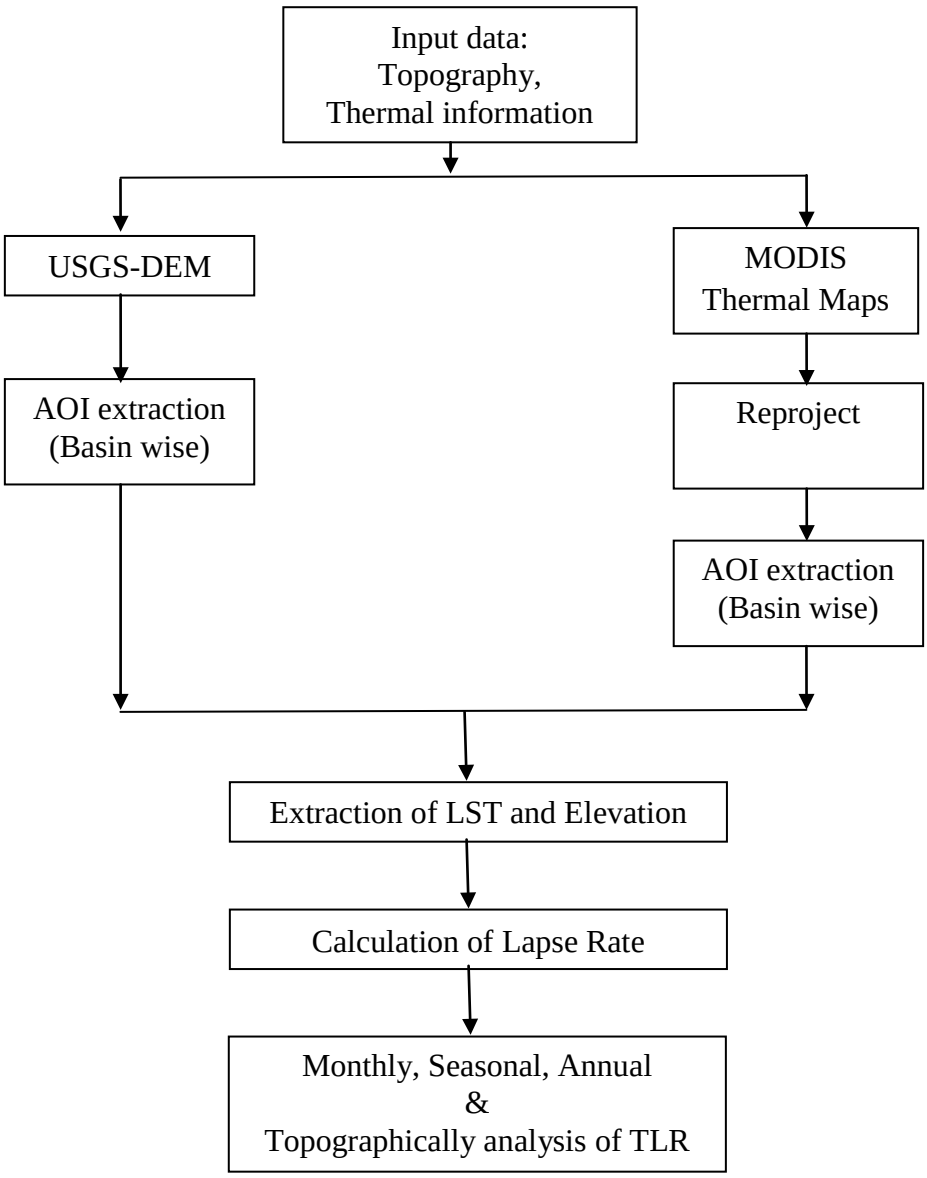

Figure 5.1: Flowchart for determining the TLR for the Beas basin

where, X= values of elevation, Y= values of temperature, –a= slope of a straight line. Negative slope of line indicates that there exists an inverse relationship between the elevation and LST. The computed coefficient of determination (R^2) values for the scatter plots signify the fraction of initial variance accounted for the relationship.

The R^2 value ranges from 0 to 1. If the value of R^2 is 1 then a good correlation is indicated between the variables whereas zero value shows a poor relation among them. For the Beas basin, R^2 values ranging from 0.66 and 0.92 were attained in case of LST from MODIS-LST maps which clearly indicate that a good negative linear correlation between elevation and LST.

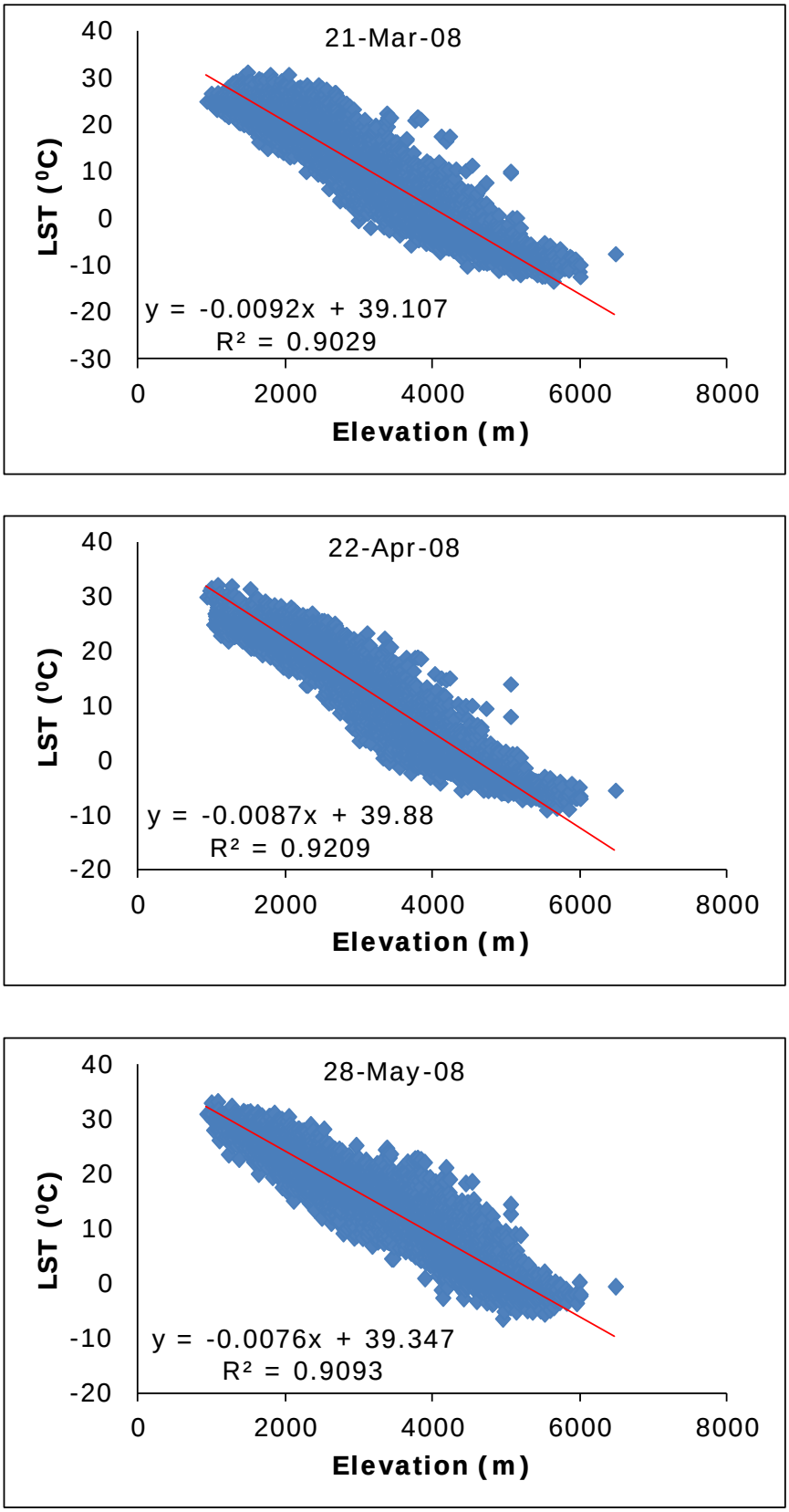

Figure 5.2: Scatter plots showing the relationship between elevation and MODIS- LST for pre-monsoon season

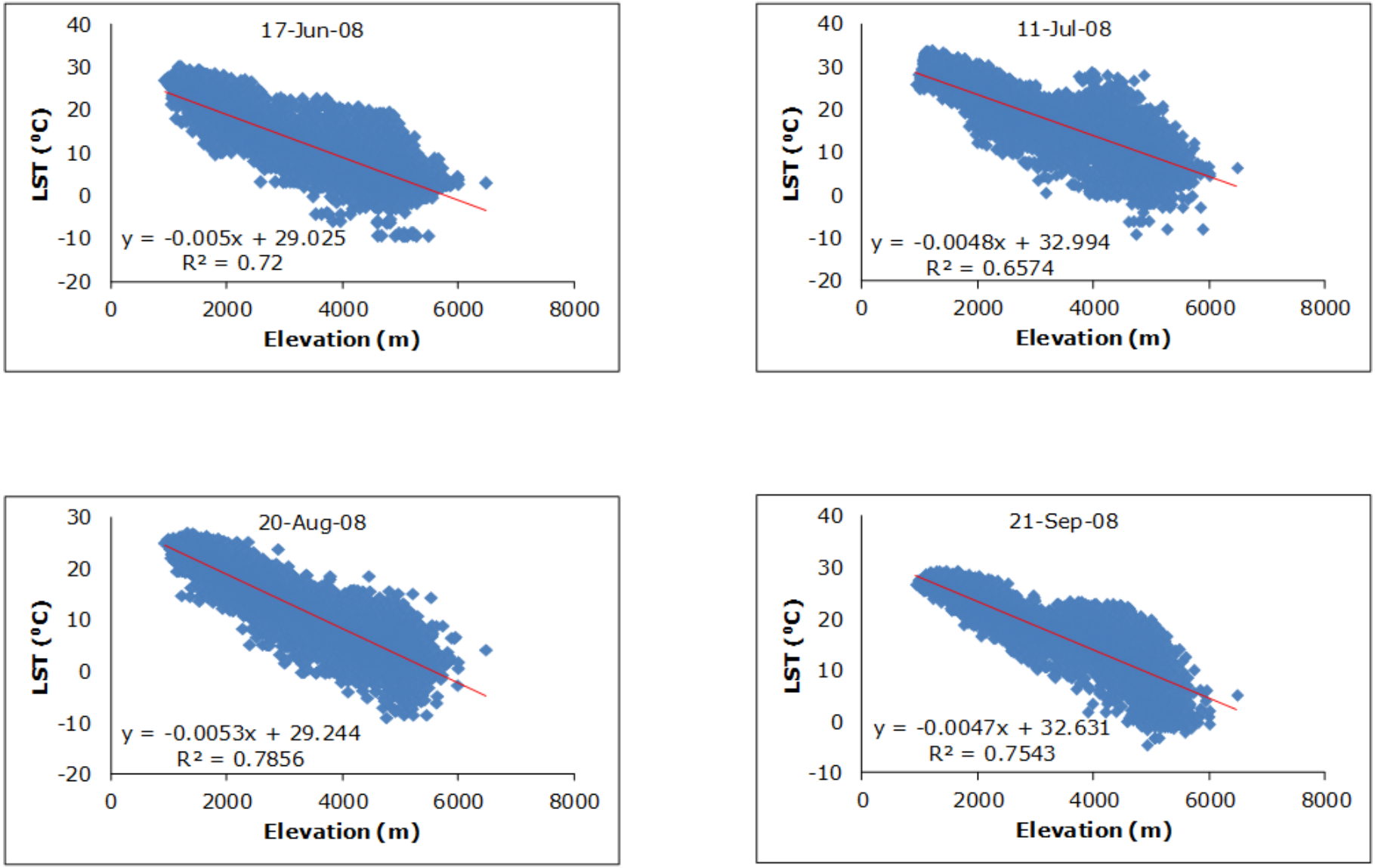

Figure 5.3: Scatter plots showing the relationship between elevation and MODIS-LST for monsoon season

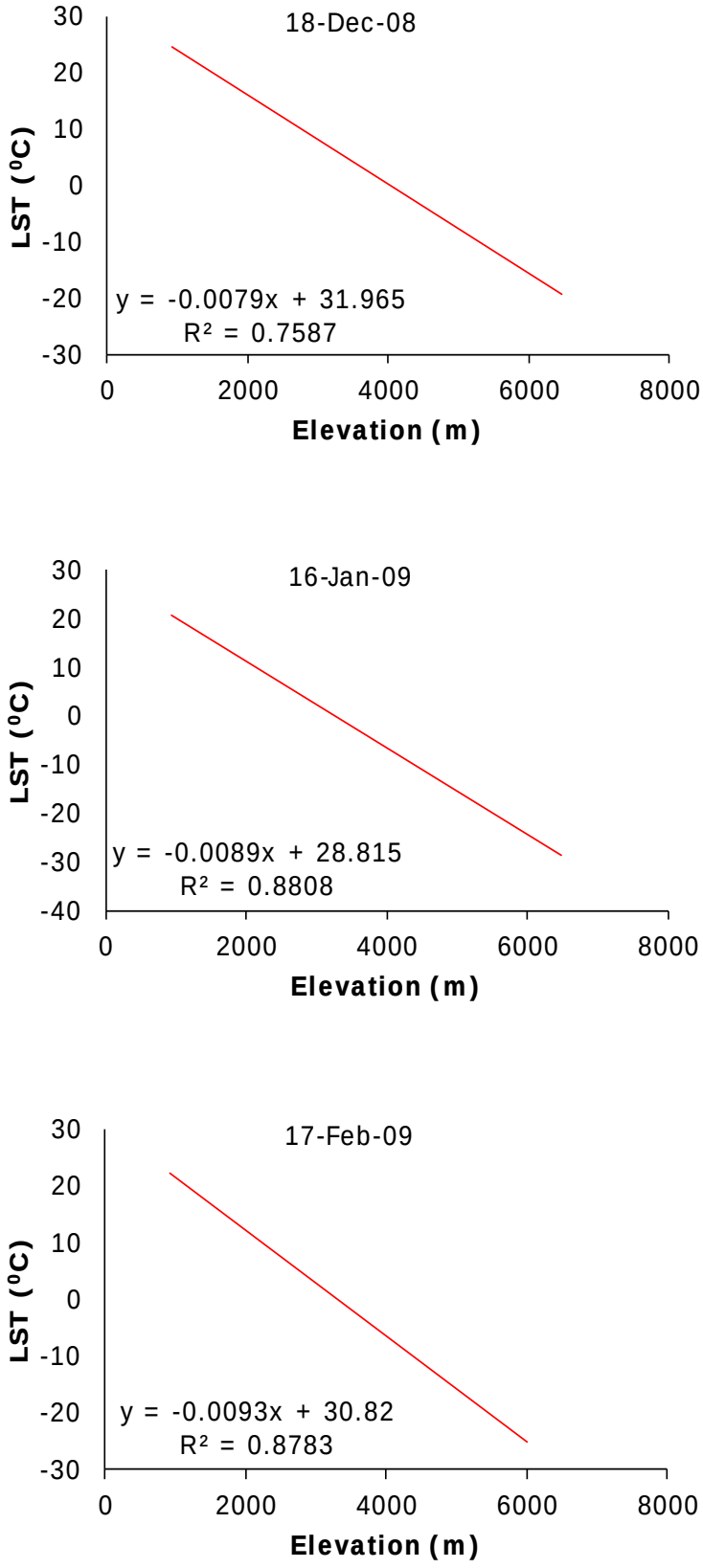

Figure 5.4: Scatter plots showing the relationship between elevation and MODIS-LST for winter season

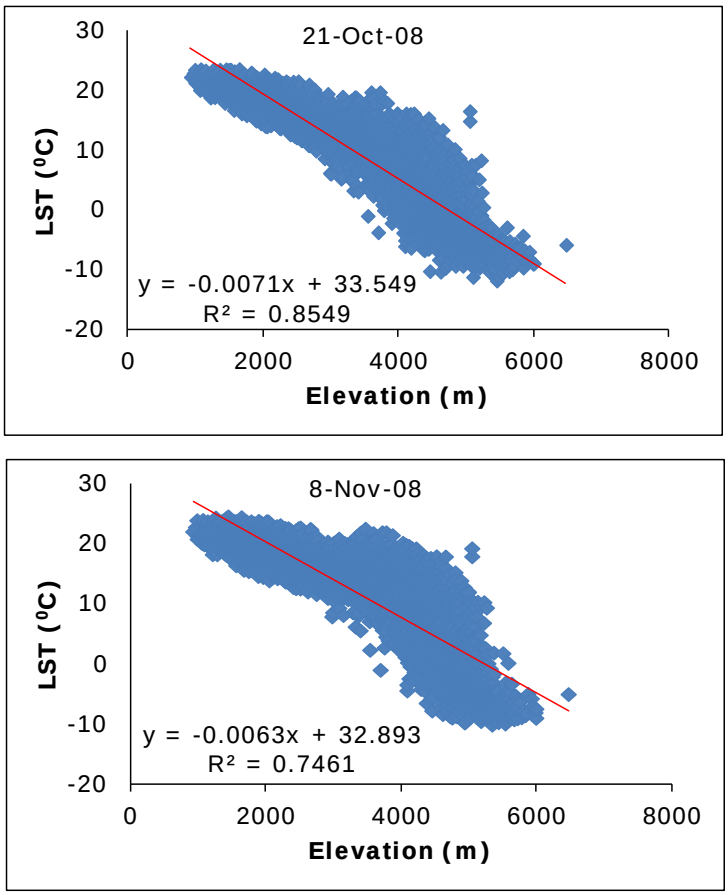

Figure 5.5: Scatter plots showing the relationship between elevation and MODIS-LST for post-monsoon season

The present study obviously exhibits an inverse linear correlation between LST and elevation. The slope of the equations is equal to the lapse rate. It equals the change in LST for each unit change in elevation. Since the slope of the best fit line is negative, LST decreases with increase in elevation. TLR is however not a constant phenomenon but changes at regional and seasonal scale. According to Bolstad et al. (1998), TLR estimated from air temperature data shows slightly seasonal trends and averaged 0.4 to 1.0°C/100 m when the maximum temperature was considered. Monthly TLR values have been estimated for the years 2001 to 2009. The summary of monthly mean values of TLR for each month in all the years for the Beas basin is given in Table 5.2. From this table, it is observed that TLR values during this period varies from 0.37 to 0.93°C/100 m and the monthly average value ranging between 0.4 to 0.82 °C/100 m. The maximum TLR value was obtained for the month of February-March whereas minimum for the month of August. Further, on the basis of this monthly data base, the TLR has been computed for different seasons and annually. The prominent and consistent variations have been observed in the basin during the study period.

Table 5.2: Monthly Temperature Lapse Rate (TLR) values in the Beas basin during the period 2001-2009

S. No	Months	January	February	March	April	May	June	July	August	September	October	November	December
1.	2001	-0.0085	-0.0090	-0.0081	-0.0085	-0.0086	-0.0079	-0.0056	-0.0042	-0.0057	-0.0063	-0.0078	-0.0083
2.	2002	-0.0079	-0.0077	-0.0084	-0.0080	-0.0078	-0.0058	-0.0045	-0.0041	-0.0054	-0.0061	-0.0073	-0.0077
3.	2003	-0.0076	-0.0089	-0.0070			-0.0063		-0.0043	-0.0039	-0.0048	-0.0070	-0.0081
4.	2004	-0.0072	-0.0079	-0.0083	-0.0071		-0.0055	-0.0044	-0.0037	-0.0038		-0.0073	-0.0077
5.	2005	-0.0079	-0.0071	-0.0078	-0.0079	-0.0079	-0.0075	-0.0050	-0.0038	-0.0044	-0.0056	-0.0062	-0.0070
6.	2006	-0.0084	-0.0080	-0.0085	-0.0079	-0.0072	-0.0063	-0.0051	-0.0047	-0.0044	-0.0054	-0.0072	-0.0082
7.	2007	-0.0086	-0.0078	-0.0080	-0.0085	-0.0067	-0.0064	-0.0042	-0.0042	-0.0046	-0.0067	-0.0060	-0.0082
8.	2008	-0.0082	-0.0082	-0.0093	-0.0082	-0.0078	-0.0054	-0.0039	-0.0046	-0.0053	-0.0067	-0.0065	-0.0079
9.	2009	-0.0085	-0.0090	-0.0081	-0.0085	-0.0086	-0.0079	-0.0053	-0.0042	-0.0057	-0.0063	-0.0078	-0.0083

The TLR was estimated for four seasons namely winter (December-February), pre-monsoon (March-May), monsoon (June-September) and post-monsoon (October-November) and given in Table 5.3. Graphically, TLR values for four seasons are shown in Figure 5.6.

Table 5.3: Seasonal and annual TLR for the Beas basin

Year	Pre-monsoon (M-A-M)	Monsoon (J-J-A-S)	Post-monsoon (O-N)	Winter (D-J-F)	ANNUAL
2001	-0.00841	-0.00584	-0.00704	-0.00797	-0.00737
2002	-0.00806	-0.00493	-0.00669	-0.00806	-0.00671
2003	-0.00695	-0.00483	-0.00588	-0.00773	-0.00642
2004	-0.00769	-0.00434	-0.00732	-0.00756	-0.00629
2005	-0.00787	-0.00518	-0.00590	-0.00779	-0.00650
2006	-0.00789	-0.00510	-0.00629	-0.00821	-0.00678
2007	-0.00772	-0.00484	-0.00632	-0.00817	-0.00665
2008	-0.00843	-0.00482	-0.00659	-0.00844	-0.00683
2009	-0.00841	-0.00576	-0.00704	-0.00818	-0.00734

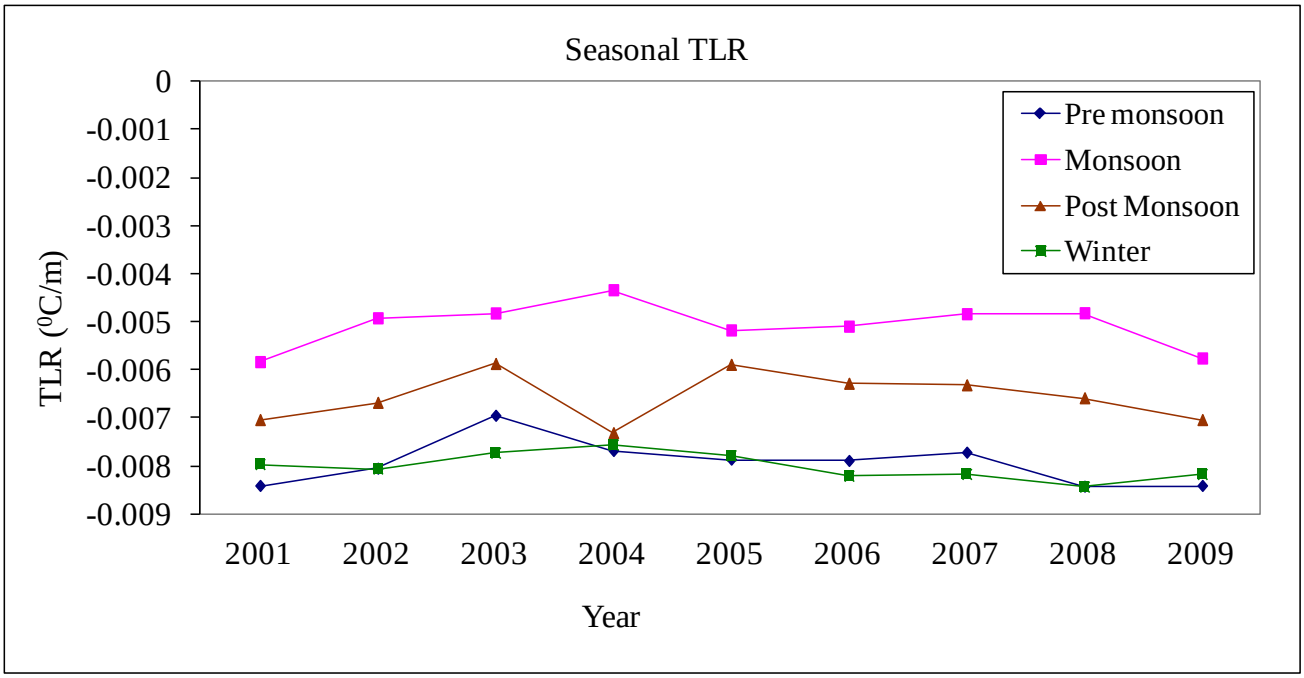

Figure 5.6: Seasonal TLR for the Beas basin during 2001-2009

On an average for all the years, TLR was found to be 0.80°C/100m for the winter season, during pre-monsoon it was 0.79°C/100m, during monsoon 0.51 °C/100m and during post monsoon the TLR was 0.66 °C/100m whereas annual TLR value was found to be 0.68 °C/100m. Figure 5.6 clearly shows that the TLR varies during different seasons with lowest values during the monsoon season which suggests that it is not appropriate to use constant lapse rate for snowmelt models in the Himalayan basins.

To see the variation of lapse rate with respect to topography, the lapse rate has been computed for three elevation ranges i.e. 1000-3000 m, 3000-6000 m and 1000-6000 m. For each month, the values of TLR for three zones are shown in Table 5.4. From this table, it can be seen that the lapse rate for lower altitude (1000-3000m) is relatively low as compared to higher altitude (3000-6000m). In the lower elevation zone, during July to December, the value of lapse rate varies between 0.40 to 0.52°C/100m while for higher elevation zones, it is low in July-September i.e. 0.46 to 0.63°C/100 m but it is high during October-December. It means that the lapse rate value is generally low in lower altitude zones.

5.5 SUMMARY

LST has been computed for the Beas river basin using MODIS-LST Products and lapse rate of LST was computed for nine years from 2001 to 2009. MODIS-LST maps are available

on internet which makes it economically more suitable. There are many advantage of this technique of estimating lapse rate using LST maps and DEM. The LST being a continuous data is well representative of the terrain. Moreover, being mapped by the satellite sensors, it is readily available throughout the year except cloudy period.

Besides, the technique of estimating the lapse rate is less time consuming. The lapse rate in case of LST varies from 0.37°C/100 m to 0.93°C/100 m. Therefore the range of lapse rate obtained from the present study can be used with confidence in snowmelt runoff and other studies. This approach can be used for estimation of seasonal and regional variation in TLR of LST. The lapse rate was found to be lowest during monsoon season and it was lower in the lower altitudes than in higher altitudes.

Table 5.4: Values of TLR for the three zones in the study area

Elevation Range	Months	January	February	March	April	May	June	July	August	September	October	November	December
1000m-3000m	2000	0.00	0.00	0.00	0.00	0.00	-0.53	-0.40	-0.41	-0.50	-0.39	-0.51	-0.39
1000m-3000m	2001	-0.52	-0.58	-0.74	-0.75	-0.57	-0.50	-0.33	-0.30	-0.37	-0.42	-0.42	-0.49
1000m-3000m	2002	-0.54	-0.67	-0.75	-0.64	-0.61	-0.50	-0.50	-0.41	-0.45	-0.39	-0.32	-0.29
1000m-3000m	2003	-0.40	-0.76	-0.64	0.00	0.00	-0.62	0.00	-0.30	-0.55	-0.40	-0.37	-0.54
1000m-3000m	2004	-0.64	-0.63	-0.63	-0.57	0.00	-0.62	-0.96	-0.41	-0.46	0.00	-0.40	-0.39
1000m-3000m	2005	-0.60	-0.61	-0.67	-0.67	-0.60	-0.70	-0.64	-0.53	-0.45	-0.42	-0.37	-0.31
1000m-3000m	2006	-0.60	-0.62	-0.74	-0.71	-0.62	-0.61	-0.55	-0.58	-0.44	-0.42	-0.50	-0.51
1000m-3000m	2007	-0.44	-0.67	-0.79	-0.66	-0.53	-0.71	-0.61	-0.60	-0.49	-0.47	-0.29	-0.50
1000m-3000m	2008	-0.64	-0.76	-0.75	-0.76	-0.73	-0.61	-0.61	-0.59	-0.46	-0.38	-0.29	-0.42
1000m-3000m	2009	-0.71	-0.81	-0.82	-0.72	-0.72	-0.73	-0.68	-0.76	-0.48	-0.51	-0.56	-0.58
1000m-6000m	2000	0.00	0.00	0.00	0.00	0.00	-0.51	-0.44	-0.44	-0.44	-0.52	-0.65	-0.73
1000m-6000m	2001	-0.75	-0.79	-0.79	-0.77	-0.70	-0.51	-0.44	-0.43	-0.45	-0.56	-0.68	-0.74
1000m-6000m	2002	-0.71	-0.69	-0.74	-0.72	-0.74	-0.58	-0.46	-0.43	-0.52	-0.62	-0.71	-0.71
1000m-6000m	2003	-0.72	-0.82	-0.64	0.00	0.00	-0.63	0.00	-0.43	-0.44	-0.52	-0.66	-0.75
1000m-6000m	2004	-0.67	-0.68	-0.75	-0.64	0.00	-0.58	-0.46	-0.42	-0.44	0.00	-0.68	-0.67
1000m-6000m	2005	-0.71	-0.63	-0.68	-0.71	-0.84	-0.75	-0.47	-0.40	-0.45	-0.59	-0.66	-0.68
1000m-6000m	2006	-0.75	-0.72	-0.76	-0.73	-0.67	-0.62	-0.49	-0.43	-0.45	-0.57	-0.68	-0.71
1000m-6000m	2007	-0.76	-0.73	-0.72	-0.76	-0.63	-0.63	-0.42	-0.42	-0.46	-0.66	-0.61	-0.74
1000m-6000m	2008	-0.75	-0.74	-0.81	-0.75	-0.74	-0.50	-0.40	-0.45	-0.54	-0.64	-0.65	-0.73
1000m-6000m	2009	-0.75	-0.80	-0.73	-0.78	-0.80	-0.79	-0.53	-0.41	-0.57	-0.66	-0.71	-0.75
3500m-6000m	2000	0.00	0.00	0.00	0.00	0.00	-0.57	-0.23	-0.64	-0.61	-0.87	-0.76	-0.84
3500m-6000m	2001	-0.81	-0.74	-0.60	-0.70	-0.81	-0.67	-0.62	-0.52	-0.77	-0.84	-0.95	-0.73
3500m-6000m	2002	-0.71	-0.60	-0.57	-0.61	-0.83	-0.78	-0.53	-0.61	-0.70	-0.95	-1.09	-0.99
3500m-6000m	2003	-1.00	-0.72	-0.53	0.00	0.00	-0.80	0.00	-0.67	-0.60	-0.83	-0.88	-0.79
3500m-6000m	2004	-0.62	-0.62	-0.72	-0.65	0.00	-0.72	-0.61	-0.65	-0.63	0.00	-0.83	-0.74
3500m-6000m	2005	-0.69	-0.59	-0.54	-0.56	-0.52	-0.70	-0.39	-0.44	-0.61	-0.94	-1.06	-1.01
3500m-6000m	2006	-0.75	-0.76	-0.65	-0.68	-0.76	-0.71	-0.48	-0.34	-0.58	-0.86	-0.81	-0.69
3500m-6000m	2007	-0.83	-0.64	-0.58	-0.69	-0.71	-0.68	-0.37	-0.32	-0.51	-0.92	-0.99	-0.81
3500m-6000m	2008	-0.78	-0.66	-0.69	-0.62	-0.73	-0.42	-0.29	-0.40	-0.70	-0.91	-1.01	-0.88
3500m-6000m	2009	-0.75	-0.80	-0.73	-0.78	-0.72	-0.79	-0.53	-0.41	-0.57	-0.66	-0.71	-0.75

Chapter 6

STREAMFLOW MODELING USING SNOWMOD

6.1 BACKGROUND

Modeling of streamflow from a basin is based on transformation of incoming precipitation to outgoing streamflow by considering atmospheric losses, temporary storages, lag and attenuation. Generally, the seasonal short-term variation in streamflow reflects variation in the rainfall. But in mountainous regions, at higher latitudes and elevations/altitudes where snowfall is a predominant component, runoff depends on the heat supplied to snowpack for melting rather than the timing of precipitation. In these mountainous regions snow and ice significantly affect the hydrology of the catchment by temporarily storing and releasing water on varied time scales (Jansson et al., 2003) causing significant distinct variations in annual and diurnal discharges differing from those of traditional landscapes (Röthlisberger and Lang, 1987). Hence, it becomes very important to model snowmelt runoff from these basins, to understand the hydrological behavior and simulate the streamflow.

This study aims to simulate the snowmelt runoff in the Beas basin up to Pandoh dam located in the western Himalayan region, India. The Beas river basin obtain substantial runoff from snow and ice, and from glaciated areas (Li et al., 2014) and the basin is also prone to floods in monsoon season and droughts during winter and post-monsoon seasons. Considering the importance of seasonal snow cover/glaciers and associated snowmelt runoff from them in this basin, a substantial effort has been made to achieve this objective. For snowmelt runoff estimation, SNOWMOD model has been integrated with the remote sensing and GIS in the present study. The structure of model, algorithms, input data, model variables/parameters, and the procedure to simulate snowmelt runoff are described in detail and simulation results for the Beas basin are presented. The inputs from space borne remote sensing satellite on extent of snow cover and seasonally/topographically varying lapse rate have been used by the model for snowmelt runoff modeling for the basin for the first time. Moreover, snow cover area (SCA) estimated using air temperature for the period when the satellites imagery are either not available or cloud covered, as discussed earlier in chapter 4 has been used in the model.

6.2 SNOWMELT RUNOFF MODELING

Precise forecasting of melt runoff can minimize the risk and loss caused by floods due to rapid melting of snow and glacier (Ferguson, 1999) and the potential impacts of climate change (IPCC, 2007) on streamflow regimes could be assessed only if, valid snow/glacier melt runoff models are available. Hydrological models generally used for simulation or forecasting streamflow are categorized as; simple regression models, black box models, conceptual models, and physically based models (Singh, 1995). Lumped-conceptual hydrological models for surface runoff analysis are considered to be useful as they integrate numerous variables and uncertainties governing surface runoff (McCuen, 2003). Conceptually, snowmelt runoff models are rainfall-runoff models with additional component or routines added to store and subsequently melt precipitation that falls as snow. The last few decades have witnessed the development of numerous snowmelt runoff models ranging from purely statistical methods, which neglects the physics of snowmelt process to the complicated energy budget equations.

The contribution of snowmelt runoff from a watershed is generally made using two types of models; energy balance models and temperature index models. There is continuing debate on the relative merits of physically based models vs. temperature index models (Franz et al., 2008). Despite of detailed physical basis and well established accuracy, application of energy balance models is limited to only small well networked watersheds and there is proclivity towards use of temperature index models. The temperature index (conceptual model) employs the concept of an index, in which a known variable is used to explain the phenomenon in a statistical rather than in a physical sense. It relates the melt to a meteorological variable (generally air temperature) through a melt factor. Temperature index models are widely used for melt modeling due to low data requirements, generally good model performance and computational simplicity (Li and Williams, 2008).

For these reasons, temperature index based snowmelt models are most widely used for snowmelt runoff evaluation. Several operational snowmelt models based on this approach like the NWSRFS model, PRMS model, HBV model, SRM model, GAWSER model, UBC model, HYMET model, HEC-1 and HEC-1F model, SSARR model, SNOWMOD as discussed earlier are available for the snowmelt modeling. The snowmelt runoff model (SRM), also referred in the literature as “Martinec model or Martinec Rango model” is developed specifically to simulate and predict snowmelt runoff and has been extensively used in the mountainous basin where snowmelt is a major runoff factor. The model uses temperature, precipitation and snow covered area as input variables and run starts with the known or estimated value of discharge

and can proceed for unlimited number of days, as long as the inputs are provided (Prasad and Roy, 2005). The major limitation lies with it, is that it does not simulate the baseflow component of runoff. For this reason, it does not contribute to the groundwater reservoir from snowmelt, rainfall and baseflow, which can be an important component of runoff in the mountainous rivers, for making them perennial in nature. (Singh and Jain, 2003) concluded that almost all the streamflow generated during winter season is from baseflow, when there is no rainfall or snowmelt. In this line another model, the SNOWMOD model (Jain, 2001) is peerless from this aspect, which takes into consideration the baseflow and simulates the entire essential components of runoff namely snowmelt runoff, rainfall induced runoff, and the baseflow with limited data.

6.3 SNOWMOD-A SNOWMELT MODEL

The SNOWMOD, a temperature index model, has been designed for the simulation of daily streamflow from the mountainous basins having contribution from both snowmelt and rainfall. The streamflow generation process from such basins involves primarily the determination of the amount of basin input derived from snowmelt, glacier melt and rainfall and then its transformation into runoff. It is a distributed model with temperature index approach in which the basin is divided into a number of elevation bands or zones for streamflow simulation, and the varied hydrological processes relevant to snowmelt and rainfall runoff are estimated for each elevation zone. For snowmelt and rainfall modeling, the model executes three operations at each time step as given below:

1. Extrapolate the available meteorological data at different altitude/elevation zones of the basin.
2. Calculate the rates of snowmelt and/or rainfall at different points.
3. Integrate the snowmelt runoff from snow cover area (SCA) and rainfall-runoff from snow-free area (SFA).

All these components are routed separately with appropriate accounting of baseflow to the basin outlet. The various parameters used in routing the snowmelt and rainfall-runoff are optimized by the model. The SNOWMOD has been applied to simulate the snowmelt runoff in the Beas basin up to Pandoh using SCA and varied lapse rate extracted from MODIS data products. The various steps involved in the model are shown schematically in Figure 6.1. The

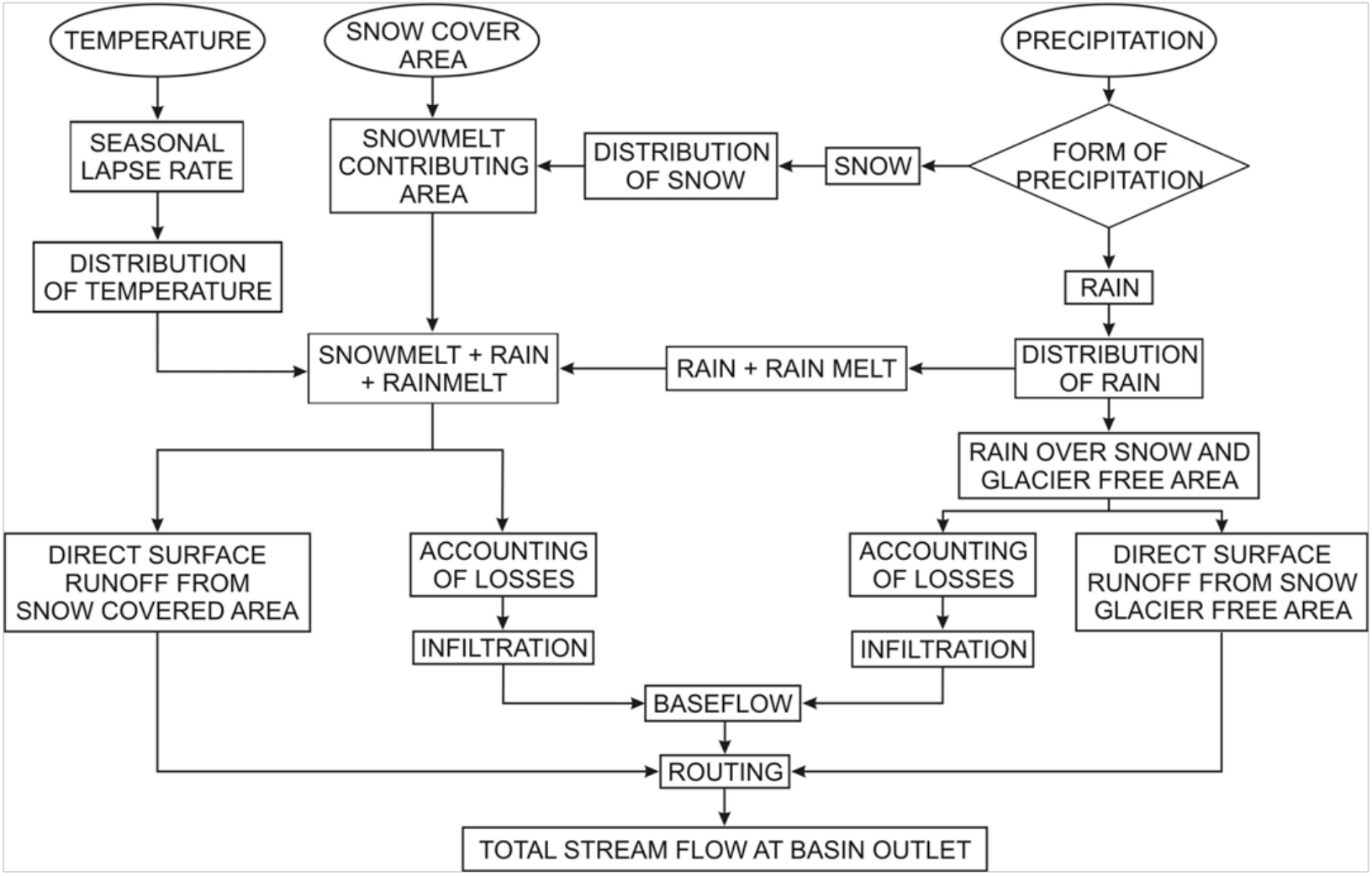

Figure 6.1: Structure of the SNOWMOD model

details of computation of snowmelt runoff and streamflow generation from the basin are discussed below.

6.4 DATA INPUT FOR SNOWMOD

The SNOWMOD model requires the following data inputs for execution:

1. Physical features of the basin, which comprise snow covered area (SCA), elevation zones or bands with their areas, altitude of meteorological stations and other essential basin characteristics affecting runoff.
2. Time variable data comprising of hydro-meteorological data like air temperatures, precipitation, streamflow and snow covered area along with other parameters determining the distribution of temperature and precipitation.
3. Information of soil moisture status of the basin.
4. Job control and time control miscellaneous data specifying the items, as total computation period routing intervals etc.

6.5 MODEL VARIABLES AND PARAMETERS

6.5.1 Division of Basin into Elevation Bands

In the mountainous areas, hydrological and meteorological conditions highly vary with the elevation. Melt is heavily affected due to topographic effects such as slope, aspect and shading, yielding high spatial variability in melt rates in mountain regions (Hock, 2003). Judicious selection of computer model thus becomes very important for such basins for the proper estimation of runoff. Distributed model is considered to be more appropriate as they take into account the spatial variability of processes in comparison to lumped model which treat whole watershed as a single entity. Moreover, distributed model can be run for continuous simulation. In such a model, the entire watershed is divided into subunits and the variables are being computed separately for each subunit. The method to sub divide the basin is more appropriate and logical, since hydro-meteorological conditions are characteristically related to elevation in mountainous regions.

SNOWMOD is a distributed model which uses the criterion of elevation bands for the spatial discretisation. Depending upon the topographic relief of the entire basin, the basin is divided into number of elevation bands. There is as such no specific range of altitude for slicing

the basin in the bands. However, an altitude difference of about 500-600 m is considered appropriate for slicing the basin into elevation bands. The sum of snowmelt and rainfall is considered as the moisture input for each elevation band. The runoff for each band is computed from the watershed runoff characteristics developed for that particular band. Streamflow for the entire basin is acquired by summing the runoff produced from all elevation bands. SNOWMOD program have a provision to store a value, for each component of flow and each routing increment for every elevation band. The program also maintains an inventory of snow cover area (SCA), snow accumulation, soil moisture and all other values needed for computing for the next period.

In the present study, using the SRTM DEM, the relief of Beas basin has been divided into nine elevation bands or zones, with an altitude difference of 600 m between each elevation band for convenience. Moreover, basin characteristics such as elevation zones and area-elevation curve have been derived. The area-elevation curve is shown in Figure 6.2. The area covered in each zone of the basin is shown in Table 6.1.

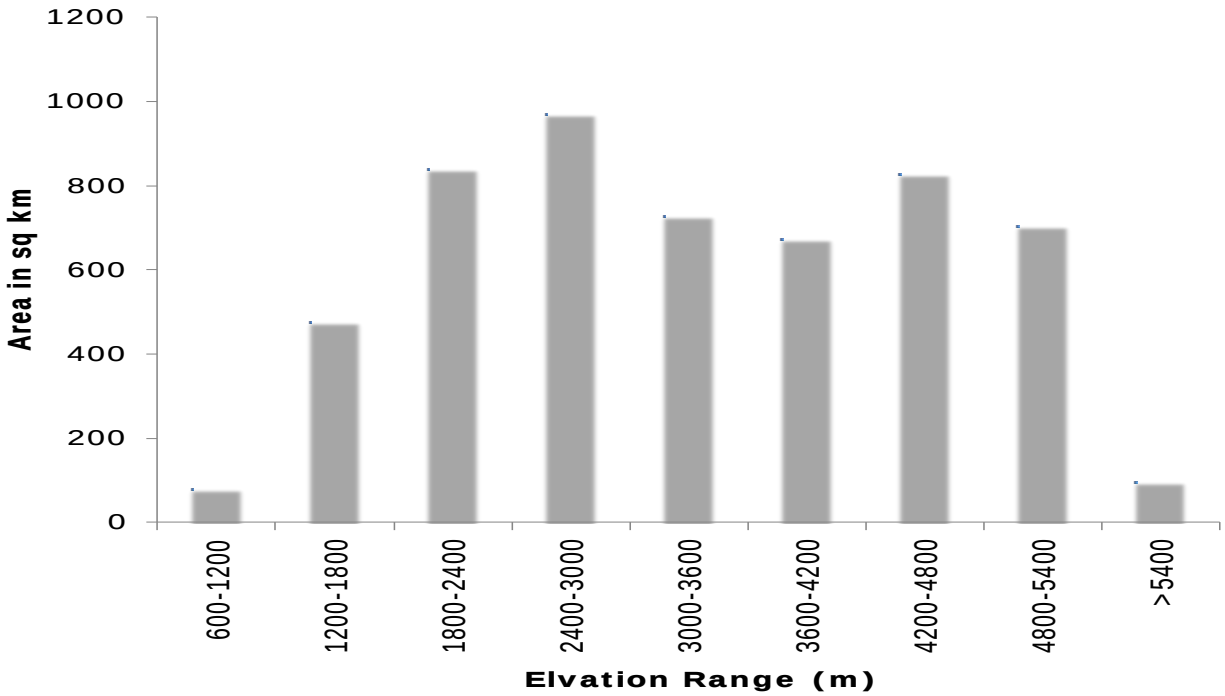

Figure 6.2: Area-elevation curve of the study area

Table 6.1: Beas basin area covered in different elevation zones

Zones	Elevation range (m)	Area (km^2)	Percentage
1	600-1200	78.67	1.46
2	1200-1800	475.81	8.84
3	1800-2400	838.07	15.57
4	2400-3000	970.52	18.03
5	3000-3600	725.45	13.47
6	3600-4200	670.97	12.46
7	4200-4800	825.48	15.33
8	4800-5400	703.40	13.06
9	>5400	95.63	1.78

From the Table 6..1, it is clearly seen that the maximum area of the basin lies in the fourth zone (2400-3000 m) and consists of 18.03% (970.52 km^2) of the total geographical area whereas minimum area is 1.46% (78.67 km^2) lying in the first zone (600-1200 m).

6.5.2 Precipitation Data and Distribution

Especially in mountainous basin, the measurement of meteorological variables is the most challenging object for hydrological simulations. Most significant data related problems are associated with the measurement of the amount of precipitation and its spatial distribution. Major problems that pose in soaring mountainous areas are continuous accessibility, accuracy of measured meteorological variables and the areal representativeness of the measurements (Panagoulia, 1992). (WMO, 1986) made a comparative study of various snowmelt models and it was concluded that the precipitation distribution assumptions and the determination of the form of precipitation were the most important factors in producing the accurate estimates of runoff volume. For a distributed model which takes into account spatial variability, it is very important to distinguish between rainfall and snowfall in each elevation band because both of these forms of precipitation behave very differently in terms of contribution to the streamflow. Among these two, the contribution of rainfall is immediate and faster to the streamflow while snowfall gets stored in the basin until it melts. The form of precipitation is mainly influenced by the meteorological and topographical factors. The meteorological factors generally includes air temperature, lapse rate, wind etc. and the topographical factors incorporate elevation,

aspect, slope, vegetation etc. Depending upon these factors in any elevation band, precipitation may fall as snow or rain. Rainfall falling on an elevation band or a part of the band is directly added to the moisture input whereas snow is added to the previously accumulated snow, if any and becomes part of the seasonal snowpack. During the early melt season, the rain falling over a cold snowpack gets frozen in the snowpack and is not immediately available to the runoff. It gets melted only when the favorable atmospheric and snowpack conditions subsist. However, if rain falls over the ripe snowpack, it gets transferred through the snow layer and contributes to the runoff.

For the present study, daily precipitation data were available for six stations namely Banjar, Bhuntar, Larji, Pandoh, Sainj and Manali within the basin. For different elevation bands, data of different stations have been used as given in Table 6.2. The rain gauges have been allocated to different elevation bands based on their proximity to the respective band according to altitude of the station. In the model critical temperature (T_c) has been specified to determine whether the measured precipitation is rain or snow. In the present study, T_c is considered to be 2ºC as recommended by Singh and Jain (2003). The following algorithm is used by the model to determine the form of precipitation:

If $T_m \geq T_c$, all precipitation is considered as rain

If $T_m \leq 0°C$, all precipitation is considered as snow

where T_m is mean air temperature. In the cases $T_m \geq 0°C$ and $T_m \leq T_c$, the precipitation is considered as a mixture of rain and snow and their proportion is determined as follows:

$$\text{Rain} = \frac{T_m}{T_c} \times P \tag{6.1}$$

$$\text{Snow} = P - \text{Rain} \tag{6.2}$$

where P is the total observed precipitation.

6.5.3 Temperature Data: Spatial and Temporal Distribution

Air temperature is an important component in the snowmelt runoff studies. It has a coherent association with many of the energy exchanges involved in melting of snow. Moreover, this meteorological variable is generally most readily available to researchers and hydrologist in near real time. Thus, air temperature is the most widely used index in snowmelt

(Sorman, 2005). Daily mean temperature is the most common parameter used for snowmelt computation. In the present study, daily mean air temperature has been calculated by using the following equation:

$$T_{air} = T_{mean} = \frac{(T_{max} + T_{min})}{2} \tag{6.3}$$

For the Beas basin, the daily maximum and minimum air temperature data were available for four meteorological stations namely Pandoh, Bhuntar, Largi and Manali. Daily mean air temperature was calculated using equation (6.3). As mentioned earlier, the basin is divided into nine elevation bands. For each band, a base station has been assigned as given in Table 6.2. For corresponding band, the temperature data was interpolated using the air temperature data of different stations and lapse rate data.

Table 6.2: Raingauge and temperature stations used for different elevation bands

Band	Elevation range (m)	Raingauge station	Temperature station
1	600-1200	Pandoh	Pandoh
2	1200-1800	Larji	Bhuntar
3	1800-2400	Manali	Larji
4	2400-3000	Manali	Manali
5	3000-3600	Manali	Manali
6	3600-4200	Sainj	Manali
7	4200-4800	Sainj	Manali
8	4800-5400	Sainj	Manali
9	>5400	Sainj	Manali

In mountainous regions for precise snowmelt runoff computation, reliable temperature data is essential for all the elevation bands of the basin. However, in Himalayan basins due to complex terrain and inaccessibility, temperature data are available only at few locations. So

these point values needs to be extrapolated or interpolated to the mid elevation of each elevation band using predefined temperature lapse rate (TLR) in the model. Traditionally, lapse rates are used for the extrapolation of measured air temperatures at stations to different elevation bands.

Temperature depicts an inverse relationship with the elevation. The rate at which temperature changes with increase in elevation is termed as lapse rate. Lapse rate is not constant value; it changes with season and region. The SRM and probably all snowmelt models are observed to be very sensitive to lapse rate, when used for temperature extrapolation. In general, mean temperature lapsed at 0.65 ^{o}C/100 m or at a specified rate to mean hypsometric elevation of each elevation zone (Singh, 1991).

The temperature lapse rate approach has been used to estimate daily temperature in various elevation bands/zones by extending the data from the base station using the equation given below:

$$T_{i,j} = T_{i,base} - \delta(h_j - h_{base}) / 100 \quad (6.4)$$

where,$T_{i,j}$ = daily mean temperature on i^{th} day in j^{th} zone (^{o}C), $T_{i,base}$ = daily mean temperature (^{o}C) on i^{th} day at the base station, h_j = zonal hypsometric mean elevation (m), h_{base} = elevation of base station (m), and δ= Temperature lapse rate in ^{o}C per 100 m

6.5.4 Degree-Days

Air temperature, a most widely available measured parameter used in snowmelt modeling has high correlation to radiation, wind and humidity which are some of the key components involved in heat transfer to the snowpack. Thus, air temperature is of great importance for the computation of melting of snow and ice. For snowmelt computations, air temperature considered as an index of complex energy balance tending to snowmelt, is expressed as degree-days. A degree-day is a unit which expresses the amount of heat in terms of persistence of temperature over a 24-hour period of ^{o}C departure from a reference temperature. In a broader sense, it refers to departure of temperature below or above a critical threshold value. Normally, the threshold temperature value of 0 ^{o}C is being used; if daily mean temperature is above it snowmelt is considered to occur. Thus, the degree-day is computed as the difference between the daily mean temperature and this critical threshold value (0 ^{o}C).

For the first time the application of a degree-day approach was made in the field of glaciology in the Alps by Finsterwalder and Schunk (1887) and ever since then this approach has been widely used for the snowmelt estimation over the world (Martinec et al, 1994; Quick and Pipes, 1995; Singh and Singh, 2001; Singh and Jain, 2003). The basic, simplest and common form of degree-day approach expression relating snowmelt to temperature index is given as:

$$M = D(T_{air} - T_{melt}) \tag{6.5}$$

where, M = daily snowmelt (mm/day), D = degree-day factor (mm $°C^{-1}$ day^{-1}), T_{air} = index air temperature (°C), and T_{melt} = threshold melt temperature (usually, 0°C). The air temperature and other hydrological conditions though varies continually throughout the day, the daily mean air temperature is the most widely used index of temperature for snowmelt in both glaciological and hydrological applications. Where only daily maximum (T_{max}) and minimum (T_{min}) air temperature are available, the daily mean air temperature is determined by equation 6.3.

6.5.5 Degree-Day Factor

The degree-day factor 'D' is a very important parameter involved in snowmelt computation and is used to convert the degree-days to snowmelt expressed in terms of depth of water. Degree-day factor is influenced largely by the physical properties of snowpack and as these properties changes with time, this factor also varies with time. Due to long melt season or large elevation difference in the basin, large variations are expected in the D factor. D factors are lower for snow and higher for ice due to higher albedo of snow as compared to ice. Anderson (1973) has well illustrated the seasonal variation in melt factor. In the literature, wide range of values has been reported with a general increase as the snowpack ripens. For instance, Garstaka (1964) observed extreme values of D_f ranging from 0.7 mm per °C per day to 9.2 mm per °C per day. Depending upon the location, time of year and meteorological conditions, values of D were reported to be between 4.0 to 8.0 mm per °C per day Yoshida (1962). Bergstrom (1992) reported that empirically fitted melt factors normally lie between 2.0-3.0 mm per °C per day in Sweden. The higher factors with an average of 6 mm per °C per day were reported for the exposed slopes of Iceland (Bergstrom, 1992). Krenke and Khodakov (1966), from various glaciers in former Soviet Union reported degree-day factor of 4.5 mm per °C per day for snow and 7 mm per °C per day for ice. The mean degree-day factor for normal snow

was computed to be 5.94 mm per °C per day whereas for dusted snow it was found to be 6.62 mm per °C per day for a normal snowpack over a glacier at an altitude of about 4000 m in the Garhwal Himalayas (Singh and Kumar, 1996). The average degree-day factor for clean and dusted snow was computed to be 5.7 and 6.4 mm per °C per day respectively while it was 7.4 and 8.4 mm per °C per day for clean and dusted ice respectively (Singh et. al., 2000).

The value of D is lower at the beginning of melt season and higher towards the end of season depending upon the snow density. At the start of melt season, the snow has low density (not much compact) related with higher albedo resulting in lower D value. As the season proceeds, snow gets older (more compacted) with higher density which is related with low albedo and hence a higher D value. Also, higher densities are allied with increased liquid water in snowpack and lower thermal quality. These different phases of snowmelt, at different elevation can change the value of D factor by zone. As discussed above that D changes with season, therefore, when using degree-day approach, changes in D with season should be taken into account. In the present study, in the starting of melt season for every month low value of degree-day factor has been taken and it goes on increasing till the end of melt season i.e. the month of September. In the present study the value of D varied from 3.0 to 7.0 mm per °C per day. The range of the values of various parameter used in this study is given in Table 6.3.

Table 6.3: Parameter values used in calibration of model

S. No.	Parameter	Symbol	Value
1.	Degree-day factor	D	3.0 – 7.0 $mm.^oC^{-1}.day^{-1}$
2.	Runoff coefficient for rain	C_r	0.40 - 0.70
3.	Runoff coefficient for snow	C_S	0.50 – 0.80
4.	Temperature lapse rate	δ	Seasonally varying
5.	Critical temperature	T_c	2^oC
6.	Number of linear reservoirs for snow free area	N_r	2
7.	Number of linear reservoirs for snow covered area	N_S	1
8.	Number of linear reservoirs for subsurface flow	N_b	1

6.5.6 Snow Cover Area (SCA)

SCA is an important and dynamic parameter to simulate snowmelt runoff for a basin. The information on spatial distribution/extent of snow cover and its depletion with time is crucial for the snowmelt runoff models. Remote sensing technologies have provided and enhanced the availability of spatial and temporal information of snow from satellite imageries for different months during the snowmelt period. The snow cover area for the present study has been extracted from the Aqua/Terra MODIS satellite data from February 2001 to December 2005. The streamflow simulation has been carried out for twelve years i.e. from 1990 to 2002 for the basin. However, MODIS data products are available since February 2000 hence; the SCA for the missing period that 1990 to 2000 were estimated by using regression technique discussed already in chapter 4. The ERDAS Imagine software has been used for processing the snow cover maps and estimating the area.

The model requires information of snow cover area for each elevation band to simulate runoff. For this purpose, classified DEM and SCA maps were overlaid for all the dates and snow cover area for each elevation band has been computed for each year. The SCA in each band were plotted against the elapsed time to obtain the snow depletion curves for different elevation bands in the basin for all the years. The SDC for the months of March to October for five years (2001, 2002, 2003, 2004 and 2005) are shown in Figure 4.9 of chapter 4.

6.5.7 Rain on Snow

Rain on snow is a common event on mountain slopes and it plays an important role in producing high streamflows. Such events are hydrologically significant phenomenon because they have much greater potential for producing floods (Colbeck, 1975; Kattleman, 1987; Brunengo, 1990; Berg et al., 1991; Archer et al., 1994). Most of the floods in British Columbia, Washington, Oregon and California were reported to have occurred due to this event. Moreover, this event is also considered as a major cause for releasing avalanches because as the rain falling over the snow weakens the bond among grains and results in alteration of snow texture leading to reduction of mechanical strength of snowpack and several studies have been conducted to study the role of rain in triggering avalanches (Conway et. al, 1988; Heywood, 1988; Conway and Raymond, 1993). In the Himalayan regions at high altitudes good rainfall occurs during the dynamic melt period (Singh et al., 1995; Singh and Kumar, 1996).

When rainwater falls on snowpack, it gets cooled to the snow temperature. The heat transferred to the snow by rainwater is the difference between its energy content before falling on the snow and its energy content on reaching thermal equilibrium within the snowpack. For snow-packs isothermal at 0°C, the release of heat results in snowmelt, while for the colder snowpack this heat tends to raise the snowpack temperature to 0ºC. In case the snowpack is isothermal at 0°C, the melt taking place due to rain is calculated by (Jain, 2001).

$$M_r = \frac{4.2\, T_r P_r}{325} \tag{6.6}$$

where M_r = melt caused by the energy supplied by rain (mm/day), T_r = temperature of the rain (°C), and P_r = depth of rain (mm day^{-1}). This component would be significant only an for high rainfall event which occurs at higher temperatures that would cause melt due to rain (Singh et al., 1997a).

6.6 COMPUTATION OF DIFFERENT RUNOFF COMPONENTS

Mainly the streamflow of a snow-fed river system has three components:

1. Runoff from snow covered area ,
2. Runoff from snow-free area and
3. Baseflow

The runoff contribution from these three components for each elevation band is computed separately and subsequently the output from all the bands/zones is integrated to provide total runoff from the basin.

6.6.1 Surface Runoff from Snow Covered Area

The runoff from snow covered area mainly consists of;

a) Snowmelt induced due to prevailing air temperature above melting temperature.
b) Snowmelt induced due to heat transfer to the snow from rain on snow-covered area.
c) Runoff depth from the rain itself, falling over the snow covered area.

(a) Snowmelt induced due to prevailing air temperature has been estimated for each elevation band/zone of the basin using the degree-day approach and SCA extent. In this approach degree-day factor (D) has been used to convert degree-days into snowmelt expressed in terms of depth of water.

$$M_{s,i,j} = C_{s,i,j} D_{i,j} T_{i,j} S_{c,i,j} \quad (6.7)$$

where, $M_{s,i,j}$ = snowmelt on i^{th} day for j^{th} band (mm), $C_{s,i,,j}$ = coefficient of runoff for snow on i^{th} day for j^{th} band, $D_{i,j}$ = degree-day factor on i^{th} day for j^{th} band ($mm.^oC^{-1}d^{-1}$), $T_{i,j}$ = temperature on i^{th} day for j^{th} band (^oC), and $S_{c,i,,j}$ = Ratio of snow covered area to the total area of j^{th} band on i^{th} day.

(b) Runoff depth due to snowmelt resulting from heat transferred to the snow from rainfall on snow covered area in an elevation band is given by the equation given below:

$$M_{r,i,j} = \frac{4.2\, T_{i,j} P_{i,j} S_{c,i,j}}{325} \quad (6.8)$$

where, $M_{r,i,j}$ = snowmelt due to rain on snow on i^{th} day for j^{th} band (mm), and $P_{i,j}$ = rainfall on snow on i^{th} day for j^{th} band (mm).

(c) Runoff from the rain itself, falling over the snow covered area is given by

$$R_{s,i,j} = C_{s,i,j} P_{i,j} S_{c,i,j} \quad (6.9)$$

For the computation of runoff from rain, the coefficient C_s is used (instead of rainfall-runoff coefficient, C_r), because runoff from the rain falling over the SCA behaves similar to runoff from the melting of snow.

The daily total discharge from the SCA is computed by adding the contribution from each elevation band/zone. Thus, discharge (Q_{SCA}) from the SCA for all the bands/zones is given by:

$$Q_{SCA} = \alpha \sum_{j-1}^{n} (M_{s,i,j} + M_{r,i,j} + R_{s,i,j}) A_{SCA,i,j} \quad (6.10)$$

where, n = total number of zones or bands, A_{SCA} = snow covered area (km^2) in the j^{th} zone on the i^{th} day, and α = factor (1000/86400 or 0.0116) used to convert the runoff depth (mm day^{-1}) into discharge (m^3 s^{-1}).

This discharge is routed to the basin outlet following the procedure described in the later section.

6.6.2 Surface Runoff from Snow-Free Area

Rainfall is the only source of surface runoff from snow-free area (SFA). Similarly to snowmelt computations, the runoff from SFA has been computed for each of the elevation band using the expression given below:

$$R_{f,i,j} = C_{r,i,j} P_{i,j} S_{f,i,j} \quad (6.11)$$

where, $C_{r,i,j}$ = coefficient of runoff for rain on i^{th} day for j^{th} band, $P_{i,j}$ = rainfall on snow on i^{th} day for j^{th} band (mm), and $S_{f,i,j}$ = Ratio of snow-free area to the total area of j^{th} band on i^{th} day. Since, SCA and SFA are complimentary to each other, $S_{f,i,j}$ can be directly calculated as 1 – $S_{c,i,j}$. The total runoff (Q_{SFA}) from SFA for all the zones is thus given by:

$$Q_{SFA} = \alpha \sum_{j=1}^{n} R_{f,i,j} A_{SFA,i,j} \quad (6.12)$$

where, $A_{SFA,j,,j}$ = snow-free area in the j^{th} zone on the i^{th} day

Similarly, the discharge from the SFA is also routed to the basin outlet before adding it to the other components of discharge.

6.6.3 Estimation of Subsurface Runoff

The runoff from unsaturated zone of the basin is represented as the subsurface or baseflow which is the main source of streamflow during the dry or fair weather periods. The

snowmelt and rainfall after accounting the direct surface runoff, contributes the remaining water to the groundwater storage through infiltration and appear as the subsurface flow or baseflow at the basin outlet with much delay. The water from this ground water storage gets with time depleted through evapo-transpiration and percolation to deep groundwater zone or aquifer. It is assumed that 50% of this groundwater water storage percolates down to the shallow groundwater and contributes to baseflow, while the remaining 50% is accounted for evapo-transpiration and percolation losses from the basin to the deeper groundwater aquifers, which may appear ahead downstream or meets deep and inactive groundwater storage. The depth of runoff contributing to baseflow from each band/zone is given by:

$$R_{b,i,j} = \beta[(1 - C_{r,i,j})R_{f,i,j} + (1 - C_{s,i,j})M_{t,i,j}] \quad (6.13)$$

where, $M_{t,i,j} = M_{s,i,j} + M_{r,i,j} + R_{s,i,j}$ and β is 0.50. The baseflow (Q_b) is computed by multiplying the depth of runoff by the conversion factor α and area, and is given as:

$$Q_b = \alpha \sum_{j=1}^{n} R_{b,i,j} A_{i,j} \quad (6.14)$$

where, A is the total area (km^2) and represents the sum of A_{SCA} and A_{SFA}. This component is also routed separately.

6.6.4 Total Runoff

The daily total runoff from the basin is computed by adding the three different routed components of runoff for each day, and is expressed as:

$$Q = Q_{sca} + Q_{sfa} + Q_b \quad (6.15)$$

As discussed above, the streamflow in the river system is a contribution resulting from direct runoff from over land or near surface flow and baseflow from the ground water discharge. The baseflow movement is very slow so also referred as delayed runoff. Infact, the contribution to the baseflow begins only after the topsoil becomes saturated.

6.7 CATCHMENT ROUTING

6.7.1 Surface Runoff Routing

The catchment routing enables to transmute the basin inputs, rainfall or/and snowmelt to the outflow of basin. The outflow which emerges from the SCA and SFA are routed independently because the hydrological response of these areas is not analogous. The technique of linear cascade reservoir is used to route the runoff, in which inflow passes via series of linear reservoirs having equal storage coefficients, to achieve integrated effect of the entire reservoirs on the outflow from end reservoir. Hence, each reservoir is involved in affecting the attenuation and lag characteristics of the outflow. The cascade of equal linear reservoirs expressed in analytical form is called as Nash Model. For cascade of n number of reservoirs, the out flow from the n^{th} reservoir is given by the equation below:

$$Q_{n+1,j+1} = C_0 Q_{n,j+1} + C_1 Q_{n,j} + C_2 Q_{n+1,j} \tag{6.16}$$

where, n = number of reservoirs and j = time index.

For a linear reservoir, $C_0 = C_1$, and hence equation is simplified as:

$$Q_{n+1,j+1} = 2C_1 \overline{Q}_{n,j+1} + C_2 Q_{n+1,j} \tag{6.17}$$

where, $$\overline{Q}_{n,j+1} = \frac{Q_{n,j+1} + Q_{n,j}}{2} \tag{6.18}$$

where, $$C_0 = \frac{\Delta t / k}{2 + \Delta t / k} \tag{6.19}$$

$$C_1 = C_0$$

$$C_2 = \frac{2 - \Delta t / k}{2 + \Delta t / k} \tag{6.20}$$

Here, C_0, C_1, C_2 are the routing coefficients and their sum equals to unity, i.e.

$$C_0 + C_1 + C_2 = 1$$

6.7.2 Subsurface Routing

After the complete discharge of the surface runoff from the basin, baseflow or subsurface flows sustain the stream. The source of these flows is soil water in excess to field capacity. This water percolates to shallow groundwater zones or moves along the slope at shallow and meets at some discharge point above the water table. The movement of subsurface runoff to channels is relatively slow as compared to direct runoff. The subsurface runoff is routed in a similar manner as surface runoff with a given value of storage coefficient (K_b), which is computed by plotting the recession period flow against time on a semi-log paper. The slope of best fit line provided the value of $K_{b.}$

$$Q_b(t) = Q_0 e^{-t/kb} \tag{6.21}$$

where, Q_b = discharge at time t, Q_0 = discharge at time t = 0, and k_b = recession constant or the depletion factor.

Equation 6.21 can be represented in logarithmic version as:

$$\ln Q = \ln Q_0 - \frac{t}{k} \tag{6.22}$$

The Beas river flow was observed to be minimum during winter season. The streamflow records were analyzed and finally an average value of $K_{b\ i.e.}$ 111.12 days was used for routing the baseflow.

6.8 EFFICIENCY CRITERIA OF THE MODEL

For the numerical evaluation of model accuracy numerous statistical criteria are available at different time steps; in each single year, in a particular season of the year or a sequence of years or seasons. The World Meteorological Organization (WMO, 1986) in a study carried out for the snowmelt models suggests numerous efficiency criteria those are particularly useful for the snowmelt modeling. In the study, WMO identified the visual inspection of linear scale plots of simulated and observed hydrographs as the most significant criteria for the evaluation of model. Several numerical criteria useful for model evaluation are also identified. The performance of the model on a daily basis is most commonly evaluated by using the non-dimensional Nash-Sutcliffe 'R^2' value (Nash and Sutcliffe, 1970) as given by the equation:

$$R^2 = 1 - \frac{\left\{\sum_{t=1}^{n}(Q_0 - Q_e)^2\right\}}{\left\{\sum_{t=1}^{n}(Q_0 - \bar{Q}_0)^2\right\}} \quad (6.23)$$

where, R^2 = Nash-Sutcliffe coefficient of goodness of fit, Q_0 = daily observed discharge from the basin, Q_e = daily estimated discharge from the basin, $\overline{Q}_o$ = mean of observed discharge, and n = number of days of discharge simulation.

Nash-Sutcliffe coefficient value is analogous to coefficient of determination, and is a direct measure of the proportion of the variance of the recorded flows explicated by the model.

The model performance can also be determined on a seasonal basis by computing the percentage volume difference between the measured and computed seasonal runoff as:

$$D_v = \frac{\left\{\sum_{t=1}^{n} Q_0 - \sum_{t=1}^{n} Q_e\right\}100}{\left\{\sum_{t=1}^{n} Q_0\right\}} \quad (6.24)$$

where, D_v is the percentage volume difference between the measured and computed seasonal runoff.

6.9 CALIBRATION OF MODEL

It is essential to calibrate the hydrological models prior to run using observed and simulated streamflow results so that the models performance intimately matches to the real system. For calibration and validation of models, an adjective function is required for checking the model performance during the simulation mode with an independent data set (Blackie et al. 1985). It is done logically with a purpose to assess goodness of fit (matching level) between the two datasets of flows i.e. observed (Qo) and (Qe) flows. The simple and commonly used objective function in a mathematical form is given as:

$$F=\Sigma\ (Qe- Qo)^2 \quad (6.25)$$

The model is believed to be optimized when any change in the values of parameter hardly reduce the F value and the model gives the optimum fit model generated values on the observed dataset. Thus, optimization endeavors to adjust the appropriate values so that

objective function value is minimized. A cascade of linear reservoirs has been used to optimize all the storage coefficients during routing of flows. The runoff generated from both snow covered and snow-free area respond very differently. For this reason, runoff generated from snow cover area (SCA) and snow-free area (SFA) was routed separately via cascades of linear reservoirs. In the study, two linear reservoirs are considered for the snow-free area because the flow generated from such areas moves faster. On the other hand, in snow covered areas the movement of runoff generated is relatively slow for which only one linear reservoir has been considered. Hence, the basin is exemplified by uneven linear reservoirs with storage coefficients Kr, for snow-free area and Ks, for snow covered area considered to be changing temporally on daily basis.

Finally, the available dataset has been divided into two parts; of which one part is used for calibration and another part (independent data set) is used for validation, to test how effectively the model executes in simulation mode. In the present work, the Rosenbrock optimization technique has been used for achieving optimal parameter values. The model has been calibrated by using a daily dataset of a period of 3 years (2002-2005). Parameters were parameterized for calibration by taking into account the overall performance of the model and reproduction of flow hydrograph. Also, four model parameters a_r, b_r, a_s and b_s have been optimized while calibrating the model.

The optimal values for the model parameters a_r, b_r, a_s and b_s are 0.568, 0.148, 1.00 and 0.149, respectively. The results of daily streamflow for the calibration period are shown in Figure 6.3. In the figure contribution from three streamflow components namely snowmelt runoff, rainfall-runoff and baseflow and comparison of observed and simulated discharge has been shown separately. For more details the yearly plots are shown in Figure 6.4 to 6.6.

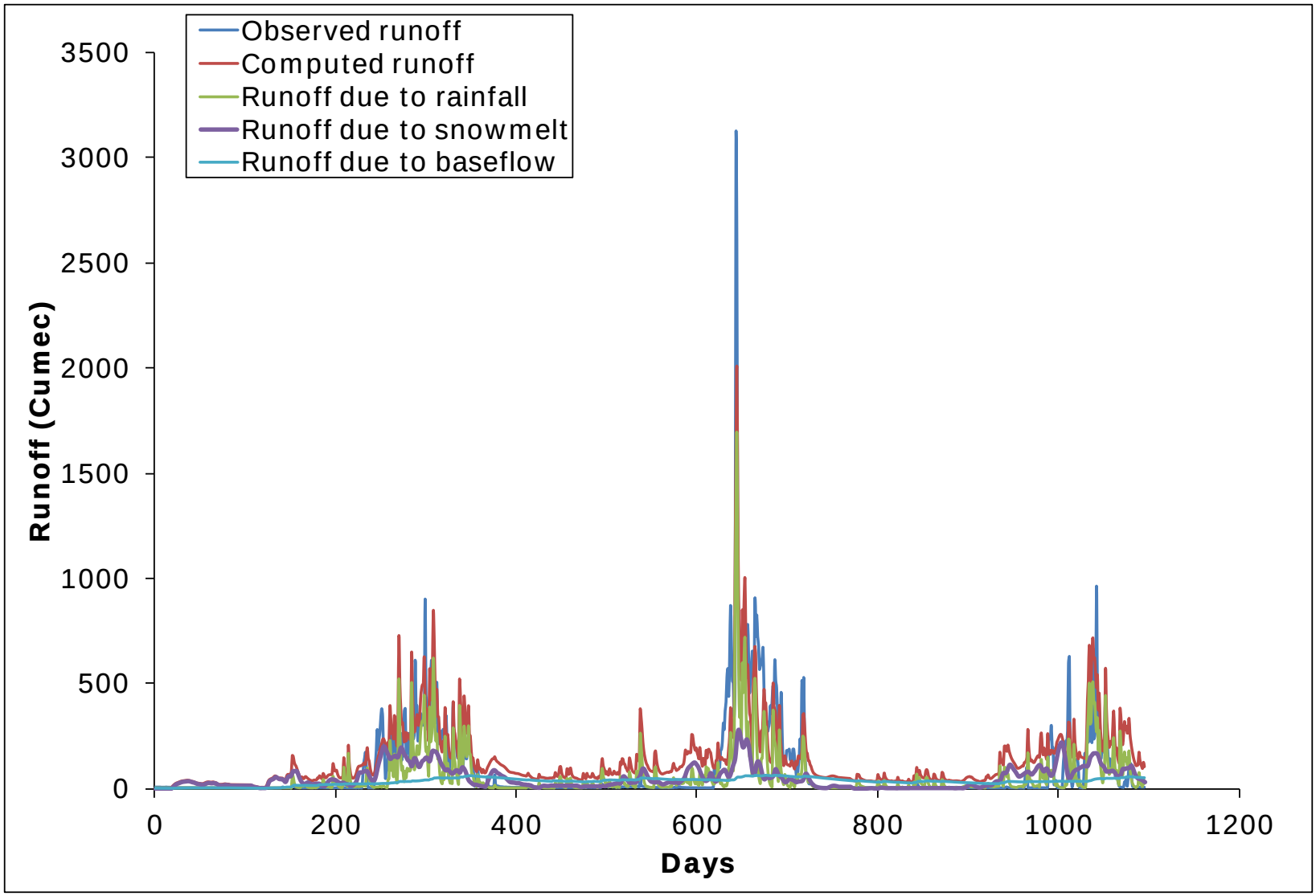

Figure 6.3: Simulated discharge of the Beas river at Pandoh for calibration period 2002-2005

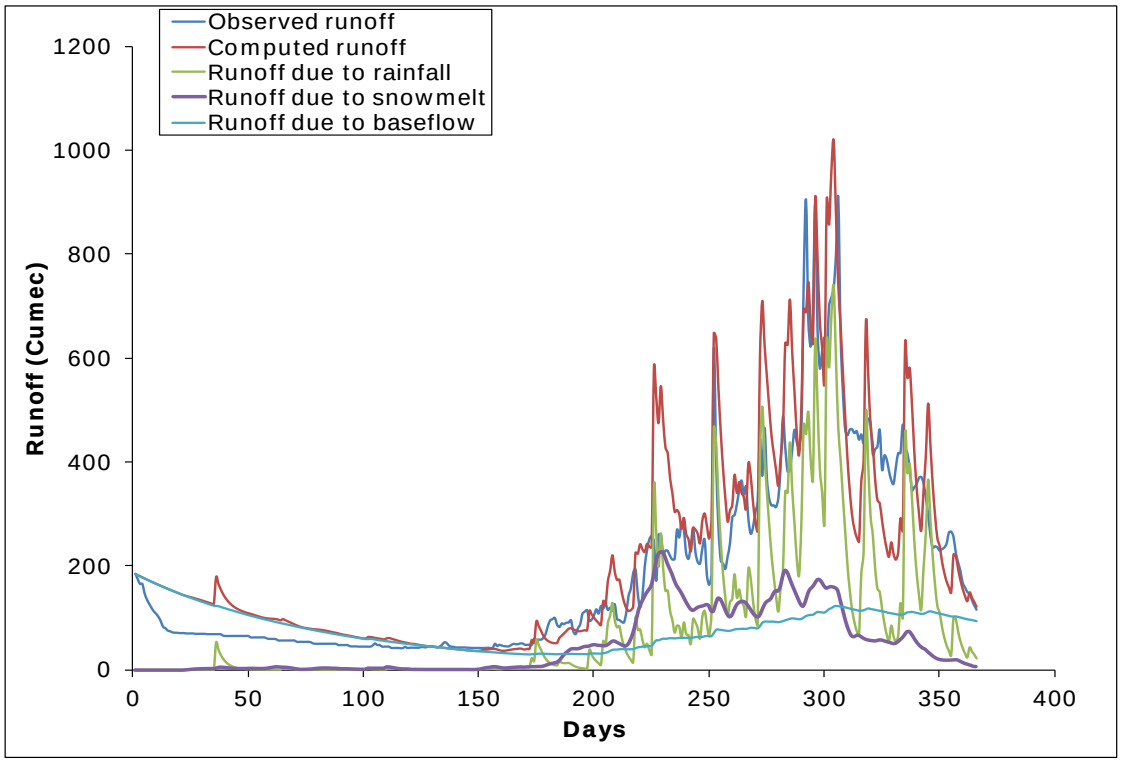

Figure 6.4: Simulated discharge of the Beas river at Pandoh for the year 1999-2000

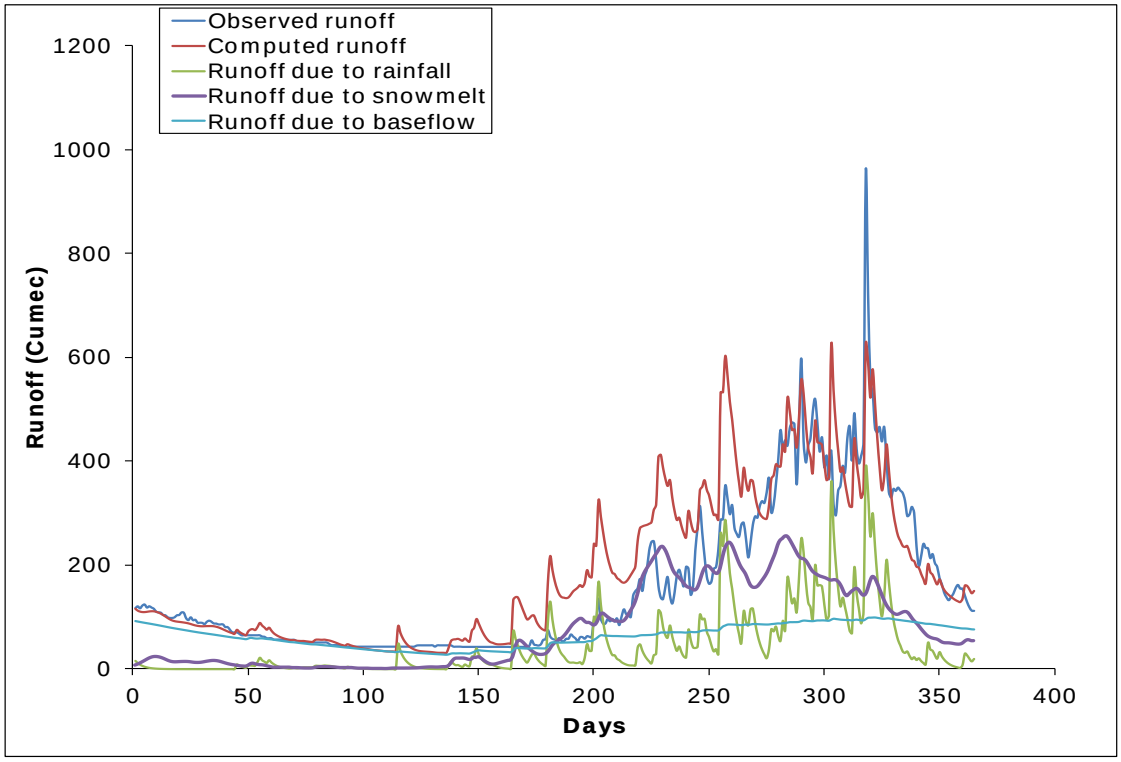

Figure 6.5 Simulated discharge of the Beas river at Pandoh for the year 2000-2001

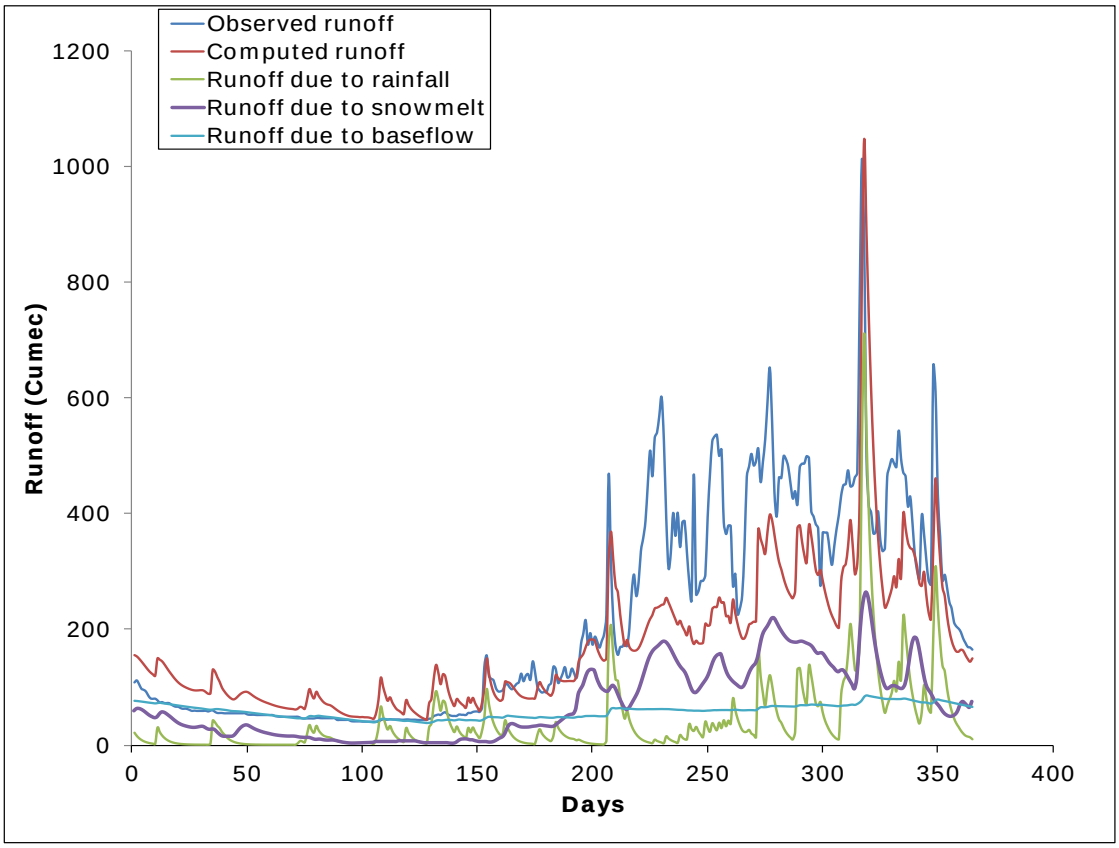

Figure 6.6: Simulated discharge of the Beas river at Pandoh for the year 2001-2002

It can be clearly seen that the estimated and observed hydrograph matches very well for the years 2002-2005. The efficiency (R^2) of the model for the melt years 2002-2005 is 0.84, whereas the difference in volume (D_V) is 1.64% and root mean square error (RMSE) is 0.28. It is revealed from the results that model performance was good for the three-year period.

6.10 SIMULATION OF STREAMFLOW

After the successful calibration of the model, it was used for simulation for a period of twelve years i.e. 1990-1993, 1993-1996, 1996-1999 and 1999-2002 for the Beas basin up to Pandoh dam. The estimated and calibrated parameters obtained during the calibration stage were utilized to simulate the runoff hydrograph for the period as mentioned above. The results of the simulation are illustrated graphically in Figure 6.7 to 6.10 and summarized in Table 6.4. These figures elucidate the five components i.e. observed discharge, simulated discharge, snowmelt contribution, rainfall contribution and contribution from baseflow. From these figures it is revealed that discharge starts rising from the month of April onwards due to increase in air temperature and reaches its peak by August and September, mainly due to

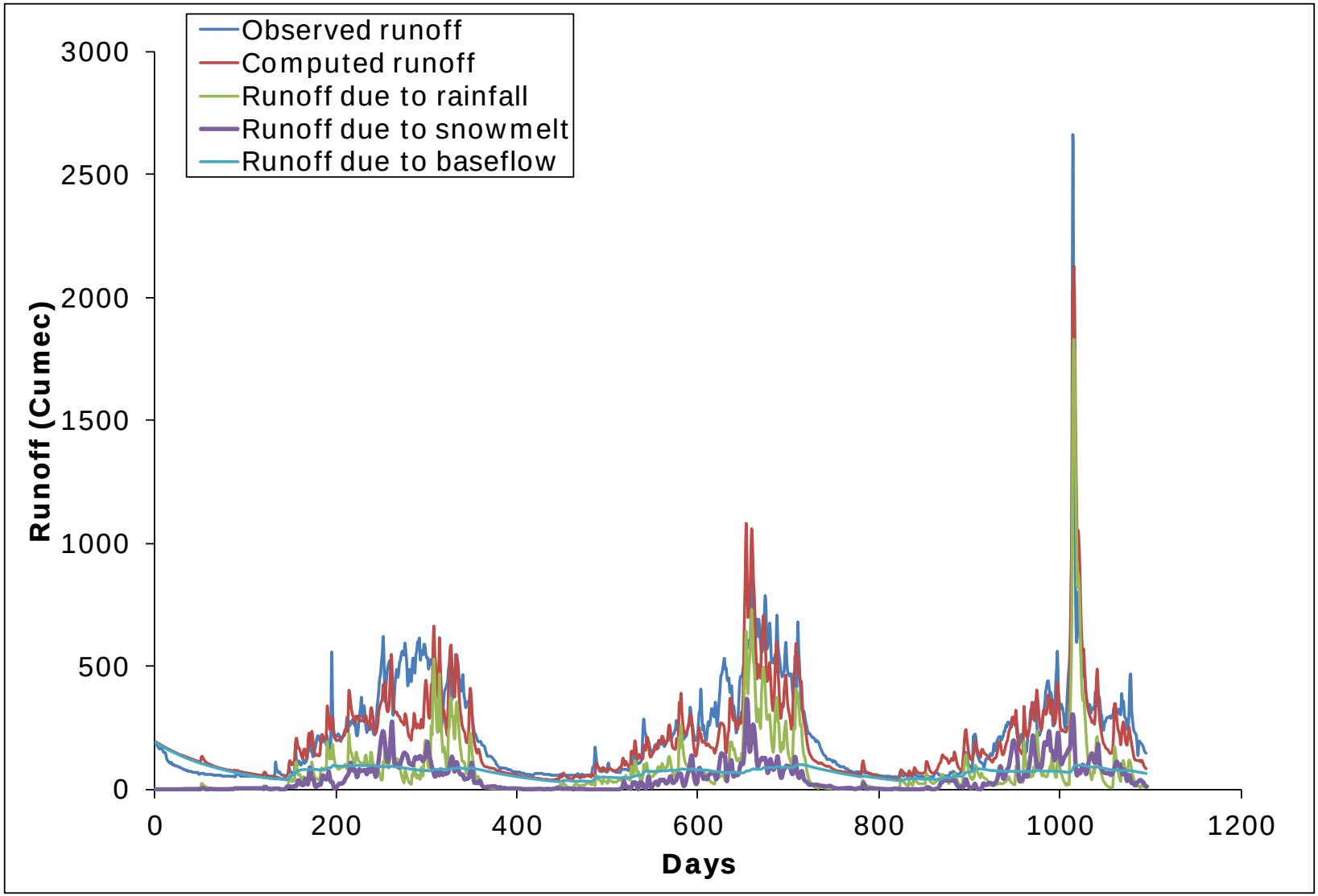

Figure 6.7: Simulated discharge of the Beas river at Pandoh for the year 1990-1993

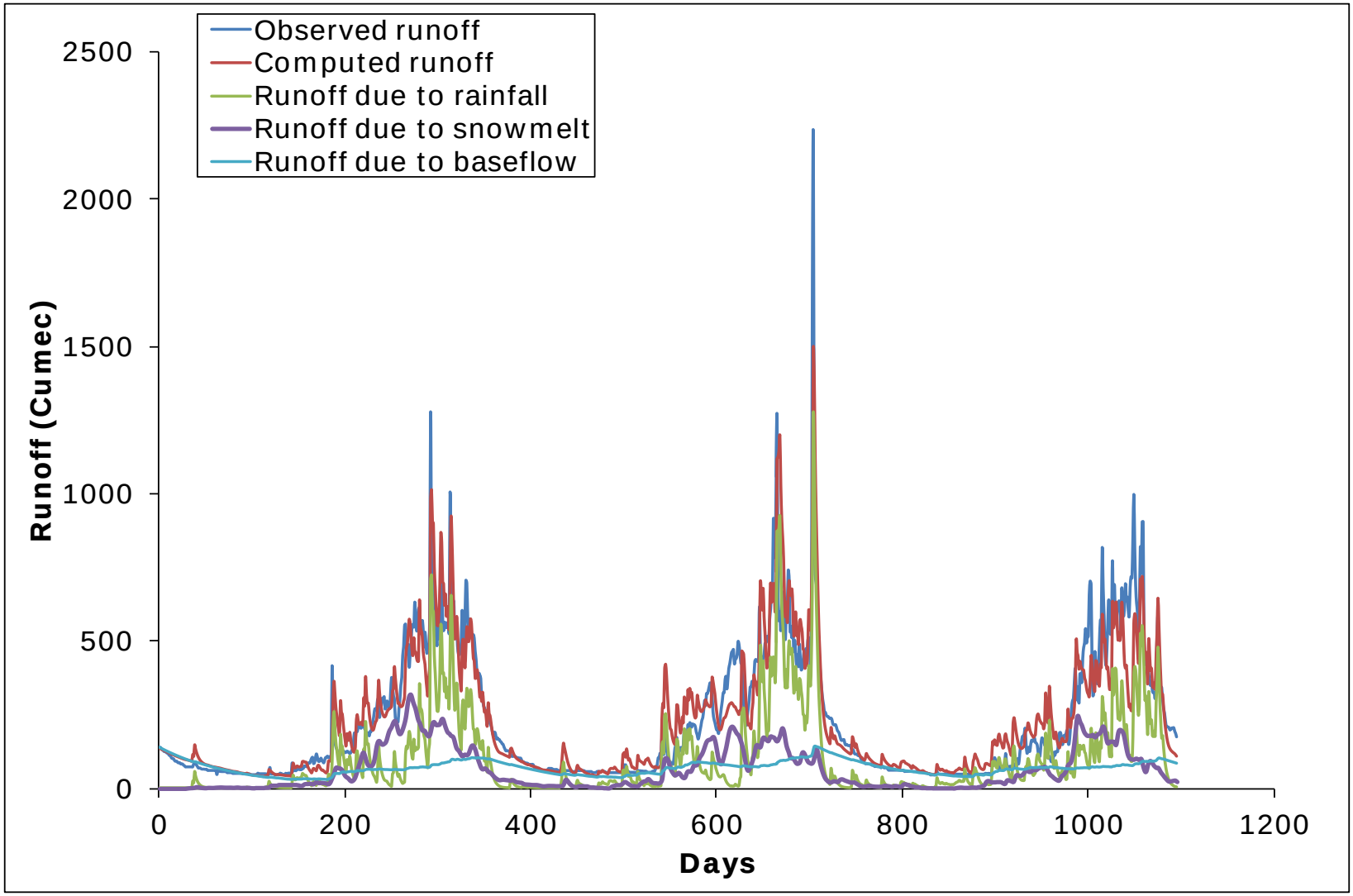

Figure 6.8: Simulated discharge of the Beas river at Pandoh for the year 1993-1996

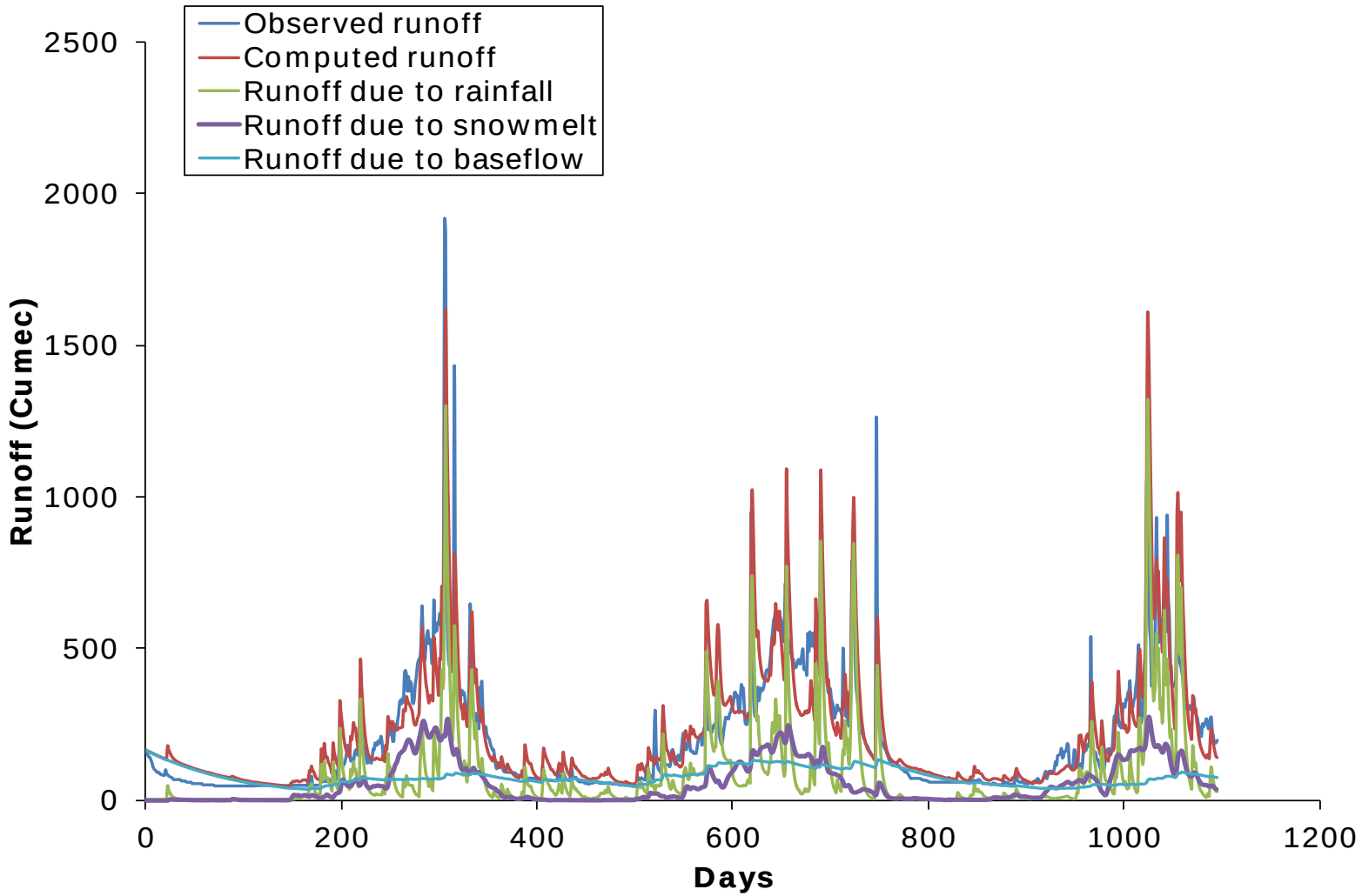

Figure 6.9: Simulated discharge of the Beas river at Pandoh for year 1996-1999

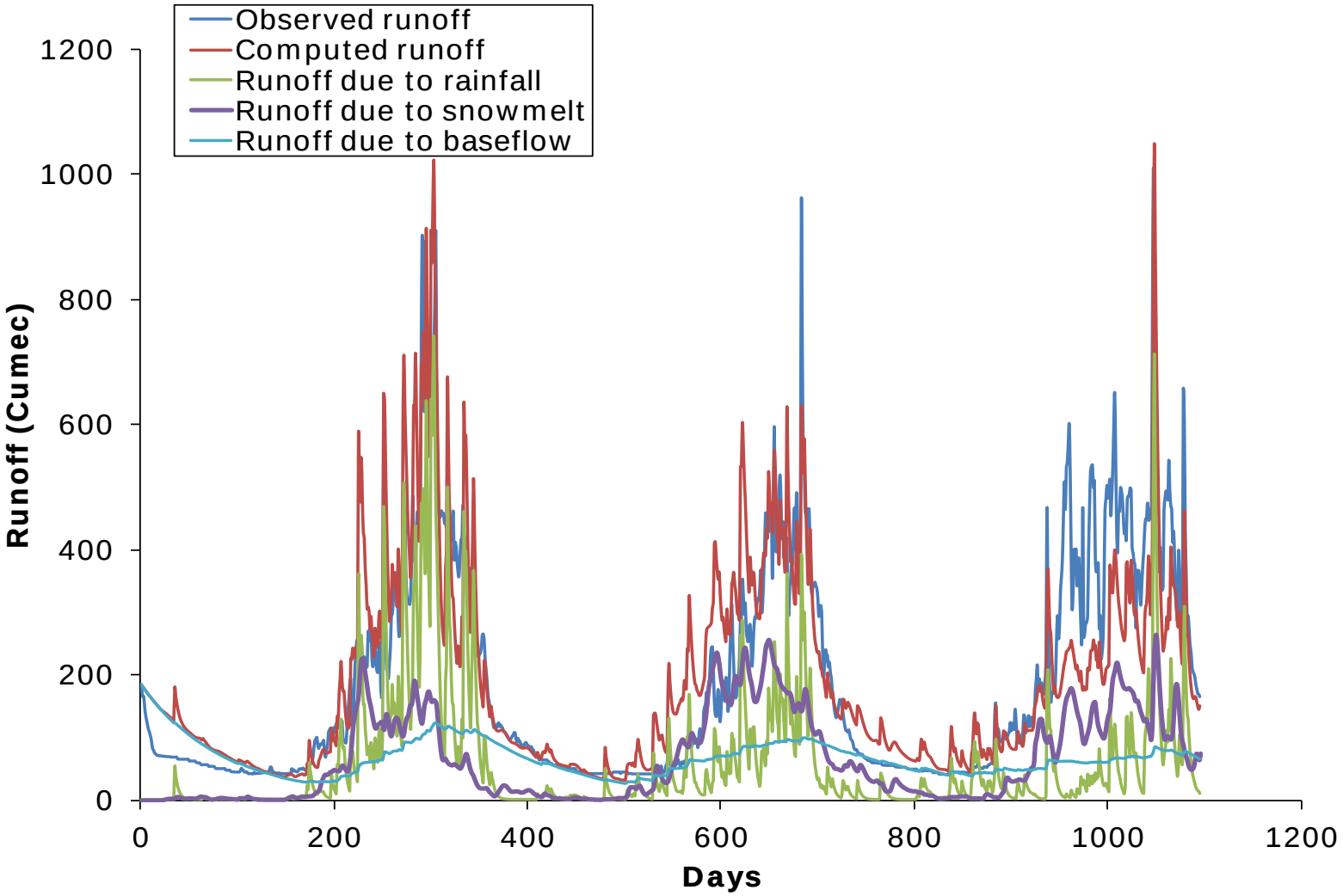

Figure 6.10: Simulated discharge of the Beas river at Pandoh for year 1999-2002

monsoonal rains and then starts reducing from the month of September onwards. It has been observed that during all the years, high flow occurred in the month of July and August. A close observation of rainfall and streamflow data signifies that most of the peaks in the streamflow were due to rainfall.

All the figures clearly depicts that the volumes and peaks of streamflow were very well reproduced by the snowmelt model for all the years. Thus, the study substantiate that SNOWMOD, a temperature index based (degree-day approach) snowmelt model worked efficiently for data scarce Beas river basin in Himalayas. The varying lapse rate has been used in the model for the first time for the study area which significantly improved the model efficiency in simulating the streamflow. The model also incorporated the estimated SCA for the missing dates using regression technique to further enhance the efficiency of the model for simulation. For more detail, yearly plots are also shown in Figure 6.11 to 6.19.

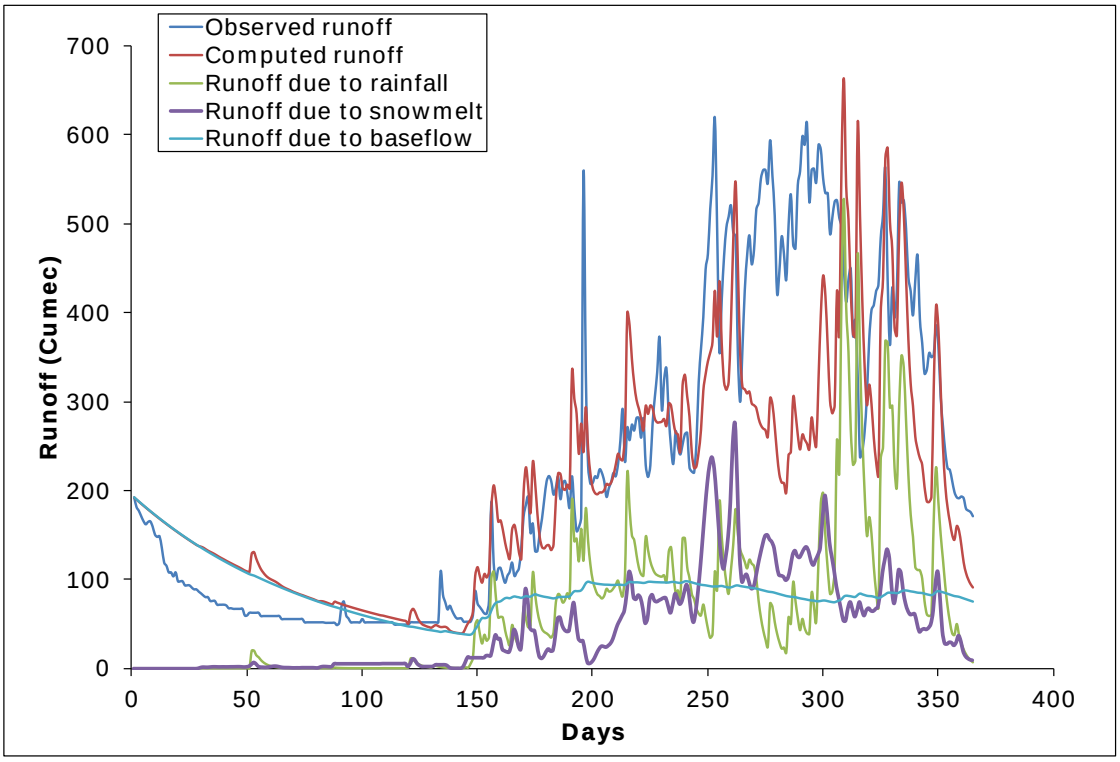

Figure 6.11: Simulated discharge of the Beas river basin at Pandoh for the year 1990-1991

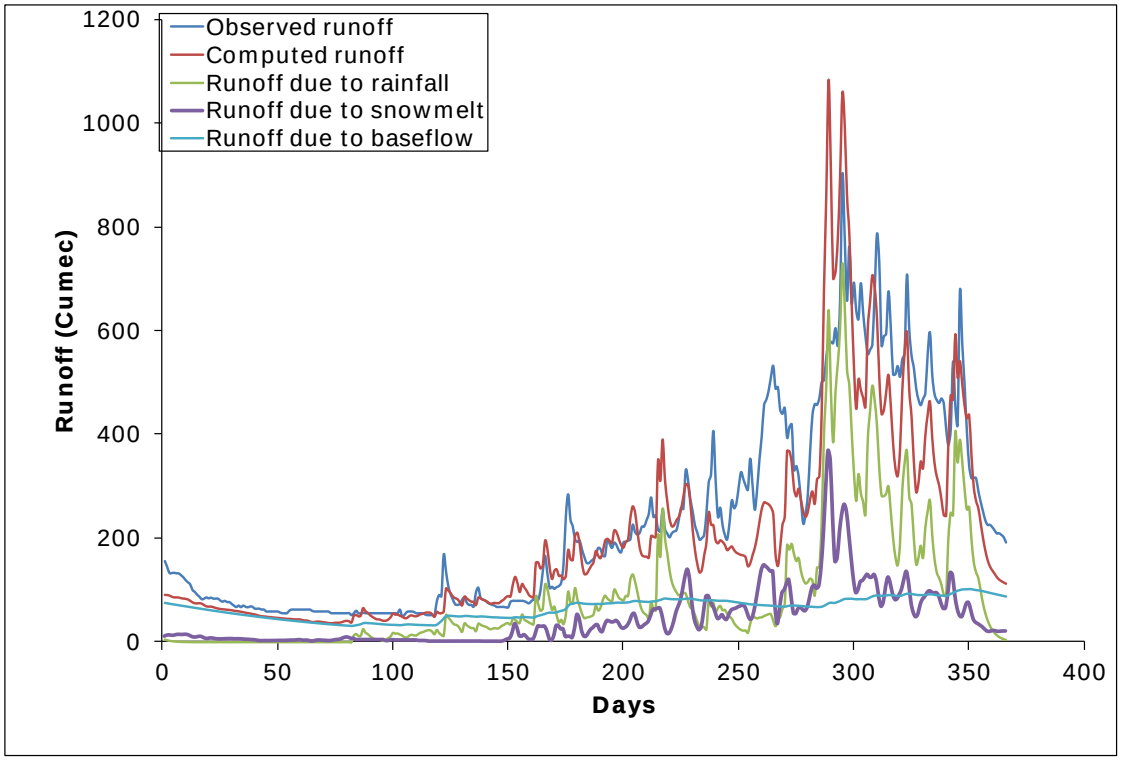

Figure 6.12: Simulated discharge of the Beas river basin at Pandoh for the year 1991-1992

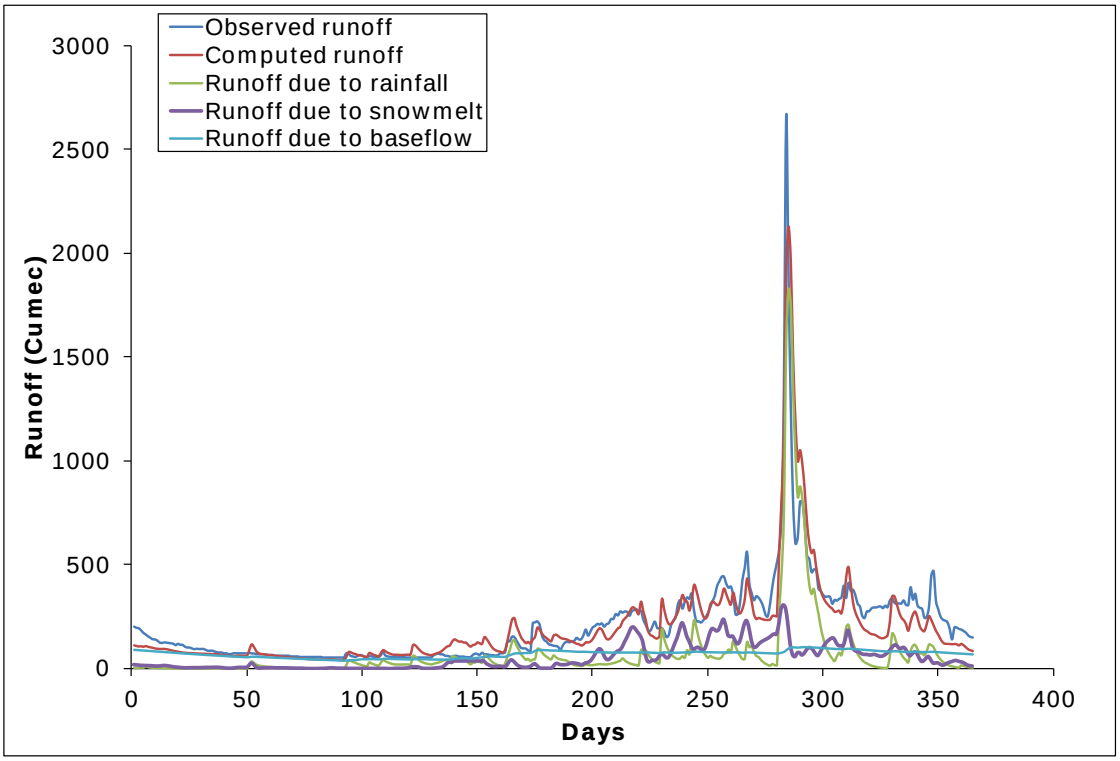

Figure 6.13: Simulated discharge of the Beas river basin at Pandoh for the year 1992-1993

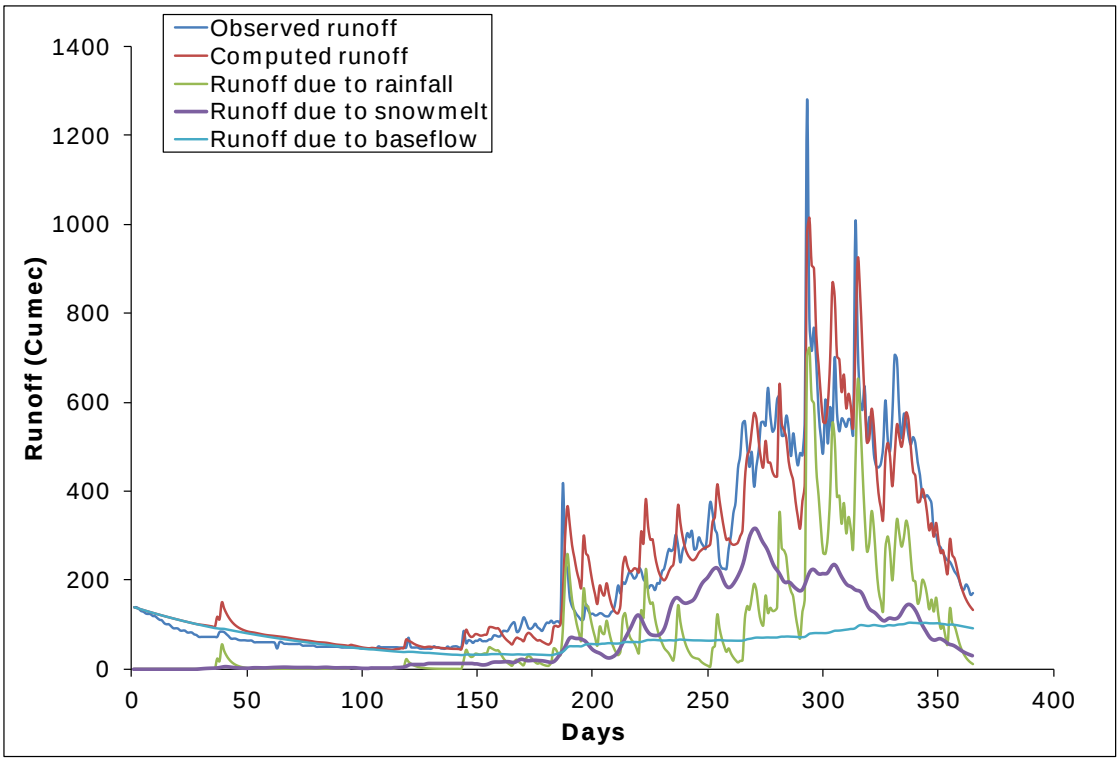

Figure 6.14: Simulated discharge of the Beas river basin at Pandoh for the year 1993-1994

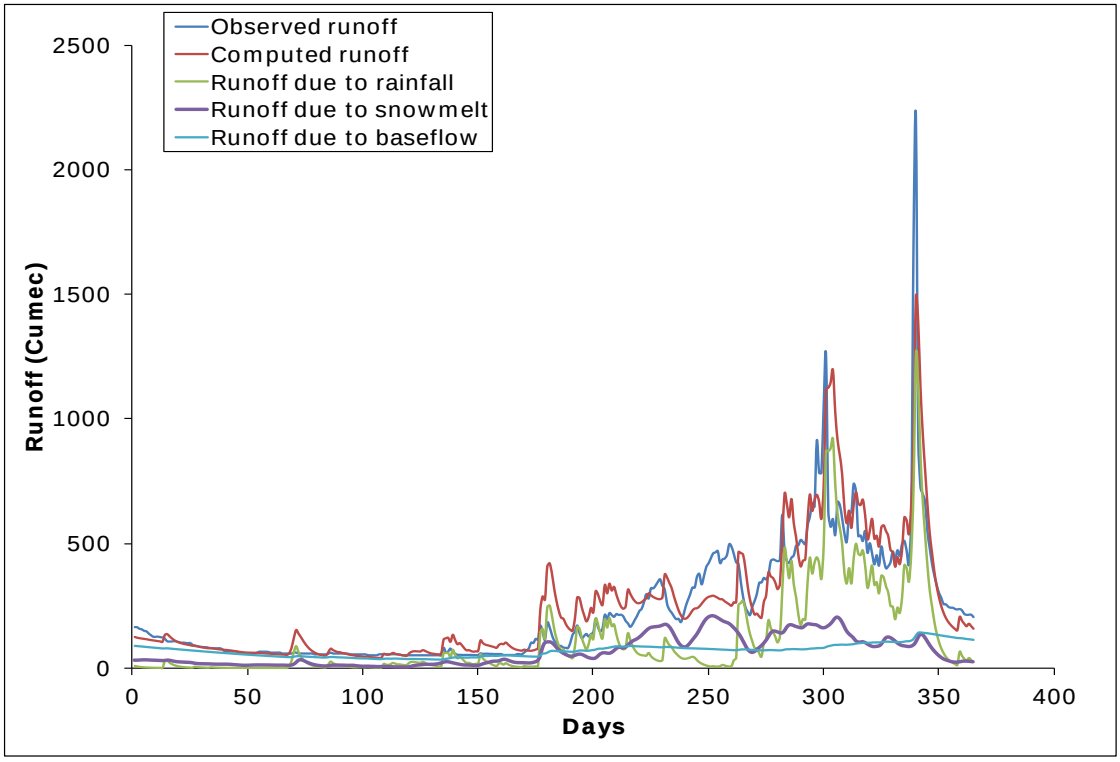

Figure 6.15: Simulated discharge of the Beas river basin at Pandoh for the year 1994-1995

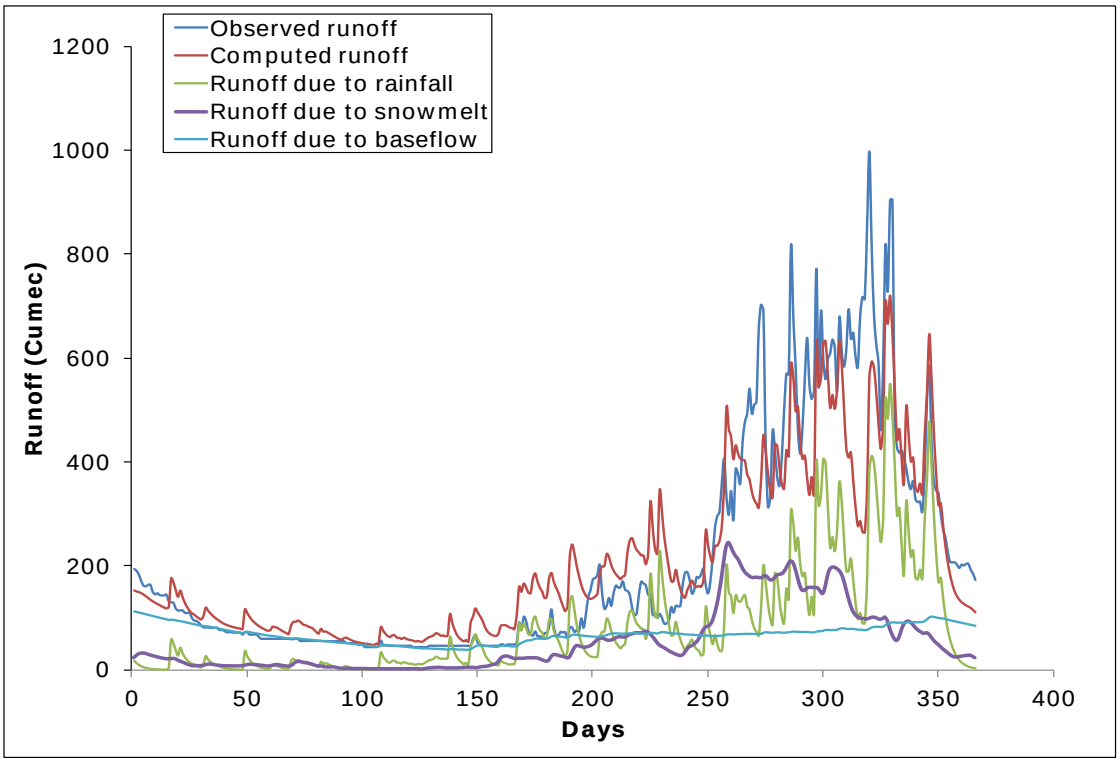

Figure 6.16: Simulated discharge of the Beas river basin at Pandoh for the year 1995-1996

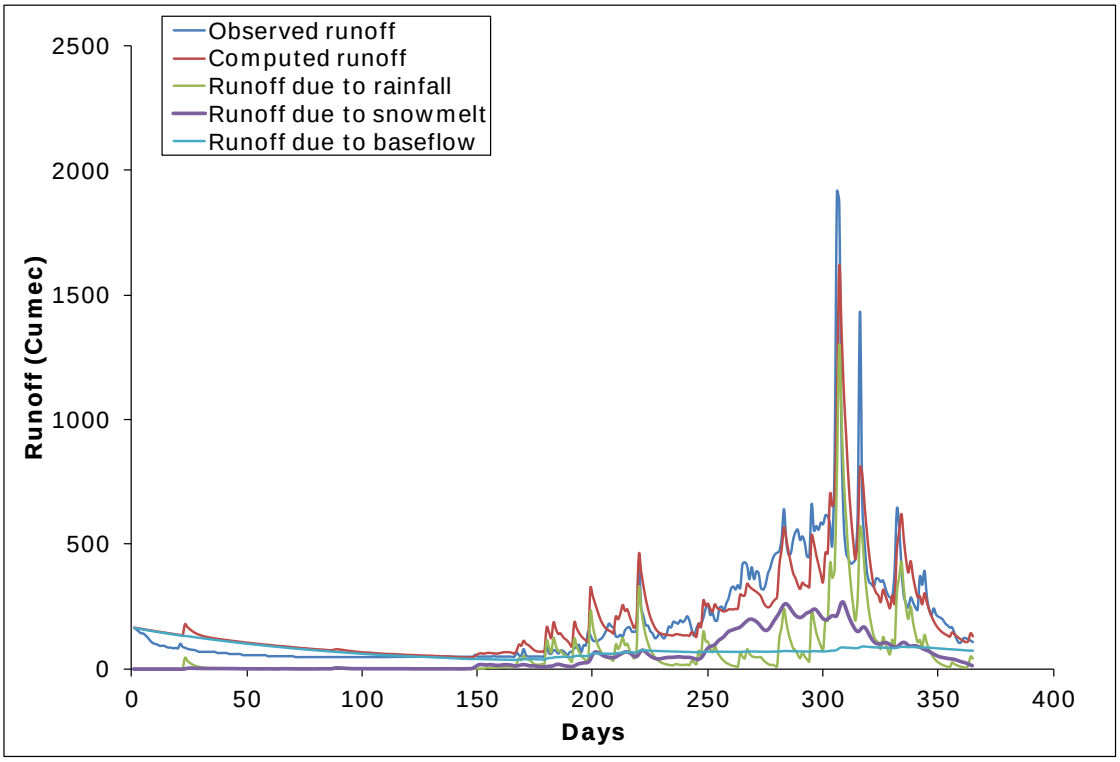

Figure 6.17: Simulated discharge of the Beas river basin at Pandoh for the year 1996-1997

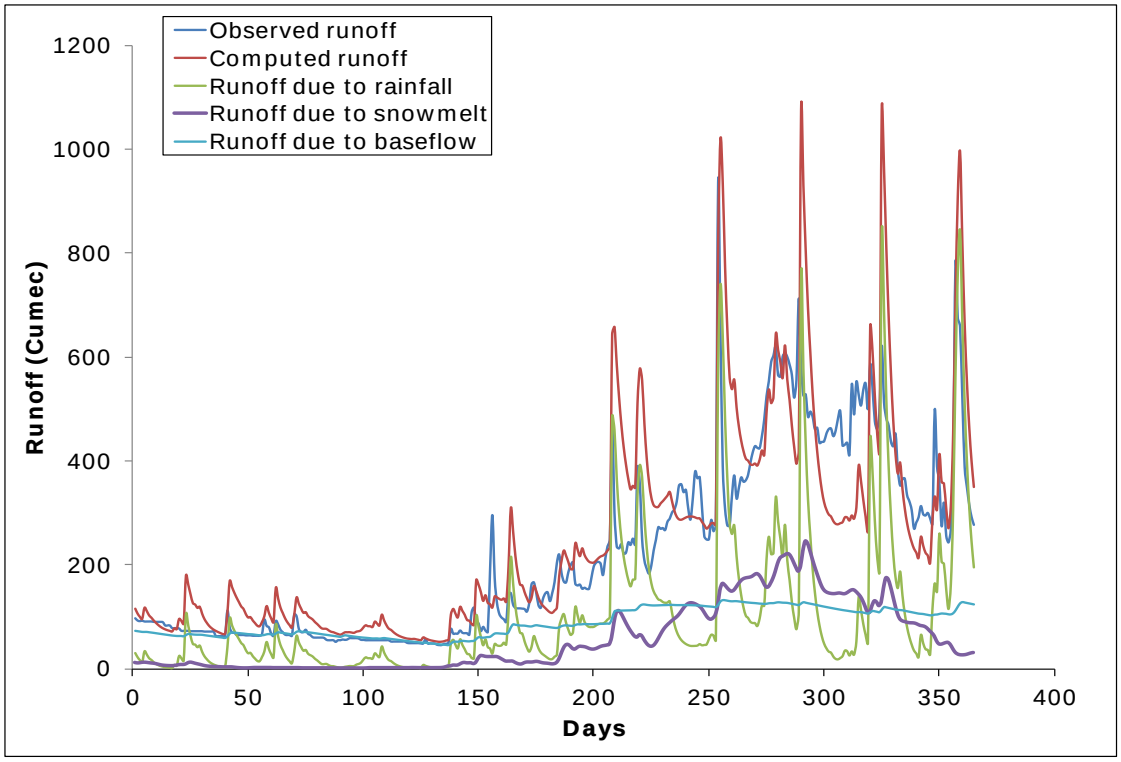

Figure 6.18: Simulation of the Beas river basin at Pandoh for the year 1997-1998

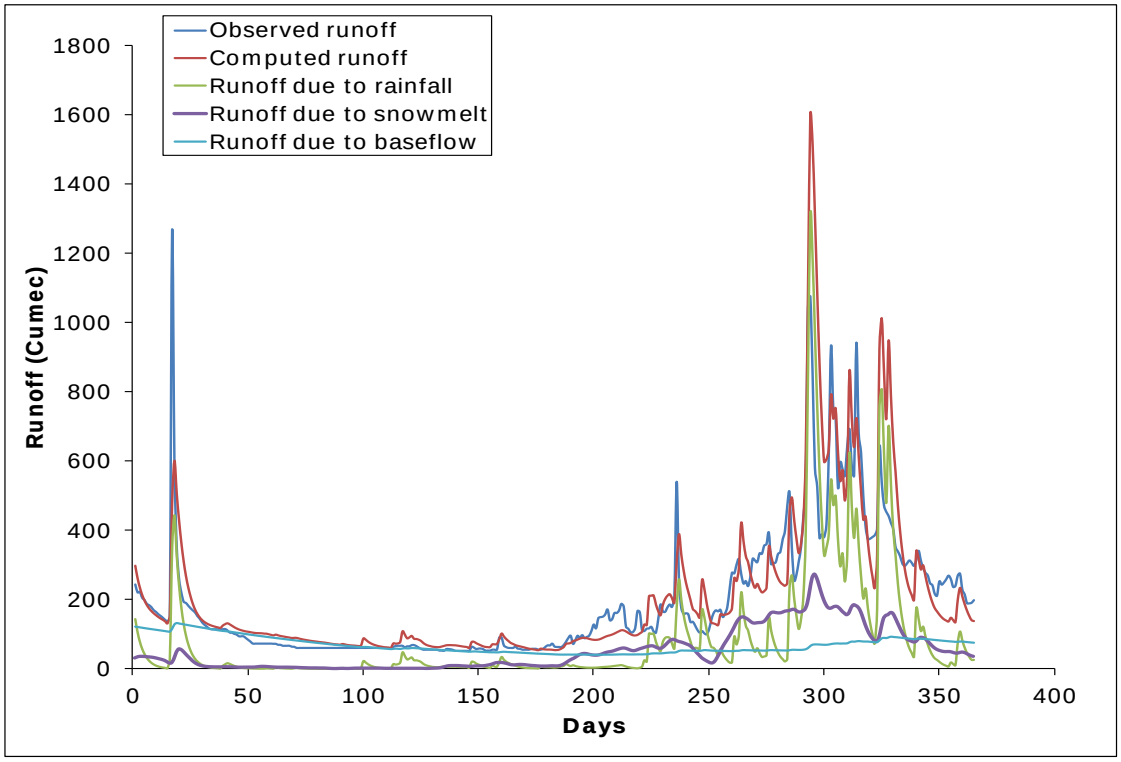

Figure 6.19: Simulation of the Beas river basin at Pandoh for the year 1998-1999

Table 6.4: Results of model simulation for the period 1990-2002 for the Beas basin

Period	Difference in Volume (Dv) (%)	Model Efficiency (R^2)	Rain (%)	Snow (%)	Base Flow (%)
1990-1993	-9.63	0.75	39.56	24.07	36.37
1993-1996	3.30	0.80	41.85	27.99	30.16
1996-1999	9.15	0.68	39.04	25.38	35.58
1999-2002	3.46	0.70	30.48	34.62	34.90

From the Table 6.4 it can be seen that efficiency of the model (R^2) for snowmelt season for 1990-2002 varied from 0.68 to 0.80. The difference in volume varies from -9.63% to 9.15%. The snowmelt contribution varies from 24.07% to 34.62% whereas rainfall contribution varied from 30.48% to 41.85% during this period. The baseflow contribution varied from 30.16 % to 36.37%.

As the model simulates snowmelt runoff and rainfall-runoff separately, the total streamflow contribution of each component has been computed for both seasonal and annual time scale. The estimated contribution of snowmelt and rainfall to the ablation and annual flows for the Beas basin is shown in Table 6.5. The ablation period is taken from the month of March upto August. The baseflow has been separated into snowmelt and rainfall components using the contribution of these components to the baseflow. It is revealed from the study that the average runoff generated during the ablation period from the snowmelt is 38.2% whereas remaining 61.8% is contributed from rainfall.

Moreover, average contributions from the snowmelt and rainfall to the annual runoff were estimated to be 39.2% and 60.8% respectively. Thus, it can be concluded that snowmelt runoff is mainly generated during the ablation period only. Kumar et al. (2007) carried out a study for this basin using the water balance approach in which the contribution of snowmelt and rainfall to the annual flows was estimated to be 35.1% and 64.9% respectively. The present study provides more accurate estimates of the snowmelt and rainfall components for the Beas basin.

Table 6.5: Contribution of snowmelt and rainfall to the ablation and annual flows

Period	Rainfall runoff (%)		Snowmelt runoff (%)	
	Ablation	Annual	Ablation	Annual
1991	60	59	40	41
1992	68	67	32	33
1993	61	59	39	41
1994	55	53	45	47
1995	66	65	34	35
1996	62	61	38	39
1997	56	56	44	44
1998	64	64	36	36
1999	62	61	38	39
2000	64	63	36	37

6.11 SUMMARY

SNOWMOD has been applied to simulate the daily runoff from the Beas basin at Pandoh. The input essential for the model included daily hydro-meteorological data of temperature, precipitation and streamflow measured at climatological observatories in the basin, and satellite derived data information on daily areal extent of snow cover and seasonally/topographic varying temperature lapse rate. Snowmelt runoff has been modeled effectively for the basin by integrating remote sensing information and hydro-meteorological data. The model simulated the contribution from three components of streamflow i.e. snowmelt runoff, rainfall-runoff and baseflow.

The model reproduced flow hydrographs very well in both calibration (2002-2005) and validation (1990-2002) period with model efficiency varying from 0.68 to 0.80 respectively. The difference in observed and simulated volume was less than 10% for total period, including calibration and validation periods. Most of the peaks in the streamflow at Pandoh dam site resulted due to rainfall. Moreover, a good database has been generated for this part of Himalayan region, especially the snow cover area and the lapse rate (seasonally and topographically) mandatory for such hydrologic models.

Chapter 7

TREND ANALYSIS

7.1 BACKGROUND

The changing climatic conditions and warming up of environment has major impact on the water resources and agricultural sectors, and overall economy of the nation. Due to intensification of hydrological cycle, drastic and oppressive change in hydrologic parameters (like precipitation, evaporation and streamflow) have occurred which substantially influences the flow regimes. Sonali and Kumar (2013) observed that among the different influential atmospheric variables, temperature has a significant and direct effect upon nearly all hydrologic variables. A small shift in climatic pattern owing to escalating air temperature and changing precipitation is likely to affect mountainous river networks (Huber et al., 2005). Moreover, warmer climate leads to the spatio-temporal variation in snow cover distribution and melt runoff from snow and glacier significantly (in different scales) which in turn will affect the water supplies in these regions. However, recent research studies by scientific community evince the well established global climatic change around the world and the effects of this alteration on regional and basin scale still needs to be probed.

The present study aims to detect and quantify the trends of hydro-climatic variables by using parametric and non-parametric statistical tools for the Beas basin. The simple regression method (parametric), Mann-Kendall test and Sens's estimator of slope method (non-parametric) have been applied to determine trend of climatic variables namely temperature, rainfall and discharge series available for various meteorological stations distributed over the basin. The trends and their magnitude for these climatic variables have been determined both at annual and seasonal time scale.

7.2 INTRODUCTION

Air temperature is generally recognised as good indicator of state of climate globally because of its ability to represent the energy exchange process over the earth's surface with reasonable accuracy (Vinnikov et al., 1990; Thapliyal and Kulshrestha, 1991). Temperature drives the hydrological cycle which directly or indirectly influences the hydrological processes.

Warmer climate leads to intensification of hydrological cycle which results in higher rates of evaporation and increase of liquid precipitation. Some studies on temperature variation on global scale (Jones et al., 1986; Folland and Parker, 1990; IPCC 2001) have established the fact that the earth's atmosphere has witnessed a significant warming in last century. The studies in mountainous areas like the Swiss and Polish Alps, the Rockies (Brown et al., 1992; Beniston et al., 1997; Wibig and Glowicki, 2002; Beniston, 2003; Diaz et al., 2003; Rebetez, 2004) and the Andes (Villaba et al., 2003; Vuille et al., 2003) have demonstrated significant rise in air temperatures with alarming effects on their environment.

Several studies in India have been carried out to determine the changes in temperature and rainfall and its association with climate change. Long–term trends in the maximum, minimum and mean temperatures over the north-western Himalaya during the 20^{th} century (Bhutiyani et al. 2007) suggest a significant rise in air temperature in the north-western Himalaya, with winter warming occurring at a faster rate. (Dimri and Ganju 2007) simulated the wintertime temperature and precipitation over the western Himalaya and found that temperature is underestimated and precipitation is overestimated in Himalaya. The changing trends of temperature and precipitation over the western Himalaya were examined and it was found that there was trend of increasing temperature and decreasing precipitation at some specific locations. (Dash et al., 2007) found an increase of 0.9 ^{o}C in annual maximum temperature over the western Himalaya. (Sharma et al., 2000) found an increasing trend in rainfall at some stations and a decreasing trend at other stations in Koshi basin in eastern Nepal and Southern Tibet. Similar trends in rainfall were found by Kumar et al. (2005) for the state of Himachal Pradesh.

The changes in temperature, precipitation and other climatic variables are likely to influence the amount and distribution of runoff in all river systems globally. No detailed study of trends for hydro-climatic data, in particular temperature and precipitation for the Beas basin has been reported. Keeping in the view, in the present study the Beas basin has been selected to comprehend the climate change in the Beas basin up to Pandoh dam by analyzing the instrumental data of air temperature, precipitation and discharge on seasonal and annual time scale. The main objective of the study was to determine trend of aforesaid hydro-meteorological variables and to understand the climate of the area.

7.3 DATA USED

The hydro-meteorological data of temperature, rainfall and discharge used in the study have been collected from the office of Bhakra Beas Management Board (BBMB) at Pandoh, as described earlier in chapter 3. The daily maximum and minimum temperature data series (1986-2009) for four distinct stations namely Bhuntar, Larji, Manali and Pandoh located at different altitudes was collected. The daily rainfall data series (1979-2009) of six stations: Banjar, Bhuntar, Larji, Pandoh, Manali and Sainj and the daily discharge data series for five stations: Bakhli, Sainj, Thalout, Tirthan and Pandoh were collected. The general details of hydro-meteorological stations is given in Table 7.1

Table 7.1 Details of the meteorological stations located in the study area

S. No	Station	Latitude	Longitude	Altitude (m)
1.	Pandoh	31° 40' 8"	77° 3' 59"	899
2.	Thalout	31° 42' 55"	77° 12' 00"	933
3.	Bakhli	31° 39' 28"	77° 05' 28"	940
4.	Larji	31° 43' 21"	77° 12' 58"	995
5.	Tirthan	31° 439' 21"	77° 13' 38"	1043
6.	Bhuntar	31° 53' 2"	77° 8' 51"	1102
7.	Sainj	31° 46' 0"	77° 18' 44"	1348
8.	Banjar	31° 39' 28"	77° 058' 28"	1353
9.	Manali	32° 14' 26"	77° 11' 37"	1842

7.4 DATA PROCESSING

The collected time series for the temperature, rainfall and streamflow was compiled and processed for the seasonal and annual analyses for the given period. The available daily maximum and minimum temperature data series has been used to compute the monthly time series of different variables; maximum (T_{max}), minimum (T_{min}) average (T_{avg}), highest maximum (H_{max}), lowest minimum (L_{min}) and range (T_{range}) for all the meteorological stations. The daily rainfall data series (1979-2009) of five stations namely Banjar, Bhuntar, Larji, Pandoh and Sainj were used to form monthly totals. Likewise, the monthly totals time series

was computed for the five streamflow stations. For investigation of changes in hydro-climatic variables at different time scales, a year was divided into four principal seasons:

1. Pre-monsoon season prevailing from March to May
2. Monsoon season prevailing from June to September
3. Post-monsoon season prevailing from October to November
4. Winter season prevailing from December to February

The monthly data of temperature, rainfall and streamflow were further used to compute the annual and seasonal time series, which were in turn used for the investigation of trend on seasonal and annual time scale.

7.5 METHODOLOGY

The term trend refers to "general tendency or inclination". In a time series of any variable, trend depicts the long smooth movement lasting over the span of observations, ignoring the short term fluctuations. It helps to determine whether the values of a series increase or decrease over the time. In statistics, trend analysis referred as an important tool and technique for extracting an underlying pattern of behaviour or trend in a time series which would otherwise be partly or nearly completely hidden by noise.

Statistic and probability plays an important role in scientific and engineering community (Ayyub and McCuen, 2002) because statistical tools help to detect spatial and temporal trends for hydrological and environmental studies. Major schemes or projects are formulated based on the historical behaviour of environment under uncertain climatic conditions. Therefore, a study of trend assists to investigate the overall pattern of change over time in hydro-meteorological variables especially for water resources project on temporal and spatial scales. Trends in data can be identified by using either parametric or non-parametric methods, and both the methods are extensively used. The parametric methods are considered to be more powerful than the non-parametric methods only when the data series is normally distributed, independent and homogeneous variance (Hamed and Rao, 1998). Conversely, non-parametric methods are more advantageous as they only require the data to be independent and are also less sensitive to outliers and missing values.

For detection of trends for climatic studies, the non-parametric methods are widely used for analyzing the trends in several hydro-climatic time series namely rainfall, temperature, pan-evaporation, wind speed etc. (Hirsch et al., 1982; Yu et al. 1993; Kothyari and Singh, 1996; Fu et al., 2004; Tebakari et al., 2005; Mishra et al., 2009; Jhajharia et al., 2009, 2011; Kumar et al.,

2010; Chattopadhyay et al., 2011; Dinpashoh et al., 2011; Jhajharia and Singh, 2011; Jain and Kumar, 2012; Jain et al., 2012b; Singh et al., 2014). Regression and other trend analysis methods have been applied by USGS to daily, monthly and annual time series of streamflow (Wurbs et al., 2011)

In the present study, to analyze the trends of the hydro-climatic series of each individual station, the popular statistical methods; simple regression method (parametric), Mann-Kendall test and Sens's estimator of slope method (non-parametric) have been applied. The systematic approach has been adopted to determine the trend in three phases. Firstly, a simple linear regression method to test the long term linear trend, secondly, non-parametric Mann-Kendall test for the presence of a monotonic increasing or decreasing trend in the time series and Thirdly, the non-parametric Sen's estimator of slope test to determine the magnitude of the trend in the time series of meteorological parameters namely temperature, rainfall and discharge at the basin scale. These are described in the following sections.

7.5.1 Regression Model

One of the most useful parametric models to detect the trend is the "Simple Linear Regression" model. The method of linear regression requires the assumptions of normality of residuals, constant variance, and true linearity of relationship (Helsel and Hirsch, 1992). The model for Y (e.g. precipitation) can be described by an equation of the form:

$$Y = at + b \tag{7.1}$$

where, t = time (year), a = slope coefficient; and b = least-squares estimate of the intercept.

The slope coefficient indicates the annual average rate of change in the hydrologic characteristic. If the slope is significantly different from zero statistically, it is entirely reasonable to interpret that there is a real change occurring over time. The sign of slope defines the direction of the trend of the variable: positive sign indicates a rising trend while negative sign indicates a falling trend.

7.5.2 Sen's Estimator of Slope

The magnitude of trend in a time series was determined using a non-parametric method known as Sen's estimator (Sen 1968). This method assumes a linear trend in the time series and has been widely used for determining the magnitude of trend in hydro-meteorological time

series (Lettenmaier et al., 1994; Yue and Hashino, 2003; Partal and Kahya, 2006). In this method, the slopes (T_i) of all data pairs are first calculated by

$$T_i = \frac{x_j - x_k}{j - k} \qquad \text{for i = 1,2,…,N} \tag{7.2}$$

where x_j and x_k are data values at time j and k ($j > k$) respectively. The median of these N values of T_i is Sen's estimator of slope which is calculated as

$$\beta = \begin{cases} T_{\frac{N+1}{2}} & \text{if } N \text{ is odd,} \\ \frac{1}{2}\left(T_{\frac{N}{2}} + T_{\frac{N+2}{2}} \right) & \text{if } N \text{ is even.} \end{cases} \tag{7.3}$$

A positive value of β indicates an upwards (increasing) trend and a negative value indicates a downwards (decreasing) trend in the time series.

7.5.3 Mann–Kendall Test

To ascertain the presence of a statistically significant trend in hydrologic climatic variables such as temperature, precipitation and streamflow with reference to climate change, the non-parametric Mann–Kendall (MK) test has been employed by a number of researchers (Yu et al. 1993; Douglas et al. 2000; Burn et al. 2004; Singh et al. 2008a, b). The MK method searches for a trend in a time series without specifying whether the trend is linear or non-linear. The MK test was also applied in the present study. The MK test checks the null hypothesis of no trend versus the alternative hypothesis of the existence of an increasing or decreasing trend. The statistic S is defined as (Salas 1993):

$$S = \sum_{i=1}^{N-1} \sum_{j=i+1}^{N} \text{sgn}(x_j - x_i) \tag{7.4}$$

where N is the number of data points. Assuming $(x_j - x_i) = \theta$, the value of sgn(θ) is computed as follows:

$$\text{sgn}(\theta) = \begin{cases} 1 & if \quad \theta > 0, \\ 0 & if \quad \theta = 0, \\ -1 & if \quad \theta < 0. \end{cases} \tag{7.5}$$

This statistic represents the number of positive differences minus the number of negative differences for all the differences considered. For large samples ($N > 10$), the test is conducted using a normal distribution (Helsel and Hirsch, 1992) with the mean and the variance as follows:

$$E[S] = 0 \tag{7.6}$$

$$Var(S) = \frac{N(N-1)(2N+5) - \sum_{k=1}^{n} t_k (t_k - 1)(2t_k + 5)}{18} \tag{7.7}$$

where n is the number of tied (zero difference between compared values) groups and t_k is the number of data points in the kth tied group. The standard normal deviate (Z-statistics) is then computed as (Hirsch *et al.* 1993):

$$Z = \begin{cases} \dfrac{S-1}{\sqrt{Var(S)}} & if \quad S > 0 \\ 0 & if \quad S = 0 \\ \dfrac{S+1}{\sqrt{Var(S)}} & if \quad S < 0. \end{cases} \tag{7.8}$$

If the computed value of $|Z| > z_{\alpha/2}$, the null hypothesis H_0 is rejected at the α level of significance in a two-sided test. In this analysis, the null hypothesis was tested at 95% confidence level.

7.6 TRENDS OF OBSERVED HYDRO-METEOROLOGICAL DATA

For better comprehension and visual interpretation of the observed trends, first of all seasonal and annual anomalies of temperature, rainfall and stream discharge for each station were computed with reference to the mean of the respective variable for the available records. Further, these anomalies were plotted against time and the trend was examined by fitting the linear regression line. The linear trend value represented by the slope of the simple least square regression provided the rate of rise/fall in the variable. Thereafter, Mann–Kendall (MK) test has been used for identification and to test the statistical significance of trend at confidence interval of 95%, prior to which data series of all the variables were checked for presence of auto-correlation. The Sen's estimator of slope (SE) was then applied to estimate the magnitude of the trend over the study period. The SE was applied to verify the outcomes of simple

regression analysis. The outcome of the analysis is shown in the form of Table and/or graph. The bold values in table refer to a statistically significant trend at 95% of confidence interval.

7.7 RESULTS AND DISCUSSION

7.7.1 Trends in Temperature

For trend analysis, initially the anomalies of maximum temperature (T_{max}), minimum temperature (T_{min}), average temperature (T_{avg}), highest maximum temperature (H_{max}), lowest minimum temperature (L_{min}) and range (T_{range}) were computed and linear regression analysis (Parametric approach) was carried out and relationship were developed for linear trends for each station at both seasonal and annual scale. Graphical representation of T_{max}, T_{min} and T_{avg} are shown in Figure 7.1 to 7.6. The results of the parametric and non-parametric test for the increasing or decreasing trend and their magnitude estimated using Sen's slope estimator (SE) are presented in Table 7.2 to 7.7.

From Table 7.2 (SE) trend analysis of annual T_{avg} indicates rising trend at Bhuntar, Larji and Pandoh and deceasing trend at Manali station. None of these trends is found statistically significant. During pre-monsoon season, all the stations indicated rising trend with rising trend at Bhuntar and Pandoh statistically significant at 95% confidence level. During monsoon, post-monsoon and winter seasons two stations (Bhuntar and Larji) experienced rising trend and remaining two stations (Manali and Pandoh) experienced decreasing trend. The rising trend at Larji (0.056 ^{0}C/yr) during monsoon season was only statistically significant at 95% confidence level.

From Table 7.3 (SE) analysis of T_{max} shows increasing non-significant at Bhuntar, Larji and Pandoh and decreasing (non-significant) at Manali. The maximum increase is found for Larji (0.076 ^{0}C/yr) and minimum increase for Pandoh (0.053 ^{0}C/yr). Seasonal analysis indicated increasing trend for Bhuntar and Larji during all seasons and decreasing trend for Manali. For all seasons, an increasing trend was observed for pre-monsoon, monsoon and winter season for Pandoh while decreasing trend during post monsoon for Pandoh. The increasing trend during pre-monsoon and winter at Bhuntar, during winter at Larji (0.112^{0}C/yr) and during pre-monsoon at Pandoh (0.11^{0}C/yr) were found statistically significant.

Maximum Temperature **Minimum Temperature**

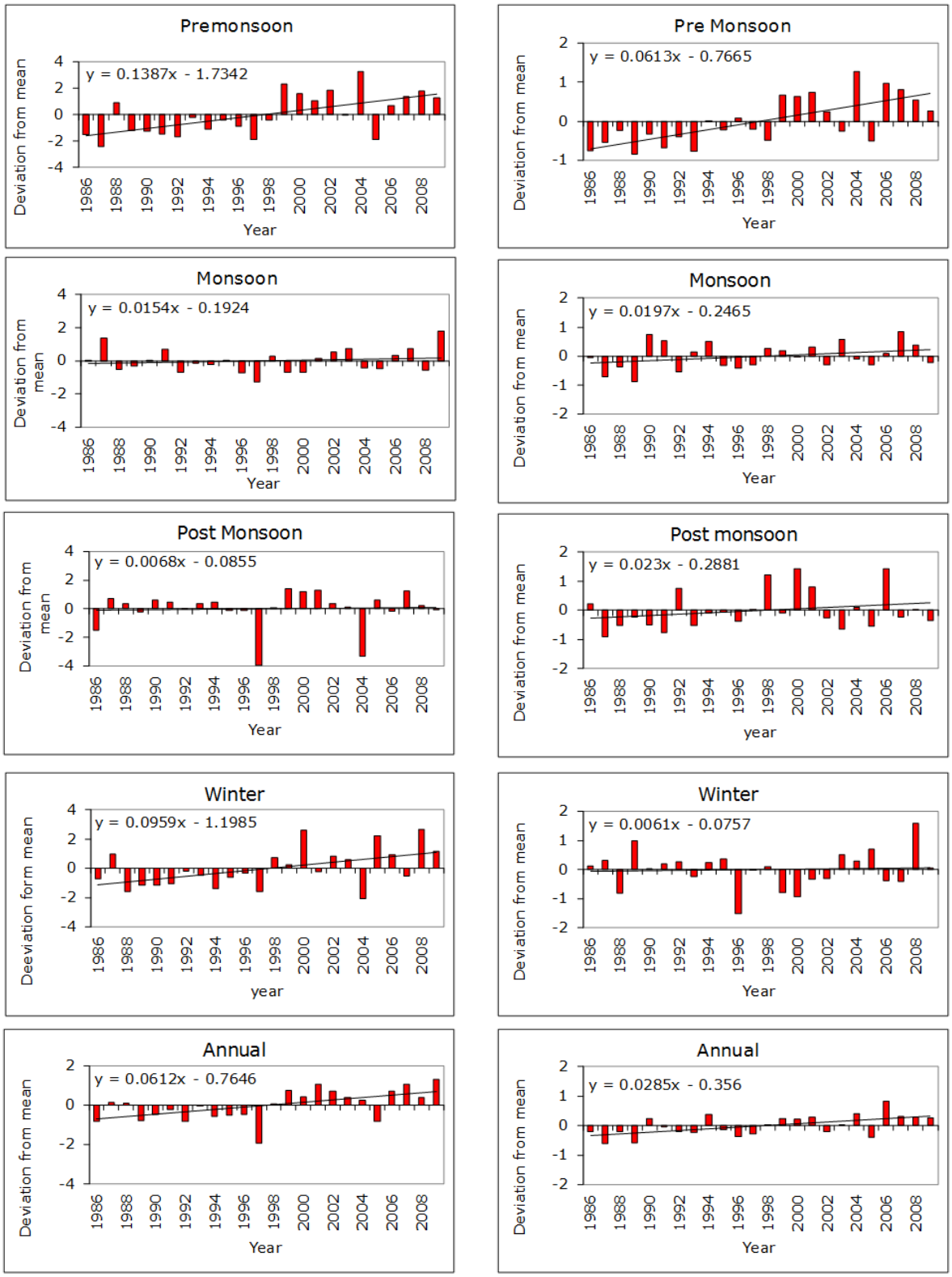

Figure 7.1: Maximum and minimum temperature trends of Bhuntar station

Maximum Temperature **Minimum Temperature**

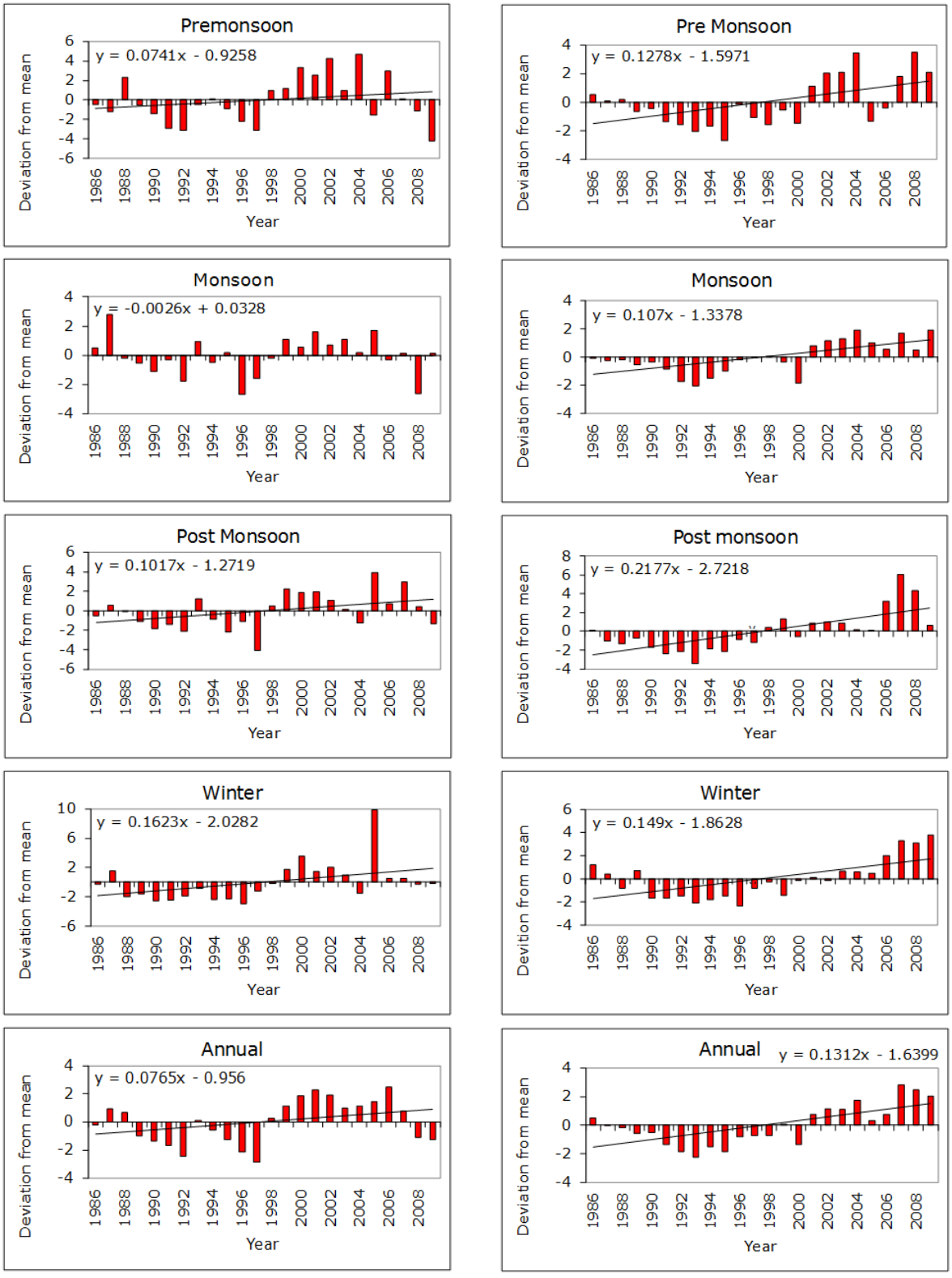

Figure 7.2: Maximum and minimum temperature trends of Larji station

Maximum Temperature **Minimum Temperature**

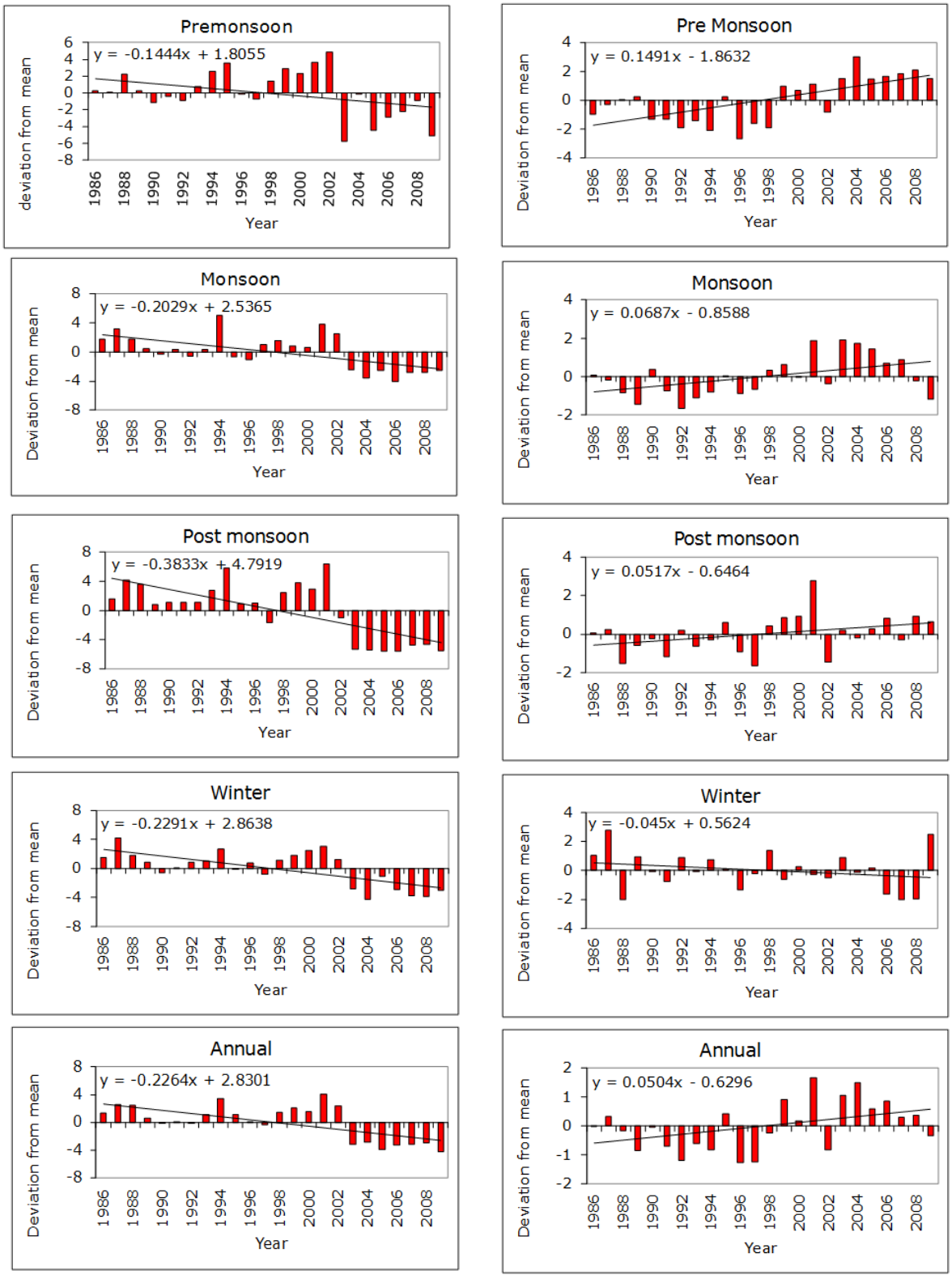

Figure 7.3: Maximum and minimum temperature trends of Manali station

Maximum Temperature **Minimum Temperature**

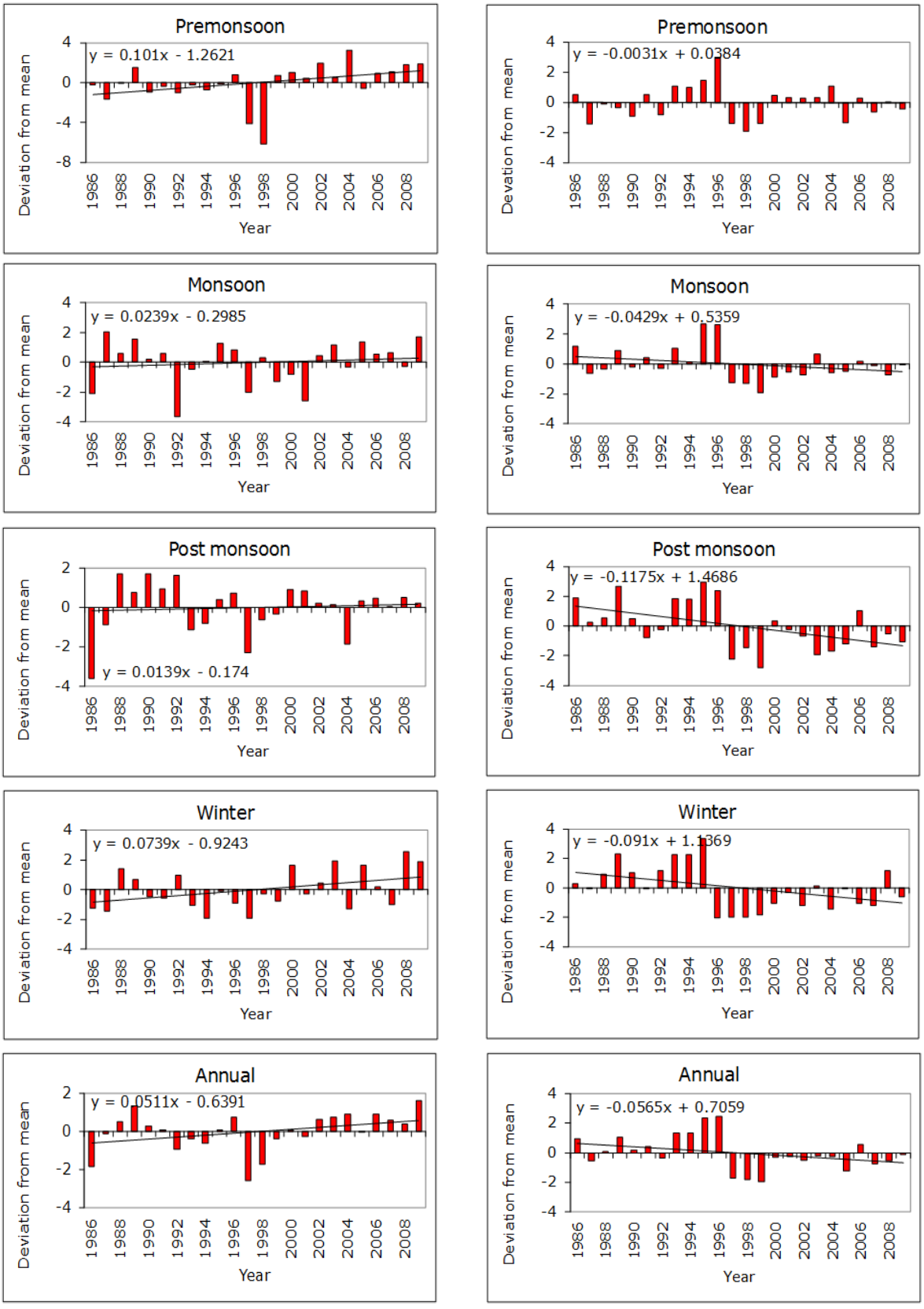

Figure 7.4: Maximum and minimum temperature trends of Pandoh station

AVG TEMPERATURE (BHUNTAR) **AVG TEMPERATURE (MANALI)**

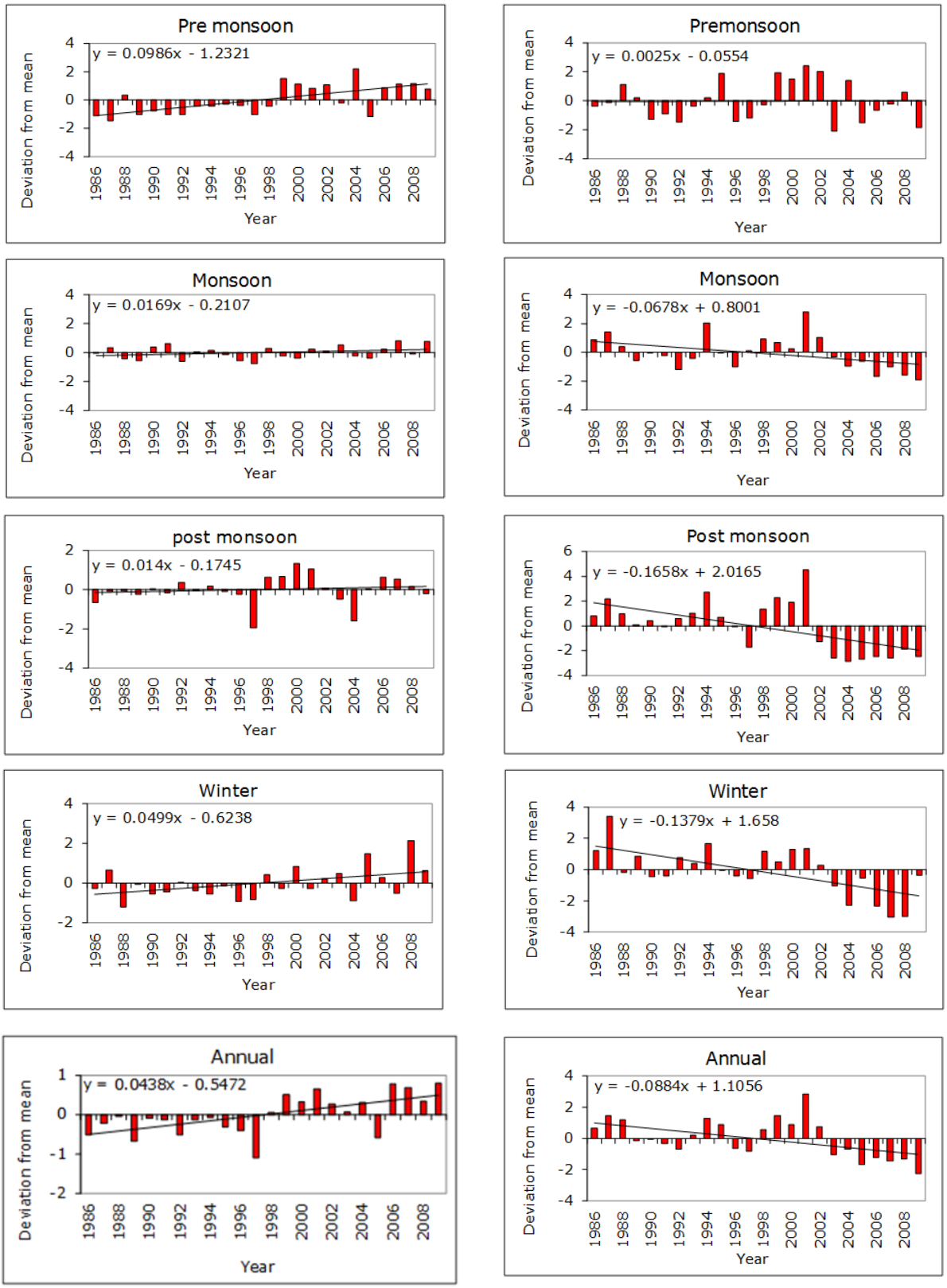

Figure 7.5: Average temperature trends of Bhuntar and Manali station

AVG TEMPERATURE (LARJI) **AVG TEMPERATURE (PANDOH)**

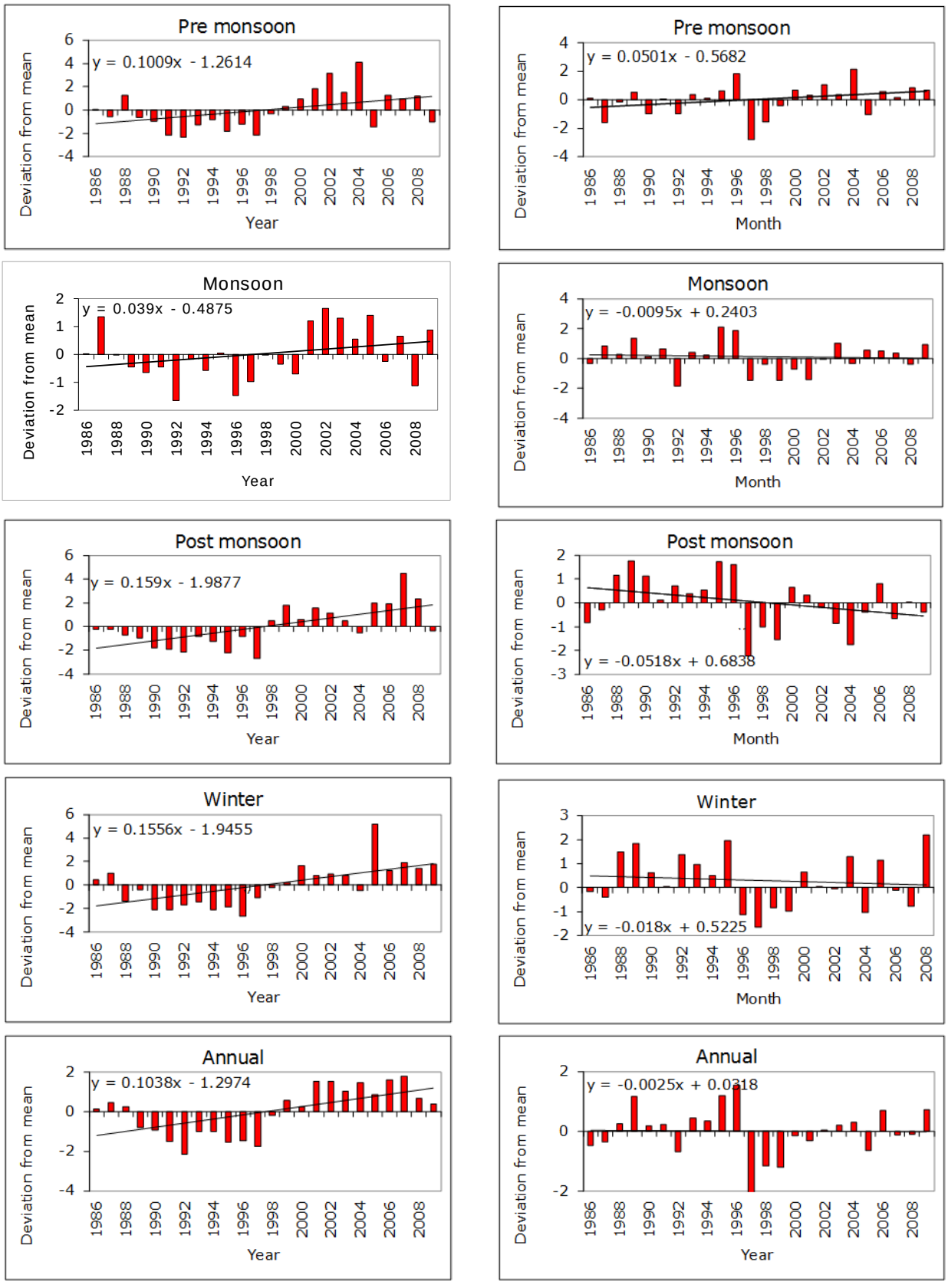

Figure 7.6: Average temperature trends of Larji and Pandoh station

Table 7.2: Seasonal and annual trends of average temperature (T_{avg})

Season	Station	Mann-Kendall test Z statistic	S	Sen Estimator	Linear regression	Trend
Annual	Bhuntar	1.95	75	0.045	0.0438	Rising
	Larji	0.9	35	0.097	0.0855	Rising
	Manali	-1.82	-70	-0.088	-0.0901	Falling
	Pandoh	0.01	19	0.01	0.0172	Rising
Pre-monsoon (Mar - May)	Bhuntar	3.32	134	**0.1**	0.0986	Rising
	Larji	1.48	57	0.09	0.0828	Rising
	Manali	0	-1	0	0.0025	No trend
	Pandoh	2.19	89	**0.043**	0.0133	Rising
Monsoon (Jun - Sept)	Bhuntar	1.12	46	0.018	0.0169	Rising
	Larji	2.01	77	**0.056**	0.039	Rising
	Manali	-1.58	-61	-0.081	-0.0678	Falling
	Pandoh	-0.2	-9	-0.006	0.0186	Falling
Post-monsoon (Oct - Nov)	Bhuntar	1.27	52	0.018	0.014	Rising
	Larji	1.08	42	0.154	0.1398	Rising
	Manali	-1.58	-61	-0.169	-0.1658	Falling
	Pandoh	-1.54	-63	-0.058	0.0002	Falling
Winter (Dec - Feb)	Bhuntar	1.84	75	0.044	0.0499	Rising
	Larji	1.8	69	0.168	0.1304	Rising
	Manali	-1.37	-53	-0.137	-0.1379	Falling
	Pandoh	-0.22	-10	-0.009	0.0302	Falling

Table 7.3: Seasonal and annual trends of maximum temperature (T_{max})

Season	Station	Mann-Kendall test Z statistic	S	Sen Estimator	Linear regression	Trend
Annual	Bhuntar	1.8	69	0.065	0.0612	Rising
	Larji	0.05	3	0.076	0.0765	Rising
	Manali	-1.8	-69	-0.233	-0.2264	Falling
	Pandoh	0.95	37	0.053	0.0511	Rising
Pre-monsoon (Mar - May)	Bhuntar	2.96	120	**0.15**	0.1387	Rising
	Larji	0.94	39	0.096	0.0741	Rising
	Manali	-1.17	-48	-0.11	-0.1444	Falling
	Pandoh	2.75	112	**0.11**	0.101	Rising
Monsoon (Jun - Sept)	Bhuntar	0.62	26	0.012	0.0154	Rising
	Larji	0.52	22	0.017	-0.0026	Rising
	Manali	-1.64	-63	-0.2	-0.2029	Falling
	Pandoh	0.4	17	0.025	0.0239	Rising
Post-monsoon (Oct - Nov)	Bhuntar	0.27	12	0.003	0.0068	Rising
	Larji	1.34	55	0.093	0.1017	Rising
	Manali	-1.53	-59	-0.372	-0.3833	Falling
	Pandoh	-0.35	-15	-0.015	0.0139	Falling
Winter (Dec - Feb)	Bhuntar	2.58	105	**0.1**	0.0959	Rising
	Larji	2.01	82	**0.112**	0.1623	Rising
	Manali	-0.79	-31	-0.22	-0.2291	Falling
	Pandoh	1.81	74	0.067	0.0739	Rising

Table 7.4: Seasonal and annual trends of minimum temperature (T_{min})

Season	Station	Mann-Kendall test Z statistic	S	Sen Estimator	Linear regression	Trend
Annual	Bhuntar	2.76	111	**0.03**	0.0285	Rising
	Larji	1.9	73	0.138	0.1312	Rising
	Manali	1.66	68	0.05	0.0504	Rising
	Pandoh	-0.58	-23	-0.043	-0.0565	Falling
Pre-monsoon (Mar - May)	Bhuntar	3.44	139	**0.062**	0.0613	Rising
	Larji	1.74	67	0.1	0.1278	Rising
	Manali	1.37	53	0.134	0.1491	Rising
	Pandoh	-0.17	-8	-0.002	-0.0031	Falling
Monsoon (Jun - Sept)	Bhuntar	1.52	62	0.021	0.0197	Rising
	Larji	1.85	71	0.1	0.107	Rising
	Manali	1	39	0.067	0.0687	Rising
	Pandoh	-0.97	-40	-0.025	-0.0429	Falling
Post-monsoon (Oct - Nov)	Bhuntar	1.27	52	0.02	0.023	Rising
	Larji	1.58	61	0.196	0.2177	Rising
	Manali	1.99	81	**0.05**	0.0517	Rising
	Pandoh	-1	-39	-0.1	-0.1175	Falling
Winter (Dec - Feb)	Bhuntar	-0.15	-7	0	0.0061	No trend
	Larji	2.75	105	**0.175**	0.149	Rising
	Manali	-1.39	-57	-0.058	-0.045	Falling
	Pandoh	-1.32	-51	-0.07	-0.091	Falling

Table 7.5: Seasonal and annual trends of highest maximum temperature (H_{max})

Season	Station	Mann-Kendall test Z statistic	S	Sen Estimator	Linear regression	Trend
Annual	Bhuntar	0.15	7	0.01	0.0049	Rising
	Larji	-1.21	-49	-0.091	-0.1243	Falling
	Manali	-1.06	-41	-0.17	-0.1696	Falling
	Pandoh	0.91	37	0	0.0354	No trend
Pre-monsoon (Mar - May)	Bhuntar	0.4	17	0.023	0.0013	Rising
	Larji	-1.22	-47	-0.2	-0.2274	Falling
	Manali	-1.14	-44	-0.267	-0.2604	Falling
	Pandoh	-0.1	-5	0	-0.0013	No trend
Monsoon (Jun - Sept)	Bhuntar	0.62	26	0.032	0.0166	Rising
	Larji	-1.46	-59	-0.125	-0.1365	Falling
	Manali	-2.47	-99	**-0.143**	-0.1457	Falling
	Pandoh	0.15	7	0	0.0033	No trend
Post-monsoon (Oct - Nov)	Bhuntar	1.59	65	0.05	0.0623	Rising
	Larji	1.71	68	0.071	0.0139	Rising
	Manali	-1.75	-67	-0.235	-0.2539	Falling
	Pandoh	1.03	42	0.054	0.0477	Rising
Winter (Dec - Feb)	Bhuntar	0.17	8	0.005	0.0561	Rising
	Larji	-0.11	-5	0	-0.0061	No trend
	Manali	-1.51	-58	-0.383	-0.3752	Falling
	Pandoh	0.95	39	0.071	0.0786	Rising

Table 7.6: Seasonal and annual trends of lowest minimum temperature (L_{min})

Season	Station	Mann-Kendall test Z statistic	S	Sen Estimator	Linear regression	Trend
Annual	Bhuntar	-0.07	-4	0	0.0182	No trend
	Larji	2.01	77	**0.205**	0.152	Rising
	Manali	0.71	29	0	0.0535	No trend
	Pandoh	-0.74	-29	-0.128	-0.1434	Falling
Pre-monsoon (Mar - May)	Bhuntar	1.19	49	0.045	0.0453	Rising
	Larji	0.97	39	0	0.0796	No trend
	Manali	-0.18	-8	0	0.0039	No trend
	Pandoh	-0.38	-16	0	-0.0148	No trend
Monsoon (Jun - Sept)	Bhuntar	0.65	27	0.023	0.03	Rising
	Larji	2.43	93	**0.083**	0.1917	Rising
	Manali	2.31	91	**0.083**	0.0978	Rising
	Pandoh	-1.75	-70	-0.063	-0.0842	Falling
Post-monsoon (Oct - Nov)	Bhuntar	-0.2	-9	-0.003	-0.0051	Falling
	Larji	1.72	66	0.2	0.2135	Rising
	Manali	1.3	52	0.057	0.0778	Rising
	Pandoh	-1.11	-43	-0.154	-0.1647	Falling
Winter (Dec - Feb)	Bhuntar	0.25	11	0.011	0.0211	Rising
	Larji	2.51	96	**0.286**	0.2211	Rising
	Manali	0.56	23	0	0.0622	No trend
	Pandoh	-1.06	-41	-0.114	-0.1244	Falling

Table 7.7: Seasonal and annual trends of temperature range (T_{range})

Season	Station	Mann-Kendall test Z statistic	S	Sen Estimator	Linear regression	Trend
Annual	Bhuntar	1.84	75	0.038	0.0327	Rising
	Larji	-1	-39	-0.025	-0.0547	Falling
	Manali	-1.9	-73	-0.22	-0.2768	Falling
	Pandoh	1.06	41	0.086	0.1082	Rising
Pre- monsoon (Mar - May)	Bhuntar	2.19	89	**0.083**	0.0774	Rising
	Larji	-0.9	-35	-0.026	-0.0537	Falling
	Manali	-1.53	-59	-0.25	-0.2935	Falling
	Pandoh	1.43	55	0.1	0.1063	Rising
Monsoon (Jun -Sept)	Bhuntar	-0.32	-14	-0.002	-0.0043	Falling
	Larji	-1.43	-55	-0.1	-0.1097	Falling
	Manali	-1.8	-69	-0.252	-0.2716	Falling
	Pandoh	1.24	51	0.05	0.0667	Rising
Post-monsoon (Oct - Nov)	Bhuntar	-0.37	-16	-0.012	-0.0162	Falling
	Larji	-1.89	-77	-0.124	-0.116	Falling
	Manali	-1.95	-75	-0.4	-0.4351	Falling
	Pandoh	0.37	15	0.12	0.1314	Rising
Winter (Dec - Feb)	Bhuntar	2.24	91	**0.089**	0.0898	Rising
	Larji	0.2	9	0.015	0.0132	Rising
	Manali	-1.8	-69	-0.15	-0.1841	Falling
	Pandoh	1.45	56	0.15	0.1649	Rising

From Table 7.4 (SE), analysis of annual T_{min} indicates that Bhuntar, Larji and Manali indicated positive trend and Pandoh indicated negative trend, with increasing trend at Bhuntar (0.03^0C/yr) found to be statistically significant. Increasing trend is observed during pre-monsoon, monsoon, post-monsoon at three stations namely Bhuntar, Larji, Manali, and as well as during winter at Larji. Pandoh station shows a decreasing trend during all seasons, with maximum decrease (-0.1 ^{0}C/yr) in post-monsoon. During winter season, decreasing trend was observed at Manali whereas Bhuntar station showed no trend.

From Table 7.5 (SE) analysis of H_{max} temperature at annual scale indicates increasing trend at Bhuntar, decreasing trend at Larji and Manali and no trend at Pandoh. No trend is found statistically significant. Season-wise analysis indicates increasing trend for all seasons for Bhuntar and decreasing trend for all seasons for Manali. Decreasing trend is found in pre-monsoon and monsoon and increasing trend in post monsoon season at Larji, and increasing trend during post-monsoon and winter season at Pandoh. Decreasing trend in monsoon season at Manali (-0.143^0C/yr) is found statistically significant.

Table 7.6 (SE) results indicates increasing trend (significant) for Larji and decreasing trend (non-significant) at Pandoh station is found for L_{min} temperature whereas stable at Bhuntar and Manali. During the pre-monsoon season, L_{min} temperature was found to be stable at all stations except at Bhuntar where it was found increasing. During monsoon season, all stations except Pandoh experienced increasing trend. In winter season L_{min} was found increasing for Bhuntar, Larji and decreasing at Pandoh station.

Table 7.7 (SE) results of annual T_{range} temperature indicate increasing trend at Bhuntar and Pandoh and decreasing trend at Larji and Manali. None of these trends is found statistically significant. Seasonal analysis indicates increasing trend at Pandoh and decreasing trend at Manali in all seasons. For Bhuntar, it is found increasing during pre-monsoon and winter (significant) and for Larji station, it is found increasing during winter season. Out of the four stations the magnitude of change varies from greatest at Larji (0.076 ^{o}C/year) to lowest at Manali (-0.233 ^{0}C/year) at annual scale. Also, Larji station shows the highest slope values for T_{avg} (0.097 ^{0}C/year), T_{max} (0.0765 ^{0}C/year), T_{min} (0.138 ^{0}C/year) temperature at annual scale. The non-parametric method results depicts the similar trend patterns in temperature variables as represented by parametric method at both seasonal and annual scale for almost all stations except in few cases. However, the results of non-parametric are considered to be more reliable, as these methods are more robust than conventional linear regression methods.

7.7.2 Trends in Rainfall

The general characteristics of seasonal and annual rainfall in the Beas river basin are given in Table 7.8. The mean annual rainfall in the basin varies from 915.8 mm at Bhuntar to 1335.9 mm at Pandoh (for the period 1979-2009). The coefficient of variation (CV) of the annual rainfall varies from 20.3% at Banjar to 33.3% at Sainj. It is evident from the Table 7.8 that all the station receives maximum rainfall during the monsoon season and least rainfall is received during the post-monsoon season. The contribution of monsoon rainfall varies from 39 % (Bhuntar) to 74% (Pandoh), while contribution of pre-monsoon season varies from 14% (Pandoh) to 30% (Bhuntar).

Table 7.8: Distribution of rainfall at different stations in Beas basin (1979-2009)

Station	Annual		Pre-monsoon		Monsoon		Post-monsoon		Winter	
	Mean	CV	Mean	% of annual	Mean	% of annual	Mean	% of annual	Mean	% of annual
Bhuntar	915.8	21.2	278	30	359	39	52	6	226	25
Larji	1009.4	24.8	242	24	525	52	50	5	193	19
Banjar	997.9	20.3	253	25	526	53	40	4	175	18
Sainj	1059.4	33.3	268	25	555	52	45	4	191	18
Pandoh	1335.9	21.6	183	14	990	74	34	3	124	9

Similar to temperature variable, the anomalies of rainfall and their trends were determined for all the stations considered in the study. The rainfall anomalies (deviation from mean) were then plotted against the time (in Year) and the linear trends observed in these have been represented graphically. Anomalies in seasonal and annual rainfall and their trends for the stations within the study area are shown graphically in figures 7.7 to 7.9. The magnitude of the seasonal and annual trend in the time series as determined using the Sen's estimator is given in Table 7.9. The annual rainfall indicates increasing trend at one station namely Banjar and decreasing trend at all other four stations with maximum decrease (-8.067mm/year) at Sainj. The increasing trend at Banjar is of the order of 8.3 mm/year. Seasonal analysis of rainfall trends shows that all stations during pre-monsoon, post-monsoon and winter season experienced decreasing trend whereas all stations experienced increasing trend in monsoon season.

RAINFALL (BANJAR) **RAINFALL (BHUNTAR)**

Figure 7.7: Rainfall trends of Banjar and Bhuntar stations

RAINFALL (LARJI) **RAINFALL (PANDOH)**

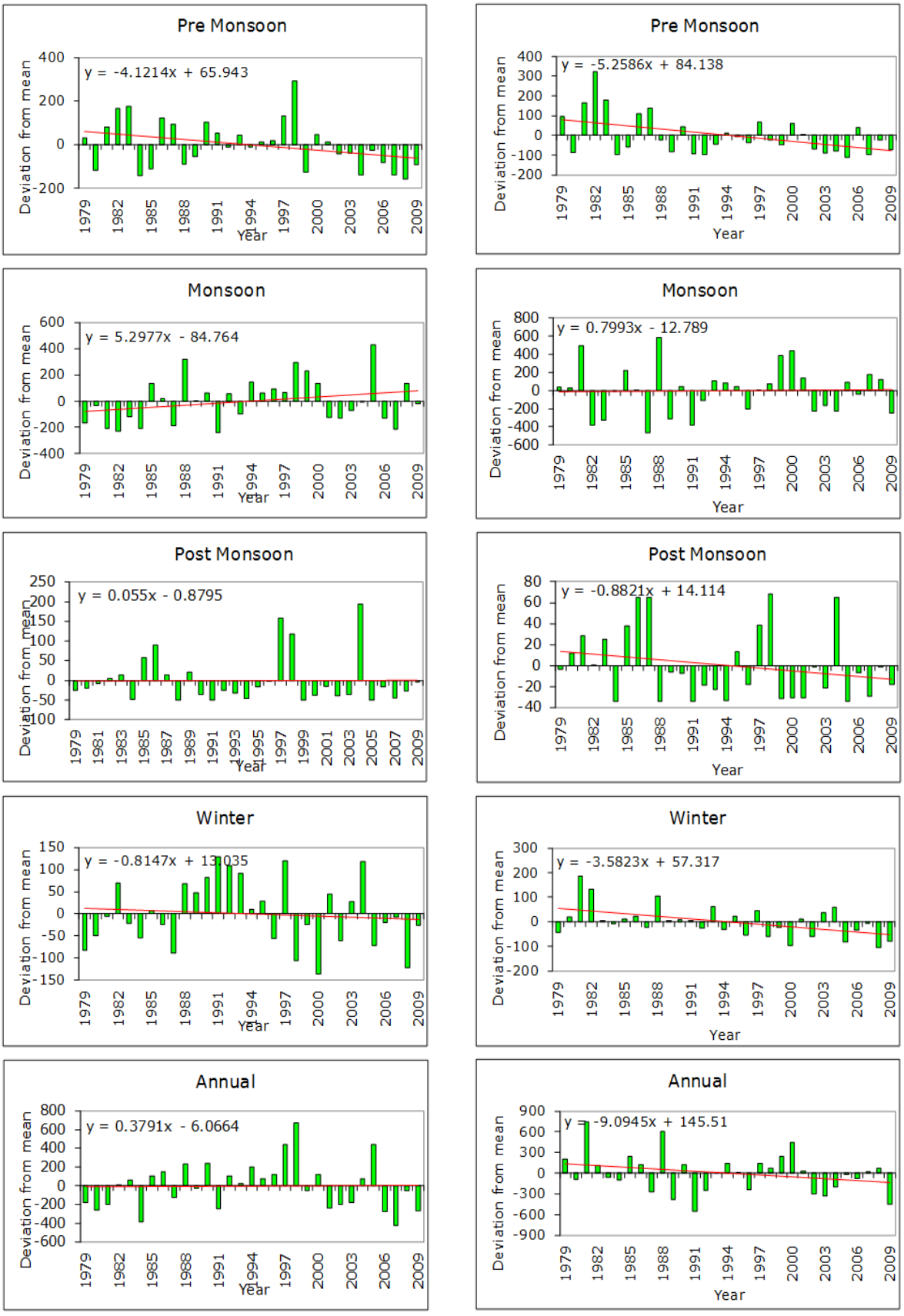

Figure 7.8: Rainfall trends of Larji and Pandoh stations

RAINFALL (SAINJ)

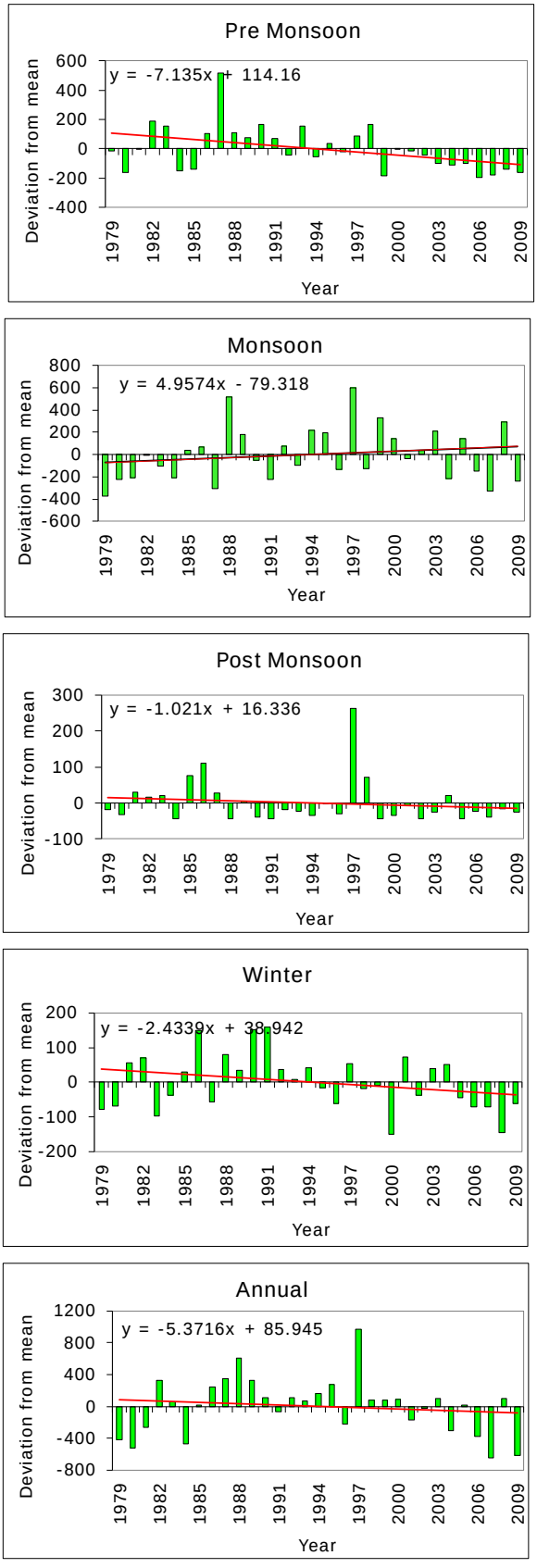

Figure 7.9: Rainfall trends of Sainj station

Table 7.9: Seasonal and annual trends in rainfall of different stations in Beas basin

Season	Station	Mann-Kendall test Z statistic	S	Sen Estimator	Linear regression	Trend
Annual	Bhuntar	-0.54	-33	-2.667	-2.0339	Falling
	Larji	-0.07	-5	-0.166	0.3791	Falling
	Banjar	1.63	97	8.3	8.5655	Rising
	Pandoh	-1.22	-73	-7.46	-9.0945	Falling
	Sainj	-0.99	-59	-8.067	-5.3716	Falling
Pre-monsoon (Mar - May)	Bhuntar	-2.14	-121	**-7.383**	-5.9845	Falling
	Larji	-2.19	-130	**-5.56**	-4.1214	Falling
	Banjar	-0.88	-53	-2.72	-1.7135	Falling
	Pandoh	-1.28	-73	-4.55	-5.2586	Falling
	Sainj	-1.96	-111	**-9.211**	-7.135	Falling
Monsoon (Jun - Sept)	Bhuntar	2.65	157	**5.936**	5.5586	Rising
	Larji	1.36	81	5.141	5.2977	Rising
	Banjar	3.09	183	**11.907**	11.605	Rising
	Pandoh	0.59	36	2.865	0.7993	Rising
	Sainj	1.12	67	6.147	4.957	Rising
Post-monsoon (Oct - Nov)	Bhuntar	-0.58	-35	-0.531	-0.427	Falling
	Larji	-0.6	-36	-0.333	0.055	Falling
	Banjar	-0.95	-57	-0.522	-0.1906	Falling
	Pandoh	-0.99	-59	-0.727	-0.8821	Falling
	Sainj	-1.29	-77	-0.736	-1.021	Falling
Winter (Dec - Feb)	Bhuntar	-0.44	-27	-0.74	-1.3051	Falling
	Larji	-0.48	-29	-0.686	-0.8147	Falling
	Banjar	-0.59	-36	-1.038	-1.4156	Falling
	Pandoh	-2.55	-151	**-3.38**	-3.5823	Falling
	Sainj	-1.39	-83	-3.083	-2.4339	Falling

In monsoon season, the maximum increase is of the order of 11.91 mm/year for Banjar and minimum increase is for Pandoh (2.86 mm/year). In pre-monsoon season, the maximum decrease is for Sainj (-9.21 mm/year) and minimum decrease is for Banjar (-2.72 mm/year). In seasons other than monsoon and pre-monsoon, the magnitude of change was quite small. The results of Mann-Kendall test applied to annual and seasonal rainfall at different stations (Table 7.9) indicates that none of the station show either increasing or decreasing significant trend in annual rainfall.

Monsoon rainfall indicated positive significant trend at Banjar and Bhuntar. Pandoh station in the winter season and three stations (Bhuntar, Larji and Sainj) in pre-monsoon season showed negative significant trend in rainfall. In post-monsoon season, all decreasing trends are found non-significant. The Mann-Kendall and Sen's slope estimator results corroborate the similar trend patterns as represented by the linear regression method at both seasonal and annual scale for rainfall.

7.7.3 Trends in Streamflow

The anomalies of stream discharge were computed and linear regression analysis was carried out and relationship was developed for linear trends for each station at both seasonal and annual scale graphically shown in figures 7.10 to 7.12. The results of Sen's slope of estimator and Mann-Kendall test applied to seasonal and annual discharge series at different stations are given in (Table 7.10). Analysis of discharge at different sites in the Beas river basin indicated decreasing trend of annual discharge at Bakhli, Pandoh and Thalout station and increasing annual discharge at Sainj and Tirthan site. All these trends are found non-significant at 95% confidence level.

Analysis of seasonal data indicated decreasing trend (non-significant) in pre-monsoon discharge for all stations; decreasing trend (non-significant) in monsoon discharge at Bakhli, Pandoh and Thalout sites and increasing trend (non-significant) of monsoon discharge at other two sites namely Sainj and Tirthan. Discharge in post-monsoon season showed increasing trend at Bakhli and Sainj and decreasing trend at Pandoh and Thalout stations. Winter season discharge indicated decreasing trend at all stations except Bakhli.

DISCHARGE (BHAKLI) **DISCHARGE (PANDOH)**

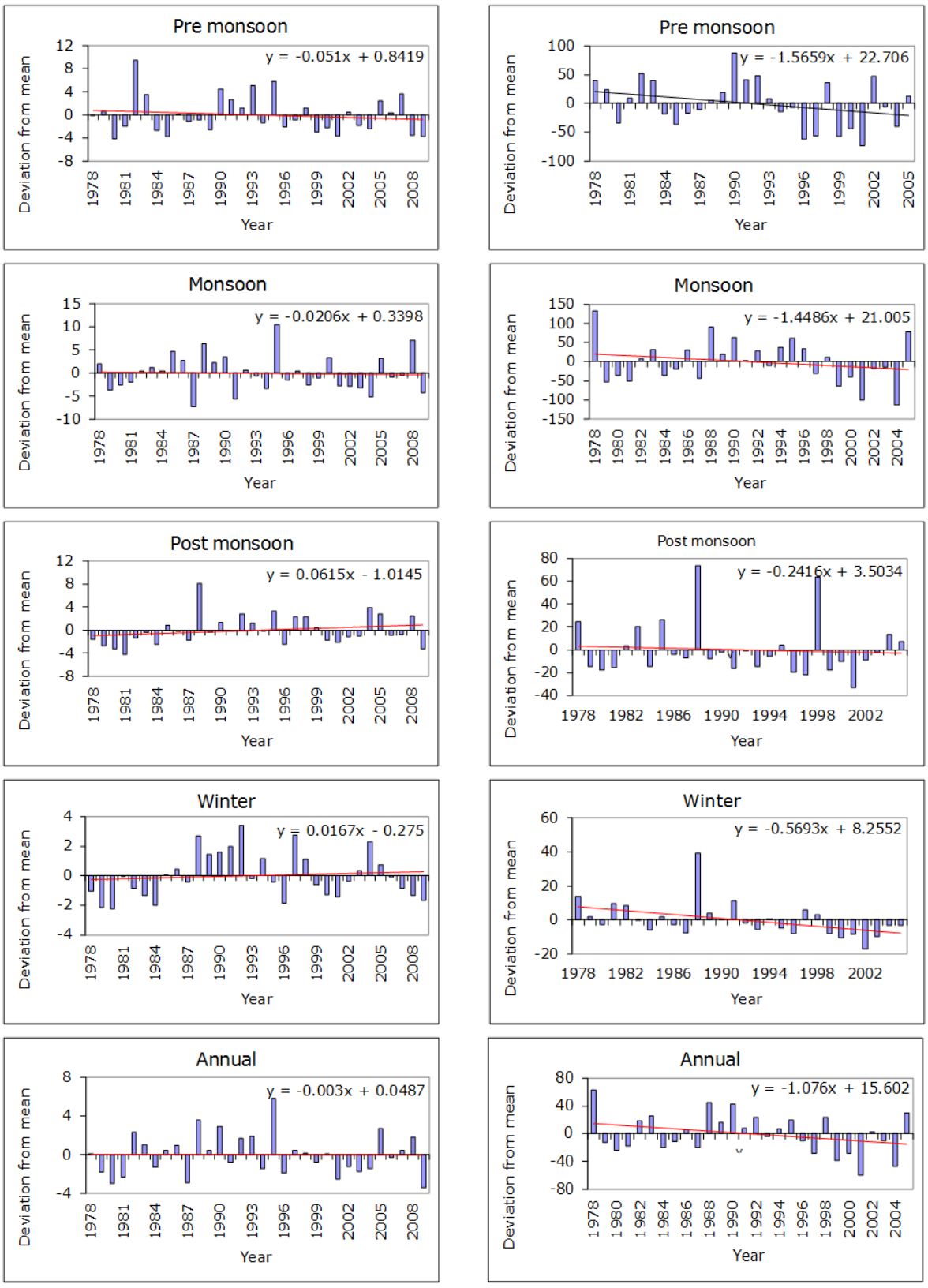

Figure 7.10: Stream discharge trends of Bakhli and Pandoh stations

DISCHARGE (THALOUT) **DISCHARGE (SAINJ)**

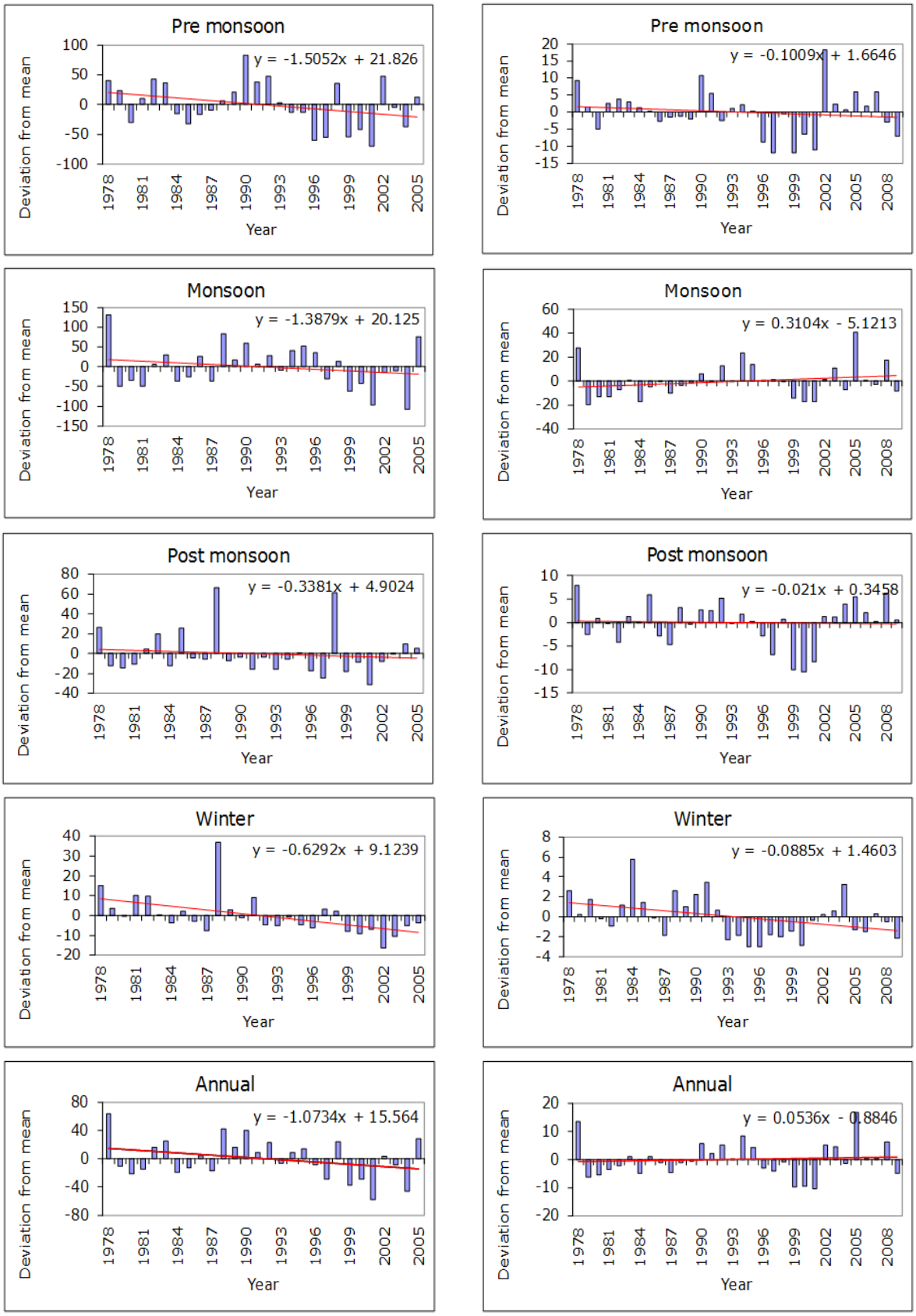

Figure 7.11: Stream discharge trends of Thalout and Sainj stations

DISCHARGE (TIRTHAN)

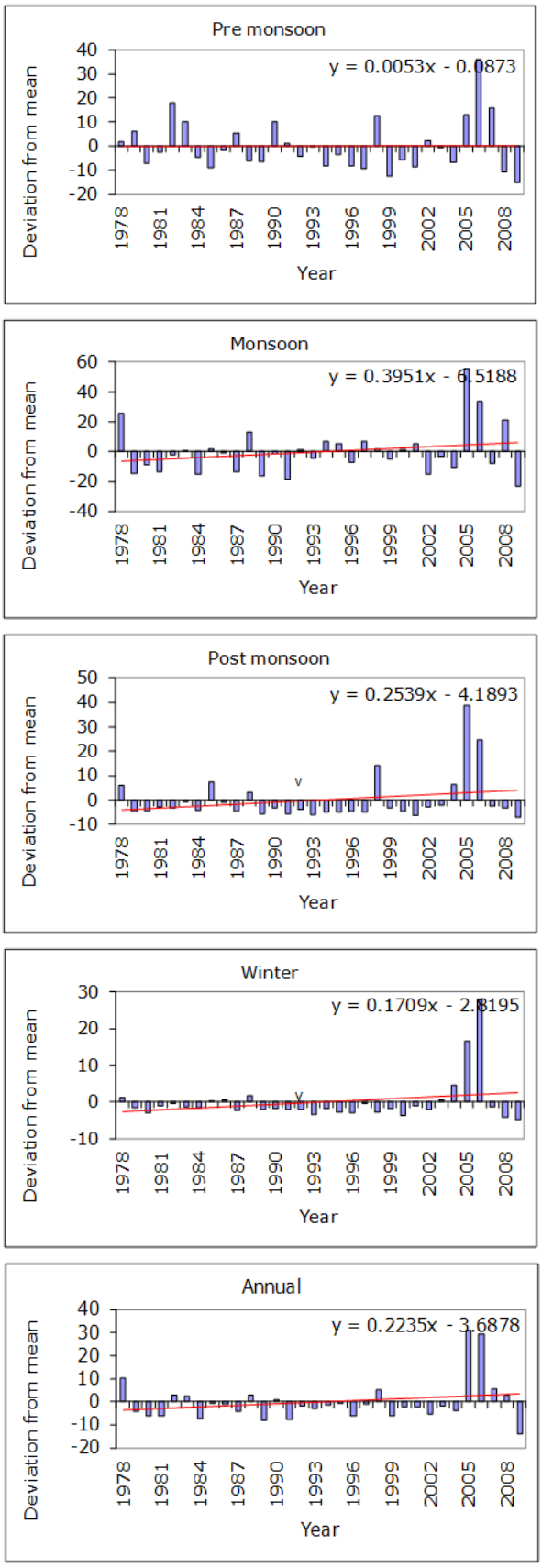

Figure 7.12: Stream discharge trends of Tirthan station

Table 7.10: Seasonal and annual trends of stream discharge

Season	Station	Mann-Kendall test Z statistic	S	Sen Estimator	Linear regression	Trend
Annual	Bhakli	-0.1	-7	-0.003	-0.003	Falling
	Pandoh	-1.13	-58	-0.996	-1.076	Falling
	Sainj	0.92	58	0.119	0.0536	Rising
	Thalout	-1.24	-64	-0.924	-1.0734	Falling
	Tirthan	0.48	35	0.08	0.2235	Rising
Pre-monsoon (Mar - May)	Bhakli	-0.63	-40	-0.051	-0.051	Falling
	Pandoh	-1.4	-72	-1.702	-1.569	Falling
	Sainj	-1.12	-70	-0.131	-0.1009	Falling
	Thalout	-1.44	-74	-1.65	-1.5052	Falling
	Tirthan	-0.96	-60	-0.196	0.0053	Falling
Monsoon (June - Sept)	Bhakli	-0.6	-38	-0.052	-0.0206	Falling
	Pandoh	-0.49	-26	-0.846	-1.4486	Falling
	Sainj	1.49	93	0.362	0.3104	Rising
	Thalout	-0.57	-30	-0.72	-1.3879	Falling
	Tirthan	0.75	47	0.263	0.3951	Rising
Post-monsoon (Oct - Nov)	Bhakli	1.64	102	0.074	0.0615	Rising
	Pandoh	-0.34	-18	-0.145	-0.2416	Falling
	Sainj	0.51	31	0.017	-0.021	Rising
	Thalout	-0.57	-30	-0.256	-0.3381	Falling
	Tirthan	0.37	23	0	0.2539	Rising
Winter (Dec - Feb)	Bhakli	0.05	4	0.016	0.0167	Rising
	Pandoh	-3.1	-158	**-0.539**	-0.5693	Falling
	Sainj	-0.65	-39	-0.079	-0.0885	Falling
	Thalout	-3.65	-186	**-0.558**	-0.6292	Falling
	Tirthan	-0.07	-5	-0.037	0.1709	Falling

7.8 SUMMARY

The mountainous basin is highly sensitive to climate change. Any change in rainfall and temperature highly influences streamflow downstream. The detection of trends and magnitude of variations due to climatic changes in hydro-climatic data, particularly temperature, precipitation and streamflow, are essential for the assessment of impacts of climate variability and change on the water resources of a region. The present study determined and analyzed the trends of temperature, rainfall and discharge data using parametric (linear regression) and non-parametric (Mann-Kendall test and Sen's estimator of slope) methods on seasonal and annual time scales for the Beas basin.

Majority of stations showed increasing trend in the mean annual temperature while one station (Manali) showed a decreasing trend over the last three decades. During pre-monsoon season, most of the stations indicated rising trends with Larji and Pandoh, statistically significant at 95% confidence level. The annual rainfall indicated increasing trend at one station namely Banjar and decreasing trend at all other four stations with maximum decrease (-8.07mm/year) at Sainj. All stations during pre-monsoon, post-monsoon and winter season experienced decreasing trends whereas all stations experienced increasing trends in monsoon season. Annual streamflow showed decreasing trend at Bakhli, Pandoh and Thalout stations @ of -0.03 cumec/year, -0.996 cumec/year and -0.924 cumec/year, respectively, whereas an increasing trend was seen at Sainj and Tirthan @ 0.119cumec/year and 0.08 cumec/year respectively.

Thus, assessment of impact of climate change is a need to understand the hydrological behaviour of Beas basin under uncertain changing scenarios of climate for optimal planning and management of water resources.

Chapter -8

CLIMATE CHANGE AND ITS IMPACT ON STREAMFLOW

8.1 BACKGROUND

Climate change refers to a statistically significant variation in either the mean state of the climate or in other statistics (such as standard deviations, the occurrence of extremes, etc.), persisting for an extended period particularly decades or longer. It is likely to affect the hydrology of river basin, especially those in Himalayan regions by intensifying the global hydrological cycle and have major impact on the streamflow of snow-fed rivers by influencing the snow/ice and glacier melt in the upstream part of the basins. It is therefore, essential to study the effects of climate change on streamflow and related variables of such river basins (both in space and time) to plan and manage the water resources effectively.

In the present study, an endeavor has been made to investigate the impact of climate change on the streamflow of Beas river under the changing climatic conditions. The SNOWMOD model has been used to estimate streamflow and thereafter to study the impact of climate change on the melt characteristics and daily runoff by defining scenarios. In the study, scenarios have been developed in two ways and applied to see the impact of climate change. First one based on the assumed plausible hypothetical scenarios derived from combination of temperature and rainfall and the second, IPCC-SRES A1B projected temperature scenario on the basis of climate modeling using actual data. A new set of Snow Depletion Curve (SDC) i.e. modified snow cover area resulting from the modified or changed climatic conditions were used by the model to simulate the runoff in both the cases. These modified SDC were prepared for the analysis using exponential relationship developed in chapter 4. The streamflow has been quantified under the applied scenarios with projected changes and presented in the following sections.

8.2 CLIMATE CHANGE MODELING

8.2.1 Climate Change and Issues

The climate of earth has never been stable for any extended period but varying naturally on all time scales. The earth's energy balance is determined by accounting the balance between

the incoming and outgoing energy which also regulates its long-term state and average temperature. Climate change has greatly affected the characteristics of climatic variables globally. These changes are not uniform but vary from place to place or region to region. Probable climate change and its perilous impacts on the hydrologic system poses a threat to global fresh water resources and aquatic ecosystems worldwide. The Himalayas are anticipated to be most vulnerable among the most environmentally fragile regions. The impact of climate change in the Himalayan regions affects the snow cover, glaciers and streamflow in the rivers by perturbing snow accumulation and snowmelt processes. The snow-fed river of mountainous regions receives significant contributions from snow and glacier melt, which affects the catchment hydrology by storing and releasing water temporarily on various time scales (Jansson et al., 2003).

The main factors which cause the climate change to occur are categorized as the natural and human influences; called 'forcings' which are held responsible for altering the flow of radiant energy in the atmosphere. Climate variability occur naturally as a result of variation in the amount of sun's energy, variation in the distance between the earth and sun, presence of volcanic pollution in the upper atmosphere (natural forcing), or occur due to addition of green house gases as a result of persistent anthropogenic forcing. Scientist have learned that the several green house gases like CO2, methane, nitrous oxide, tropospheric ozone, chlorofluorocarbons (CFCs) and water vapor are responsible for the global warming. Except water vapor, the concentration of intact greenhouse gases more or less depends on human activities. The water vapors levels in the atmosphere are dependent on the temperature of Earth and availability of liquid water thus its concentration in the air is indirectly affected by the human activities. Moreover, the human activities such as industrial development, deforestation for extension of cities, pollution of waterways and cities, construction of dams etc. could possibly alter the climatic conditions.

In rugged alpine terrain, the snow distribution patterns are the most visible outcome of topography and its interaction with climatic variables namely radiation, precipitation and wind (K¨orner, 1992; Gottfried et al., 1999; K¨orner, 1999). Klien-Tank et al., (2006) has revealed variation in indices of temperature and precipitation, the associated climatic extremes over the central and south Asia. From the analysis of observed global changes in daily climate extremes (temperature and precipitation), temperature extremes associated with global warming shows significant changes (Alexander et al., 2006). Various studies over the mountainous regions such as (the Swiss and Polish Alps, the Rockies (Brown et al. 1992; Diaz and Bradley 1997; Beniston at al. 1997; Wibig and Glowicki 2002; Beniston 2003; David et al. 2003; Rebetez

2004) and Andes (Villaba et al.2003; Vuille et al. 2003) have publicized the significant increase in the surface air temperature.

The important climatic variables which influence the ecosystem are precipitation, radiation, temperature and streamflow. The recently growing scientific evidences have been widely recognized that over the past century climate has changed globally due to anthropogenic factors altering the natural environment. The increase in global temperatures and modified precipitation distribution are the most explicit changes on the climate (Houghton et al., 1995) consequently leading to significant alteration in the regional hydrological cycles and subsequent changes in the regional water availability. The global warming has resulted in increase in the average temperature. Moreover, these long-term changes in the temperature have significant impact on the hydrological cycle. Disturbance in the hydrological cycle may result in significant temporal and spatial change in occurrence of hydrological events like rainfall pattern, extreme precipitation events and drought conditions ensuing in unequal distribution of accessible fresh water and in turn affecting the socio-economic planning of the region. The prominent indications of the climatic change and their prejudicial effects are; formation, growth and outburst of glacial lakes, glacial retreat, increase in frequency of flood/flash flood, reduction in seasonal snow cover, and rise in sea level etc.

In mountainous regions due to topographic forcings the climate varies at shorter distances. In addition, amplitude of such changes is higher at high elevations owing to relatively larger sensitivity to climate change (Diaz and Bradley, 1997; Shrestha et al., 1999). Thus, mountains are more susceptible to the impacts of rapid climate change and endow appealing location for early detection, study climate change signals and its impacts on the hydrological, ecological and societal systems (Beniston M., 2003).

In Indian context, the rivers of Himalayan regions would have immense impact of climate change. The rivers draining from the Himalayan basins, in which precipitation enhances with orography, the major proportion of streamflow is derived from both contemporaneous precipitation and melt from snow and glacier. Thus, snow and glacial melt are imperative hydrological processes in the mountainous river basins (Kure et al., 2013b) and climatic variability in temperature and precipitation may gravely affect the water availability of the region.

Snow cover is a decisive hydrological parameter in the water cycle as it influences the dynamics of global water cycle directly. For a region, regardless of snow depth, duration of snow cover is a gesture of climatic condition (Leathers and Luf, 1997; Butt and Kelly, 2008). Snow cover is a major factor for climate change studies globally (Butt, 2006). The snow cover

extent is governed by the climatic features such as solar radiation, temperature and precipitation. Thus, snowfall and temperature are the main determinant factors of the streamflow. Earlier studies on climate change revealed that the areal extent of snow cover and glaciated areas have reduced owing to change in climate. (Schetinnikov, 1998; Paul et al., 2004; Barnett et al., 2005; Aizen et al., 2006; Paul et al., 2007; Makhmadaliev et al., 2008; Hirabayashi et al., 2010; Ohara et al., 2014b). Impacts of climate change in the northwestern Himalayan river basin have been reported in the form of rising temperature, depleting snowfall precipitation which coincide with the rapid reduction of glaciers (Ageta 2001; Hewitt 2005; Bhutiyani et al., 2007; Shekhar et al., 2010). Each and every aspect of the society, from agriculture production and energy consumption to flood control, water supply and ecosystem management will be affected due to such hydrological changes. The tremendous importance of water for both society and the environment necessitate and emphasize the hydrologists and researchers to study and understand the affect of climate change on the regional water availabilities. The impacts of climate change on the hydrological regime are normally investigated by defining scenarios.

8.2.2 Climate Scenarios

A scenario refers to probable portrayal of the future climate based on the internally consistent set of climatological relationship among the climatic parameters. These scenarios facilitates in providing the alternative images of the future state of sphere under the changing environment. Scenarios are generated for the investigation of possible repercussion of climatic change and are considered as potential tools for analyzing the driving forces such as demographic evolution, socio-economic progression, and technological transformation which may affect the emission of green house gases (GHGs) in near future. These generated scenarios render support for climate change studies comprising climate modeling and impact assessments along with adaption and mitigation.

For better understanding and estimating the plausible trends and uncertainties involved in future emissions of GHG affecting the environmental conditions, the IPCC-International Panel on Climate Change evolved a series of GHG emission scenarios (Nakicenovic and Swart, 2000) based on the assorted set of driving forces covering periods of a century. The four diverse storylines A1, B1, A2 and B2 were used to develop self-consistent numerous different scenarios to envisage how the future might unfold under future from present world in terms of political, social, economical and technical evolution. In the present study attempt has been

made to study the hydrological response of streamflow of Beas river basin under the changing climate using A1B scenario. A1B scenario comes from the family of A1 scenario. This scenario technically emphasizes not to rely profoundly on a particular energy source in future world of very swift economic progress, global population peaking by mid-century and declining subsequently, and with better and more proficient technologies.

For better understanding the dynamic, complicated and catastrophic impacts of climate change on the hydrological systems, climate model are customary in use. The climate model is a mathematical description of large scale physical processes governing the climate system. Presently, General Circulation Models or Global Climate Models (GCMs), the numerical models are considered as reliable tools designed to simulate present climate and future climatic conditions (Kure et al., 2013a). In climate change studies, wide variation in spatial and temporal scales ranging from few minutes to a year and from few kilometers to thousands of kilometer, adds more complexity for hydrological studies. GCM models are well accredited for reasonably representing the basic climatic parameters at large scale but they are not able to reproduce the details of climatic conditions well at the regional scale. Therefore, GCMs output cannot be directly utilized in any regional hydrological model (Wigley et al., 1990; Carter et al., 1994) to make reliable predictions about the regional hydrological changes owing to its coarser resolution and simplification of hydrologic cycle in climate models (Arora, 2001). The new generation super high resolution atmospheric model GCM model AGCM20 developed by Japan reproduces the data at the spatial and temporal resolution of 20 km and 1 hour respectively (Mizuta et al., 2006; Kiem et al., 2008; Kitoh and Kusunoki, 2008; Kim et al., 2010, Kure et al., 2013b). However, the data is not publicly available at present. Optimal water resources planning require fine scale information which could be achieved by downscaling the output of GCM projections.

A framework is being provided by the hydrological models to conceptualize and investigate the relationship between climate and water resources. In climatic change studies, the hydrological models are utilized for the evaluation of annual and seasonal streamflow variation using simple water balance models (e.g., Arnell, 1992). Global and regional climate models and the hydrologic models are the imperative tools in such climatic studies (Glieck, 1987; Xu, 2000; Guo et al., 2002; Xu et al., 2005; Chen et al., 2007; Boe et al., 2007), though there exist many major challenges in the application of GCM and hydrological models (Xu, 1999; Fowler et al., 2007).

8.3 HYDROLOGICAL MODELING FOR CLIMATE CHANGE

Normally there are three categories for simulating the hydrological responses due to climate change using hydrologic models.

1. Coupling GCMs and macroscale hydrological models
2. Downscaled GCM climate output for use in hydrological models
3. Based on hypothetical scenarios as input to hydrological models

These are described in the following sections.

8.3.1 Coupling GCMS and Macroscale Hydrological Models

Basically, two approaches based on simulation models are available to study the impact of climate change on runoff in rivers. The first approach obtains the runoff directly as a part of a GCM simulation which is then distributed to the specific river basins (Russell and Miller, 1990; Kuhl and Miller, 1992). This approach does not confer good assessment of the hydrological responses of climatic changes. Thus there is strong urge to couple hydrologic models to GCMs. The second approach employs the meteorological parameters temperature and precipitation from climate simulations of GCMs as input to the hydrologic models for runoff simulation (Nash and Glieck, 1993; Hostetler and Giorgi, 1993; Kite et al., 1994; Kamga, 2001; Evans and Schreder, 2002; Chiew and McMahon, 2002; Muttiah et al., 2002; Arnell, 2003; Mirza et al., 2003). This approach employing coupled hydrological model with GCM provided better results for river runoff.

8.3.2 Downscaled GCM Climate Output for Use in Hydrological Models

Usually, GCMs run at coarse grid resolution as a result of which they are inherently unable to represent sub-grid scale features (like orography and land use) and dynamics of mesoscale processes. Thus, output of GCMs cannot be used directly to simulate climate variables at local scale for the climate impact assessment. Consequently, to overcome this limitation downscaling methods gained recognition. In past decade, several downscaling methods have been developed which transfers the GCM simulated information to a local (finer, at sight) scale.

Presently, in climatic studies two approaches namely dynamic (physical dynamics are solved explicitly) and statistical (empirical) downscaling are used to downscale the output of a GCM to the specified locations. These two approaches of downscaling are most commonly in

use in the one way coupling of GCMs and hydrological models (Wilby et al, 1999; Bergstrom et al., 2001; Fowler et al., 2007; Schoof et al., 2009; Pinto et al., 2010).

The main target of dynamic downscaling is accomplished by developing and utilizing limited area models or regional models (RCM). The dynamic downscaling approach involves nesting of Regional Climate Model (RCM) into GCM. The RCM is basically a numerical model which possess horizontal grid spacing (about 20-50 km) which is driven by initial conditions, time dependent lateral meteorological conditions and surface boundary conditions (Srinivas et. al, 2013). The GCM is being used to specify the time varying atmospheric boundary conditions. Even though RCMs have obvious physical meanings, yet its intricate design and high computational cost restricts its use in climatic studies.

The statistical downscaling approach involves in developing quantitative statistical relationships, that transforms large–scale climatic/atmospheric variables (or predictors) simulated by GCM to local scale variable (or predictands). Hence, requires less time for computations. Broadly, statistical downscaling techniques are classified into three classes; transfer function, weather generators, weather classification schemes (Wilby et al., 2004; Wilby and Dawson, 2007). The most commonly statistical downscaling approaches are based on the transfer functions in which direct relationships between the predictors and predictands are modeled (Schoof et al., 2007) and regression models based on transfer functions (eg. Wigley et al. 1990; Wilby, 1998; Wilby et al., 2003, 2004; Buishand et al., 2004; Ghosh and Mujumdar, 2008) are simple conceptual way of depicting linear and non-linear association between predictor and predictands.

8.3.3 Based on Hypothetical Scenarios as Input to Hydrological Models

Different GCMs give different values of climate variable changes hence a single consistent estimate cannot be arrived that could be advanced as deterministic forecast for hydrological planning. Thus, another most commonly used approach in climate change impact studies is based on hypothetical scenarios (Chang, 1999). This approach follows four steps for the estimation of the hypothetical climate change impacts on hydrological behavior:

1. To determine the parameters of a hydrological model for the study basin by utilizing the present climatic inputs and observed river flows for model validation.
2. To perturb the historical time series of climatic data (usually, temperature or precipitation) based on a climate change scenarios.

3. To simulate the hydrological characteristics of the study basin under the perturbed climate by usage of calibrated hydrological model.
4. To compare the current and feasible future hydrological characteristics simulated by the model.

The simplicity in representing the wide range of alternative scenarios makes the hypothetical scenario approach more advantageous. Moreover, these scenarios can be utilized for determining the sensitivity of a particular basin due to the changing climatic conditions. Numerous studies have been carried out using the altered time series for the assessment of potential impacts of climate change. (Nemec and Schaake, 1982; Gleick, 1986,1987; McCabe and Ayers, 1989; Schaake and Liu, 1989; Lettenmaier and Gan, 1990; Vehvilainen and Lohvansuu, 1991; Panagoulia, 1991; Arnell, 1992; Ng and Marsalek, 1992; Cayan et al., 1993; Singh and kumar, 1997 b, Mehrotra, 1999; Baron et al., 2000; Sharma et al., 2000; Xu, 2000; Garg et al., 2013).

In the present study, as discussed earlier, the model developed for the Beas basin was calibrated using the dataset of 3 years (2002-2005) has been used to assess the impact of climate change on the streamflow of the Beas river up to Pandoh dam under assumed ten plausible hypothetical scenarios for period 1990-2002 and future projected temperature based on IPCC-SRES A1B scenario for years 2040-43, 2043-46, 2046-2049, 2049-2052, 2093-96 and 2096-99. Since it was observed from the trend analysis that average temperature at all meteorological stations showed a rising trend, except Manali whereas decreasing trend except monsoon has been observed in case of rainfall. Hence, the adopted changes in temperature considered are $T+1^0C$ and $T+2^0C$ and for rainfall increase/decrease are 5%, 10%, −5%, -10% in the study area with an aim to study the influence of rise in temperature and rainfall variation on the various runoff components under wide range of possible hypothetical scenarios.

8.4 STREAMFLOW MODELING UNDER CHANGED CLIMATE

8.4.1 Using Hypothetical Scenario

Areal snow cover extent globally has also been recognized as one of the essential climate variables for the climate change monitoring. Snow cover equally affects and gets affected by the patterns of climate and climate change. It is directly related to temperature of an area and rise in temperature speed up the melting rate of snow. Thus, when modeling a climate change, it becomes indispensable to incorporate the effect of different melt rates on the daily

snow cover values. In order to signify the extent of impacts of climate change on water resources, it is essential to properly assess the streamflow under the changing climatic conditions and have reliable estimate of its variability. Streamflow exemplify an integrated response to hydrological inputs. The snowmelt model applied in the study simulates both components of runoff, i.e. melt runoff as well as the rainfall-runoff. However, snowmelt runoff component is mainly affected due to change in temperature.

In the present study, in order to cover a wide range of climate variability, ten hypothetical climate change scenarios were derived from combination of two temperature (T+1, T+2) and four precipitation (5%, 10%, -5%, -10%) changes based on plausible projections. For the assessment of climate change using distributed model, SCA are required as input to prepare modified SCA depletion curves under the changed climatic scenarios. Since, the Beas basin has been divided into nine elevation zones and four of them are partially snow covered, modified SCA depletion curves have been prepared for these four zones as discussed earlier in previous chapter. With the modified meteorological and snow cover depletion data, streamflow has been simulated for all the hypothetical scenarios mentioned above. Figure 8.1 to 8.4 and Figure 8.5 to 8.8 illustrates the results of simulations for a period i.e. 1990-2002 for $T+1^0C$ and $T+2\ ^0C$ temperature increase scenario respectively for the Beas basin. It is revealed from the study that with the increase in temperature, streamflow increases in the beginning of the melt season and produces small peaks. In the later part of the summer season, these peaks increase and found to be reduced without much change in their timings. These peaks are mainly due to the heavy rainfall with a small contribution from snowmelt. The streamflow as well as snowmelt runoff have been computed for each month under a number of hypothetical scenarios.

As described earlier that streamflow as well as snowmelt runoff components have been computed for a number of hypothetical scenarios. These have been computed for each month. The mean annual flows have been computed using the data of a period of 1990 to 2002. The details of computed mean annual flow values are given in Table 8.1 and the streamflow and snowmelt are depicted graphically in Figure 8.9 and 8.10 for the Beas basin. Figure 8.11 and 8.12 shows the mean monthly streamflow and snowmelt runoff. In the table/figure, change in streamflow and snowmelt runoff is given with respect to reference scenarios. In figure 8.13 to 8.16 the change in snowmelt only has been shown for the basin. Figure 8.17 and 8.18 more clearly depicts the effects of temperature change ($T+1^0C$, $T+2^0C$) scenarios on the mean streamflow and snowmelt runoff on monthly scale respectively. It is observed that both runoff

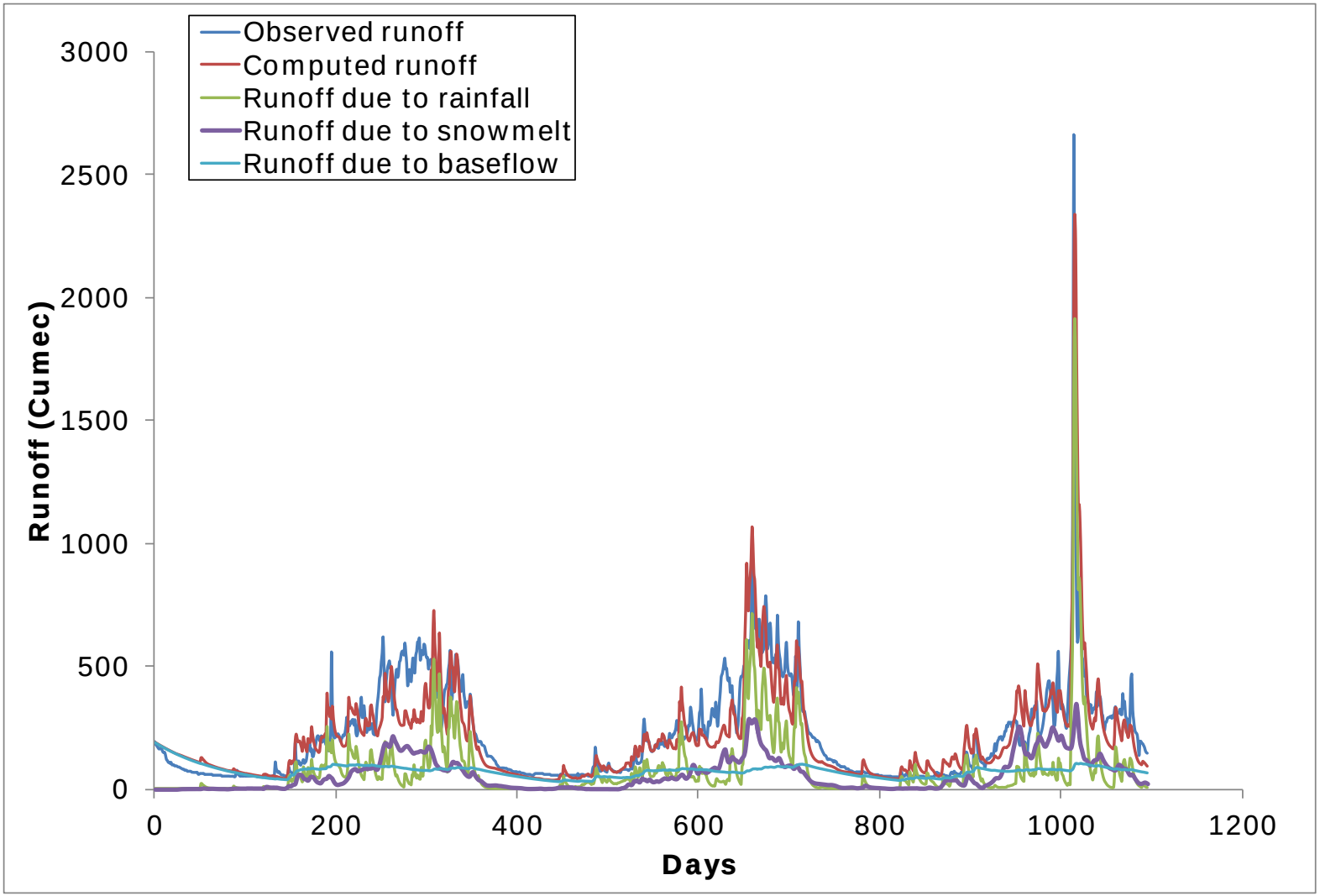

Figure 8.1: Simulation for the years 1990-1993 under temperature rise of 1^0C

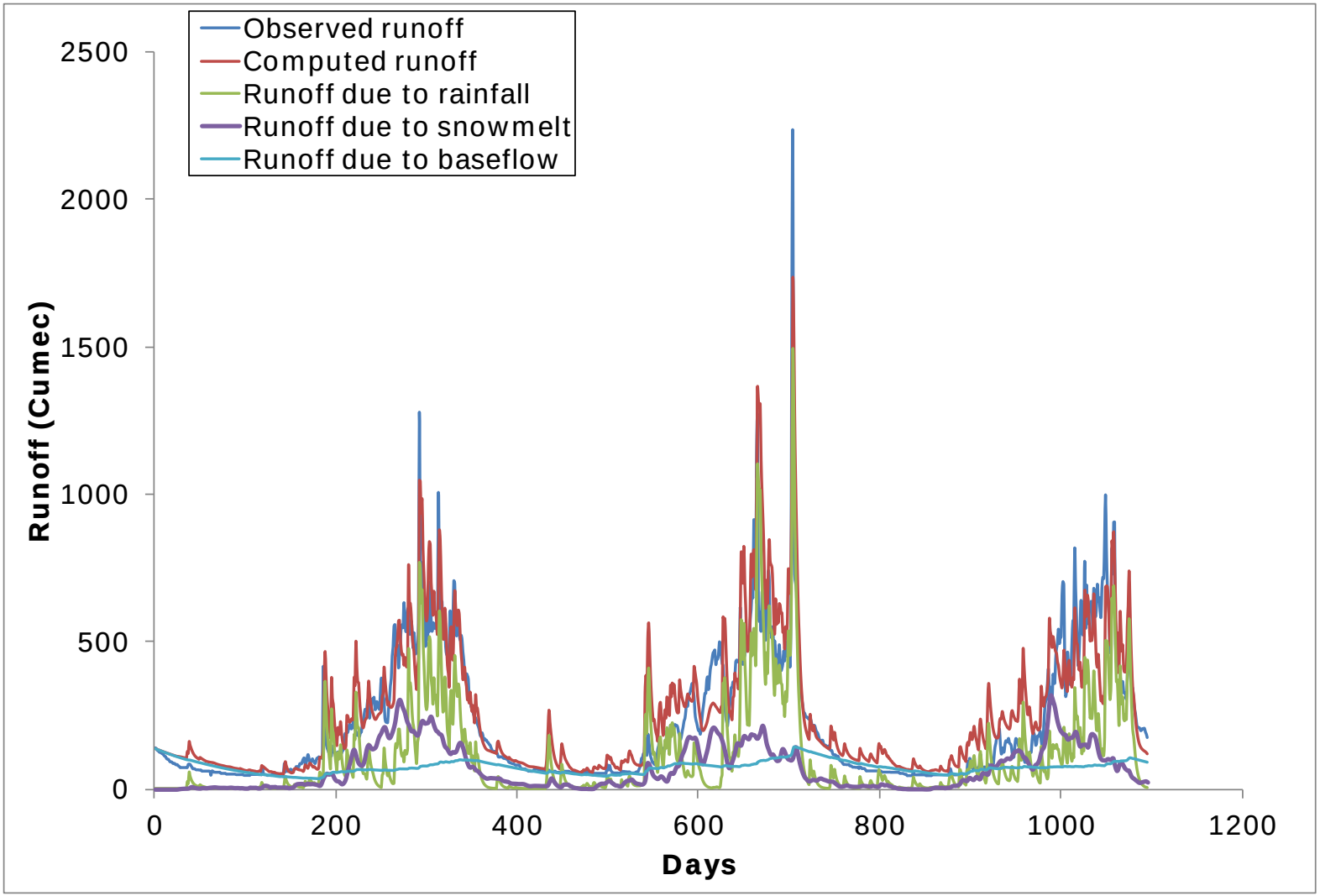

Figure 8.2: Simulation for the years 1993-1996 under temperature rise of 1^0C

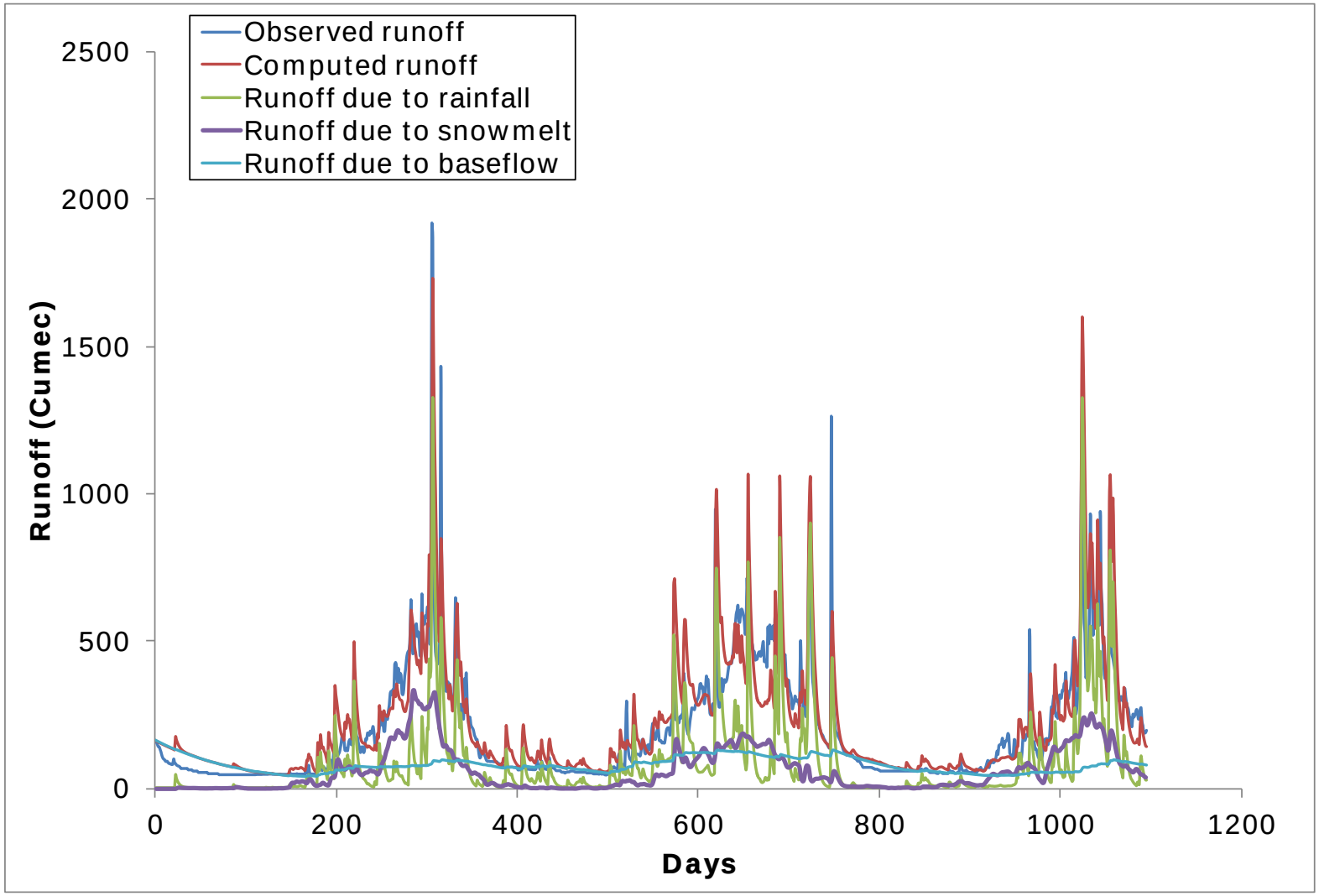

Figure 8.3: Simulation for the years 1996-1999 under temperature rise of 1^0C

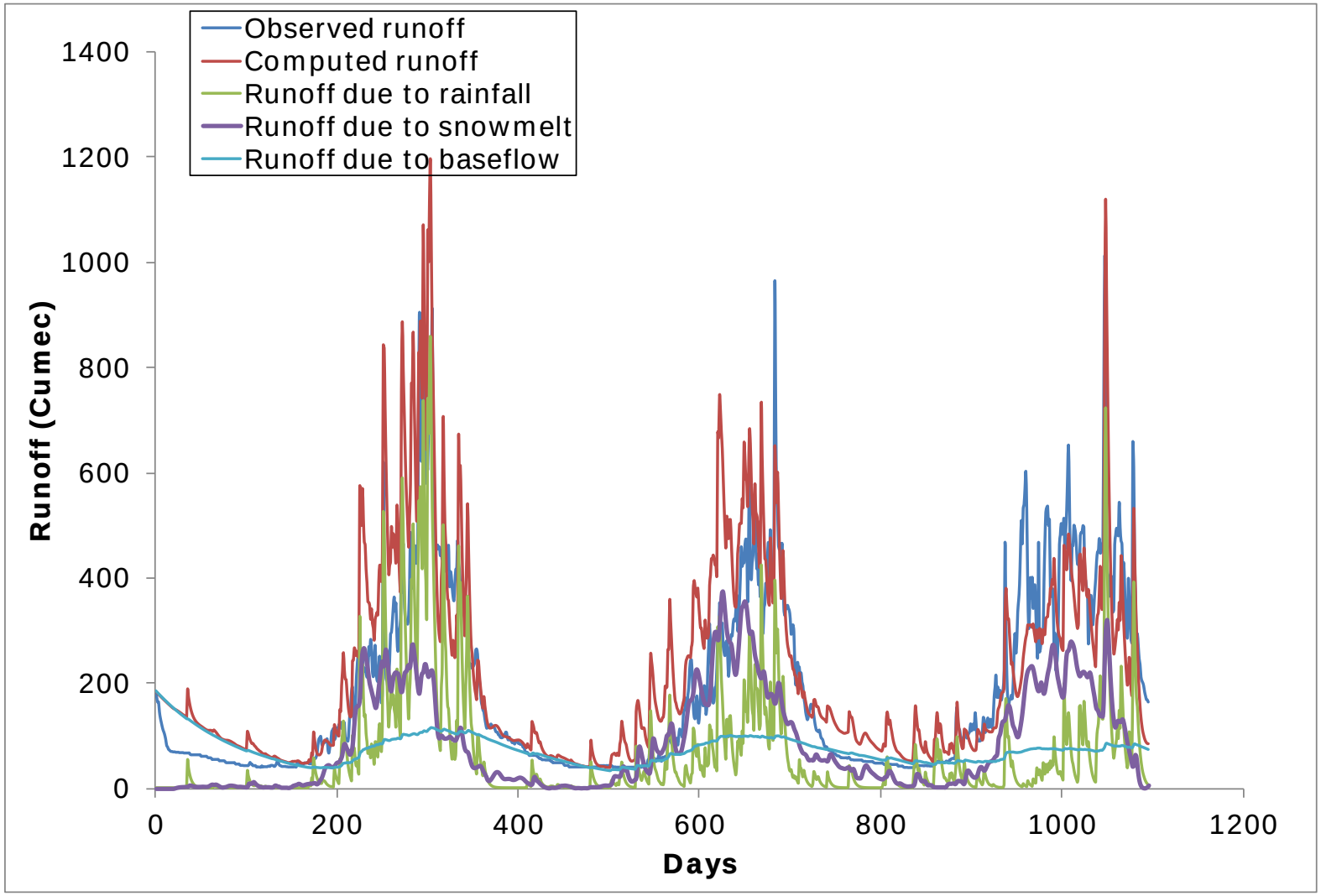

Figure 8.4: Simulation for the years 1999-2002 under temperature rise of 1^0C

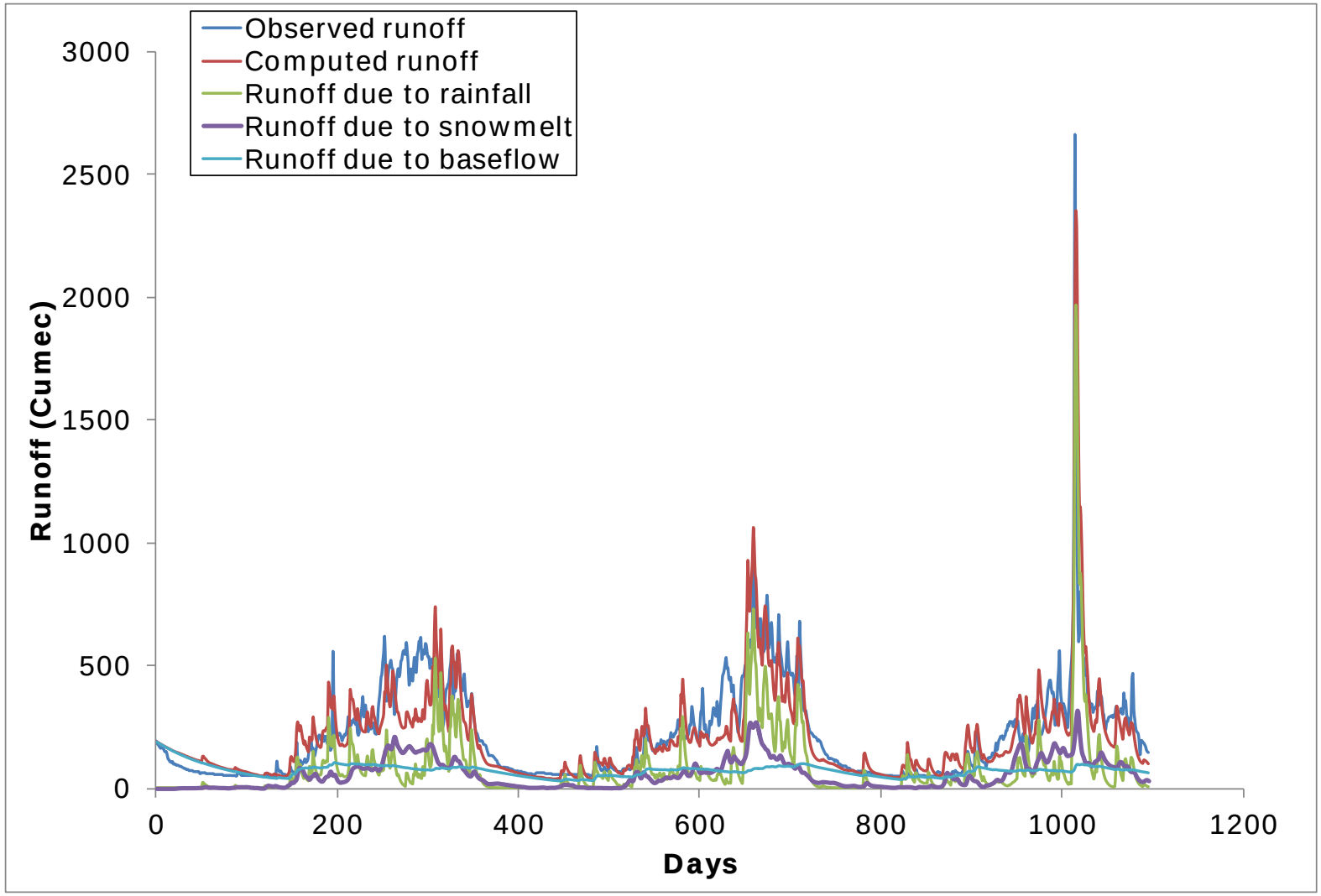

Figure 8.5: Simulation for the years 1990-1993 under temperature rise of 2^0C

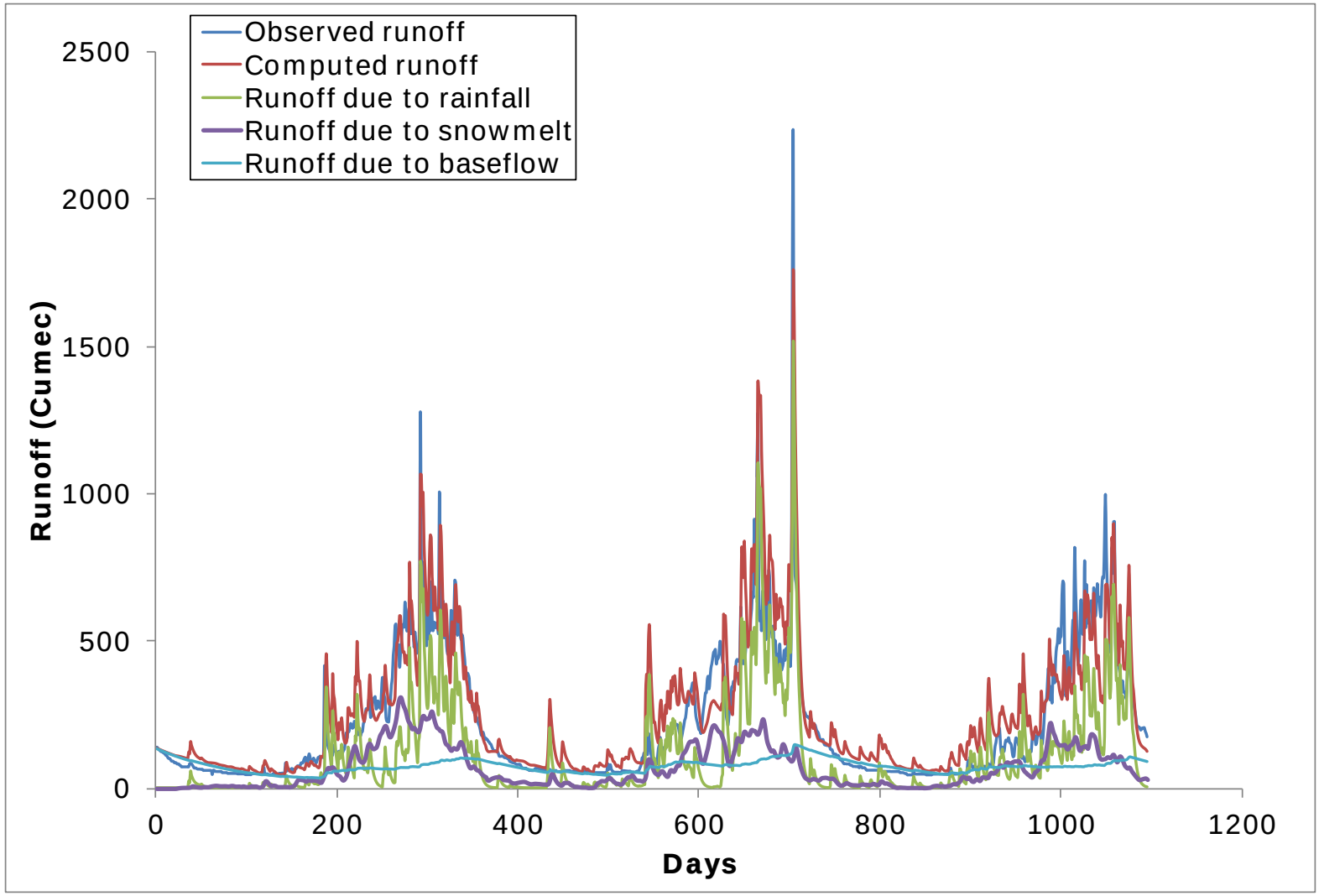

Figure 8.6: Simulation for the years 1993-1996 under temperature rise of 2^0C

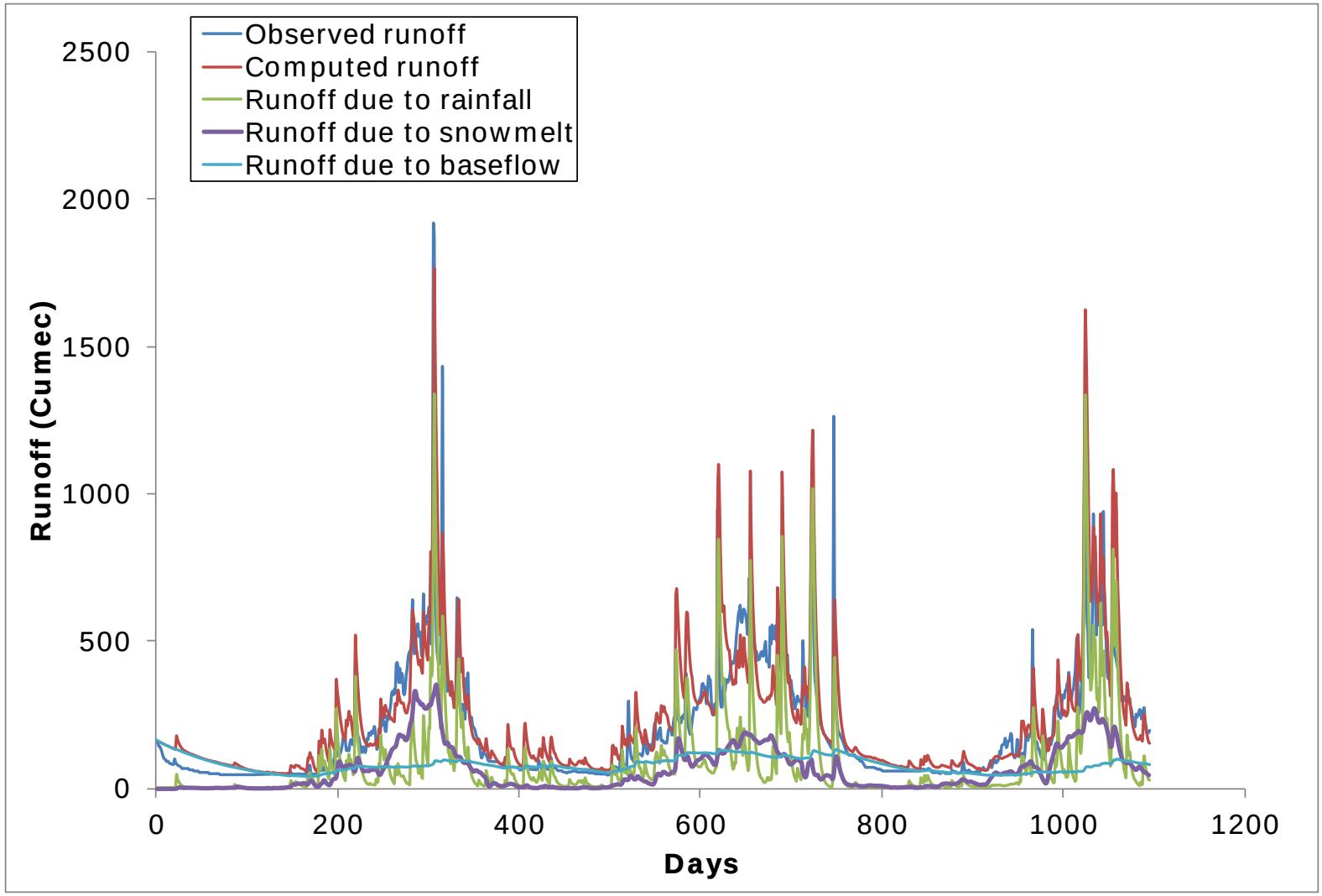

Figure 8.7: Simulation for the years 1996-1999 under temperature rise of 2^0C

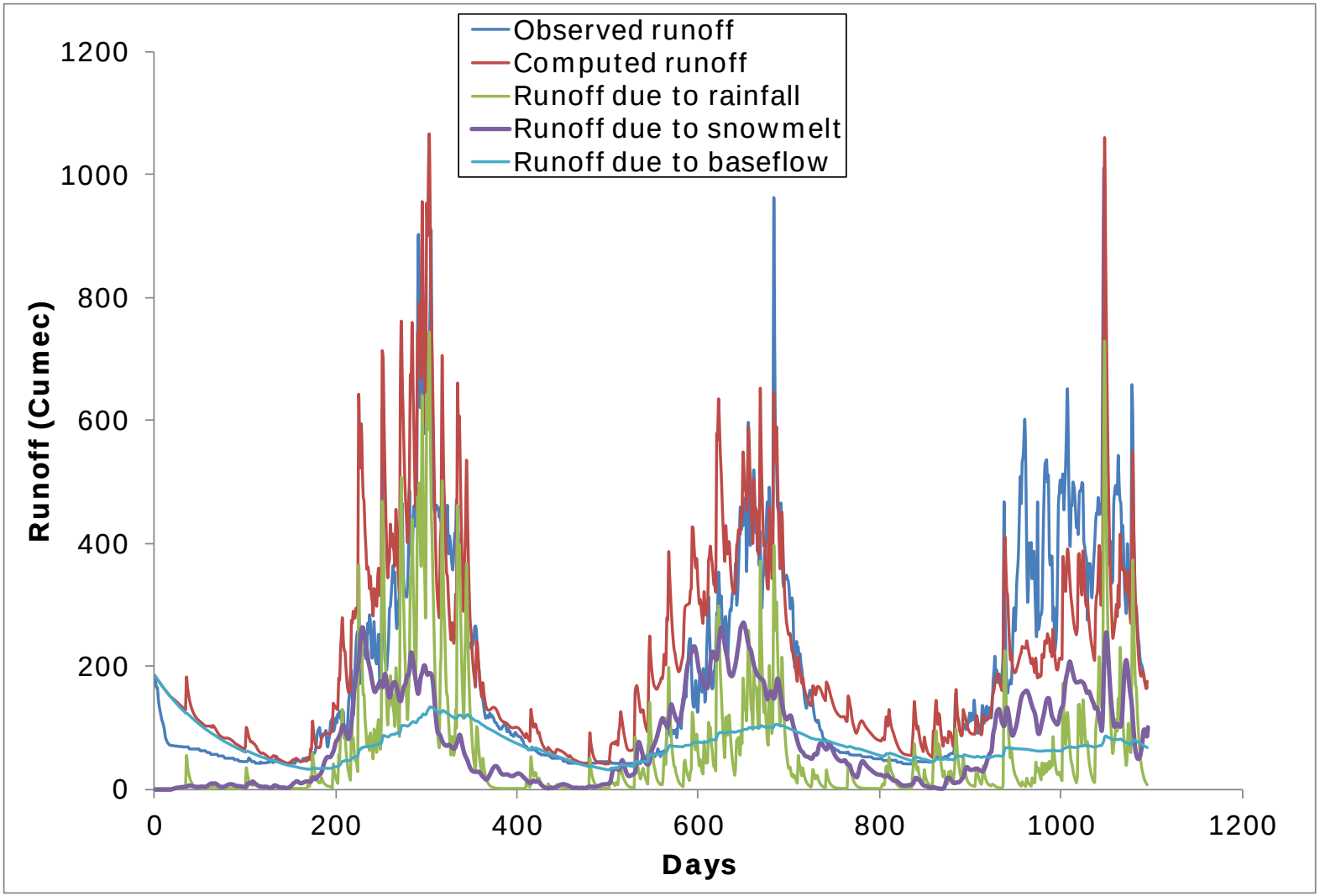

Figure 8.8: Simulation for the years 1999-2002 under temperature rise of 2^0C

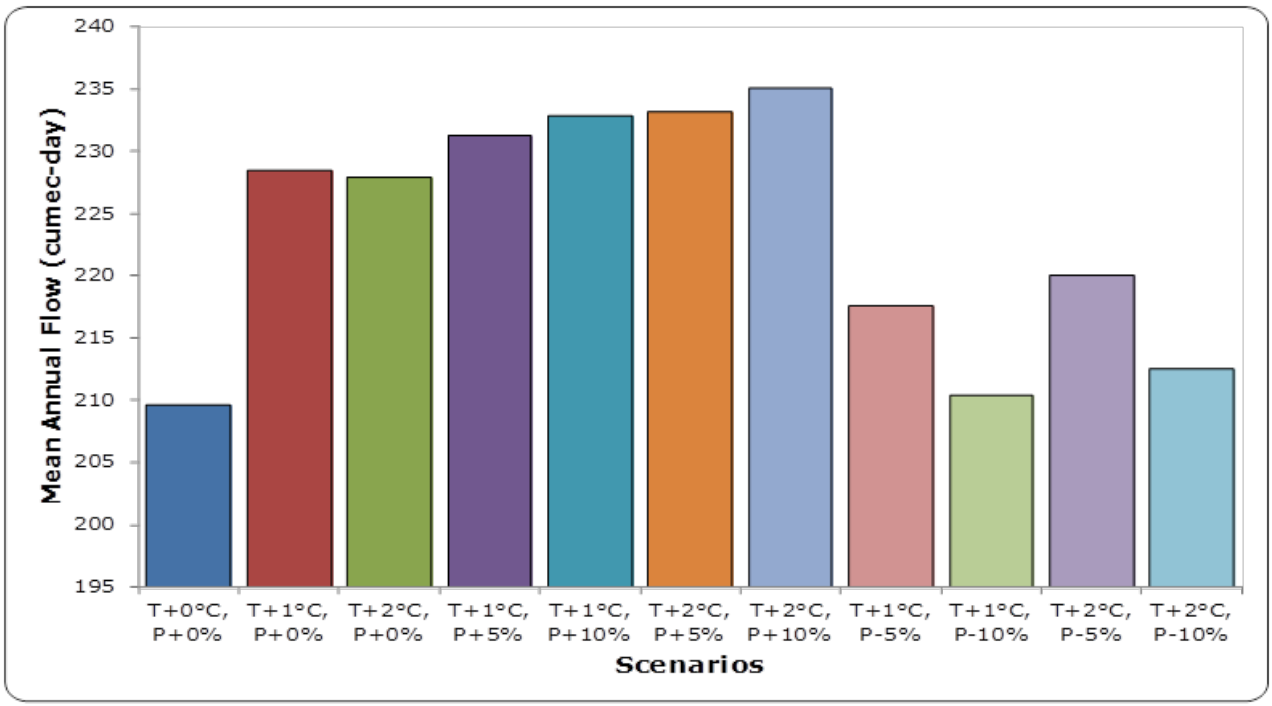

Figure 8.9: Mean annual streamflow for various scenarios in Beas basin

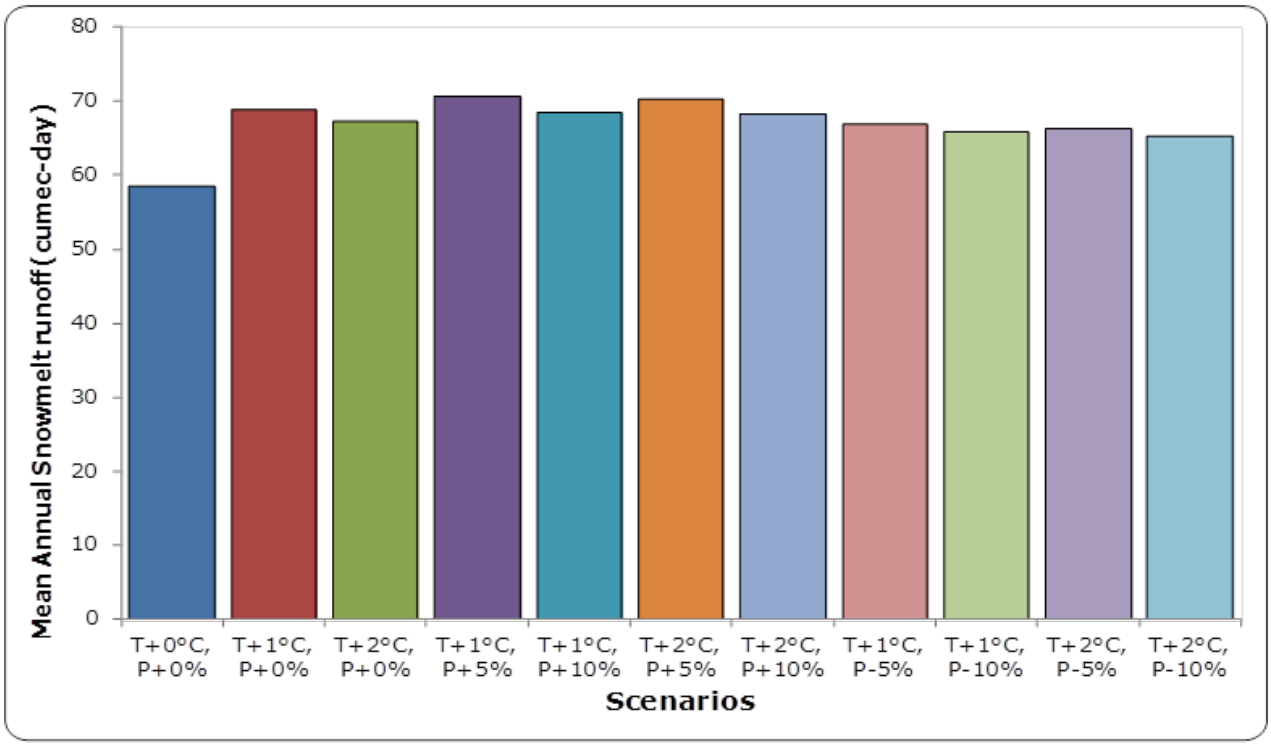

Figure 8.10: Mean annual snowmelt runoff for various scenarios in Beas basin

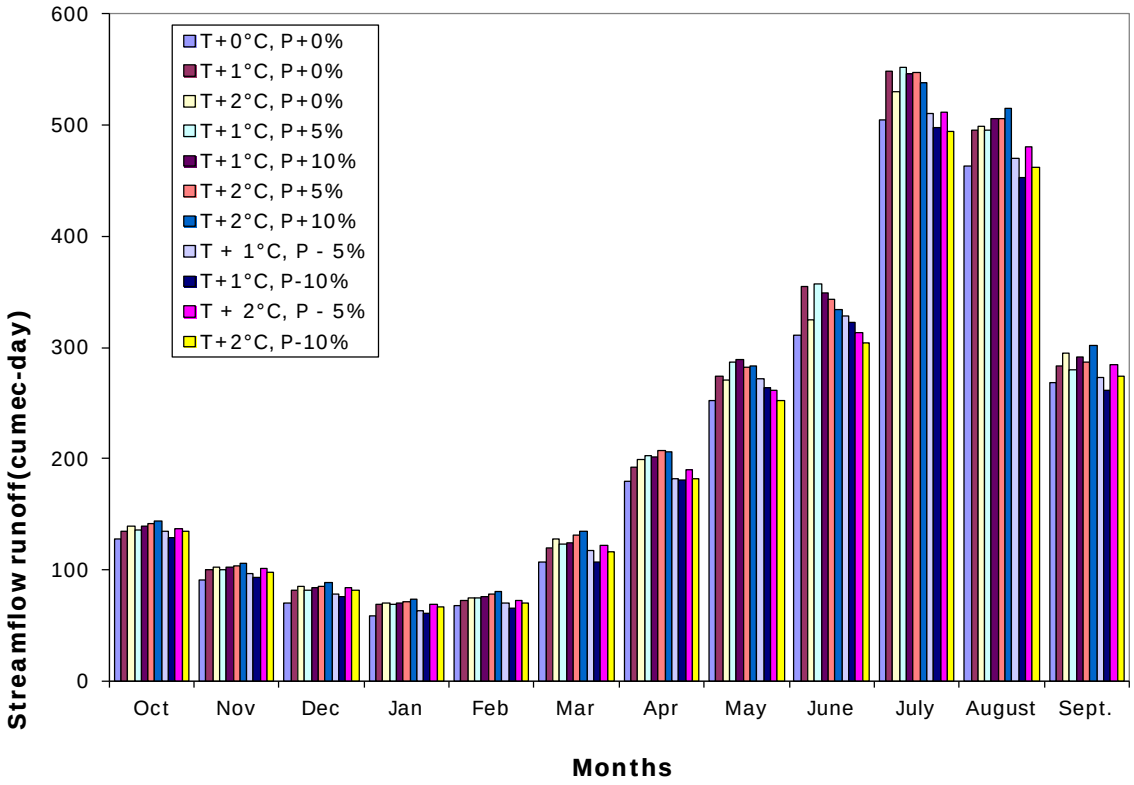

Figure 8.11: Mean annual streamflow for different scenarios for each month in Beas basin

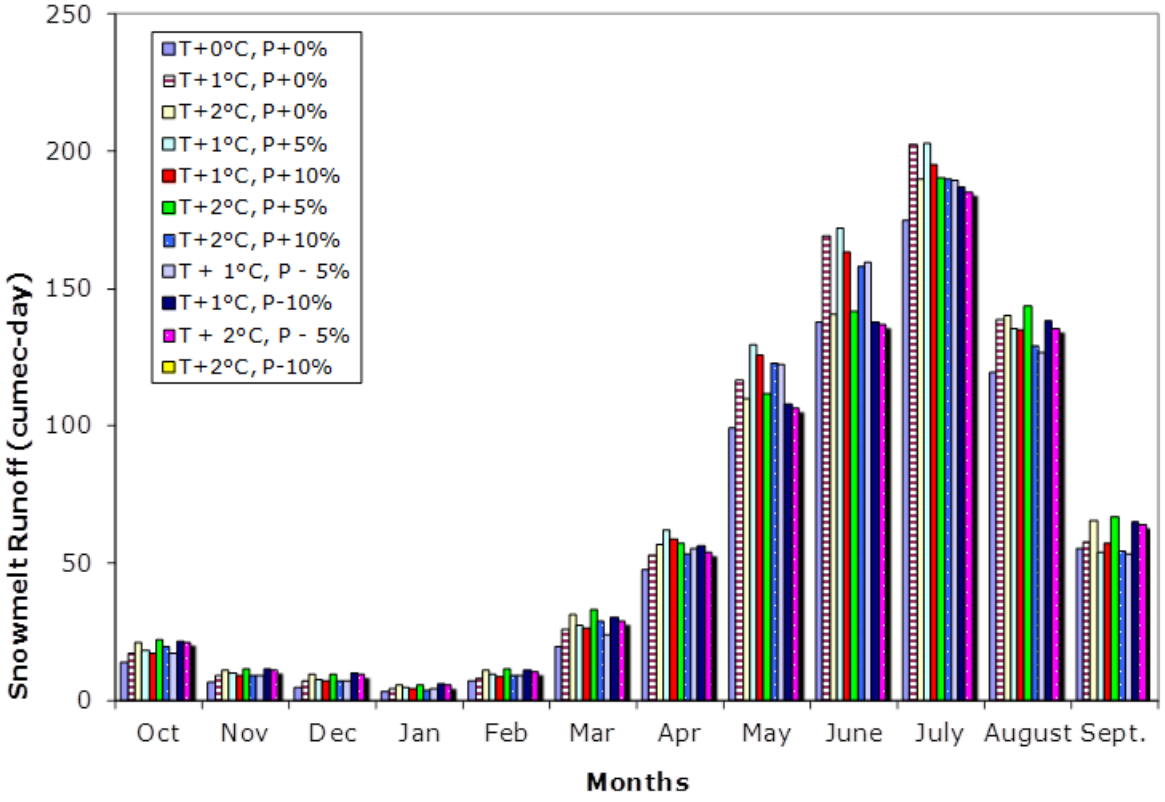

Figure 8.12: Mean annual snowmelt runoff for different scenarios for each month in Beas basin

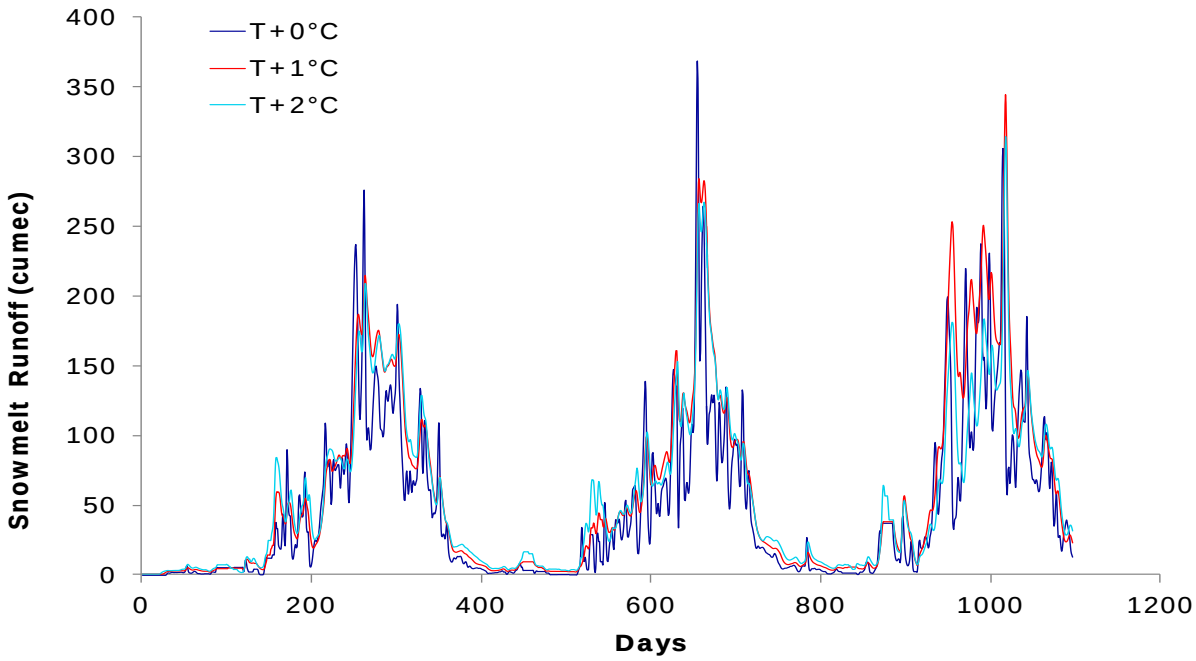

Figure 8.13: Snowmelt runoff for temperature rise of 1^0C and 2^0C for year 1990-1993

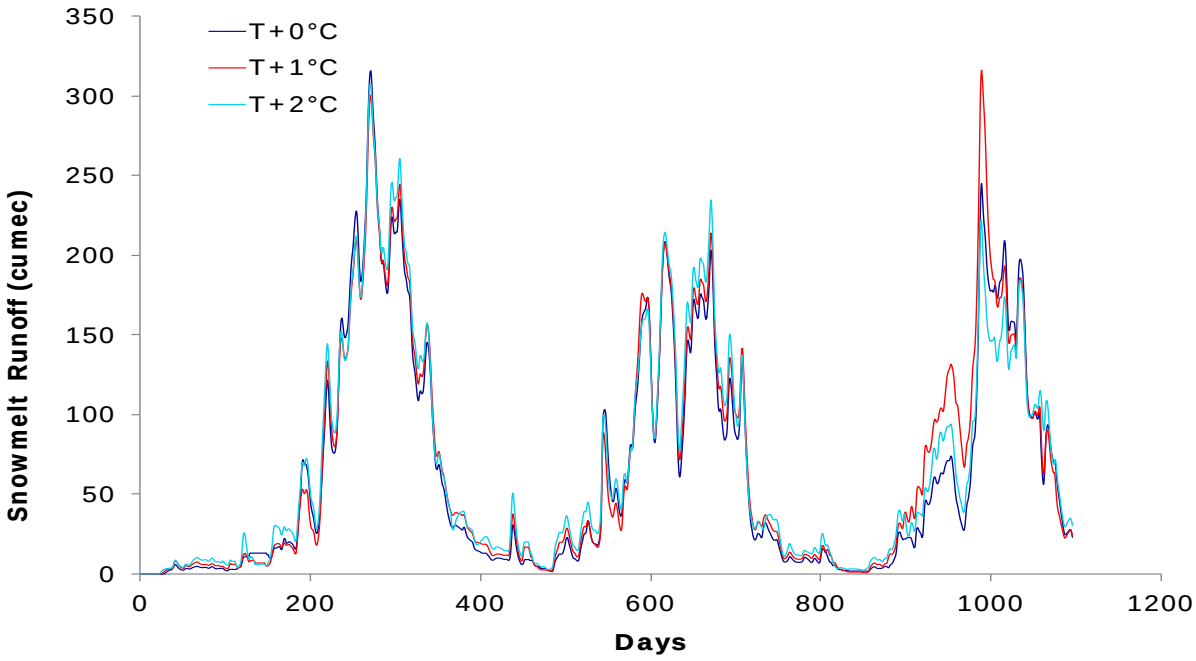

Figure 8.14: Snowmelt runoff for temperature rise of 1^0C and 2^0C for year 1993-1996

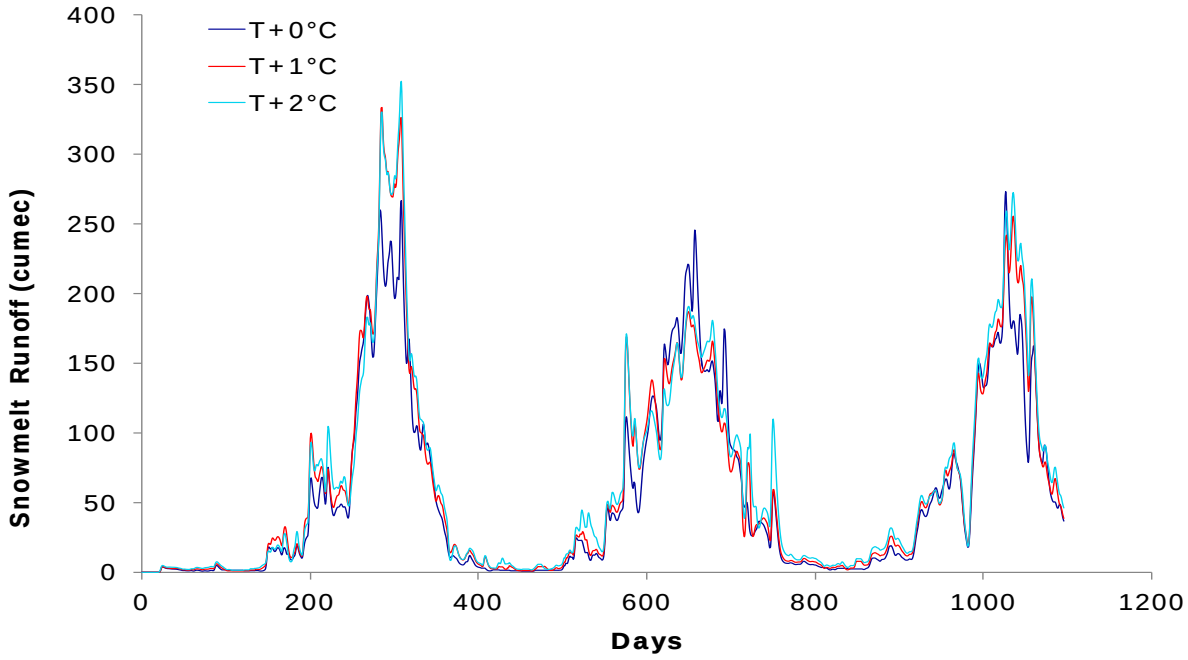

Figure 8.15: Snowmelt runoff for temperature rise of 1^0C and 2^0C for year 1996-1999

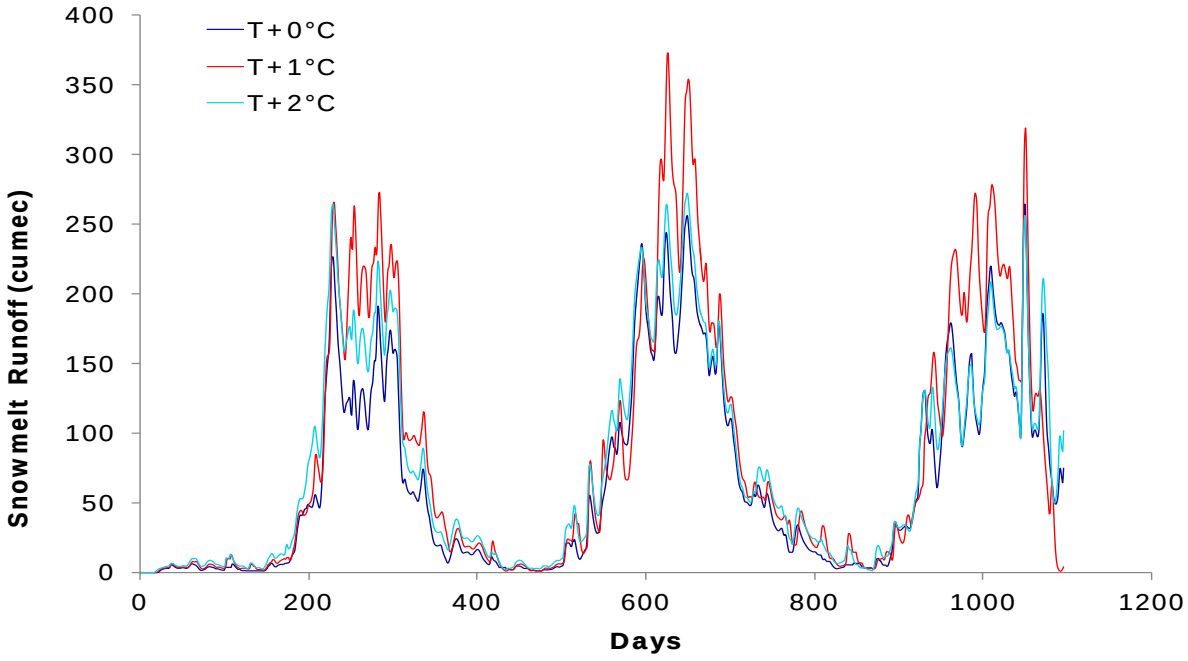

Figure 8.16: Snowmelt runoff for temperature rise of 1^0C and 2^0C for year 1999-2002

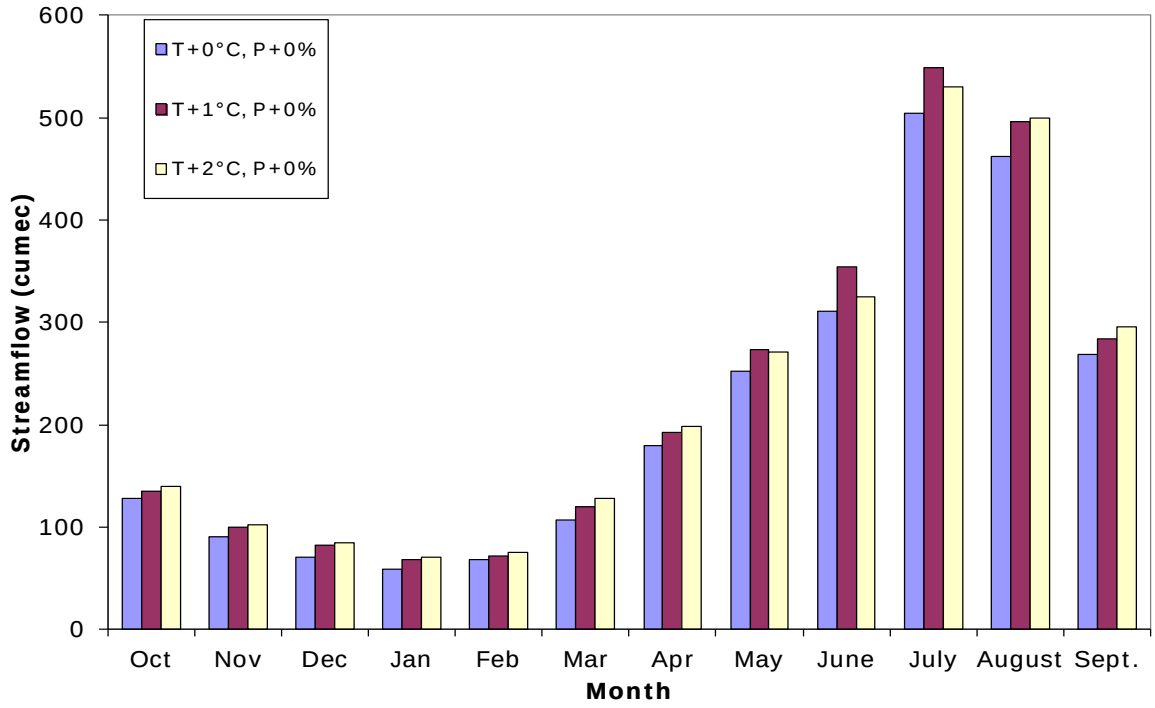

Figure 8.17: Mean annual streamflow for temperature change only scenarios for each month in Beas basin

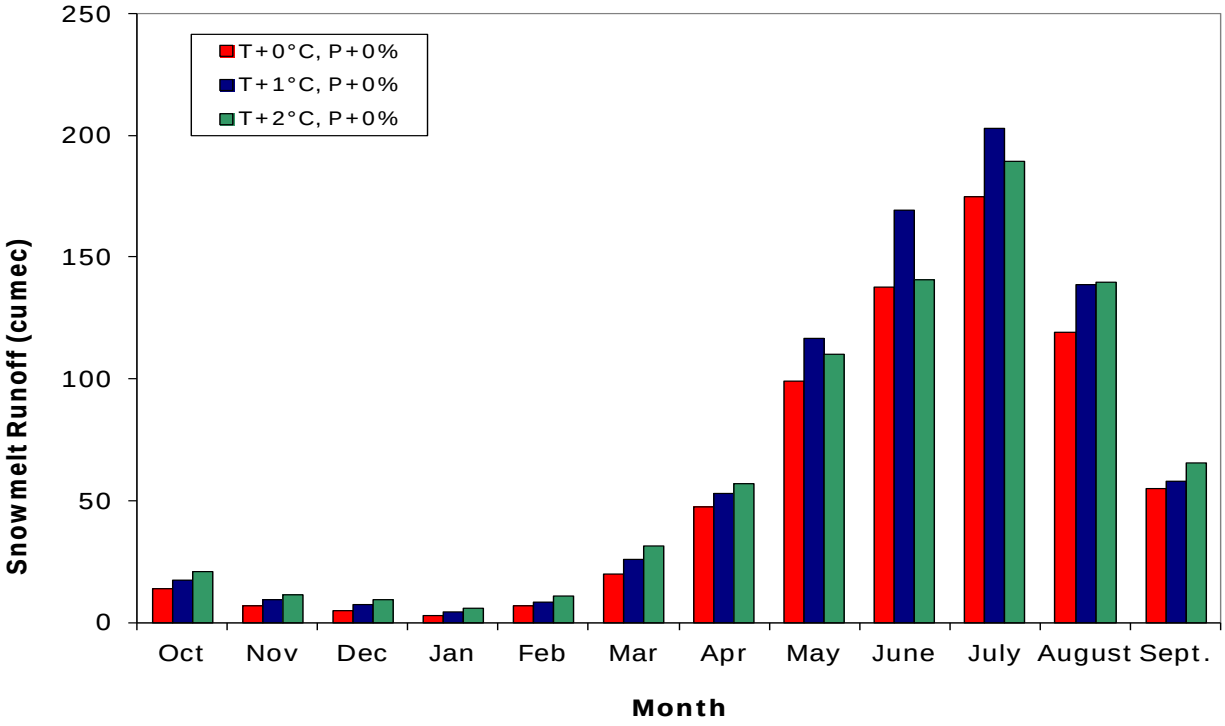

Figure 8.18: Mean annual snowmelt runoff for temperature change only scenarios for each month in Beas basin

Table 8.1: Mean annual runoff for different hypothetical scenarios for the Beas basin (Year: 1990-2002)

Scenarios	Mean Annual Streamflow (cumec-day)	Change (%)	Mean Annual Snowmelt runoff (cumec-day)	Change (%)
T+0°C, P+0%	209.44	-	58.42	-
T+1°C, P+0%	228.49	9	68.84	17.72
T+2°C, P+0%	227.85	8.69	67.22	14.95
T+1°C, P+5%	231.23	10.3	70.74	20.97
T+1°C, P+10%	232.8	11.05	68.49	17.12
T+2°C, P+5%	233.19	11.23	70.18	20
T+2°C, P+10%	235.06	12.12	68.27	16.74
T+1°C, P-5%	217.54	3.77	66.83	14.28
T+1°C, P-10%	210.42	0.37	65.94	12.75
T+2°C, P-5%	220.06	4.9	66.38	13.51
T+2°C, P-10%	212.49	1.36	65.38	11.8

(streamflow and snowmelt) components increase with the increase in temperature. Because under warmer climate higher melting rate takes place which accelerates the melting of snow resulting in increased snowmelt runoff from the basin. However in case of T+2°C, the increase in streamflow/snowmelt runoff is slightly less than the case of increase of T+1°C. The reason for this may be availability of lesser snow cover in case of T+2°C due to more melting.

During the ablation period in the Beas basin, snowmelt runoff increases in the months of March and April with the increase in temperature. It is also found that the streamflow is more with increase in temperature by 1°C in comparison to the increase in temperature by 2°C for the months of May, June and July. It is also observed that for 1°C and 2°C increase in temperature, the mean annual streamflow increases by 9% and 8.69% respectively. The maximum percentage increase in mean annual streamflow is 12.12% for the T+2°C, P+10% scenario whereas with the T+1°C, P-10% scenario the minimum % increase in mean annual streamflow is 0.37%.

8.4.2 Streamflow under Future Projected Scenario

The hydro-climatic heterogeneity of the Himalayan regions complicates understanding the hydrology and hydrologic response of snow-fed rivers to projected changes in climatic conditions. Under these warmer climatic conditions, melt from snow/ice and glacier adds a dominant component of flow to runoff from glacierized basins in addition to contemporary precipitation. An appropriate assessment of probable future temperature and precipitation and its variability is required for various climatic scenarios. The changes in the streamflow timing are probable to occur in the future under the warmer climate. Thus, assessment of projected climate change on the vulnerable resources of planet earth can be extremely useful to develop strategies for sustainable planning, management and conservation of these resources (Srinivas et al., 2013). Much of the literature on hydrologic simulation aims to find the sensitivity of streamflow and glacier to climate warming by using step increases in temperature.

Many studies based on the projected changes in the climatic variables have been carried out to connote the influence of climate change on the water resources. At basin scale study, the streamflow in the upper reaches (greater than 2000 amsl) was projected to reduce by 8.4%, 17.6% and 19.6% in the Indus, the Ganges and the Brahmaputra river basins in 2046-2065 comparative to the base year (2001-2007), exhibiting the relative significance of glacier melt contribution (Immerzeel et al., 2009). However, reduction in the streamflow due to declining contributions from the glacier is likely to be compensated from the projected future increase in precipitation. Immerzeel et al., (2011) quite recently, used output from five GCMs to high-resolution combined cyrospheric hydrologic model under A1B emission scenarios to study the repercussions of climate change on the hydrology of Langtang river catchment and witnessed that both downscaled temperature and precipitation increased by 0.06^{0}C/year and 1.9 mm/year respectively. Immerzeel et al. (2011) projected that glaciers would shrink and retreat by 32% in 2035 resulting in reduction in glacier melt contribution to streamflow. However, this loss in glacier runoff is compensated by increased rainfall-runoff and baseflow leading to an overall increase in streamflow by 4 mm/year.

In order to provide an indication of the extent of impacts of climatic change on water resources, streamflow represents an integrated response to hydrologic inputs on the drainage basin. The model applied in the present study simulates melt runoff as well as rainfall runoff. However there is effect mainly on snowmelt runoff due to change in climate. In this study impact of temperature change on streamflow have been presented. The precipitation change was not considered as the precipitation has less effect on streamflow in comparison to

temperature rise (Arora et al., 2008; Jain et al., 2010b), also it is massive and difficult in projecting precipitation at river basin level in complex, rugged topography and varying climatology of Himalayan region (Sharma et al., 2013). Hence, efforts have been made to study the impact of change of temperature on streamflow for the Beas basin using future climatic scenarios based on realistic temperature records available for the area.

The impact of climate change on the streamflow has been quantified in response to future climate change by using the projected temperature IPCC-SRES A1B scenario on the basis of a study by Srinivas et al. (2013). The daily maximum and minimum temperature have been projected up to the year 2100 using simulations of Canadian coupled global climate model (CGCM3.1/T63). From these projected values, computations for the period of 2001-2020, 2021-2040, 2041-2060, 2061-2080, 2081-2100 have been carried out and given in Table 8.2, 8.3, 8.4 and 8.5 for the stations Manali, Larji, Bhuntar and Pandoh. These values are also shown graphically in Figure 8.19 to 8.23 for the stations Manali, Larji, Bhuntar and Pandoh.

It is observed from these tables/figures that at Manali station, future maximum mean monthly temperature is projected to decrease during April-August and increase during January-February and October-December. At Bhuntar, the maximum monthly temperature is projected to increase in future during January-April. Further, there is decrease in the value for June-August over the period 2081-2100. At Larji station, maximum mean temperature is projected to increase in future during January-March and October-December. At Pandoh, future maximum temperature for almost all the months is projected to increase.

Since the Beas basin has been divided into nine zones and four of them are partially snow covered, modified SCA depletion curves were prepared for four zones as described in chapter 4. Also, the daily temperature projections have been prepared for the study area. With these modified meteorological and snow cover depletion data, streamflow has been simulated for the scenarios A1B for the Beas river basin for the years 2040-43, 43-46, 46-49, 49-52 and also for the years 2093-96, 2096-99. The results of these simulations are given in Table 8.6.

Table 8.2: Projected maximum temperature for different time period for Manali station

A1B	Observed	2001-2020	2021-2040	2041-2060	2061-2080	2081-2100	2001-2020	2021-2040	2041-2060	2061-2080	2081-2100
							Change				
Jan	11.79	10.74	13.83	15.60	16.04	15.23	-1.06	2.04	3.81	4.25	3.44
Feb	12.94	12.96	13.29	14.83	16.17	17.69	0.02	0.35	1.89	3.23	4.75
Mar	16.66	15.50	16.48	17.76	18.36	17.26	-1.16	-0.17	1.10	1.71	0.61
Apr	22.53	18.94	19.80	21.54	21.44	23.15	-3.59	-2.73	-0.99	-1.09	0.62
May	26.16	24.12	24.94	22.47	24.67	24.66	-2.04	-1.21	-3.69	-1.48	-1.49
Jun	27.52	23.02	24.97	24.81	23.80	24.84	-4.49	-2.55	-2.70	-3.71	-2.68
Jul	27.07	25.19	25.34	25.08	25.76	25.65	-1.88	-1.73	-1.99	-1.31	-1.42
Aug	26.59	24.39	24.54	23.73	23.65	23.83	-2.20	-2.05	-2.86	-2.94	-2.76
Sep	25.62	24.58	24.90	24.96	24.65	25.01	-1.05	-0.72	-0.66	-0.97	-0.61
Oct	22.55	24.54	24.43	25.26	24.72	25.46	1.99	1.89	2.72	2.18	2.91
Nov	18.08	19.44	21.37	21.11	22.49	23.18	1.36	3.28	3.02	4.41	5.10
Dec	13.66	13.83	14.05	16.76	16.70	16.64	0.17	0.39	3.10	3.04	2.98

Table 8.3: Projected maximum temperature for different time period for Larji station

A1B	Observed	2001-2020	2021-2040	2041-2060	2061-2080	2081-2100	2001-2020	2021-2040	2041-2060	2061-2080	2081-2100
							Change				
Jan	13.92	16.45	18.98	20.73	21.04	19.92	2.53	5.06	6.81	7.12	6.00
Feb	16.60	17.95	18.23	19.75	21.16	22.93	1.35	1.63	3.15	4.56	6.33
Mar	20.25	20.94	22.00	23.34	23.96	22.82	0.69	1.75	3.09	3.71	2.58
Apr	26.92	24.50	25.35	27.31	27.40	29.02	-2.42	-1.57	0.39	0.48	2.10
May	31.09	30.86	32.50	31.32	31.96	32.79	-0.23	1.41	0.23	0.87	1.70
Jun	33.64	32.03	32.05	32.96	32.97	32.10	-1.61	-1.59	-0.68	-0.67	-1.53
Jul	31.20	31.29	32.42	30.84	31.75	31.51	0.09	1.21	-0.36	0.55	0.31
Aug	30.49	30.07	30.35	29.50	29.15	29.33	-0.42	-0.14	-0.99	-1.34	-1.16
Sep	29.27	30.34	30.81	30.69	30.48	30.83	1.07	1.54	1.42	1.21	1.56
Oct	25.97	30.10	30.11	31.08	30.81	31.66	4.13	4.14	5.11	4.84	5.69
Nov	21.01	24.90	26.73	26.62	27.84	28.70	3.89	5.72	5.61	6.83	7.69
Dec	15.07	18.93	19.42	22.36	21.90	21.95	3.86	4.35	7.29	6.83	6.88

Table 8.4: Projected maximum temperature for different time period for Bhuntar station

A1B	Observed	2001-2020	2021-2040	2041-2060	2061-2080	2081-2100	2001-2020	2021-2040	2041-2060	2061-2080	2081-2100
							Change				
Jan	15.56	13.89	18.72	20.95	21.37	23.95	-1.67	3.16	5.39	5.81	8.39
Feb	17.23	17.85	18.35	20.39	21.90	23.72	0.62	1.12	3.16	4.67	6.49
Mar	20.94	21.73	22.68	23.98	24.52	24.71	0.79	1.74	3.04	3.59	3.77
Apr	26.58	25.07	25.94	27.78	28.13	29.04	-1.51	-0.63	1.20	1.56	2.47
May	30.45	31.74	33.37	34.84	33.09	32.07	1.29	2.91	4.38	2.63	1.61
Jun	32.78	35.22	32.91	34.47	35.52	27.67	2.44	0.13	1.69	2.74	-5.11
Jul	31.03	31.39	32.93	30.83	31.63	26.66	0.36	1.90	-0.20	0.60	-4.37
Aug	30.41	30.22	30.53	29.91	29.41	27.57	-0.19	0.12	-0.50	-1.00	-2.84
Sep	29.88	30.43	30.89	30.70	30.60	30.84	0.56	1.01	0.82	0.72	0.96
Oct	27.51	30.14	30.14	31.01	30.97	29.61	2.63	2.63	3.50	3.46	2.11
Nov	22.74	25.53	27.05	27.14	28.10	24.99	2.79	4.31	4.40	5.36	2.25
Dec	17.45	18.76	19.28	22.15	22.09	23.79	1.31	1.84	4.71	4.65	6.34

Table 8.5: Projected maximum temperature for different time period for Pandoh station

A1B	Observed	2001-2020	2021-2040	2041-2060	2061-2080	2081-2100	2001-2020	2021-2040	2041-2060	2061-2080	2081-2100
							Change				
Jan	19.04	20.11	23.04	24.80	24.86	24.04	1.07	4.00	5.76	5.82	5.00
Feb	20.65	22.04	22.27	23.95	25.21	26.70	1.38	1.62	3.30	4.56	6.05
Mar	24.25	24.86	25.78	27.08	27.51	26.64	0.61	1.53	2.83	3.25	2.39
Apr	30.07	28.12	29.10	30.73	30.76	31.95	-1.95	-0.97	0.66	0.69	1.88
May	33.86	33.51	35.49	35.30	34.68	35.99	-0.34	1.63	1.44	0.82	2.13
Jun	34.29	35.96	34.55	36.04	36.90	34.79	1.67	0.26	1.75	2.61	0.50
Jul	32.07	33.34	34.93	32.72	33.39	33.11	1.27	2.86	0.65	1.32	1.04
Aug	31.73	32.32	32.57	32.18	31.78	31.83	0.59	0.84	0.44	0.04	0.10
Sep	31.80	32.51	32.84	32.63	32.68	32.81	0.71	1.04	0.83	0.88	1.01
Oct	30.04	32.11	32.13	32.88	33.08	33.44	2.07	2.09	2.84	3.04	3.40
Nov	25.70	28.65	29.75	29.98	30.53	31.05	2.95	4.05	4.28	4.83	5.35
Dec	20.45	22.80	23.48	26.13	25.86	25.51	2.35	3.03	5.68	5.41	5.06

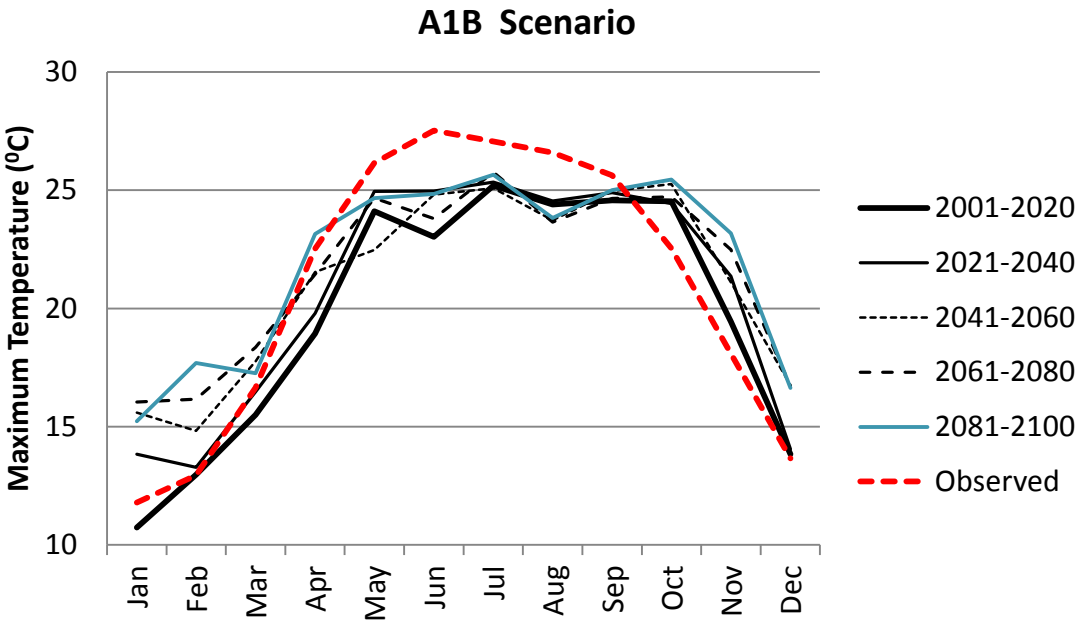

Figure 8.19: Projected daily max. temperature for different time period for Manali station

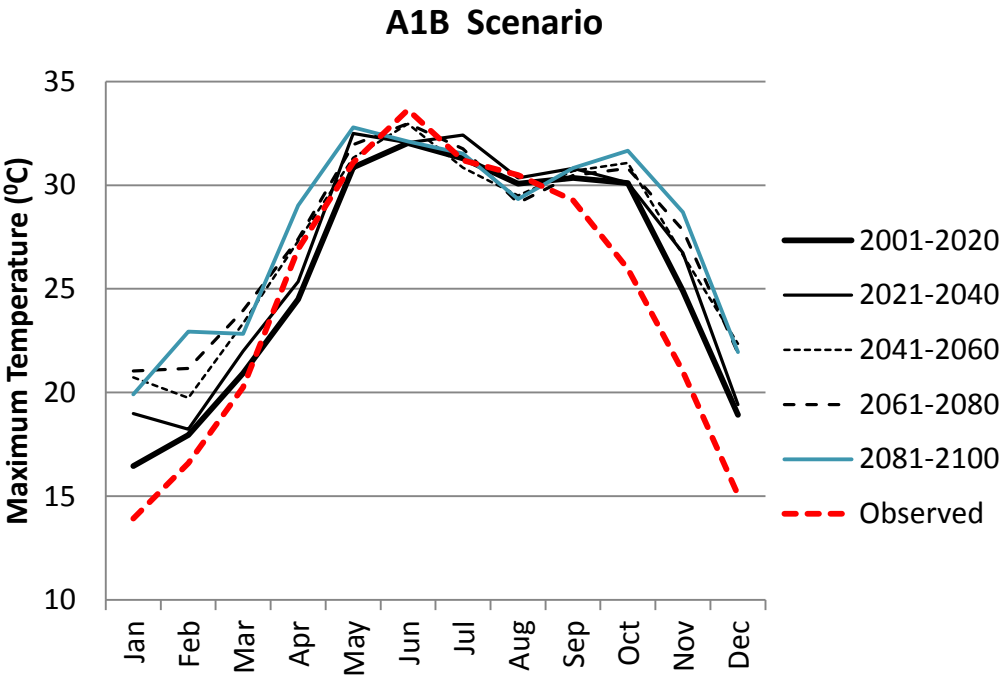

Figure 8.20: Projected daily max. temperature for different time period for Larji station

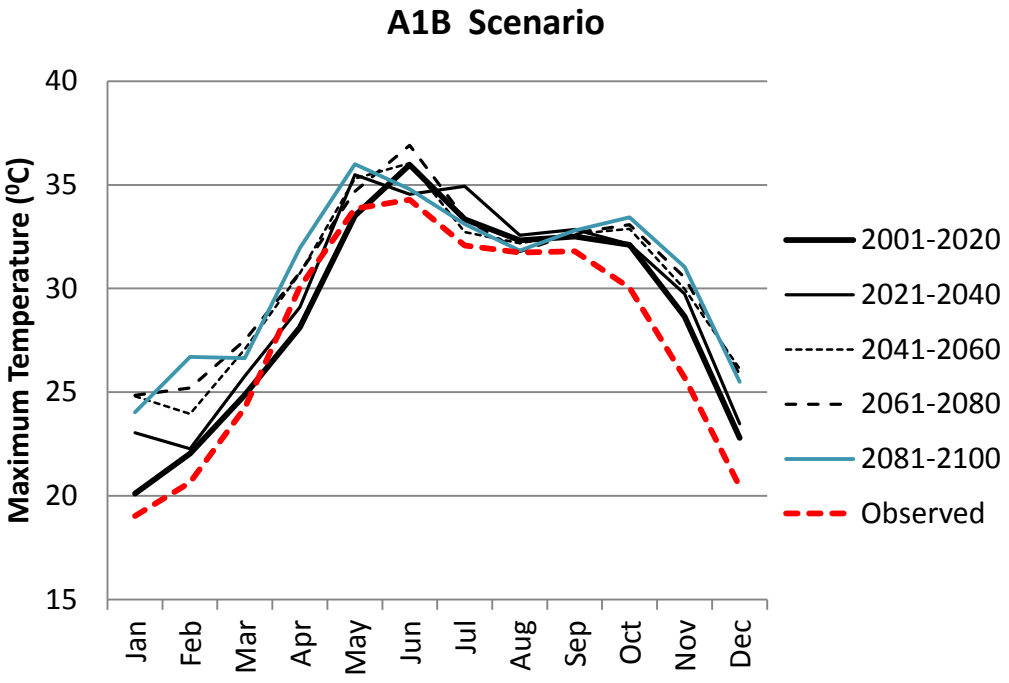

Figure 8.21: Projected daily max. temperature for different time period for Bhuntar station

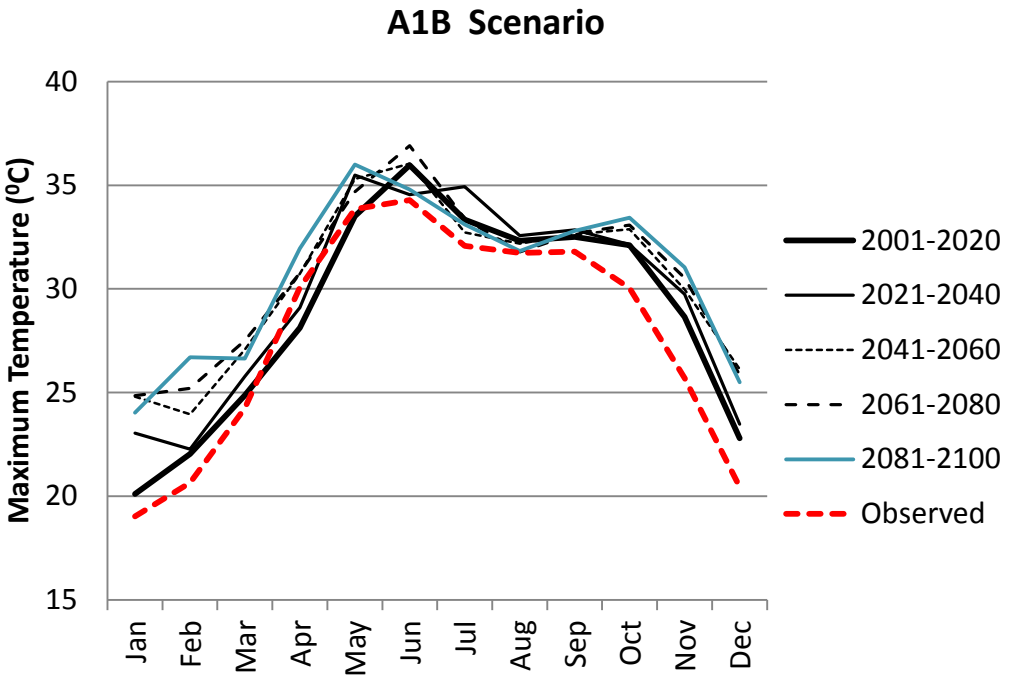

Figure 8.22: Projected daily max. temperature for different time period for Pandoh station

Table 8.6: Simulation of streamflow for the Beas Basin up to Pandoh

Period	Simulated Streamflow (cumec-day)	Rainfall contribution (cumec-day)	Snowmelt runoff contribution (cumec-day)	Base flow contribution (cumec-day)
1990-2002	209.44	79.52	58.42	71.49
2040-43	179.90	77.17	30.49	72.25
2043-46	182.70	85.27	26.54	70.88
2046-49	180.89	75.87	30.67	74.36
2049-52	183.08	79.04	30.16	73.88
2093-96	217.44	96.44	51.56	69.44
2096-99	212.75	84.69	49.78	78.28

The average simulated flow for the years 1990-2002 was compared with the simulated projected flows for the different years, as given in the Table 8.6. The results are depicted in graphical form in Figure 8.23. The change in annual flow as well as snowmelt runoff is given in Table 8.7. From this table it can be seen that the total streamflow will reduce for the years 2040-43, 2043-46, 2046-49 and 2049-52 while for the years 2093-96 and 2096-99 it will increase marginally. The snowmelt runoff will decrease in all the future scenarios. For the project period up to 2052, the reduction in total streamflow is of the order of 12-14% while reduction in snowmelt runoff is 47-54%. For the period of 2093 to 2096, the there is reduction in snowmelt runoff of the order of 11-15% while there is slight increase in the total streamflow i.e. of the order of 1.5 to 4%. From the analysis of projected temperature, it was found that temperature is higher during 2080-2100 in comparison to 2040-60. Due to which the snow cover will reduce more in 2080-2100 and hence snowmelt runoff will be more which increases the total streamflow marginally. However, during the last decade of the century, temperature change is not significant therefore projected streamflow is not showing much change.

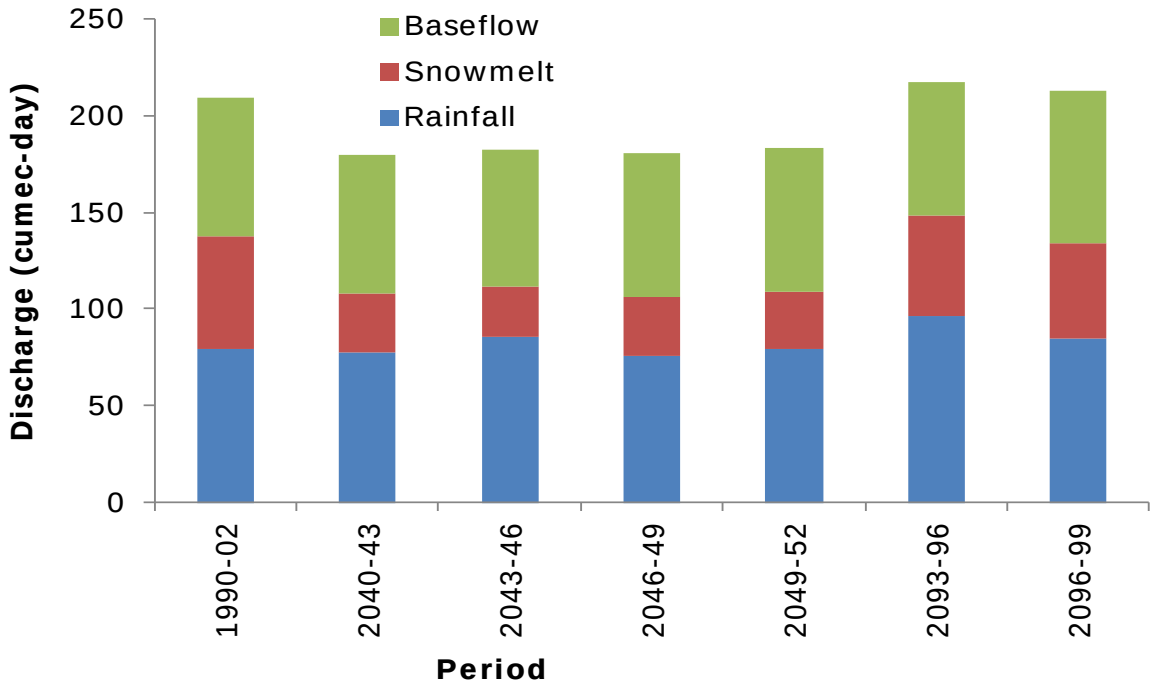

Figure 8.23: Simulation of streamflow for the Beas basin up to Pandoh

Table 8.7: Mean (annual) runoff for A1B scenario for Beas basin

Scenarios	Average annual streamflow (cumec-day)	Percentage change	Average annual snowmelt runoff (cumec-day)	Percentage change
1990-2002	209.44	-	58.42	-
2040-43	179.90	-14.10	30.49	-47.81
2043-46	182.70	-12.77	26.54	-54.57
2046-49	180.89	-13.63	30.67	-47.50
2049-52	183.08	-12.59	30.16	-48.37
2093-96	217.44	+3.82	51.56	-11.74
2096-99	212.75	+1.58	49.78	-14.79

8.5 SUMMARY

SNOWMOD model has been used to estimate the streamflow and evaluate the impact of climate change in Beas river basin for 10 plausible hypothetical scenarios and IPCC-SRES A1B projected scenarios as well. Snow cover depletion curves were modified with respect to change in temperature. Since the Beas basin is divided into nine zones and four of them are partially snow covered, modified SDCs were prepared for these four zones. The change in computed streamflow under different generated scenarios indicated the effect of climate change. For 1°C and 2°C increase in temperature, the mean annual streamflow increased by about 9% and 8.69%, respectively. The maximum percentage increase in mean annual streamflow was 12.12% for T+2°C, P+10%. Minimum percentage increase in mean annual streamflow was 0.37% for T+1°C, P-10%.

With projected temperature and snow cover depletion data, streamflow has been simulated for scenarios A1B and the effect of different climate scenarios on the melt runoff as well as streamflow has been studied for Beas basin. The streamflow and snowmelt runoff both are decreasing for projected daily temperature. For the project period up to 2052, the reduction in total streamflow was of the order of 12-14% while it was 47-54% in snowmelt runoff. For the period of 2093 to 2096, the reduction in snowmelt runoff was of the order of 11-15% while there was slight increase in the total streamflow i.e. of the order of 1.5 to 4%. In case of hypothetical scenarios the change in temperature has been considered by adding same value e.g. 1 or 2°C throughout the year. Therefore in this case the projected runoff is always increasing while in other case, temperature projection based on climate modeling decreases during monsoon months. Hence the projected streamflow is showing different opposite behavior i.e. decreasing during the mid-century.

Chapter 9

SUMMARY AND CONCLUSIONS

9.1 SUMMARY

The snow-fed Beas river system in Himalayas has high water resources prospective to meet the demands of growing population in the region. Besides many hydropower schemes are in progress or in operation to harness the potential of river water. A simple, logistic and systematic assessment of Beas river streamflow is imperative for the success of such existing and upcoming schemes, and to properly manage the water resources for the socio-economic development of the society in the region. Moreover, in recent decades global warming and climate change issues have added another dimension of intricacy. It is a major issue of concern and there is need to study the impacts of climate change on streamflow.

With this perspective, efforts have been made to model the streamflow and evaluate the impacts of climate change on streamflow for Beas river basin by conducting sequential studies involved for simulation of streamflow and assessment of impact of climate change on streamflow involving snow cover mapping, spatio-temporal variation in temperature lapse rate, trend analysis and plausible impacts of climate change under different hypothetical and projected scenarios using SNOWMOD model. The whole study can be summarized in brief as follows:

- Snow forms an integral part of hydrological model in Himalayan basin. Snow cover mapping in such complex, rugged terrains with highly varied topography becomes arduous to acquire spatial and temporal areal extent of snow cover. In this direction, snow cover area estimated from remote sensing satellite data proved to be a better option.
- Snow depletion curves (SDCs) prepared from snow cover area information are imperative for simulation of runoff in snow-fed river basins. MODIS data is used to prepare SDC, for the years 2001 to 2005. For the period 1990 to 2000, an exponential relationship was generated between the Snow Cover Area (SCA) and Cumulative Mean Air Temperature (CMAT) for the Beas basin. This technique was used to prepare snow cover area maps for years 1990 to 2000 and thereafter SDCs were prepared and used in the model.

- MODIS-LST dataset was used to determine spatial and temporal temperature lapse rate for Beas basin. Monthly, seasonally and topographically (elevation based) varying lapse rate values were developed for a period of nine years i.e. from 2001 to 2009.
- The snowmelt runoff model was applied with varied lapse rate computed in the study and the daily streamflow components namely snowmelt runoff, rainfall-runoff and baseflow were estimated
- The simple regression method (parametric), Mann-Kendall test and Sens's estimator of slope method (non-parametric) were applied to determine trends in hydro-meteorological parameters namely temperature, rainfall and discharge over the last three decades.
- To investigate the impact of climate change on streamflow, plausible hypothetical scenarios and IPCC-SRES A1B projected temperature scenarios were applied.

9.2 CONCLUSIONS

The conclusions drawn from the present work are enumerated as below:

1. Estimation of snow cover area from remote sensing data, such as MODIS is found to be more reliable as it provides continuous data at greater temporal resolution.
2. The proposed exponential relationship generated between the Snow Cover Area (SCA) and Cumulative Mean Air Temperature (CMAT) performs well for determination of snow depletion curves (SDCs) when regular SCA is not available at regular interval.
3. The use of monthly, seasonal and topographically varied TLR in the present study has shown to be more promising than the fixed (or constant) TLR values used in the past.
4. The application of SNOWMOD model with varied TLR for estimation of snowmelt runoff in Beas basin yielded satisfactory results exhibiting its applicability to Himalayan basin. The daily streamflow components namely snowmelt runoff, rainfall-runoff and baseflow were estimated to be 24.07 % to 34.62 %, 30.48 % to 41.85 % and 30.16 % to 36.37% respectively with model efficiency varying from 0.68 to 0.80.
5. Majority of stations showed increasing trend in the mean annual temperature whereas one station (Manali) depicted decreasing trend during the study period. The annual and seasonal rainfall in general indicated decreasing trend at majority of stations. The trend analysis of discharge at Pandoh and Thalout indicated decreasing trend at annual and seasonal scale.

6. The study shows changes in the mean streamflow by about 9% and 8.69% with rise in 1°C and 2°C temperature respectively. The maximum percentage increase in mean annual streamflow was found to be 12.12% for T+2°C, P+10% scenario whereas minimum percentage increase was 0.37% for T+1°C, P-10% scenario
7. The study reveals a reduction in streamflow by 12-14% and that in snowmelt runoff by 47-54% by the year 2052. However by the end of century there is slight increase in streamflow while reduction in snowmelt of the order 11-15%.

9.3 SCOPE OF FUTURE RESEARCH WORK

Streamflow modeling and impact of probable climate change under the different hypothetical and projected scenario explored in Beas basin with limited data has extended the application of modeling approach in this part of Himalayas. Some of the issues for future research work are briefed as follows:

1. Retrieval of temperature lapse rate from LST maps of MODIS provides better representation of TLR in the area. For streamflow modeling, seasonally as well as topographically varying lapse rates have been considered instead of fixed value. As lapse rate varies with season and region, there is a scope to establish actual lapse rate for hydrological modeling in other parts of Himalayas.
2. Variation in streamflow at seasonal and annual scale is governed by the climate of the region. Hence seasonal and annual trends have been examined for climatic variables (temperature and rainfall) during the last three decades for Beas basin. There is a need to expand the work along with other parameters such as snowfall, relative humidity etc. at greater spatial and temporal resolutions for other parts of Himalayas.
3. The present study was done to evaluate the impact of climate change on the streamflow under hypothetical scenarios and real projected temperature scenarios based on IPCC-SRES A1B. Other plausible IPCC SRES based scenarios for temperature and rainfall change may be considered to understand the changes in model parameters and investigate the catchment process behavior.

9.4 MAJOR CONTRIBUTIONS

The main objectives of the present study were stream/snowmelt runoff modeling and to evaluate the impact of climate change on snowmelt runoff for a Himalayan basin. For

estimation of SCA when sufficient satellite data were not available, a temperature based approach has been proposed and applied for generating SCA and, in turn modified SDCs to study the impact of climate change. The use of temporally and topographically varying temperature lapse rate has shown to be more rational than the currently used fixed value.

REFERENCES

Aber, J. and Federer, C. (1992). A generalized lumped-parameter model of photosynthesis, evapotranspiration and net primary production in temperate and boreal forest ecosystems, Oecologia, Vol. 92, pp. 463-474.

Agarwal, K.C., Kumar, V. and Das, T. (1983). Snowmelt runoff for a catchment of Beas basin. Proc. of the First National Symposium on Seasonal Snowcover. 28-30, April, SASE, Manali, II:43-63.

Ageta, Y. (2001). Study project on the recent shrinkage of summer accumulation type glaciers in the Himalayas, 1997-1999. Bulletin of Glaciological Research, 18:45-49.

Aggarwal, S.P., Garg, V., Gupta, P.K., Nikam, B.R., Thakur, P.K. and Roy, P.S. (2013). Run-off potential assessment over Indian landmass: a macro-scale hydrological modelling approach. Current Science, 104 (7):950-959.

Aggarwal, S.P., Thakur, P.K., Nikam, B.R. and Garg, V. (2014). Integrated approach for snowmelt run-off estimate using temperature index model, remote sensing and GIS. Current Science, 106 (3): 397-407.

Aizen, V.B., Kuzmichenok, V.A., Surazakov, A.B. and Aizen, E.M. (2006). Glacier change in the central and northern Tien Shan during the last 140 years based on surface and remote-sensing data. Annals of Glaciology, 43:202-213.

Alexander, L.V., Zhang, X., Peterson, T.C., Caesar, J., Gleason, B., Klein Tank, A.M.G., Haylock, M., Collins, D., Trewin, B., Rahim, F., Tagipour, A., Rupa Kumar, K., Revadekar,J., Griffiths, G., Vincent, L., Stephenson, D.B., Burn, J., Aguilar, E., Brunet, M., Taylor, M., New, M., Zhai, P., Rusticucci, M. and Vazquez-Aguirre, J.L. (2006). Global observed changes in daily climate extremes of temperature and precipitation. Journal of Geophysical Research-Atmospheres, 111, D05109.

Anderson, E.A. (1973). National Weather Service River Forecast System-Snow Accumulation and Ablation Model, NOAA Technical Memorandum NWS HYDRO-17, U.S. Dept. Commerce, Silver Spring, MD.

Archer, D.R., Bailey, J.O., Barret, E.C. and Greenhill, D. (1994). The potential of satellite remote sensing of snow cover Great Britain in relation to snow cover. Nordic Hydrology, 25:39-52.

Arnell, N.W. (1992). Factors controlling the effects of climate change on river flow regime in a humid temperate environment. Journal of Hydrology, 132:321-342.

Arnell, N.W. (2003). Relative effects of multi-decadal climatic variability and changes in the mean and variability of climate due to global warming: future streamflows in Britain. Journal of Hydrology, 270:195-213.

Arnold, N.S., Rees, W.G., Hodson, A.J. and Kohler, J. (2006). Topographic controls on the surface energy balance of a high Arctic valley glacier. J. Geophys. Res., 111, F02011, doi: 10.1029/2005JF000426.

Arora, V.K. (2001). Streamflow simulations for continental scale river basins in a global atmospheric general circulation model. Advances in Water Resources Research, 28:1247-1260.

Arora, M., Singh, P., Goel, N.K. and Singh, R.D. (2008). Climate variability influences on hydrological responses of a large Himalayan basin. Water Resources Management, 22 (10):1461-1475.

Arora, M., Rathore, D.S., Singh, R.D., Kumar, R. and Kumar, A. (2010). Estimation of Melt Contribution to Total Streamflow in River Bhagirathi and River Dhauli Ganga at Loharinag Pala and Tapovan Vishnugad Project Sites. Journal of Water Resource and Protection, 2 (7):636-643.

Ayyub, B. and McCuen, R.H. (2002). Probability, Statistics, and Reliability for Engineers and Scientists. CRC Press.

Bagchi, A.K. (1981). Snowmelt runoff in Beas basin using satellite images. PhD thesis, Department of Civil Engineering, University of Roorkee, India.

Barnett, T.P., Dumenil, L., Schlese, U., Roeckner, E. and Latif, M. (1989). The effect of Eurasian snow-cover on regional and global climate variations. Journal of Atmospheric Science, 46:661-685.

Barnnet, T.P., Adam, J.C. and Lettenmaier, D.P. (2005). Potential impacts of a warming climate on water availability in snow-dominated regions. Nature, 438(17):303-309, DOI: 10.1038/nature04141.

Baron, J.S., Hartman, D.M., Band, L.E. and Lammers, R.B. (2000). Sensitivity of a high elevation Rocky mountain watershed to altered climate and CO_2. Water Resources Research, 36:89-99.

Barsi, J.A., Schott, J.R., Palluconi, F.D., Helder, D.L., Hook, S.J., Markham, B.L., Chander, G. and O'Donnell, E.M. (2003). Landsat TM and ETM+ thermal band calibration. Can. J. Remote Sens., 29:141–153.

Basistha, A., Arya, D.S. and Goel N.K. (2009). Analysis of historical changes in rainfall in the Indian Himalayas. Int. J. Climatol., 29:555-572.

Becker, F. (1987). The impact of spectral emissivity on the measurement of land surface temperature from a satellite. International Journal of Remote Sensing, 8:1509-1522.

Becker, F. and Li, Z.L. (1990). Towards a local split window method over land surfaces. International Journal of Remote Sensing, 11(3):369-393.

Beniston, M., Diaz, F.D. and Bradley, R.S. (1997). Climate change at high elevation sites: an overview. Climate change, 36:233-251.

Beniston, M. (2003). Climate Change in mountainous region: a review of possible impacts. Climate Change, 59:5-31.

Berg, N., Osterhuber, R. and Bergman, J. (1991). Rain-induced outflow from deep snowpacks in the central Sierra Nevada, California. Hydrologic Sciences Journal, Vol. 36:611-629.

Bergeron, J., Royer, A., Turcotte, R. and Roy, A. (2013). Snow covers estimation using blended MODIS and AMSR-E data for improved watershed-scale spring streamflow simulation in Quebec. Canada. Hydrol. Process. Published online in Wiley Online libraryDOI:10.1002/hyp.10123.

Bergstrom, S. (1992). The HBV Model-Its Structure and Applications, SMHI, RH 4, Norrkoping.

Bergstrom, S., Carlsson, B., Gardelin, M., Lindstrom, G., Pettersson, A. and Rummukainen, M. (2001). Climate change impacts on runoff in Sweden-assessments by global climate models, dynamical downscaling and hydrological modeling. Climate Res. 16 (2):101-112.

Bernstein, L. and Bosch, P. (2007). Climate Change 2007: Synthesis Report, assessed on 1/4/2014.http://www.unep.org/geo/geo_ice/PDF/GEO_C2_LowRes.pdf assessed on 1/4/2014

Bharati, L., Gurung, P., Jayakody, P., Smakhtin, V. and Bhattarai, U. (2014). The projected impact of climate change on water availability and development in the Koshi basin, Nepal. Mountain Research and Development, 34 (2):118-130.

Bhutiyani, M.R., Kala, V.S. and Power, N.J. (2007). Long-term trends in maximum, minimum and mean annual air temperatures across the northwest Himalaya during the twentieth century. Climatic Change, 85(1-2):159-177.

Blackie, J.R. and Eles, C.W.O. (1985). Lumped catchment models, Chapter 11, In: Hydrological Forecasting, Edited by M.G. Anderson and T. P. Burt, John Wiley & sons.

Blandford, T., Humes, K., Harshburger, B., Moore, B., Walden, V. and Ye, H. (2008). Seasonal and synoptic variations in near surface air temperature lapse rates in a mountainous basin, J. Appl. Meteorol. Climatol., 47(1):249–261, doi:10.1175/ 2007JAMC1565.1.

Boe, J., Terray, L., Habets, F. and Martin, E. (2007). Statistical and dynamical downscaling of the Seine basin climate for hydro-meteorological studies. Int. J. Climatol., 27 (12):1643-1655.

Bohui, T., Yuyun, Bi., Zhao-Liang, Li and Xia, Jun. (2008). Generalized split-window algorithm for estimate of Land surface temperature from Chinese geostationary FengYun Meteorological Satellite (FY-2C) Data, sensors, 8:933-951.

Bolstad, P.V., Swift, L., Collins, F. and Regniere, J. (1998). Measured and predicted air temperatures at basin to regional scales in the southern Appalachian Mountains, Agric. For. Meteorol., 91(3–4):161–176.

Brown, T.B., Berry, R.G. and Doesken, N.J. (1992). An exploratory study of temperature trends for Colorado paired mountain–high plains stations. American Meteorology Society sixth conference on mountain meteorology, Portland, OR, pp 181-184.

Brunengo, M.J. (1990). A method of modeling the frequency characteristics of daily snow amount for stochastic simulation of rain-on-snowmelt events. Proceeding of Western Snow Conference, 58:110-121.

Buishand, T., Shabalova, M. and Brandsma, T. (2004). On the choice of the temporal aggregation level for statistical downscaling of precipitation. J Clim., 17:1816–1827.

Bunting, J.T. and d'Entremont, R.P. (1982). Improved cloud detection utilizing Defense Meteorological Satellite Program near infrared measurement, Air Force Geophysics Laboratory. Environmental Research Papers, No. 765, AFGL-TR-82-0027, 27 January 1982, 91.

Burn, D.H., Cunderlick, J.M. and Pietroniero, A. (2004). Hydrological trends and variability in the Liard river basins. Hydrol. Sci.J. 49(1):53-67.

Bussieres, N., Louie, P.Y.T. and Hogg, W. (1990). Progress report on the implementation of an algorithm to estimate regional evaportanspiration using satellite data. Proceeding of the workshop on applications of remote sensing in hydrology, Saskaton Saskatchewan, 13-14 February 1990.

Butt, M.J. (2006). Passive microwave methods to retrieve snow pack characteristics in UK. Scottish Geographical Journal, Vol. 122(1):19-31.

Butt, M.J. and Kelly, R.E.J. (2008). Estimation of snow depth in the UK using the HUT snow emission model. International Journal of Remote Sensing, 29(14):4249-4267.

Carsey, F., Dozier, J. and Marks, D. (1987). Snow mapping and classification from Landsat Thematic Mapper ™ data. Annals of Glaciology, 9:97-103.

Carsey, F. (1992). Remote sensing of ice and snow, review and status. Intl. J. remote Sens., 13(1):5-11.

Carter, T.R., Parry, M.L., Harasawa, H. and Nishioka, S. (1994). IPCC technical guidelines for assessing climate change impacts and adaptations, IPCC Special Report to Working Group II of IPCC, London.

Caselles, V., Coll, C. and Valor, E. (1997). Land surface temperature determination in the whole Hapex Sahell area from AVHRR data. Int. J. Remote Sens., 18 (5):1009-1027.

Cayan, D.R., Riddle, L.G. and Aguado, E. (1993). The influence of temperature and precipitation on seasonal streamflow in California. Water Resources Research, 29:1127-1140.

Chaku, S.K. (1972). Geology of Chauri Tehsil and adjacent area, Chamba Dist., H.P. Himalayan Geo., 2:404-414.

Chang, A.T.C., Foster, L. and Hall, D.K. (1987). Nimbus-7 SMMR derived global snow cover parameters. Annals of Glaciology, 9:39-44.

Chang, Yu-Xu. (1999). Climate change and hydrologic models: A review of existing gaps and recent research developments. Water Resource Management, 13:369-382.

Chattopadhyay, S., Jhajharia, D. and Chatopadhyay, G. (2011). Univariate modeling of monthly maximum temperature time series over North East India: neural network versus Yule-walker equation based approach. Meteorological Applications, 18:70-82, doi:10.1002/met.2011.

Chen, H., Guo, S.L., Xu, C.Y. and Singh, V.P. (2007). Historical temporal trends of hydro Climatic variables and runoff response to climate to climate variability and their relevance in water resource management in the Hanjiang basin. J. Hydrol., 344:171-184.

Chiew, F.H.S. and McMohan, T.A. (2002). Modelling the impacts of climate change on Australian streamflow. Hydrological Processes, 16 (6):1235-1245.

Choudhury, B.U., Das, A., Ngachan, S.V., Slong, A., Bordoloi, L.J. and Chouwdhury, P. (2012). Trend analysis of long term weather variables in Mid altitude Meghalaya, North-East India. Journal of Agricultural Physics, ISSN 0973-032X, 12 (1):12-22.

Colbeck, S.C. (1975). A theory of water flow through a layered snowpack. Water Resources Research, 11:261-266.

Coll, C., Casselles, V., Sobrino, J.A. and Valor, E. (1994). On the atmospheric dependence of the split-window equation for land surface temperature. International Journal of Remote Sensing, 15:105-122.

Coll, C. and Casselles, V. (1997). A split window algorithm for land surface temperature from advanced very high resolution radiometer data: validation and algorithm comparison. Journal of Geophysical Research, 102:16697-16713.

Conway, H., Breyfogle, S. and Wilbour, C.R. (1988). Observations relating to wet snow stability. International Snow Science Workshop, ISSW'88 Comm. Whitler, B.C., Canada.

Conway, H. and Raymond, C.F. (1993). Snow stability during rain. Journal of Glaciology, 39:635-642.

Dash, P., Gottsche, F.M., Olesen, F.S. and Fischer, H. (2002). Land surface temperature and Emissivity estimation from passive sensor data: Theory and Practice-Current Trends. International Journal of Remote Sensing, 23 (13):2563-2594.

Dash, S.K., Jenamani, R.K., Kalsi, S.R. and Panda, S.K. (2007). Some evidence of Climate change in twentieth-century India. Climatic Change, 85(3-4), 299-321.

David, G.V., Gareth, J.M., Connolley, W.M., Parkinson, C., Mulavaney, R., Hodgson, D.A., King, J.C., Pudsey, C.J. and Turner, J. (2003). Recent rapid regional climatic warming on the Antarctic Peninsula. Climate Change 60:243–274.

Debele, B., Srinivasan, R. and Gosain, A.K. (2009). Comparison of process-based and temperature-index snowmelt modeling in SWAT. Water Resour. Manage, 24:1065-1088, doi: 10.1007/s11269-009-9486-2.

De Scally, F.A. (1997). Deriving lapse rate of slope air temperature for meltwater runoff modeling in subtropical mountains, An example from Punjab Himalaya, Pakistan, Mountain Research and Development, 17 (4):353-362.

Deshmukh, A.G., Rao, E.P. and Eldho, T.I. (2004). Surface Runoff Estimation using remote sensing, GIS and SCS Method. Intern. Conf. on Advanced Modeling Techniques for Sustainable Management of Water Resources, NIT Warangal, January.

Dey, B. and Goswami, D.C. (1983). Application of Remote Sensing for seasonal runoff prediction in the Indus basin, Pakistan. Hydrological Applications of Remote Sensing and Remote Data Transmission (Proceedings of the Hamburg Symposium, August 1983), IAHS Publication No. 145:637-645.

Dey, B., Sharma, V.K., Goswami, D.C. and SubbaRao, P. (1988). Snow cover, snowmelt and runoff in the Himalayan river basins: final technical report. National Aeronautics and Space Administration, NASA-CR-182434, 37.

Diak, G.R. and Whipple, M.S. (1993). Improvements to models and methods for evaluating the land-surface energy balance and effective roughness using radiosonde reports and satellite-measured skin temperature data. Agriculture and Forestry Meteorology, 63:189-218..

Diaz, H.F. and Bradley, R.S. (1997). Temperature Variation during the last century at high elevation sites. Clim Change, 36:253-279.

Diaz, H.F., Grosjean, M. and Graumlich, L. (2003). Climate variability and change in high elevation regions: past, present and future. Climate Change 59:1-4.

Dimri, A.P. and Ganju, A. (2007). Wintertime Seasonal scale simulation over western Himalaya using RegCM3. Pure Appl. Geophys., 164(8-9):1733-1746.

Dinpashoh, Y., Jhajharia, D., Fakheri-Fard, A., Singh, V.P. and Kahya, E. (2011). Trends in reference evapotranspiration over Iran. J. Hydrol, 399:422-433, doi:10.1016/ j.jhydrol. 2011.01.021.

Douglas, E.M., Vogel, R.M. and Knoll, C.N. (2000). Trends in flood and low flows in the United States: impact of spatial correlation. J. Hydrol, 240:90-105.

Dousset, B. and Gourmelon, F. (2003). Satellite multi-sensor data analysis of urban surface temperature and landcover. ISPRS Journal of Photogrammetry and Remote Sensing. 58, (1-2):43-54.

Dozier, J. and Marks, D. (1987). Snow mapping and classification from Landsat Thematic mapper. Remote Sensing of Environment, 28:9-22.

Dozier, J. (1989). Spectral signatures of alpine snow cover from the landsat thematic mapper. Remote Sens Environ, 28:9–22.

Dozier, J. (1998). Remote sensing of the alpine snow cover: a review of techniques and accomplishments from the visible wavelengths through the microwave. In proceedings of International Conference of Snow Hydrology the Integration of Physical, Chemical, and Biological Systems, 6-9 October, Brownsville, Vermont, USA, U.S. Army Cold Regions Research and Engineering Laboratory Hanover, New Hampshire 03755-1290, Special Report 98-10.

Eldho, T.I., Jha, A. and Singh, A.K. (2006). Integrated Watershed Modelling using A Finite Element Method and a GIS Approach. International Journal of River Basin Management, IAHR, 4 (1):1-9.

Eldho, T.I. (2009). Integrated Watershed Modeling and Characterization Using FEM, GIS and Remote Sensing techniques". ISH Journal of Hydraulics Engineering, 15:227-243.

Euromap (2007). IRS-1C, IRS-1D, IRS-P6, Available online at http://www.euromap.de/ docs/ doc_005.html (accessed on August 12, 2014).

Evans, J. and Schreider, S. (2002). Hydrological impacts of climate change on inflows to Perth, Australia. Climatic Change, 55 (3):361-393.

Ferguson, R.I. (1999). Snowmelt runoff models. Progress in physical Geography 23: 205-227.

Finsterwalder, S. and Schunk, H. (1887). Der Suldenferner (in German). Z. Deutsch. u. Osterr. Alpenverein, 18:72–89.

Folland, C.K. and Parker, D.E. (1990). Observed variation of sea surface temperature. In: Schlesinger ME (ed) Climate-ocean interaction. Kluwer, Dordrecht, pp 21-52.

Foster, J.L., Hall, D.K. and Chang, A.T.C. (1987). Remote sensing of snow. Eos 68(32):681-4.

Fowler, H.J., Blenkinsop, S. and Tebaldi, C. (2007). Linking climate change modelling to impact studies: recent advances in downscaling techniques for hydrological modelling. Int. J. Climatol. 27 (12):1547-1578.

Frank, W., Hoinkes, G., Purtshcellar, C.M., Ritcher, W. and Thoni, M. (1973). Relation between metamorphism and orogeny in a typical section of the Indian Himalayas. Tschermak's Mineral. Petrogr. Mitt., 20:303-312.

Franz, K.J., Hogue, T.S. and Sorrooshian, S. (2008). Operational snow modeling: addressing the challenges of an energy balance model for national weather service forecast. J. Hydrol. 360 (1-4):48-66.

Frei, A. and Robinson, D. A. (1998). Evaluation of snow extent and its variability in atmospheric model intercomparison project. Journal of Geophysical Research, 103:8859–8871.

Frei, A. and Robinson, D.A. (1999). Northern Hemisphere Snow Extent: Regional Variability 1972 to 1994. International Journal of Climatology 19:1535-1560.

Friedl, M.A. (2002). Forward and inverse modeling of land surface energy balance using surface temperature measurements. Remote Sensing of Environment, 79:344-354.

Fu, G., Chen, S., Liu, C. and Shepard, D. (2004). Hydro-climatic trends of the Yellow river basin for the last 50 years. Climate change 65, 149-178.

Fuchs, G. and Gupta, V.J. (1971). Palaeozoic stratigraphy of Kashmir, Kishtwar and Chamba (Punjab Himalayas). Verh. Geol. Bundesanst. Vienna, 1:68-97.

Gain, A.K., Immerzeel, W.W., Sperna-Weiland, F.C. and Bierkens, M.F.P. (2011). Impact of climate change on the stream flow of the lower Brahmaputra: trends in high and low flows based on discharge-weighted ensemble modeling. Hydrol. Earth Syst. Sci., 15:1537–1545, doi:10.5194/hess-15-1537-2011.

Gangodagamage, C. and Aggarwal, S.P. (2012). Integrating satellite based remote sensing observations with SCS curve number method for simplified hydrologic modeling in ungauged basins. Asian journal of Geoinformatics, 12 (3):29-39.

Garg, V., Aggarwal, S.P., Nikam, B.R. and Thakur, P.K. (2013). Hypothetical Scenario Based Impact Assessment of Climate Change on Runoff Potential of a Basin. ISH Journal of hydraulic engineering. 19(3):244-249.

Garstka, W.U. (1964). Snow and Snow surveys. In Handbook of Applied Hydrology (V. T. Chow Ed.), McGraw-Hill Book Company, New York, 10-34.

Ghosh, S. and Mujumdar, P.P. (2008). Statistical downscaling of GCM simulations to streamflow using relevance vector machine. Adv Water Resour, 31:132–146.

Gleick, P.H. (1986). Methods for evaluating regional hydrologic impacts of global climate change. Journal of Hydrology, 88:97-116.

Gleick, P.H. (1987). Regional hydrologic consequences of increase in atmospheric CO2 and other trace gases. Climatic Change, 10:137-161.

Goswami, A. (2007). Spatial techniques in snowcover and snowmelt runoff studies in western Himalaya. PhD Thesis unpublished, University of Roorkee.

Gottfried, M., Pauli, H., Reiter, K. and Grabherr, G. (1999). A fine-scaled predictive model for changes in species distribution patterns of high mountain plants induced by climate warming. Divers, Distr., 5:241-251.

Gunreisussen, T., Johnsen, H. and Lauknes, I. (2001). Snow covers mapping capabilities using RADARSAT standard mode data. Can J Remote Sens 27:109–117.

Guo, S.L., Wang, J.X., Xiong, L.H., Ying, A.W. and Li, D.F. (2002). A macro-scale and semi-distributed monthly water balance model to predict climate change impacts in China. J. Hydrol., 268 (1-4):1-15.

Gupta, R.D., Srivastava, R.K. and Prakash, D.V.S.S. (2002). Remote Sensing Based Resource Mapping using Digital Satellite Data, Indian Geotechnical Conference on Geotechnical Engineering: Environmental Challenges, 20-22 December, Allahabad, India.

Gupta, R.D., Singh, M.K., Snehmani. and Ganju, A. (2014). Validation of SRTM X band DEM over Himalayan mountain. The International Archives of the Phogrammetry, Remote Sensing and Spatial Information Sciences, XL-4, ISPRS Technical Commission IV Symposium, 14-16 May 2014, Suzhou, China.

Gupta, R.P., Duggal, A.J., Rao,, S.N., Sankar, G. and Singhal, B.B.S. (1982). Snow covers area vs snowmelt runoff relations and its dependence on geomorphology-a study from Beas catchment (Himalayas India). Journal of Hydrology, 58:325-339.

Gupta, R.P., Haritashya, U.K. and Singh, P. (2005). Mapping dry/wet snow cover in the Indian Himalayas using IRS multispectral images, Remote Sensing of Environment, 97:458-469.

Gurung, D.R, Kulkarni, A.V., Griraj, A, Aung, K.S., Shrestha, B. and Srinivasan, J. (2011). Changes in seasonal snow cover in Hindu Kush-Himalayan region. The Cryosphere Discuss., 5:755-777, doi: 10.5194/tcd-5-755-2011.

Gusso, A. and Fontana, D.C. (2005). Vertical variation survey of the nocturnal air temperature using NOAA/AVHRR satellite data. Anais XII Simpósio Brasileiro de Sensoriamento Remoto, Goiânia, Brasil, 16-21 April 2005, INPE, pp. 173-179, available online at http://marte.dpi.inpe.br/col/ltid.inpe.br/sbsr/2004/11.22.17.56/ doc/173.pdf, (accessed on December 10, 2007).

Hall, D.K. and Martinec, J. (1985). Remote sensing of Ice and Snow, Chapman and Hall, Newyork.

Hall, D.K., Riggs, G.A. and Salomonson, V.V. (1995). Development of methods for mapping global snow cover using moderate resolution imaging spectrometer (MODIS) data. Remote Sens Environ, 4:127–140.

Hall, D.K., Riggs, G.A., Salomonson, V.V., Barton, J.S., Casey, K., Chien, J.Y.L., DiGirolamo, N.E., Klein, A.G., Powell, H.W. and Tait, A.B. (2001). Algorithm theoretical basis document (ATBD) for the MODIS snow and sea ice-mapping algorithms. Available

online at http://www.modis-snow-ice.gsfc.nasa.gov/atbd01.html (accessed on February 18, 2014).

Hall, D.K., Rigges, G.A. Salomonson, V.V. DiGirolamo, N.E. and Bayr, K.A. (2002a). MODIS sonw-cover products. Remote Sensing of Environment, 83:181-194.

Hall, D.K., Kelly, R.J.E., Riggs, G.A., Chang A.T.C. and Foster, J.L. (2002b). Assessment of the relative accuracy of hemispheric-scale snow –cover maps. Annals of Glaciology, 34:24-30.

Hall, D.K., Riggs, G.A. and Salomonson, V.V. (2006). updated weekly. MODIS/Terra snow cover 8-day L3 global 500m grid V005, [January 01, 2001 to December 31, 2005 list the dates of the data used]. Boulder, Colorado USA: National Snow and Ice Data Center. Digital media.

Hall, D.K. and Riggs, G.A. (2007). Accuracy assessment of the MODIS snow-cover products, Hydrological Processes, 21:1534-1547.

Hall, D.K., Riggs, G.A. and Salomonson, V.V. (2007). Updated daily MODIS/Aqua Snow Cover Daily L3 Global 500 m Grid.

Hallikainen, M.T. (1984). Retrieval of snow water equivalent from Nimbus-7 SSMR data: effect of land cover categories and weather conditions. IEEE Oceanic Engineering. 9(5):372-376.

Hallikainen, M.T., Sokol, J., Pultz, T.J. and Walker, A.E. (2003a). Passive and active microwave remote sensing of snow cover. International Journal of Remote Sensing, 24(24):5327-5344.

Hallikainen, M.T., Halme, P., Takala, M. and Pulliainen, J. (2003b). Combined active and passive microwave remote sensing of snow in Finland. In Proceedings of IEEE. Geoscience and Remote Sensing Symposium, IGARSS ‘03’, 21-25 July 2003, Toulouse, France, IEEE International, 2:830-832.

Hallikainen, M.T., Lahtinen, P., Yuanzhi, Z., Takala, M. and Pulliainen, J. (2004). Feasibility of satellite Ku-band scattermeter data for retrieval of seasonal snow characteristics in Finland. In Proceedings of IEEE Geoscience and Remote Sensing Symposium, IGARSS ‘04’, 20-24 September 2004, Anchorage, AK, USA, IEEE International, 3:1936-1939.

Hamed, K.H. and Rao, A.R. (1998). A modified Mann-Kendall trend test for auto correlated data. Journal of Hydrology, 204:182 196.

Haritashya, U.K. (2005). Glacio-hydrological studies of the Gangotri Glacier basin. Himalayas. PhD thesis, IIT Roorkee, India.

Helsel, D.R. and Hirsch, R.M. (1992). Statistical Methods in Water Resources, Elsevier, Amsterdam, 522.

Hewitt, K. (2005). The Karakoram anomaly Glacier expansion and the 'elevation effect,' Karakoram Himalaya. Mountain Resource Development 25(4):332-340. DOI: 10.1659/0276-4747(2005)025[0332: TKAGEA] 2.0.CO; 2.

Heywood, L. (1988). Rain on snow avalanche events-some observations, Proceeding of International Snow Science Workshop, ISSW'88 Comm. Whistler, B.C. Canada.

Hirabayashi, Y., Doll, P. and Kanae, S. (2010). Global-scale modeling of glacier mass balances for water resources assessments: Glacier mass changes between 1948 and 2006. Journal of Hydrology, 390:245-256.

Hirsch, R.M., Slack, J.R. and Slack, R.A. (1982). Techniques of trend analysis for monthly water quality data. Water Resour. Res. 18(1): 107-121.

Hirsch, R.M., Helsel, D.R., Cohn, T.A. and Gilroy, E.J. (1993). Statistical treatment of Hydrologic data. In: Handbook of Hydrology (ed. By D. R. Maidment), 17.1-17.52. McGraw-Hill, York, USA.

Hock, R. (2003). Temperature index melt modeling in mountain areas. J. Hydrol., 282: 104-115.

Hostetler, S.W. and Giorgi, F. (1993). Use of output from high-resolution atmospheric models in landscape scale hydrologic models: an assessment. Water Resources Research, 29:1685-1695.

Houghton, J.T., Meira Filho, L.G., Callander, B.A., Harris, N., Kattenberg, A. and Maskell. (eds): (1995). Climate change (1995) the science of climate change: Contribution of working group I to the second assessment report of the Intergovernmental panel on climate change, Cambridge University press., 572.

Huber, U.M., Bugmann, H.K.M. and Reasoner, A.M. (2005). Global change and mountain regions: An overview of current knowledge, Advances in Global Change Research series 23:650 ISBN 978-1-4020-3508-1.

ICIMOD (2001). Inventory of Glaciers, glacial Lakes and Glacial Lake outburst Floods, monitoring and early warning system in the Hindu Kush-Himalayan region, Nepal, (UNEP/RCAP)/ ICIMOD, Kathmandu.

Immerzeel, W.W., Beek, L.P.H., Konz, M., Shrestha, A.B. and Bierkens, M.F.P. (2011). Hydrological response to climate change in a glacerized catchment in the Himalayas. Climatic Change, 110:721-736.

Immerzeel, W.W., Droogers, P., de Jong, S.M. and Bierkens, M.F.P. (2009). Monitoring of snow cover and runoff simulation in Himalayan river basins using remote sensing. Remote Sensing of Environment, 113:40-49.

IPCC (2001). Climate change. The IPCC third assessment report, Cambridge University Press, Cambridge and New York. Vol. I (The Scientific basis), II (impact adaption and vulnerability) and III (Mitigation)

IPCC (Intergovernmental Panel on Climate Change) (2001). In: Houghton JT et al. (eds) The third assessment report of working group I of the intergovernmental panel on climate change (IPCC). Cambridge Univ. Press, New York, 881.

IPCC (2007). Climate Change. The physical science basis, contribution of working group 1 to the fourth assessment report of the intergovernmental panel on climate change. In: Solomon S, Qin D, Manning M, Chen Z, Marquis MC, Averyt K, Tignor M, Miller HL (eds) Intergovernmental panel on climate change, Cambridge and New York.

Jacob, F., Petitcolin, F., Schmugge, T., Vermote, E., French, A. and Ogawa, K. (2004). Comparison of land surface emissivity and radiometric temperature derived from MODIS and ASTER sensors. Rem. Sens. Environ., 90:137–152.

Jain, S.K. (2001). Snowmelt runoff modeling and sedimentation studies in Satluj basin using remote sensing and GIS. PhD Thesis unpublished, University of Roorkee.

Jain, S.K., Goswami, A. and Saraf, A.K. (2008a). Accuracy assessment of MODIS, NOAA and IRS data in snow cover mapping under Himalayan condition. Int J Remote Sens 29(20):5863–5878.

Jain S.K., Goswami, A. and Saraf, A. K. (2008b). Determination of land surface temperature and its lapse rate in the Satluj River basin using NOAA data. International Journal of Remote Sensing, 29:11:3091-3103, DOI: 10.1080/01431160701468992

Jain, S.K. Goswami, A. and Saraf, A.K. (2010a). Snowmelt run-off modeling in a Himalayan basin with the aid of satellite data. Int. J. Remote Sensing, 31(24):6603-6618.

Jain S.K., Goswami, A. and Saraf, A.K. (2010b). Assessment of snowmelt runoff using remote sensing and effect of climate change on runoff. Water Resources Management Journal, 24(9):1763-1777.

Jain, S.K. and Kumar, V. (2012). Trend analysis of rainfall and temperature data for India. Current Science, 102(1):37-49.

Jain S.K., Lohani, A.K. and Singh, R.D. (2012a). Snowmelt runoff modelling in a basin located in Bhutan Himalaya. India Water Week, Water Energy and Food Security: Call for solutions, April 10-14, New Delhi.

Jain, S.K., Kumar, V. and Saharia, M. (2012b). Analysis of rainfall and temperature trends in northeast India. Int. J. Climatol., Published online in Wiley online library, DOI: 10.1002/ joc.3483.

Jansson, P., Hock, R. and Schneider, T. (2003). The concept of glacier storage-a review. Journal of Hydrology, 282:116-129.

Jeyram, A., Tiwari, R.S. and Sharma, K.P. (1983). Snowmelt runoff using Landsat imageries. In Proceedings of the First National Symposium on Snowcover, 28–30 April, SASE, Manali, (Manali: Snow & Avalanche Study Establishment), II:11–21.

Jhajharia, D., Shrivastava, S.K. and Sarkar, S. (2009). Temporal characteristics of pan evaporation trend under the humid conditions of Northeast India. Agric. Forest Meteorol., 149:763-770.

Jhajharia, D. and Singh, V.P. (2011). Trends in temperature, diurnal temperature range and sunshine duration in Northern India. International Journal of Climatology, 31(9):1353-1367,doi:10.1002/joc.2164/

Jhajharia, D., Dinpashoh, Y., Kahya, E., Singh, V.P. and Fakheri-Farid, A. (2011). Trends in reference evapotranspiration in the humid region of North-east India. Hydrol. Process, 26(3):421-435, doi:10,1002/hyp.8140 (In Press).

Jones, P.D., Raper, S.C.B., Bredley, R.S., Diaz, H.F., Kelly, P.M. and Wiglay, T.M.C. (1986). Northern hemispheric surface air variation: 1851-1984. J Clim Appl Meteorol., 25:161-179.

Justice, C.O., Townshed, J.R.G., Vermote, E.F., Masuoka, E, Wolfe, R.E., Saleous, N., Roy, D.P. and Morisette, J.T. (2002). An overview of MODIS Land data processing and product status. Remote Sensing of Environment, 83:3-15.

Kaab, A., Paul, F., Maisch, M., Hoelzle, M. and Haeberli, W. (2002). The new remote sensing –derived Swiss glacier inventory: II, first results. Annals of Glaciology, 34: 362-366.

Kamga, F.M. (2001). Impact of greenhouse gas induced climate change on the runoff of the Upper Benue river (Cameroon). Journal of Hydrology, 252:145-156.

Kargel, J., Abrams, M., Bishop, M., Bush, A., Hamilton, G., Jiskoot, H., Kaab, A., Kieffer, H., Lee, E.M., Paul, F., Rau, F., Raup, B., Shroder, J.F., Soltesz, D., Stainforth, D., Sterns, L. and Wessels, R. (2005). Multispectral imaging contributions to global land ice measurements from space. Remote Sensing of Environments, 99 (1-20):187-219.

Kattel, D.B., Yao, T., Yang, K., Tian, L. and Yang, G. (2013). Temperature lapse rate in complex mountain terrain on the southern slope of the central Himalayas, Theor. Appl. Climatol. 113:671-682.

Kattel, D.B. and Yao, T. (2013). Recent temperature trends at mountain stations on the southern slope of the central Himalayas. Journal of Earth System Science, 122:215-227.

Kattelmann, R. (1987). Uncertainty in Assessing Himalayan Water Resources. Mountain Research and Development, 7(3):279-286.

Kattleman, R. (1997). Rapid changes in snow cover at lower elevations in Sierra Neveda, California. USA Ann Glaciol, 25:367–370.

Kaul, M.K. (1999). Inventory of Himalayan glaciers, Sp. Pub. No.34, Geological Survey of India.

Kaur, R., Saikumar, D., Kulkarni, A.V. and Chaudhary, B.S. (2009). Variations in snow cover and snowline altitude in Baspa basin. Current Science, 96(9):1255-1258.

Kavvas, M.L., Chen, Z.Q., Ohara, N., A.J. and Amin, M.Z.M. (2006). Impact of Climate Change on the Hydrology and Water resources of Peninsular Malaysia. International Congress on River Basin Management, 529-537.

Kawashima, S., Ishida, T., Minomura, M., Miwa, T. (2000). Relations between Surface Temperature and Air Temperature on a Local Scale during Winter Nights, Journal of Applied Meteorology, Vol. 39, pp. 1570-1579.

Kaya, I. (1999). Application of snowmelt runoff model using remote sensing and GIS, Msc. Thesis. Civil Engineering Department, Middle East Technical University, Ankara, Turkey.

Keshri, A.K., Shukla, A. and Gupta, R.P. (2009). ASTER ratio indices for supraglacial terrain mapping. International Journal of Remote Sensing, 30 (2):519-524.

Khattak, M.S., Babel, M.S. and Sharif, M. (2011). Hydro-meteorological trends in the upper Indus River basin in Pakistan. Climate research, 46:103-119. doi:10.3354/cr00957.

Kiem, A.S., Ishidaria, Hapuarachchi, H.P., Zhour, M.C., Hirabayashi, Y. and Takeuchi K. (2008). Future hydroclimatology of the Mekong River basin simulated using the high-resolution Japan Meteorological Agency (JMA) AGCM. Hydrological Processes 22: 1382.DOI: 10.1002/hyp.6947.

Kim, A.S, Tachikawa, Y., Nakakita, E. and Kaorn, T. (2010). Hydrologic Evaluation on the AGCM20 Output Using Observed River Discharge Data. Hydrological Research Letters 4:35-39. DOI: 10.3178/HRL.4.35.

Kite, G.W., Dalton, A. and Dion, K. (1994). Simulation of streamflow in a macroscale watershed using GCM model data. Water Resources Research, 30:1547-1559.

Kitoh, A. and Kusunoki, S. (2008). East Asian summer monsoon simulation by a 20-km mesh AGCM. Climate Dynamics 31: 389 -401. DOI: 10.1007/s00382-007-0285-2.

Klien, A.G., Hall, D.K. and Riggs, G.A. (1998). Improving snow cover mapping in forests through the use of a canopy reflectance model, Hydrological Processes, 12: 1723-1744.

Klein, A.G. and Barnett, A.G. (2003). Validation of daily MODIS snow cover maps of the Upper Rio Grande River Basin for the 2000–2001 snow year, Remote Sensing of Environment, 86:162–176.

Klein Tank, A.M.G., Peterson, T.C., Quadir, D.A., Dorji, S. and Zou, X et al., (2006). Changes in daily temperature and precipitation extremes in central and south Asia. Journal of Geophysical Research, 111:D16105.

Koing, M., Winther, J.G. and Isaksson, E. (2001). Measuring snow and glacier ice properties from satellite. Reviews of Geophysics. 39 (1):1-27.

K¨orner, Ch. (1992). Response of alpine vegetation to global climate change. Catena Suppl., 22:85-68.

K¨orner, Ch. (1999). Alpine plant Life: Functional plant ecology of high mountain ecosystems, Springer, Berlin Heidelberg, p. 343.

Kothyari, U.C. and Singh, V.P. (1996). Rainfall and Temperature Trends in India. Hydrological Processes, 10 (3):357-372.

Krenke, A.K. and Khodakov, V.G. (1966). O svyazi poverkhnostnogo tayaniya lednikov s temperaturoy vozdukha [The relationship between surface ice melting and air temperature]. Mater. Glyatsiol. Issled .12, 153-164. [In Russian with English summary].

Krishna, A.P. (1996). Satellite remote sensing applications for snow cover characterization in the morphogenetic regions of upper Tista River basin, Sikkim Himalaya. International Journal of Remote Sensing, 17(4): 651–656.

Krishna, A.P. (1999). Snow cover and glacier assessments in parts of the Sikkim Himalaya by remote sensing and GIS. In Proceedings of NSSW'99 National Snow Science Workshop, Snow and Avalanche Study Establishment (SASE), Manali, DRDO, Govt. of India, 33–40.

Krishna, A.P. (2005). Snow and glacier cover assessment in the high mountains of Sikkim Himalaya. Hydrological Processes, 19:2375–2383,doi:10.1002/hyp.5890.

Krishna, A.P. and Sharma, A. (2013). Snow cover and land surface temperature assessment of Gangotri basin in the Indian Himalayan Region (IHR) using MODIS satellite data for climate change inferences. Proc SPIE 10/2013; DOI: 10.1117/12.2029084

Krishna, A.P. (2014) Characteristics of snow and glacier fed rivers in mountainous regions with special reference to Himalayan basins. In book: Encyclopedia of Snow, Ice and Glaciers, Edition: 1st, Chapter: Encyclopedia of Earth Science Series, Publisher: Springer, The Netherlands, Editors: V.P. Singh, P. Singh, U.K. Haritashya, 128-133.

Kuhl, S.C. and Miller, J.R. (1992). Seasonal river runoff calculated from a global atmospheric model. Water resources Research. 28:2029-2039.

Kulkarni, A.V. (1991). Glacier inventory in Himachal Pradesh using satellite data. Journal of Indian Society of Remote Sensing, 19(3):195-203.

Kulkarni, A.V. and Bahuguna, I.M. (2001). Role of satellite images in snow and glacial investigations. Proceedings of the symposium on snow, ice and glaciers-a Himalayan perspective. GSI special publication, 53:233-240.

Kulkarni, A.V. Singh, S.K., Mathur, P. and Mishra, V.D. (2006). Algorithm to monitor snow cover using AWiFS data of Resourcesat-1 for the Himalayan region. International Journal of Remote Sensing, 27:2449-2457.

Kulkarni, A., Rathore, B.P., Singh, S.K. and Ajai, A. (2010). Distribution of seasonal snow cover in central and western Himalaya. Annals of Glaciology, 51(54):121-128.

Kulkarni, A., Patwardhan, S.K., Kumar, K., Karamuri, A. and Krishnan, R. (2013). Projected Climate Change in the Hindu Kush-Himalayan Region By Using the High-resolution Regional Climate Model PRECIS, Mountain Research and Development, 33(2):142-151,doi: http://dx.doi.org/10.1659/MRD-JOURNAL-D-11-00131.1.

Kumar, V., Singh, P. and Jain, S.K. (2005). Rainfall trend over Himachal Pradesh, Western Himalaya, India Proc. Conf. Development of Hydro Power projects –A Prospective Challenge, Shimla.

Kumar, V., Singh, P. and Singh, V. (2007). Snow and glacier melt contribution in the Beas River at Pandoh Dam, Himachal Pradesh, India. Hydrological Sciences Journal, 52 (2):376-378.

Kumar, V., Jain, S.K. and Singh, Y. (2010). Analysis of long-term rainfall trends in India. Hydrological Sciences Journal, 55 (4):484-496.

Kumar, V. and Jain, S.K. (2010). Trends in seasonal and annual rainfall and rainy days in Kashmir valley in the last century. Quaternary International, 64-69.

Kure, S., Jang, S., Ohara, N., Kavvas, M.L. and Chen, Z.Q. (2013a). Hydrologic impact of regional climate change for the snow-fed and glacier-fed river basins in the Republic of Tajikistan: statistical downscaling of global climate model projections. Hydrol. Process., 27:4071-4090. DOI: 10.1002/hyp.9536.

Kure, S., Jang, S., Ohara, N., Kavvas, M.L. and Chen, Z.Q. (2013b). Hydrologic impact of regional climate change for the snow-fed and glacier-fed river basins in the Republic of Tajikistan: hydrological response of flow to climate change. Hydrol. Process., 27:4057-4070. DOI: 10.1002/hyp.9535.

Kyle, H.L., Curran, R.J., Barnes, W.L. and Escoe, D. (1978). A cloud physics radiometer, Third Conference on Atmosphere Radiation. American Meteorological Society, 28-30 June 1978, Davis, Calif., 107-109.

Lakshmi, V.K., Czajkowski, K.P., Dubayah, R.O. and Susskind, J. (2001). Land surface air temperature mapping using TOVS and AVHRR. International Journal of Remote Sensing, Vol. 22, No. 4, pp. 643-662.

LP DAAC. (2014). Land surface temperature and emissivity 8-day L3 Global 1 km. http://lpdaac.usgs.gov/products/modis_products_table/mod11a2, accessed on 26.9.2014.

Lavalleée, S., Brissette, F.P., Leconte, R. and Larouche, B. (2006). Monitoring snow-cover Depletion by Coupling Satellite Imagery with a distributed Snowmelt Model. Journal of water resources and management 132 (2):71-78. DOI: 10.1061/ (ASCE) 0733-9496.132:2(71).

Leathers, D.J. and Luff, B.L. (1997). Characteristics of snow cover duration across the northeast United States of America. International Journal of Climatology, 17:1535-1547.

Lettenmaier, D.P. and Gan, T.Y. (1990). Hydrological sensitivities of the Sacromento San Joaquin river basin, California to global warming. Water Resources Research, 26: 69-86.

Lettenmaier, D.P., Wood, E.F. and Wallis, J.R. (1994). Hydro-climatological trends in the continental United States, 1948-88. J. Climate, 7:586-607.

Li, B., Zhu, A-X., Zhou, C., Zhang, Y., Pei, T. and Qin, C (2008). Automatic mapping of snow cover depletion curves using optical remote sensing data under conditions of frequent cloud cover and temporary snow. Hydrol Process, 22 (16):2930-2942,30.

Li, H., Beldring, S., Xu, C.Y. and Jain, S.K. (2014). Modelling runoff and its components in Himalayan basins. Hydrology in a changing world: Environmental and Human Dimensions, Proc. FRIEND-Water 2014, Montpellier, France, October 2014 (IAHS Publ. 363, 158-164, 2014).

Li, X. and Williams, M.W. (2008). Snowmelt runoff modeling in an arid mountain watershed. Tarim Basin, China. Hydrological Processes, 22 (19):3931-3940.

Li, Z.L. and Becker, F. (1993). Feasibility of land surface temperature and emissivity determination from AVHRR data. Remote Sensing of Environment, 43:67-85.

Li, Z-L., Tang, B-H., Wu, H., Ren, H., Yan, G., Wan, Z., Trigo, I.F. and Sobrino, J.A. (2013). Satellite-derived land surface temperature: Current status and perspectives. Remote Sensing of Environment, 131:14-37.

Makhmadaliev, B., Kayumov, A., Novikov, V., Mustaeva, N. and Rajabov, I. (2008). The second national communication of the Republic of Tajikistan under the United Nations Framework convention on climate change. Available at: http://unfccc.int/resource/docs/natc/tainc2.pdf

Mannstein, H. (1987). Surface energy budget, surface temperature and thermal inertia, Remote Sensing Applications in Meteorology and Climatology, 201:391-410.

Mao, K., Qin, Z., Shi, J. and Gong, P. (2005). A practical split-window algorithm for retrieving land-surface temperature from MODIS data. Int. J of Remote Sensing, 26(15):3181-3204.

Marshall, S.J., Sharp, M.J., Burgess, D.O. and Anslow, F.S. (2007). Near-surface temperature lapse rates on the Prince of Wales Icefield, Ellesmere Island, Canada: implications for regional downscaling of temperature. Int. J. Climatol., 27:385-398.

Martinec, J., Rango, A. and Roberts, R. (1994). Snowmelt Runoff Model (SRM) User's Manual (Version 3.0). Department of Geography, University of Bern, Switzerland.

Martinec J, Rango A. and Roberts R. (1998). Snowmelt Runoff Model (SRM) User's Manual (ed. By M. F. Baumgartner & G. M. Apfl), University of Berne, Switzerland

Massom, R. (1991). Satellite Remote sensing of Polar Regions: Applications, Limitations and Data Availability. Belhaven Press, London, and Lewis Publishers (CRC), Boca Raton, USA.

Matson, M., Roeplewski, C.F. and Varnadore, M.S. (1986). An atlas of satellite-derived northern hemisphere snow cover frequency. National Weather Service, Washington D.C., 75.

McCabe, G.J. and Ayers, M.A. (1989). Hydrologic effects of climate change in the Deaware river basin. Water Resources Bulletin, 25(6):1231-1241.

McCuen, R.H., Rawls, W.J. and Brakensiek, D.L. (1981). Statistical Analysis of the Brooks-Corey and the Green-Ampt Parameters Across Soil Textures. Water Resources Research, 17(4):1005-1013.

McCuen, R.H. (2003). Hydrologic analysis and design, 3rd edn. Prentice Hall, Englewood Cliffs.

McMillin, L.M. (1975). Estimation of sea surface temperature from two infrared window measurements with different absorption. Journal of Geophysical Research, 80:5113-5117.

Mehrotra, R. (1999). Sensitivity of runoff, soil moisture and reservoir design to climate change in central Indian River basins. Climatic Change, 42 (4):725-757.

Minder, J.R., Mote, P.W. and Lundquist, J.D. (2010). Surface temperature lapse rates over complex terrain: Lessons from the cascade Mountains. Journal of Geophysical Research, 115 (D14122):1-13.

Mirza, M.Q., Warrick, R.A., Ericksen, N.J. and Kenny, G.J. (1998). Trends and persistence in precipitation in the Ganges, Brahamputra and Meghna river basins. Hydrological Sciences Journal, 43 (6):845-858.

Mirza, M.Q., Warrick, R.A. and Ericksen, N.J. (2003). The implications of climatic change on floods of the Ganges, Brahmaputra and Meghana rivers in Bangladesh. Climatic Change, 57(3):287-318.

Mishra, A.K., Ozger, M. and Singh, V.P. (2009). Trend and Persistence of Precipitation under Climate Change Scenarios. Hydrological Processes, 23:2345-2357.

Mishra, M., Babel, M.S. and Tripathi, N.K. (2013) Analysis of climatic variability and snow cover in the Kaligandaki Rivr basin, Himalaya, Neapl. Theor Appl Climatol., 116 (3-4):681-694, DOI 10.1007/s00704-013-0966-1.

Mizuta, R., Oouchi, K., Yoshimura, H., Noda, A., Yukimoto, S., Hosaka, M., Kusunoki, S., Kawai, H. and Nakagawa, M. (2006). 20-km-mesh global climate simulations using JMA-GSM model –mesh climate States. Journal of the Meteorological Society of Japan 84(1): 165-185, DOI: 10.2151/jmsi.84.165.

MODIS (2007). About MODIS, NASA, available online at http://modis.gsfc.nasa.gov/ about/, (accessed on February17, 2014).

Mokhov, I.I. and Akperov, M.G. (2006). Tropospheric lapse rate and its relation to surface temperature from reanalysis data. Atmospheric and Oceanic Physics, 42 (4):430-438.

Muttiah, R.S. and Wurbs, R.A. (2002). Modeling the Impacts of Climate Change on Water Supply Reliabilities. Water International-WATER INT, 27(3):407-419.

Nakicenovic, N. and Swart, R. eds. (2000). Special Report on emissions scenarios: a special report of Working Group III of the Intergovernmental Panel on Climate Change. Cambridge, UK: Cambridge University Press.

Nash, J.E. and Sutcliffe, J.V. (1970). River flow forecasting through conceptual model, Part 1 a discussion of principles, Journal of Hydrology, 10:282-290.

Nash, L. and Gleick, P. (1993). The Colorado River basin and climate change, Rep. EPA 230-R-93-009, United States Environmental Agency, Washington, DC.

Negi, H.S., Kulkarni, A.V. and Semwal, B.S. (2009). Estimation of snow cover distribution in Beas basin, Indian Himalaya using satellite data and ground measurements. J. Earth Syst. Sci., 118 (5):525-538.

Negi, H.S., Thakur, N.K., Kumar, R. and Kumar, M. (2009). Monitoring and evaluation of seasonal snow cover in Kashmir valley using remote sensing, GIS and ancillary data. J. Earth Syst. Sci.118, 6:711–720.

Nemec, J. and Schaake, J. (1982). Sensitivity of water resources to climate variation. Hydrological Sciences Journal, 27:327-343.

Neupane, R.P., Yao, J., Joseph, D. and White. (2013). Estimating the effects of climate change on the intensification of monsoonal-driven stream discharge in a Himalayan watershed. Article first published online: 6 Dec 2013,DOI: 10.1002/hyp.10115.

Ng, H.Y.F. and Marsalek, J. (1992). Sensitivity of streamflow simulation to changes in climatic inputs. Nordic Hydrology, 23:257-272.

Nolin, A.W. and Stroeve, J. (1997). The changing albedo of Greenland ice sheet: implications for climate modeling. Annals of Glaciology, 25:51-57.

Nolin, A.W. and Liang, S. (2000). Progress in bi-directional reflectance modeling and applications for surface particulate media: snow and soils, Remote Sensing Reviews, 18:307-342.

Ohara, N., Kavvas, M.L., Chen, Z.Q., Liang, L., Anderson, M., Wilcox, J. and Mink, L. (2014a). Modelling atmospheric and hydrologic processes for assessment of meadow restoration impact on flow and sediment in a sparsely gauged California watershed. Hydrol. Process., 28:3053–3066. DOI: 10.1002/hyp.9821.

Ohara, N., Jang, S., Kure, S., Chen, Z.Q. and Kavvas, M.L. (2014b). Modeling of interannual snow and ice storage in high-altitude regions by dynamic equilibrium concept. J. Hydrol. Eng., 19:04014034-11.

Otto-Bliesner, B.L., Marsha, S.J., Overpeck, J.T., Miller, G.H. and Hu, A.X. (2006). Simulating Arctic climate warmth and ice field retreat in the last interglaciation, Science, 311(5768):1751–1753, doi:10.1126/science.1120808

Panagoulia, D. (1991). Hydrological response of a medium-sized mountainous catchment to climate changes. Hydrological Sciences Journal, 36 (6):525-547.

Panagoulia, D. (1992). Hydrological modelling of a medium size mountainous catchment from incomplete meteorological data, Journal of Hydrology, 137:279-310.

Panday, P.K., Christopher, A.W., Frey, K.E. and Brown, M.E. (2013). Application and evaluation of a snowmelt runoff model in the Tamor River basin, Eastern Himalayas using Markov Chain Monte Carlo (MCMC) data assimilation approach. Hydrological Processes, DOI:101002/hyp.10005.

Pant, N.C., Kumar, M., Rawat, J.S. and Rani, N. (2014). Study of Snow Cover Dynamics of Pinder Watershed in Central Himalaya using Remote Sensing and GIS Techniques. International Journal of Advanced Earth Science and Engineering, 3 (1):122-128.

Panwar, A. and Singh, D. (2014). Monitoring of seasonal snow cover in Yamuna basin of Uttarakhand Himalaya using Remote Sensing techniques. International Journal of Engineering Sciences and Emerging Technologies, 6 (5):447-453.

Partal, T. and Kahya, E. (2006). Trend analysis in Turkish precipitation data. Hydrol. Processes, 20:2011-2026.

Paul, F., Kaab, A., Maisch, M., Kellenberger, T. and Haeberli W. (2004). Rapid disintegration of Alpine glaciers observed with satellite data. Geophysical Research Letters 31: L21402. DOI: 10.1029/2004GL020816.

Paul, F., Maich, M., Rothenbuhler, C. and Haeberli, W. (2007). Calculation and visualization of future glacier extent in the Swiss Alps by means of hypsographic modeling. Global and Planetary Change 55:343-357. DOI: 10.1016/j.gloplacha. 2006.08.003.

Pinto, J.G., Neuhaus, C.P., Leckebusch, G.C., Reyers, M. and Kerschgens, M. (2010). Estimation of wind storm impacts over Western Germany under future climate conditions using a statistical-dynamical downscaling approach. Tellus Ser. A- Dynam. Meteorol. Oceanogr., 62(2):188-201.

Prasad, V.H. and Roy, P. (2005). Estimation of snowmelt runoff in Beas Basin, India. Geocarto Int. 20(2):41-47.

Prata, A.J. and Platt, C.M.R. (1991). Land surface temperature measurements from the AVHRR, Proceeding of the 5th AVHRR Data Users' Meeting, Tromso, Norway, 433-438.

Pratap, B., Dobhal, D.P., Bhambri, R. and Mehta, M. (2013). Near-surface temperature lapse rate in Dokriani Glacier catchment, Garhwal Himalaya, India. Himalayan Geology, 34 (2):183-186.

Prentice, I.C., Cramer, W., Harrison, S.P., Leemans, R., Monserud, R.A. and Solomon, A.M. (1992). A global biome model based on plant physiology and dominance, soil properties and climate, J. Biogeogr., 19(2):117–134

Price, J.C. (1982). On the use of satellite data to infer surface fluxes at meteorological scales. Journal of Applied Meteorology, 21:1111-1112.

Price, J.C. (1984). Land surface temperature measurements from the split window channels of the NOAA 7 Advanced Very High Resolution Radiometer. J. Geophys. Res., 89:7231-7237.

Price, J.C. (1990). The potential of Remotely Sensed Thermal Infrared data to Infer Surface Soil Moisture and Evaporation. Water Resources, 16:787-795.

Quick, M.C. and Pipes, A. (1995). UBC Watershed Model Manual (Version 4.0). Univ. of British Columbia, Vancouver, Canada.

Rai, R.K., Upadhyay, A. and Ojha, C.S.P. (2010). Temporal Variability of Climatic Parameters of Yamuna River Basin: Spatial Analysis of Persistence, Trend and Periodicity. The Open Hydrology ournal, 4:184-210.

Rai, S.C. and Gurung, A. (2005). Raising awareness of the impacts of climate changes, Mt. Res. Dev., 25(4):316–320.

Raj, K.B.G. and Fleming, K. (2008). Surface temperature estimation from Landsat ETM^{+} data for a part of the Baspa basin, NW Himalaya, India. Bulletin of Glaciological Research, 25:19-26.

Rajbhandari, R**.**, Shrestha, A.B., Kulkarni, A., Patwardhan, S.K., Bajracharya, S.R. (2014)**.** Projected changes in climate over the Indus river basin using high resolution regional climate model (PRECIS). Clim Dyn, DOI 10.1007/s00382-014-2183-8.

Rango, A., Saalomonson, V.V. and Foster, J.L. (1977). Seasonal streamflow estimation in the Himalayan region employing meteorological satellite snow covers observations. Water Resources research, 13(1):109-112.

Rango, A. (1996). Space borne remote sensing for snow hydrology application. J Hydrol Sci., 41:477–494.

Rebetez, M. (2004) Summer 2003 maximum and minimum daily temperature over a 3,300 m altitudinal range in the Alps. Climate Res., 27:45–50.

Rees, W.G. (2006). Remote sensing of snow and ice. CRC Press, Taylor &Francis, p. 285.

Riggs, G.A. and Hall, D.K. (2002). Reduction of Cloud Obscuration in the MODIS Snow Data Product, Presentation at the 59th Eastern Snow Conference, 5-7 June 2002, Stowe, VT.

Riggs, G., Hall, D.K. and Salomonson, V.V. (2006). MODIS snow products users guide to collection 5.

Ritter, M. (2007). Air Temperature Patterns, Geography 101; The physical environment, available online at http://www.uwsp.edu/geo/faculty/ritter/geog101/ Default.htm, (accessed on December 10, 2007).

Robinson, D.A., Dewey, K.F. and Heim, R.R. (1993). Global snow cover monitoring-an update. Bulletin of the American Meteorological Society,74(9):1689–1696.

Roe, G.H. and O'Neal, M.A. (2010). The response of glaciers to intrinsic climate variability: Observations and models of late Holocene variations, J. Glaciol., 55(193): 839–854.

Rolland, C. (2003). Spatial and seasonal variations of air temperature lapse rates in Alpine regions, J. Clim., 16(7):1032–1046.

Ross, B. and Walash, J. (1986). Synoptic-scale influences of snow cover and sea ice . Monthly Weather Review, 114(10):1790-1810.

Rossow, W.B. and Gardner, L.C. (1993). Cloud detection using satellite measurements of infrared and visible radiances for ISCCP. J. Clim., 6, 2341-2369.

Rothlisberger, H. and Lang, H. (1987). Glacial hydrology. In:Gurmell,A.M., Clark,M.J. (Eds), Glacial-fluvial Sediment Transfer , An Alpine Perspective, Wiley , New York, Chapter 10, 207-284.

Running, S., Nemani, R., Hungerford, R. (1987). Extrapolation of synoptic meteorological data in mountainous terrain and its use for simulating forest evapotranspiration and photosynthesis, Canadian Journal of Forest Research, Vol. 17, pp. 472-483.

Running, W.S, Justice, C.O., Salomonson, V., Hall, D., Barker, J., Kaufman, Y., Strahler, A.H., Huete, A.R., Muller, J.P., Vanderbilt, V., Wan, Z.M. and Teillet, P. and Carneggie, D. (1994). Terrestrial remote sensing science and algorithms planned for EOS/MODIS. Int. J. Remote Sensing, 15 (17):3587-3620.

Russell, G. and Miller, J. (1990). Global river runoff calculated from a global atmospheric GCM. Journal of Hydrology, 117:241-254.

Sahu, R.K., Mishra, S.K., Eldho, T.I. and Jain, M.K. (2007). An Advanced Soil Moisture Accounting Procedure for SCS Curve Number Method. J. Hydrologic Processes, 21(21):2872-2881.

Salama, M.S., Van der Velde, R., Zhong, L., Ma, Y., Ofwono, M. and Su, Z. (2012). Decadal variations of land surface temperature anomalies observed over the Tibetan. Mountain Research Mountain Research and Development 93

http://dx.doi.org/10.1659/MRD-JOURNAL-D-12-00090.1 Plateau by the Special Sensor Microwave Imager (SSMI) from 1987 to 2008. Climate Change, 114:769–781.

Salas, J.D. (1993). Analysis and modeling of hydrologic time series. In Handbook of Hydrology, Maidment DR (ed). McGraw-Hill: New York, 19.1-19.72.

Salomonson, V.V. and Appel, I. (2004). Estimating fractional snow cover from MODIS using the normalized difference snow index. Remote Sensing of Environment, 89:351-360.

Saraf, A.K., Foster, J.L., Singh, P. and Tarafdar, S. (1999). Passive microwave data for snow depth and snow extent estimation in the Himalayan mountains, International Journal of Remote Sensing, 20 (1):83-95.

Schaake, J.C. and Liu, C. (1989). Development and applications of simple water balance models to understand the relationship between climate and water resources. New directions for surface water modeling (Proceedings of the Baltimore symposium, May 1989) IAHS Publ. No. 181:343-352.

Scharfen, G.R., Hall, D.K., Khalsa, S.J.S., Wolfe, J.D., Marquis, Riggs, G.A. and McLean, B. (2000). Accessing the MODIS snow and ice products at the NSIDC DAAC. Proceeding of IGARSS'00, 23-28 July 2000, Honolulu, Hi pp. 2059-2061.

Schetinnikov, A.S. (1998). Morphology and regime of glaciers of Pamirs-Alay (in Russian). SANIGMI Publications: Tashkent, Uzbekistan; 219.

Schmugge, T.J. and Andre, J.C., Eds. (1991). Land Surface Evaporation: Measurements and Parameterization. New York: Springer- Verlag.

Schmugge, T., Hook, S.J. and Coll, C. (1998). Recovering surface temperature and emissivity from thermal infrared multispectral data. Remote Sensing of Environment, 65:121-131.

Schoof, J.T., Pryor, S.C. and Robeson, S.M. (2007): Downscaling daily maximum and minimum temperatures in the Midwestern USA: a hybrid empirical approach. Int. J. Climatol., 27 (4):439-454.

Schoof, J.T., Shin, D.W., Cocke, S., LaRow, T.E., Lim, Y.K. and O'Brien, J.J. (2009). Dynamically and statistically downscaled seasonal temperature and precipitation hindcast ensembles for the southeastern USA. Int. J. Climatol., 29 (2): 243-257.

Sellers, P.J., Hall, F.G., Asrar, G., Strebel, D.E. and R.E. Murphy. (1988). The first ISLSCP Field Experiment (FIFE). Bulletin of American Meteorological Society, 69 (1):22-27.

Sen, P.K. (1968). Estimates of the regression coefficient based on Kendall's tau. J. Am. Statist. Assoc., 63:1379-1389.

Serafinni, V.V. (1987). Estimation of evapotranspiration using surface and satellite data. International Journal of Remote Sensing, 8:1547-1562.

Seth, S.M. (1983). Modelling of daily snowmelt runoff during pre-monsoon month for Beas basin up to Manali. In Proceedings of the First National Symposium on Seasonal Snowcover, 28–30 April, SASE, Manali, (Manali: Snow & Avalanche Study Establishment), II:104–115.

Sharma, K.P., Moore, B. and Vorosamarty, C.J. (2000). Anthropogenic, climatic and hydrologic trends in the Kosi basin, Himalaya. Climate Change, 47:141-165.

Sharma, V., Mishra, V.D. and Joshi, P. K. (2012). Snow cover variation and streamflow simulation in a snow-fed river basin of the Northwest Himalaya. Journal of Mountain Science, 9 (6):853-868.

Sharma, V., Mishra, V.D. and Joshi, P.K. (2013). Implications of climate change on streamflow of a snow-fed river system of the Northwest Himalaya. J. Mt. Sci, 10 (4):574-587.

Shashi Kumar, V., Paul, P.R., Ramana Rao, Ch.L.V., Haefner, H. and Seidel, K. (1993). Snowmelt runoff forecasting studies in Himalayan basins. (In: Young, G.J., ed. Snow and Glacier Hydrology. International Symposium, Kathmandu, Nepal, 16-21 November 1992. Proceedings. International Association of Hydrological Sciences, IAHS/AIHS Publications, 218:85-94.

Shekhar, M.S., Chand, H., Kumar, S., Srinivasan, K. and Ganju, A. (2010), Climate change studies in the western Himalaya. Annals of Glaciology 51(54):105-112(8), DOI: 10.3189/172756410791386508.

Shimamura, Y., Izumi, T. and Matsuyama, H. (2006). Evaluation of a useful method to identify snow-covered areas under vegetation-comparisons among a newly proposed snow index, normalized difference snow index, and visible reflectance. International Journal of Remote Sensing, 27(21):4867-4884.

Shrestha, A.B., Wake, C.P., Mayewski, P.A. and Dibb, J.E. (1999). Maximum Temperature trends in the Himalaya and its vicinity: an analysis based on temperature records from Nepal for the period 1971-94. Journal of Climate, 9(12):2775-2786.

Shroder, Jr. J.F., Owen, L. and Derbyshire, E. (1993). Quanternary glaciations of the Karakoram and Nanga Parbat Himalaya. In J.F. Schroder, Jr. (Ed.), Himalaya to the sea. 132-158, London: Routledge.

Singer, F.S. and Popham, R.W. (1963). Non- Meteorological observations from satellites. Astronautics and Aerospace Engineering, 1(3):89-92.

Singh, D., Jain, S.K. and Gupta, R.D. (2014). Trend analysis of historical and downscaled future precipitation data in Sutlej basin, India. International Journal of Earth Sciences and Engineering, 7:118-127.

Singh, P. (1991). A temperature lapse rate study in Western Himalayas. Hydrol J., 14:156–163.

Singh, P. and Quick, M.C. (1993). Streamflow simulation of Satluj River in the Western Himalayas. Snow and Glacier Hydrology. IAHS publication 218:261-271.

Singh, P., Ramashastri, K.S. and Kumar, N. (1995). Topographical influence on precipitation distribution in different ranges of western Himalayas. Nordic Hydrology, 26:259-284.

Singh, P. and Kumar, N. (1996). Determination of snowmelt factor in the Himalayan region, Hydrological Sciences Journal, 41:301-310.

Singh, P., Jain, S.K. and Kumar, N. (1997a). Estimation of snow and glacier contribution to the Chenab River, Western Himalaya. Mt. Res. Dev., 17 (1):49-56.

Singh, P., Spitzbart, G., Huebl, H. and Weinmeister, H.W. (1997b). Hydrological response of a snowpack under rain-on-snow events: a field study, Journal of Hydrology, 202:1-20.

Singh, P. and Kumar, N. (1997a). Effect of orography on precipitation in the western Himalayan region. J. Hydrol., 199:183-206.

Singh, P. and Kumar, N. (1997b). Impact of climate change on the hydrological response of a snow and glacier melt runoff dominated Himalayan River. J Hydrol., 193:316–350.

Singh, P., Kumar, N. and Arora, M. (2000). Degree –day factors far snow and ice for Dokriani Glacier, Garhwal Himalayas. Journal of Hydrology, 235:1–11.

Singh, P. and Singh, V.P. (2001) Snow and Glacier Hydrology. Kluwer, Dordrecth, The Netherlands.

Singh, P. and Jain, S.K. (2002). Snow and glacier melt in the Satluj river at Bhakra Dam in the Western Himalayan region. Hydrological Sciences Journal, 47:93-106.

Singh, P. and Jain. S.K. (2003). Modelling of streamflow and its components for a large Himalayan basin with predominant snow melt yields. Hydrological Sciences Journal, 48:257-276.

Singh, P., Bengtsson, L. and Berndtsson, R. (2003). Relating air temperatures to the depletion of snow covered area in a Himalayan basin. Nordic Hydrol., 34(4):267–280.

Singh, P. and Bengtsson, L. (2004). Hydrological sensitivity of a large Himalayan basin to climate change. Hydrological processes, 18 (13):2363-2385.

Singh, P. and Bengtsson, L. (2005). Impact of warmer climate on melt and evaporation for the rainfed, snowfed and glacierfed basins in the Himalayan region. Journal of Hydrology, 300(1-4):140–154.

Singh, P., Arora, M. and Goel, N. K. (2006). Effect of climate change on runoff of a glacierized Himalayan basin. Hydrological Processes, 20 (9):1979-1992.

Singh, P., Kumar, V., Thomas, T. and Arora. M. (2008a). Change in rainfall and relative humidity in different river basins in the northwest and central India. Hydrol. Processes, 22:2982-2992.

Singh, P., Kumar, V., Thomas, T. and Arora, M. (2008b). Basin-wide assessment of temperature trends in the northwest and central India. Hydrol. Sci. J. 53(2):421-433.

Singh, P., Haritashya, U.K. and Kumar, N. (2008c). Modelling and estimation of different components of streamflow for Gangotri Glacier basin, Himalayas. Hydrological Sciences–Journal–des Sciences Hydrologiques,53(2):309-322.

Singh, R.K., Prasad, V.H. and Bhatt, C.M. (2004). Remote sensing and GIS approach for assessment of the water balance of a watershed. Hydrological Sciences Journal, 49(1):131-141.

Singh, V.P. (ed). (1995). Computer Models of watershed Hydrology, Water Resources Publications, Littleton, Colorado, 1995.

Slariya, M. (2013). Hydroelectric Power Generation: Himachal Pradesh's Perspective. EXCEL International Journal of Multidisciplinary Management Studies, EIJMMS, 3 (5):192-205, ISSN 2249-8834.

Snehmani, Singh, M.K., Gupta, R.D. and Ganju, A. (2013a). DTM Generation and Avalanche Hazard Mapping using Large Format Digital Photogrammetric Data and Geomatics Technique. Journal of Remote Sensing & GIS, 4 (2):4-13.

Snehmani, Singh, M.K., Gupta, R.D. and Ganju, A. (2013b). Extraction of high resolution DEM from Cartosat-1 stereo imagery using rational Math model and its accuracy assessment for a part of snow covered NW-Himalaya. Journal of Remote Sensing & GIS, 4 (2):23-34.

Sobrino, J.A., Li, Z., Stoll M.P. and Becker, F. (1994). Improvements in the split-window technique for land surface temperature determination. IEEE Trans. Geosci. Remote sens., 32 (32):243-253.

Sobrino, J.A. and Raissouni, N. (2000). Toward remote sensing methods for land cover dynamic monitoring: Application to Morocco. Int. J. Remote Sens., 21:353– 366.

Sobrino, J.A., El-Kharraz, J. and Li, Z. (2003). Surface temperature and water vapour retrieval from MODIS data; Int. J. Remote Sens.24 (24):5161–5182.

Sonali, P. and Kumar, D.N. (2013). Review of trend detection methods and their application to detect temperature changes in India. Journal of Hydrology, 476:212-227.

Sorman, A.A. (2005). Use of Satellite Observed Seasonal snow cover in Hydrological Modelling and Snowmelt Runoff Prediction in Upper Euphrates Basin, Turkey. PhD Thesis, Middle East Technical University.

Srinivas, V.V., Basu, B., Nagesh Kumar, D. and Jain, S.K. (2013). Multi-site downscaling of maximum and minimum daily temperature using support vector machine. Int. J. Climatol., 34:1538-1560, DOI: 10.1002/joc.3782.

Srivastava, S.K. and Gupta, R.D. (2003). Monitoring of Changes in Land Use/ Land Cover using Multi-sensor Satellite Data. 6th International Conference on GIS/GPS/RS: Map India 2003, Jan.28-31, New Delhi.

Steinacker, R., Ratheiser, M., Bica, B., Chimani, B., Dorninger, M., Gepp, W., Lotteraner, C., Schneider, S. and Tschannett, S. (2006). A mesoscale data analysis and downscaling method over complex terrain. Mon. Weather Rev, 134:2758-2771.

Strovold, R. and Malnes, E. (2004). Snow covered area retrieval using ENVISAT ASAR wide swath in mountainous areas. In: IEEE international geosciences and remote sensing symposium proceedings, 1–7:1845–1848.

Subramaniam, S., Suresh Babu, A.V., Sivasankar, E., Venkateshwar Rao, V. and Behera, G. (2011). Snow Cover Estimation from Resourcesat-1 AWiFS–Image Processing With an Automated Approach, International Journal of Image Processing (IJIP), 5 (3):298-320.

Tang, Z.Y. and Fang, J.Y. (2006). Temperature variation along the northern and southern slopes of Mt. Taibai, China, Agric. For. Meteorol., 139(3–4):200–207, doi:10.1016/ j.agrformet.2006.07.001.

Tebakari, T., Yoshitani, J. and Suvanpiomol, C. (2005). Time-space trend analysis in pan evaporation Kingdom of Thailand. J. Hydrol. Eng., 10 (3):205-215.

Tekeli, A.E., Akyurek, Z., Sensoy, A., Sorman, A.A. and Sorman, A.U. (2005a). Modelling the temporal variation in snow-covered area derived from satellite images for simulating/forecasting of snowmelt runoff in Turkey, Hydrological Sciences Journal, 50 (4):669-682.

Tekeli, A.E., Aky¨urek, Z., Sorman, A.A., Sensoy, A. and Sorman, A.U. (2005b). Using MODIS snow cover maps in modeling snowmelt runoff process in the eastern part of Turkey. Remote Sens Environ., 97:216–230.

Thakur, P.K. and Prasad, V.H. (2006). Study of Frosting Patterns, Polar Ice of Mars, Terrestrial Analog Studies of Gangotari Glacier of India Using Remote Sensing and Spectral Nature of CO2/H2O Ice LPI Contributions. In the Fourth Int. Conf. on Mars Polar Science and Exploration Meeting at SLF Davos, Switzerland, 2-6 October, 2006.

Thakur, P.K., Duishonakunov, M., Prasad, V.H., Garg, P.K. and Garg, R.D. (2008). Hydrology study in Manali Sub-Basin of Beas River using HEC-HMS. Hydro2008, National conference on Hydraulics and Water Resources, MNIT Jaipur, 15-16 , 681-693.

Thakur, P.K., Aggarwal, S.P. and Radchenko, Y. (2009). Snowmelt runoff and Climate Change studies in Manali sub-basin of Beas river, India. In Proceeding of National Symposium on climate change and Water Resources in India, NIH Roorkee, 18-19.

Thakur, P.K., Murgan, A.V., Aggarwal, S.P. and Prasad, V.H. (2011). Automatic Extraction of Information in a Glacial Terrain using Remote Sensing. Hydrology Journal. 34(1and 2):65-75.

Thakur, P.K., Aggarwal, S.P., Garg, P.K., Garg, R.D., Mani, S., Pandit, A. and Kumar, S. (2012). Snow physical parameters estimation using space-based Synthetic Aperture Radar. Geocarto International, 27(3):263-288.

Thakur, P.K., Garg, R.D., Aggarwal, S. P., Garg, P. K., Mani, S. and Shi, J. (2013). Snow density retrieval using SAR data: algorithm validation and applications in part of North Western Himalaya. The Cryosphere Discussions 05/2013; 7(3):1927-1960.

Thapa, K.B. (1980). Analysis for snowmelt runoff during premonsoon months in Beas basin using satellite imageries. M.E. dissertation, Department of Hydrology, University of Roorkee, India.

Thapa, K.B. (1993). Estimation of snowmelt runoff in Himalayan catchments incorporating remote sensing data, In: Young, G. J., ed. Snow and Glacier Hydrology. International Symposium, Kathmandu, Nepal, 16-21 November 1992, Proceedings International Association of Hydrological Sciences. IAHS/AISH Publication 218:69-74.

Thapliyal, V. and Kulshrestha, S.M. (1991). Decadal changes and trends over India. Mausam, 42:333-338.

Thayyen, R.J., Gergan, J.T. and Dobhal, D.P. (2005). Slope lapse rates of temperature in Din Gad (Dokriani Glacier) catchment, Garhwal Himalaya, India, Bulletin of Glaciological Research 22:31-37.

Townshend, J.R.G. and Tucker, C.J. (1984). Objectives assessment of advanced very high resolution radiometer data for land cover mapping; Int. J. Remote Sens., 5:497-504.

Tseng, K.H., Shum, C.K., Lee, H., Duan, J., Kuo, C., Song, S. and Zhu, W. (2011). Satellite observed environmental changes over the Qinghai–Tibetan Plateau. Atmospheric and Oceanic Sciences, 22:229–239.

Tucker, C.J. (1979a). Maximum normalized difference vegetation index images for sub-Saharan Africa for 1983-1985. Int. J. Remote Sens., 7:1383-1384.

Tucker, C.J. (1986): Maximum normalized difference vegetation index images for sub-Saharan Africa for 1983-1985, International Journal of Remote Sensing, 7, pp 1383-1384.

Ulivieri, C., Castronouvo, M.M., Francioni, R. and Cardillo, A. (1992). A SW algorithm for estimating land surface temperature from satellites, Adv. Space Res., 14 (3):59-65.

Upadhyay, D.S., Mishra, D.K., Johri, A.P., Mishra D.K. and Srivastava, A.K. (1991). Use of satellite based information in snowmelt run-off studies, Mausam, 42 (2):187-194.

U.S. Army Corps of Engineers. (1956). Snow Hydrology, Summary report of snow investigations. U.S. Army Corps of Engineers, North Pacific Division, Portland, Oregon, 1956.

USGS (2004). Shuttle Radar Topography Mission, 3 Arc Second scene SRTM_u03, Unfilled Unfinished 2.0, 13 Global Land Cover Facility, University of Maryland, College Park, Maryland, February 2000. 14 Vogt J.V., 1996. Land surface temperature retrieval from NOAA AVHRR data. Dans : G. D'Souza., A. 15 Belward & J.P. Malingreau (eds.). Brussels & Luxembourg, 125-151. USGS (2004) http://srtm.usgs.gov/. access on 14 May 2008.

Vehvilainen, B. and Lohvansuu, J. (1991). The effects of climate change on discharges and snow cover in Finland. Hydrological Sciences, 36:109-121.

Vidal, A. (1991). Atmospheric and emissivity correction of land surface temperature measured from satellite using ground measurements or satellite data. Int. J. Remote Sens., 12 (12):2449-2460.

Villaba, R., Lara, A., Boninsegna, J.A., Masiokas, M., Delgado, S., Aravena, J.C., Roig, F.A., Schmelter, A., Wolodarsky, A. and Ripalta, A. (2003). Large-scale temporal changes across the southern Andes: 20th century variations in the context of the past 400 years. Climate Change, 59:177–232.

Vinnikov, K., Graisman, P.Y. and Lugina, K.M. (1990). Empirical data on contemporary global climate changes (Temperature and precipitation). J Climate, 3:662-677.

Vuille, M., Bradley, R.S., Werner, M. and Keimig, F. (2003). 20th century climate change in the tropical Andes: observations and model results. Climate Change, 59:75–99.

Wan, Z. and Dozier, J. (1996). A generalized split-window algorithm for retrieving land surface temperature measurement from space, IEEE Transactions on Geoscience and Remote Sensing, 34:892-905.

Wan, Z., Zhang, Y., Zhang, Q. and Li, Z.L. (2004). Quality assessment and validation of the MODIS global land surface temperature. International Journal of Remote Sensing, 25 (1):261-274.

Wang, J. and Li, W. (2003). Comparison of methods of snow cover mapping by analyzing the solar spectrum of satellite remote sensing data in China. International Journal of Remote Sensing, 24(21):4129-4136.

Weng, Q., Lu, D. and Schubring, J. (2004). Estimation of land surface temperature-vegetation abundance relationship for urban heat island studies. Remote Sensing of Environment, 89(4):467-483.

Wibig, J. and Glowicki, B. (2002). Trends in minimum and maximum temperature in Poland. Climate Res, 20:123–133.

Wigley, T.M.L, Jones, P.D., Briffa, K.R. and Smith, G. (1990). Obtaining sub-grid-scale information from coarse-resolution general circulation model output. J Geophys Res, 95 (D2):1943–1953.

Wilby, R.L. (1998). Statistical downscaling of daily precipitation using daily airflow and seasonal teleconnection indices. Clim Res10:163–178.

Wilby, R.L., Hay, L.E. and Leavesley, G.H. (1999). A comparison of downscaled and raw GCM output: implications for climate change scenarios in the San Juan River basin, Colorado. J. Hydrol., 225 (1-2):67-91.

Wilby, R.L., Tomlinson, O.J. and Dawson, C.W. (2003). Multi-site simulation of precipitation by conditional resampling. Clim Res, 23:183–194.

Wilby, R.L., Charles, S.P., Zorita, E., Timbal, B., Whetton, P. and Mearns, L.O. (2004). Guidelines for use of climate scenarios developed from statistical downscaling methods. Supporting material of the Intergovernmental Panel on Climate Change (IPCC), prepared on behalf of Task Group of Data and Scenario Support for Impacts and Climate Analysis (TGICA), 1-27.

Wilby, R.L. and Dawson, C.W. (2007). Statistical downscaling model, SDSM, Version 4.2 – A decision support tool for the assessment of regional climate change impacts. User Manual.

Wiscombe, W.J. and Warren, S.G. (1980). A model for the spectral albedo of snow, I, pure snow . Journal of Atmosphere Sciences, 37:2712-2733.

World Meteorological Organization (WMO) (1986). Intercomparison of models of snowmelt runoff. Operation Hydrological Report No. 23, (WMO No. 646), World Meteorological Organization, Geneva.

Wurbs, R., Ranjan, A., Muttiah, S. and Felden, F. (2005). Incorporation of Climate Change in Water Availability Modeling. Journal: Journal of Hydrologic Engineering – Journal of Hydrologic Engineering10 (5):375-385.

Wurbs, R.A. and Kim, T.J. (2011). River Flows for Alternative Conditions of Water Resources Development. Journal: Journal of Hydrologic Engineering, 16:148-156.

Xu, CY. (1999). From GCMs to river flow: a review of downscaling methods and hydrologic modelling approaches. Progress in Physical Geography, 23 (2): 229–249.

Xu, C.Y. (2000). Modelling the effects of climate change on water resources in central Sweden. Water Resour. Manage., 14:177-189.

Xu, C.Y., Widen, E. and Halldin, S. (2005). Modelling hydrological consequences of climate change- progress and challenges. Adv. Atmos. Sci., 22 (6):789-797.

Xu, Y., Shen, Y. and Wu, Z. (2013). Spatial and Temporal Variations of Land surface Temperature over the Tibetan Plateau Based on Harmonic Analysis. Mountain Research and Development, 33(1):85-94.

Xu, Z., Liu, Z., Fu, G. and Chen, Y. (2010). Trends of major hydroclimatic variables in the Tarim river basin during the past 50 years. Journal of Arid Environments, 74 (2):256-267.

Yao, T., Duan, K., Thompson, L.G., Wang, N., Tian, L., Xu, B., Wang, Y. and Yu, W. (2007) Temperature variations over the past millennium on the Tibetan Plateau revealed by four ice cores; Ann. Glaciol., 46:362–366.

Yoshida, S. (1962). Hydrometerological study on snowmelt, Journal of Meteorological Research, 14:879-899.

Yu, Y., Privette, J.L. and Pinheiro, A.C. (2008). Evaluation of split-window land surface temperature algorithms for generating climate data records. IEEE Trans. Geoscience and Remote Sensing, 46 (1):179-192.

Yu, Y., Tarpley, D., Privette, J.L., Goldberg, M.D., Raja, M.K.R.V., Vinnikov, K.Y. and Xu, H. (2009). Developing algorithm for operational GOES-R land surface temperature product. IEEE Transactions on Geoscience and Remote Sensing, 47:936-951.

Yu, Y.S., Zou, S. and Whittemore, D. (1993). Non-Parametric trend analysis of water quality data of rivers in Kansas. J. Hydrol., 150:61-80.

Yue, S. and Hashino, M. (2003). Temperature trends in Japan: 1900-1990. Theoret. Appl. Climatol., 75:15-27.

Zhengming, W. (1999). MODIS Land-Surface Temperature Algorithm Theoretical Basis Document, available online at http://modis.gsfc.nasa.gov/data/atbd/ atbd_mod11.pdf, (accessed on September 22,, 2014).

Zhengming, W. (2006). MODIS Land Surface Temperature Products Users' Guide, available online at http://www.icess.ucsb.edu/modis/LstUsrGuide/usrguide.html, (accessed on May 13, 2014).

Zhong, L., Su, Z., Ma, Y., Salama, M.S. and Sobrino, J.A. (2011). Accelerated changes of environmental conditions on the Tibetan Plateau caused by climate change. Journal of Climate 24:6540–6550.

ANNEXURE-I

LIST OF PUBLICATIONS

INTERNATIONAL JOURNALS:

1. Jain S.K., Thakural, L.N., Singh, R.D., Lohani, A.K. and Mishra and S.K. (2011). Snow cover depletion under changed climate with the help of remote sensing and temperature data. Natural Hazards, 58 (3):891-904.

INTERNATIONAL CONFERENCES:

1. Thakural, L. N., Jain, Sanjay K. and Singh, R. D. 2012. Trends Analysis of Temperature in Beas Basin, Western Himalayas. International Symposium on Cryosphere and Climate change 2012, Manali, pg 101, 2-4 April.
2. Thakural, L.N., Jain, S.K., Singh, R.D., Jain, S.K., Mishra, S.K. 2013. Trend analysis of Temperature and Rainfall in Beas basin, Western Himalayas. International Humboldt Kolleg in Management of Water, Energy and Bio-resources in Changing Climate Regime: Emerging Issues and Environmental Challenges, Feb. 8-9, 2013 organized by School of Environmental Sciences, Jawaharlal Nehru University, New Delhi.

NATIONAL CONFERENCES:

1. Retrieval of snow cover using MODIS for the Himalayan basin. Climate Change: Past, Present and Future, 12-13 January, 2015 organized by Department of Geology, Poona College of Arts, Science and Commerce, Pune, Maharashtra. (Accepted)

ANNEXURE-II

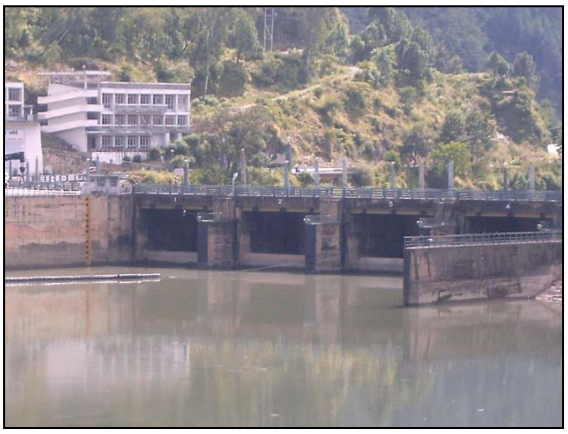

Pandoh Dam
(Pandoh, Mandi district)

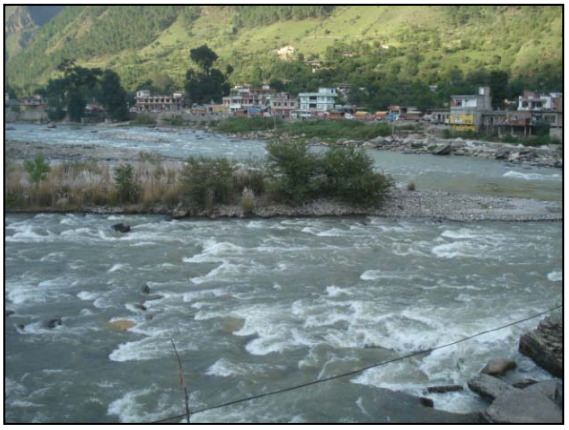

Confluence of river Beas and Parvati
(Bhuntar)

Upstream of Pandoh dam

Sase's meteorological observatory, Dhundi

Melting of snow, Marhi

Snow field, Dhundi (January 2010)

Field photographs taken during the field visit